

Louisiana State University

LSU Scholarly Repository

---

LSU Doctoral Dissertations

Graduate School

---

November 2021

## Reaction Pathways of Molecular Growth for Bay-Region Methyl-Substituted Polycyclic Aromatic Hydrocarbons During Supercritical Pyrolysis of n-Decane

Venkata Sai Krishna Karthik Vutukuru

Follow this and additional works at: [https://repository.lsu.edu/gradschool\\_dissertations](https://repository.lsu.edu/gradschool_dissertations)

 Part of the [Chemical Engineering Commons](#)

---

### Recommended Citation

Vutukuru, Venkata Sai Krishna Karthik, "Reaction Pathways of Molecular Growth for Bay-Region Methyl-Substituted Polycyclic Aromatic Hydrocarbons During Supercritical Pyrolysis of n-Decane" (2021). *LSU Doctoral Dissertations*. 5709.

[https://repository.lsu.edu/gradschool\\_dissertations/5709](https://repository.lsu.edu/gradschool_dissertations/5709)

This Dissertation is brought to you for free and open access by the Graduate School at LSU Scholarly Repository. It has been accepted for inclusion in LSU Doctoral Dissertations by an authorized graduate school editor of LSU Scholarly Repository. For more information, please contact [gradetd@lsu.edu](mailto:gradetd@lsu.edu).

REACTION PATHWAYS OF MOLECULAR GROWTH FOR BAY-  
REGION METHYL-SUBSTITUTED POLYCYCLIC AROMATIC  
HYDROCARBONS DURING SUPERCRITICAL PYROLYSIS  
OF *n*-DECANE

A Dissertation

Submitted to the Graduate Faculty of the  
Louisiana State University and  
Agricultural and Mechanical College  
in partial fulfillment of the  
requirements for the degree of  
Doctor in Philosophy

in

The Gordon A. and Mary Cain Department of Chemical Engineering

by  
Venkata Sai Krishna Karthik Vutukuru  
B.Tech., Osmania University, India, 2015  
December 2021

*For my Parents and Grandparents*

## Acknowledgments

First and foremost, I would like to thank the most important person in this journey, my Ph.D. advisor, Prof. Mary J. Wornat. Without her guidance and support, this dissertation would not have been possible. I am forever grateful for her constant encouragement and passing on her knowledge not only about how to conduct research and present data but also about life in general. Throughout my journey as a graduate student, she has been a constant source of inspiration and I am honored to be given the opportunity to work under her.

Next, I would like to thank the other members on my committee, Prof. John C. Flake, Prof. Michael Benton, and Prof. Shengmin Guo for their valuable input and willingness to be a part of my committee. I would also like to thank the Air Office of Scientific Research for providing funding for my research. For providing specially synthesized compounds, I would like to thank Dr. Albrecht Seidel of Biochemical Institute for Environmental Carcinogens, Germany. For providing reference standards and UV spectra, I would like to thank the following people: Dr. Arthur Lafleur and Ms. Elaine Plummer of Massachusetts Institute of Technology; Dr. John Fetzer of FETZPAHS; Dr. Hilan Kaplan of Boston College; Dr. Markus Braun and Prof. Maximilian Zander of RÜTGERS Basic Aromatics GmbH; Dr. Michael J. Krische of University of Texas; Prof. Bonsup Cho of University of Rhode Island; Prof. Thomas E. Prisinzana and Mr. Benjamin Neuenswander of University of Kansas, Prof. Yasushi Nishihara and Prof. Masayuki Iwasaki of Okayama University; Dr. Qingsu Xia of National Center for Toxicological Research; Dr. Yao-Ting Wu of National Chang Kung University; Dr. Dianne Poster of National Institute of Standards and Technology; Dr. Diego Peña of CiQUS, Spain.

I would also like to thank Dr. Nimesh B. Poddar for being a wonderful mentor. I will always be grateful to him for sharing his knowledge and expertise in UV spectra. I would also

like to thank another important member of the research group, Dr. Subramanian V. Kalpathy. He taught me how to perform complicated experiments, and I will always be grateful for that. The third member in our group I would like to thank is Dr. Elizabeth Hurst for teaching me how to perform extremely complex product analyses. Dr. Eva Caspary, Ms. Catherine Poddar, Mr. Avinash Mali, Mr. Matthew Skapura, Ms. Leah Potylchansky, and Ms. Erin Cochran are the other members of our group I would like to thank for their help during my time in the lab.

I would like to thank Joe, Darla, Rachel, and Danny—the workshop and administrative staff at the Department of Chemical Engineering—for their constant support. I would also like to thank the Combustion Institute and the Coates Travel Awards program at LSU for providing me with funding to present my research around the world.

Finally, I would like to thank my parents, Kumari Vutukuru and Ramana Vutukuru for their constant love and support. I also want to thank my sisters, Dr. Navya Vutukuru and Teja Vutukuru, for believing in me and for being my role models.

## Table of Contents

Acknowledgements.....	iii
List of Tables .....	vii
List of Figures .....	ix
Abstract .....	xix
Chapter 1. Introduction .....	1
1.1. Background and Motivation .....	1
1.2. Purpose of This Study .....	6
1.3. Structure of the Dissertation.....	8
Chapter 2. Experimental Equipment and Analytical Techniques .....	11
2.1. Introduction .....	11
2.2. Supercritical Fuel Pyrolysis Reactor System .....	11
2.3. Product Analysis .....	14
2.4. Concluding Remarks .....	28
Chapter 3. New identifications of Aliphatic and Aromatic Products .....	29
3.1. Introduction .....	29
3.2. Identification of <i>n</i> -Alkanes, Alkenes, and Dienes .....	29
3.3. Identification of Cyclic Aliphatic Products .....	31
3.4. Identification of One-Ring Aromatic Products .....	31
3.5. Identification of PAH Products .....	34
3.6. Concluding Remarks .....	37
Chapter 4. Effects of Temperature on the Yields of Aliphatic and Aromatic Products .....	38
4.1. Introduction .....	38
4.2. Effects of Temperature on the Yields of Major Straight-Chain Aliphatic Products .....	39
4.3. Effects of Temperature on the Yields of Cyclic Aliphatic Products .....	44
4.4. Effects of Temperature on the Yields of Aromatic Products .....	49
4.5. Concluding Remarks .....	58
Chapter 5. Reaction Pathways of Molecular Growth for Bay-Region Methyl-Substituted Polycyclic Aromatic Hydrocarbons During Supercritical Pyrolysis of <i>n</i> -Decane, as Determined from Experiments with 4-Methylchrysene Dopant .....	63
5.1. Introduction .....	63
5.2. Experimental Equipment and Procedures .....	66
5.3. Results and Discussion .....	67
5.4. Concluding Remarks .....	90

Chapter 6. Reaction Pathways of Molecular Growth for Bay-Region Methyl-Substituted Polycyclic Aromatic Hydrocarbons During Supercritical Pyrolysis of <i>n</i> -Decane, as Determined from Experiments with 4-Methylphenanthrene Dopant .....	92
6.1. Introduction .....	92
6.2. Experimental Equipment and Procedures .....	95
6.3. Results and Discussion .....	96
6.4. Concluding Remarks .....	117
Chapter 7. Conclusions and Recommendations .....	118
7.1. Summary .....	118
7.2. Supercritical Pyrolysis of <i>n</i> -Decane at Low Temperatures .....	120
7.3. Mechanistic Findings from Dopant Experiments with Bay-Region Methyl-Substituted PAH .....	122
7.4. Recommendations for Future Work .....	127
Appendix A. Supporting Information for Chapter 2 .....	128
Appendix B. Supporting Information for Chapter 4 and Chapter 5 .....	137
Appendix C. Supporting Information for Chapter 6 .....	176
Appendix D. Letter of Permission .....	211
References .....	212
Vita .....	216

## List of Tables

2.1. Constituents of the 15 normal-phase HPLC fractions of an <i>n</i> -decane product mixture. ....	20
2.2. Solvent methods used for the reversed-phase HPLC analysis of PAH products produced from the supercritical pyrolysis of <i>n</i> -decane. ....	24
3.1. Newly identified <i>n</i> -alkanes, alkenes, and dienes of supercritical <i>n</i> -decane pyrolysis. ....	30
3.2. Newly identified C <sub>5</sub> -ring aliphatic products of supercritical <i>n</i> -decane pyrolysis. ....	32
3.3. Newly identified C <sub>6</sub> -ring aliphatic products of supercritical <i>n</i> -decane pyrolysis. ....	33
3.4. Newly identified one-ring aromatic products of supercritical <i>n</i> -decane pyrolysis. ....	34
3.5. Newly identified PAH products of supercritical <i>n</i> -decane pyrolysis. ....	36
3.6. Newly identified PAH products from the supercritical pyrolysis of <i>n</i> -decane to which 4-methylchrysene has been added as a dopant. ....	36
5.1. Ring-expansion reactions of 9-methylfluorene and of 9-fluorenyl (with ethylene), as determined from supercritical <i>n</i> -decane pyrolysis experiments with the dopant fluorene. ...	75
6.1. Proposed pathways for the formation of benzo[ <i>pqr</i> ]naphtho[8,1,2- <i>bcd</i> ]perylene and benzo[ <i>ghi</i> ]naphtho[8,1,2- <i>bcd</i> ]perylene from reactions of 4-pyrenylmethyl with the principal aliphatic growth species—methyl, ethylene, and 1-butene—in the supercritical <i>n</i> -decane pyrolysis environment. ....	112
A1. GC retention times and response factors for C <sub>1</sub> -C <sub>6</sub> hydrocarbons. ....	128
A2. GC retention times and responses factor for the Agilent model 7890B GC/FID. ....	129
A3. Surrogate compounds for GC calibration. ....	130
A4. HPLC elution times and response factors for polycyclic aromatic hydrocarbons. ....	133
A5. Surrogate compounds for HPLC calibration. ....	134
B1. Quantified aromatic products of supercritical <i>n</i> -decane pyrolysis. ....	137
B2. PAH growth reactions of 1-naphthylmethyl and phenalenyl, as determined from supercritical <i>n</i> -decane pyrolysis experiments with the dopant 1-methylnaphthalene. ....	156



B3. PAH growth reactions of 1-pyrenylmethyl and benzo[ <i>cd</i> ]pyrenyl, as determined from supercritical <i>n</i> -decane pyrolysis experiments with the dopant 1-methylnaphthalene (which greatly increased the production of 1-methylpyrene). .....	157
B4. PAH growth reactions of 1-phenanthrylmethyl and benz[ <i>de</i> ]anthracenyl, as determined from supercritical <i>n</i> -decane pyrolysis experiments with the dopant 1-methylphenanthrene. ....	158
B5. Proposed pathways for the formation of benzo[ <i>pqr</i> ]naphtho[8,1,2- <i>bcd</i> ]perylene, benzo[ <i>ghi</i> ]naphtho[8,1,2- <i>bcd</i> ]perylene, and naphtho[8,1,2- <i>abc</i> ]coronene from reactions of 4-benzo[ <i>a</i> ]pyrenylmethyl and 5-benzo[ <i>a</i> ]pyrenylmethyl with the principal aliphatic growth species—methyl, ethylene, propene, and 1-butene—in the supercritical <i>n</i> -decane pyrolysis environment. ....	159
C1. Quantified aromatic products of supercritical <i>n</i> -decane pyrolysis. ....	176

## List of Figures

1.1. Molecular structure and bond-dissociation energies for model fuel <i>n</i> -decane. ....	2
1.2. Molecular structures of 1-methylnaphthalene, 2-methylnaphthalene, and 1-methylphenanthrene, and relevant bond-dissociation energies. ....	6
1.3. Molecular structures of 4-methylchrysene and the three- to six-ring bay-region methyl-substituted PAH products of supercritical <i>n</i> -decane pyrolysis at 568 °C, 94.6 atm, and 133 sec: 4-methylphenanthrene, 1-methyltriphenylene, 9-methylbenzo[ <i>e</i> ]pyrene, 10-methylbenzo[ <i>a</i> ]pyrene, 11-methylbenzo[ <i>a</i> ]pyrene, 1-methylbenzo[ <i>e</i> ]pyrene, and 7-methylbenzo[ <i>ghi</i> ]perylene. ....	7
2.1. Schematic of the supercritical fuel pyrolysis reactor system. ....	12
2.2. Analyses scheme for the fractionation of the liquid-phase products from the supercritical pyrolysis of <i>n</i> -decane. ....	17
2.3. Reversed-phase HPLC chromatogram of five-ring C <sub>20</sub> H <sub>12</sub> PAH and their alkylated derivatives from the supercritical pyrolysis of <i>n</i> -decane at 570 °C, 94.6 atm, and 133 sec. ....	25
2.4. The black line is the UV spectrum of a PAH product from the supercritical pyrolysis of <i>n</i> -decane overlaid with the red line, which is the UV spectrum of a reference standard. ....	27
3.1. The black line is the UV spectrum of a PAH product from the supercritical pyrolysis of <i>n</i> -decane overlaid with the red line, which is the UV spectrum of a reference standard. ....	35
3.2. Comparisons of the UV spectra of 4-methylchrysene-doped <i>n</i> -decane pyrolysis products (black lines) to reference spectra (red lines). ....	37
4.1. Yields, as functions of temperature, of the major straight-chain <i>n</i> -alkanes and 1-alkenes of supercritical <i>n</i> -decane pyrolysis at 94.6 atm and 133 sec. ....	40
4.2. Yields, as functions of temperature, of the major straight-chain 2-alkenes, 3- & 4-alkenes, and dienes of supercritical <i>n</i> -decane pyrolysis at 94.6 atm and 133 sec. ....	41
4.3. Molecular structure of <i>n</i> -decane and relevant bond-dissociation energies. ....	42
4.4. Yields, as functions of temperature, of the major C <sub>6</sub> -ring cyclic aliphatic products of supercritical <i>n</i> -decane pyrolysis at 94.6 atm and 133 sec. ....	46
4.5. Yields, as functions of temperature, of the major C <sub>5</sub> -ring cyclic aliphatic products of supercritical <i>n</i> -decane pyrolysis at 94.6 atm and 133 sec. ....	47

4.6. Yields, as functions of temperature, of the major one-ring aromatic products of supercritical <i>n</i> -decane pyrolysis at 94.6 atm and 133 sec. ....	51
4.7. Yields, as functions of temperature, of the major two-ring aromatic products of supercritical <i>n</i> -decane pyrolysis at 94.6 atm and 133 sec. ....	52
4.8. Yields, as functions of temperature, of selected benzenoid PAH products produced from the supercritical <i>n</i> -decane pyrolysis experiments conducted at 94.6 atm and 133 sec: (a) 3-ring PAH; (b) 4-ring PAH; (c) 5-ring PAH; (d) 5-ring C <sub>22</sub> H <sub>14</sub> PAH; (e) 6-ring PAH; (f) 7-ring PAH; (g) 8-ring PAH; and (h) 9-ring PAH. ....	55
5.1. Molecular structures of 1-methylnaphthalene, 2-methylnaphthalene, 1-methyl phenanthrene, and 4-methylchrysene and relevant bond-dissociation energies. ....	64
5.2. Molecular structures of 4-methylchrysene (242h) and seven three- to six-ring bay-region methyl-substituted PAH products of supercritical <i>n</i> -decane pyrolysis at 568 °C, 94.6 atm, and 133 sec: 4-methylphenanthrene (192f), 1-methyltriphenylene (242b), 9-methylbenzo[ <i>e</i> ]pyrene (266x), 10-methylbenzo[ <i>a</i> ]pyrene (266o), 11-methylbenzo[ <i>a</i> ]pyrene (266n), 1-methylbenzo[ <i>e</i> ]pyrene (266w), and 7-methylbenzo[ <i>ghi</i> ]perylene (290b). ....	65
5.3. Yields of selected PAH products of supercritical <i>n</i> -decane pyrolysis at 568 °C, 94.6 atm, and 133 sec: (a) four- to six-ring PAH, (b) benzo[ <i>a</i> ]pyrene and alkyl derivatives, (c) six- to nine-ring benzenoid PAH and derivatives, and (d) five- to seven-ring PAH with internal five-membered rings. ....	70
5.4. Yields of five-ring C <sub>22</sub> H <sub>14</sub> PAH and their methyl derivatives from supercritical <i>n</i> -decane pyrolysis at 568 °C, 94.6 atm, and 133 sec: benzo[ <i>c</i> ]chrysene (278i), benzo[ <i>b</i> ]chrysene (278a), dibenz[ <i>a,h</i> ]anthracene (278b), dibenz[ <i>a,j</i> ]anthracene (278c), benzo[ <i>a</i> ]naphthacene (278d), pentaphene (278e), picene (278f), benzo[ <i>g</i> ]chrysene (278g), dibenz[ <i>a,c</i> ]anthracene (278h), three methyl dibenz[ <i>a,c</i> ]anthracenes (292b-d), and a methylbenzo[ <i>g</i> ]chrysene (292a). ....	73
5.5. Molecular structures of 4 <i>H</i> -cyclopenta[ <i>def</i> ]chrysene and fluorene and relevant bond-dissociation energies. ....	74
5.6. Yields of five-ring C <sub>20</sub> H <sub>12</sub> PAH, their derivatives, and an associated C <sub>18</sub> H <sub>10</sub> PAH product from supercritical <i>n</i> -decane pyrolysis at 568 °C, 94.6 atm, and 133 sec: benzo[ <i>a</i> ]pyrene (252e), benzo[ <i>e</i> ]pyrene (252g), perylene (252f), benzo[ <i>b</i> ]fluoranthene (252b), benzo[ <i>a</i> ]fluoranthene (252a), a methylbenzo[ <i>a</i> ]fluoranthene (266c), benzo[ <i>k</i> ]fluoranthene (252c), benzo[ <i>j</i> ]fluoranthene (252d), and benzo[ <i>ghi</i> ]fluoranthene (226a). ....	76
5.7. Yields of five-ring C <sub>20</sub> H <sub>12</sub> PAH, and their methyl derivatives, from supercritical <i>n</i> -decane pyrolysis at 568 °C, 94.6 atm, and 133 sec: benzo[ <i>a</i> ]pyrene (252e), 4-methylbenzo[ <i>a</i> ]pyrene (266r), 5-methylbenzo[ <i>a</i> ]pyrene (266m), 12-methylbenzo[ <i>a</i> ]pyrene (266l), 11-	

methylbenzo[ <i>a</i> ]pyrene (266n), 6-methylbenzo[ <i>a</i> ]pyrene (266p), 10-methylbenzo[ <i>a</i> ]pyrene (266o), 7-methylbenzo[ <i>a</i> ]pyrene (266h), 9-methylbenzo[ <i>a</i> ]pyrene (266i), 1-methylbenzo[ <i>a</i> ]pyrene (266q), 3-methylbenzo[ <i>a</i> ]pyrene (266s), and 2-methylbenzo[ <i>a</i> ]pyrene (266k) co-eluting with 8-methylbenzo[ <i>a</i> ]pyrene (266j). . . . .	77
5.8. PAH growth reactions—as determined from supercritical <i>n</i> -decane pyrolysis experiments with 1-methylnaphthalene and 1-methylphenanthrene as dopants—of (a) 1-naphthylmethyl, (b) 1-pyrenylmethyl, and (c) 1-phenanthrylmethyl and their respective phenalenyl-type radicals with <i>n</i> -decane’s highest-yield alkenes: ethylene, propene, and 1-butene. . . . .	80
5.9. Reaction pathways, stemming from the 5-benzo[ <i>a</i> ]pyrenylmethyl and 4-benzo[ <i>a</i> ]pyrenylmethyl radicals, for PAH growth in the supercritical <i>n</i> -decane pyrolysis environment. . . . .	81
5.10. Yields of six-ring C <sub>24</sub> H <sub>14</sub> PAH from supercritical <i>n</i> -decane pyrolysis at 568 °C, 94.6 atm, and 133 sec: dibenzo[ <i>a,e</i> ]pyrene (302d), dibenzo[ <i>e,l</i> ]pyrene (302f), dibenzo[ <i>a,l</i> ]pyrene (302g), naphtho[2,1- <i>a</i> ]pyrene (302h), naphtho[2,3- <i>a</i> ]pyrene (302i), naphtho[2,3- <i>e</i> ]pyrene (302j), naphtho[1,2- <i>e</i> ]pyrene (302k), dibenzo[ <i>a,i</i> ]pyrene (302l), benzo[ <i>b</i> ]perylene (302e), naphtho[2,3- <i>b</i> ]fluoranthene (302a), naphtho[1,2- <i>b</i> ]fluoranthene (302b), dibenzo[ <i>b,j</i> ]fluoranthene (302m), and dibenzo[ <i>j,l</i> ]fluoranthene (302c). . . . .	82
5.11. Reactions 1-butene with the phenalenyl-type radicals (green structures) (a) dibenz[ <i>a,cd</i> ]pyrenyl and (b) dibenz[ <i>a,fg</i> ]pyrenyl to produce the seven methyl-substituted C <sub>26</sub> H <sub>14</sub> PAH products (black and purple structures). . . . .	84
5.12. Yields of seven-ring C <sub>26</sub> H <sub>14</sub> PAH, and their methyl derivatives, from supercritical <i>n</i> -decane pyrolysis at 568 °C, 94.6 atm, and 133 sec: dibenzo[ <i>e,ghi</i> ]perylene (326d), dibenzo[ <i>b,ghi</i> ]perylene (326f), naphtho[1,2,3,4- <i>ghi</i> ]perylene (326g), naphtho[8,1,2- <i>bcd</i> ]perylene (326h), dibenzo[ <i>cd,lm</i> ]perylene (326i), three methyldibenzo[ <i>e,ghi</i> ]perylenes (340e-g), two methyldibenzo[ <i>b,ghi</i> ]perylenes (340a-b), and two methylnaphtho[1,2,3,4- <i>ghi</i> ]perylenes (340c-d). . . . .	85
5.13. Reaction pathways of 4 <i>H</i> -benzo[ <i>cd</i> ]fluoranthene (240a), 1 <i>H</i> -benzo[ <i>cd</i> ]fluoranthene (240e), 4-methyl-4 <i>H</i> -benzo[ <i>cd</i> ]fluoranthene (254a), and 1-methyl-1 <i>H</i> -benzo[ <i>cd</i> ]fluoranthene (254c)—via their phenalenyl-type radicals (green structures)—to produce indeno[1,2,3- <i>cd</i> ]pyrene (276a), 12-methylindeno[1,2,3- <i>cd</i> ]pyrene (290j), 3-methylindeno[1,2,3- <i>cd</i> ]pyrene (290h), 5-methylindeno[1,2,3- <i>cd</i> ]pyrene (290i), 1-methylindeno[1,2,3- <i>cd</i> ]pyrene (290g), benz[ <i>a</i> ]indeno[1,2,3- <i>cd</i> ]pyrene (326c), benz[ <i>i</i> ]indeno[1,2,3- <i>cd</i> ]pyrene (326j), benz[ <i>h</i> ]indeno[1,2,3- <i>cd</i> ]pyrene (326b), and benz[ <i>l</i> ]indeno[1,2,3- <i>cd</i> ]pyrene (326k). . . . .	89
6.1. Molecular structures of 2-methylnaphthalene, 1-methylnaphthalene, and 1-methylphenanthrene and relevant bond-dissociation energies. . . . .	93

6.2. Molecular structures of 4-methylchrysene and 4-methylphenanthrene and relevant bond-dissociation energies. ....	94
6.3. Yields of selected PAH products of supercritical <i>n</i> -decane pyrolysis at 568 °C, 94.6 atm, and 133 sec: (a) three- to five-ring PAH, (b) pyrene and its methyl derivatives, (c) five- to eight-ring benzenoid PAH and derivatives, and (d) five- and six-ring PAH with internal five-membered rings. ....	98
6.4. Yields of four-ring C <sub>18</sub> H <sub>12</sub> PAH, and their alkyl derivatives, from supercritical <i>n</i> -decane pyrolysis at 568 °C, 94.6 atm, and 133 sec: (a) chrysene (228b), 1-methylchrysene (242a), 2-methylchrysene (242g), 3-methylchrysene (242d), 6-methylchrysene (242f), benz[ <i>a</i> ]anthracene (228a), triphenylene (228c), 1-methyltriphenylene (242b), and 2-methyltriphenylene (242c). ....	101
6.5. Molecular structures of 4 <i>H</i> -cyclopenta[ <i>def</i> ]phenanthrene and fluorene and relevant bond-dissociation energies. ....	102
6.6. Yields of four-ring PAH, and their derivatives, from supercritical <i>n</i> -decane pyrolysis at 568 °C, 94.6 atm, and 133 sec: (a) acephenanthrylene (202b), fluoranthene (202a), the five methylfluoranthenes (216b-f) (one of which co-elutes with benzo[ <i>a</i> ]fluorene (216g) and benzo[ <i>b</i> ]fluorene (216h)), benzo[ <i>c</i> ]fluorene (216i), and a methylbenzo[ <i>c</i> ]fluorene (230a); (b) pyrene (202c), 1-methylpyrene (216j), 2-methylpyrene (216k), 4-methylpyrene (216l), 1-ethylpyrene (230b), 2-vinylpyrene (228d), 3,4-dihydrocyclopenta[ <i>cd</i> ]pyrene (228e), cyclopenta[ <i>cd</i> ]pyrene (226b), 4-methylcyclopenta[ <i>cd</i> ]pyrene (240b), and 6 <i>H</i> -benzo[ <i>cd</i> ]pyrene (240c). ....	105
6.7. Reaction pathways, stemming from the 4-pyrenylmethyl and 2-pyrenylmethyl radicals, for PAH growth in the supercritical <i>n</i> -decane pyrolysis environment. ....	107
6.8. Yields of five-ring C <sub>20</sub> H <sub>12</sub> PAH, and their methyl derivatives, from supercritical <i>n</i> -decane pyrolysis at 568 °C, 94.6 atm, and 133 sec: (a) benzo[ <i>a</i> ]pyrene (252e), 12-methylbenzo[ <i>a</i> ]pyrene (266l), 5-methylbenzo[ <i>a</i> ]pyrene (266m), 11-methylbenzo[ <i>a</i> ]pyrene (266n), 6-methylbenzo[ <i>a</i> ]pyrene (266p), 10-methylbenzo[ <i>a</i> ]pyrene (266o), 7-methylbenzo[ <i>a</i> ]pyrene (266h), 9-methylbenzo[ <i>a</i> ]pyrene (266i), 1-methylbenzo[ <i>a</i> ]pyrene (266q), 4-methylbenzo[ <i>a</i> ]pyrene (266r), 3-methylbenzo[ <i>a</i> ]pyrene (266s), and 2-methylbenzo[ <i>a</i> ]pyrene (266k) co-eluting with 8-methylbenzo[ <i>a</i> ]pyrene (266j); (b) benzo[ <i>e</i> ]pyrene (252g), 3-methylbenzo[ <i>e</i> ]pyrene (266b), 4-methylbenzo[ <i>e</i> ]pyrene (266t), 2-methylbenzo[ <i>e</i> ]pyrene (266u), 1-methylbenzo[ <i>e</i> ]pyrene (266w), 9-methylbenzo[ <i>e</i> ]pyrene (266x), and 10-methylbenzo[ <i>e</i> ]pyrene (266v). ....	109
6.9. Yields of benzo[ <i>ghi</i> ]perylene (276b) and the six methylbenzo[ <i>ghi</i> ]perylenes (290a-f), from supercritical <i>n</i> -decane pyrolysis at 568 °C, 94.6 atm, and 133 sec. ....	110
6.10. Reaction pathways of 4 <i>H</i> -benzo[ <i>cd</i> ]fluoranthene (240a), 1 <i>H</i> -benzo[ <i>cd</i> ]fluoranthene (240e), 4-methyl-4 <i>H</i> -benzo[ <i>cd</i> ]fluoranthene (254a), and	

1-methyl-1 <i>H</i> -benzo[ <i>cd</i> ]fluoranthene (254c)—via their phenalenyl-type radicals (green structures)—to produce indeno[1,2,3- <i>cd</i> ]pyrene (276a), 12-methylindeno[1,2,3- <i>cd</i> ]pyrene (290j), 3-methylindeno[1,2,3- <i>cd</i> ]pyrene (290h), 5-methylindeno[1,2,3- <i>cd</i> ]pyrene (290i), and 1-methylindeno[1,2,3- <i>cd</i> ]pyrene (290g). .....	116
B1. Yields of (a) alkanes (including unreacted fuel <i>n</i> -decane) and (b) C <sub>2</sub> -C <sub>6</sub> alkenes from the supercritical pyrolysis of <i>n</i> -decane at 568 °C, 94.6 atm, and 133 sec. ....	160
B2. Yields of (a) C <sub>7</sub> -C <sub>14</sub> alkenes and (b) dienes from the supercritical pyrolysis of <i>n</i> -decane at 568 °C, 94.6 atm, and 133 sec. ....	161
B3. Yields of (a) C <sub>5</sub> -ring and (b) C <sub>6</sub> -ring cyclic aliphatic products from the supercritical pyrolysis of <i>n</i> -decane at 568 °C, 94.6 atm, and 133 sec. ....	162
B4. Yields of one- and two-ring aromatics from supercritical <i>n</i> -decane pyrolysis at 568 °C, 94.6 atm, and 133 sec: (a) benzene and substituted benzenes; (b) indene (116a), 1-methylindene (130a), 2-methylindene (130b), 3-methylindene (130c), naphthalene (128a), 1-methylnaphthalene (142a), and 2-methylnaphthalene (142b). ....	163
B5. Yields of two- and three-ring aromatics from supercritical <i>n</i> -decane pyrolysis at 568 °C, 94.6 atm, and 133 sec: (a) 1-ethylnaphthalene (156b), 2-ethylnaphthalene (156a), and the ten dimethylnaphthalenes (156c–l); (b) 2-vinylnaphthalene (154a), acenaphthene (154b), acenaphthylene (152a), 1-methylacenaphthylene (166a), phenalene (166d), benz[ <i>f</i> ]indene (166b), and benz[ <i>e</i> ]indene(166c). ....	164
B6. Yields of three- and four-ring PAH from supercritical <i>n</i> -decane pyrolysis at 568 °C, 94.6 atm, and 133 sec: (a) fluorene (166e), the five methylfluorenes (180a–e), dibenzofulvene (178a), 9-ethylfluorene (194a), and 9-ethylidene fluorene (192a); (b) phenanthrene (178b), the five methylphenanthrenes (192b–f), 4 <i>H</i> -cyclopenta[ <i>def</i> ]phenanthrene (190a), anthracene (178c), the three methylanthracenes (192g–i), and 7 <i>H</i> -benz[ <i>de</i> ]anthracene (216a). ....	165
B7. Yields of four-ring PAH, and their derivatives, from supercritical <i>n</i> -decane pyrolysis at 568 °C, 94.6 atm, and 133 sec: (a) acephenanthrylene (202b), fluoranthene (202a), the five methylfluoranthenes (216b–f) (one of which co-elutes with benzo[ <i>a</i> ]fluorene (216g) and benzo[ <i>b</i> ]fluorene (216h)), benzo[ <i>c</i> ]fluorene (216i), and a methylbenzo[ <i>c</i> ]fluorene (230a); (b) pyrene (202c), 1-methylpyrene (216j), 2-methylpyrene (216k), 4-methylpyrene (216l), 1-ethylpyrene (230b), 2-vinylpyrene (228d), 3,4-dihydrocyclopenta[ <i>cd</i> ]pyrene (228e), cyclopenta[ <i>cd</i> ]pyrene (226b), 4-methylcyclopenta[ <i>cd</i> ]pyrene (240b), and 6 <i>H</i> -benzo[ <i>cd</i> ]pyrene (240c). ....	166
B8. Yields of four-ring C <sub>18</sub> H <sub>12</sub> and five-ring C <sub>19</sub> H <sub>12</sub> PAH, and their alkyl derivatives, from supercritical <i>n</i> -decane pyrolysis at 568 °C, 94.6 atm, and 133 sec: (a) chrysene (228b), 3-methylchrysene (242d), 2-methylchrysene (242g), 1-methylchrysene (242a), 6-methylchrysene (242f), benz[ <i>a</i> ]anthracene (228a), triphenylene (228c), 1-methyltriphenylene (242b), and 2-methyltriphenylene (242c); (b) chrysene (228b),	

- 3-methylchrysene (242d), 2-methylchrysene (242g), 1-methylchrysene (242a), 6-methylchrysene (242f), 4*H*-cyclopenta[*def*]chrysene (240d), 4-methyl-4*H*-cyclopenta[*def*]chrysene (254b), 4-ethyl-4*H*-cyclopenta[*def*]chrysene (268a), 4-propyl-4*H*-cyclopenta[*def*]chrysene (282a), and 4-methylchrysene (242h). ..... 167
- B9. Yields of five-ring C<sub>19</sub>H<sub>12</sub> and C<sub>21</sub>H<sub>14</sub> PAH, and their methyl derivatives, from supercritical *n*-decane pyrolysis at 568 °C, 94.6 atm, and 133 sec: (a) 4*H*-benzo[*cd*]fluoranthene (240a), 4-methyl-4*H*-benzo[*cd*]fluoranthene (254a), 1*H*-benzo[*cd*]fluoranthene (240e), and 1-methyl-1*H*-benzo[*cd*]fluoranthene (254c); (b) dibenzo[*a,c*]fluorene (266a), methyl-dibenzo[*a,c*]fluorene (280a), dibenzo[*a,h*]fluorene (266d), naphtho[1,2-*a*]fluorene (266e), naphtho[2,1-*a*]fluorene (266f), and naphtho[2,3-*a*]fluorene (266g). ..... 168
- B10. Yields of five-ring C<sub>20</sub>H<sub>12</sub> PAH, their derivatives, and an associated C<sub>18</sub>H<sub>10</sub> PAH product from supercritical *n*-decane pyrolysis at 568 °C, 94.6 atm, and 133 sec: (a) benzo[*a*]pyrene (252e), benzo[*e*]pyrene (252g), perylene (252f), benzo[*b*]fluoranthene (252b), benzo[*a*]fluoranthene (252a), a methylbenzo[*a*]fluoranthene (266c), benzo[*k*]fluoranthene (252c), benzo[*j*]fluoranthene (252d), and benzo[*ghi*]fluoranthene (226a); (b) benzo[*a*]pyrene (252e), 4-methylbenzo[*a*]pyrene (266r), 5-methylbenzo[*a*]pyrene (266m), 4-ethylbenzo[*a*]pyrene (280b), 5-ethylbenzo[*a*]pyrene (280c), 4-vinylbenzo[*a*]pyrene (278j), and 5-vinylbenzo[*a*]pyrene (278k). ..... 169
- B11. Yields of five-ring C<sub>20</sub>H<sub>12</sub> PAH, and their methyl derivatives, from Supercritical *n*-decane pyrolysis at 568 °C, 94.6 atm, and 133 sec: (a) benzo[*a*]pyrene (252e), 4-methylbenzo[*a*]pyrene (266r), 5-methylbenzo[*a*]pyrene (266m), 12-methylbenzo[*a*]pyrene (266l), 11-methylbenzo[*a*]pyrene (266n), 6-methylbenzo[*a*]pyrene (266p), 10-methylbenzo[*a*]pyrene (266o), 7-methylbenzo[*a*]pyrene (266h), 9-methylbenzo[*a*]pyrene (266i), 1-methylbenzo[*a*]pyrene (266q), 3-methylbenzo[*a*]pyrene (266s), and 2-methylbenzo[*a*]pyrene (266k) co-eluting with 8-methylbenzo[*a*]pyrene (266j); (b) benzo[*e*]pyrene (252g), 3-methylbenzo[*e*]pyrene (266b), 4-methylbenzo[*e*]pyrene (266t), 2-methylbenzo[*e*]pyrene (266u), 10-methylbenzo[*e*]pyrene (266v), 1-methylbenzo[*e*]pyrene (266w), and 9-methylbenzo[*e*]pyrene (266x). ..... 170
- B12. Yields of five-ring C<sub>22</sub>H<sub>14</sub> PAH, and their methyl derivatives, and six-ring C<sub>22</sub>H<sub>12</sub> PAH from supercritical *n*-decane pyrolysis at 568 °C, 94.6 atm, and 133 sec: (a) benzo[*c*]chrysene (278i), benzo[*b*]chrysene (278a), dibenz[*a,h*]anthracene (278b), dibenz[*a,j*]anthracene (278c), benzo[*a*]naphthacene (278d), pentaphene (278e), picene (278f), benzo[*g*]chrysene (278g), dibenz[*a,c*]anthracene (278h), three methyl-dibenz[*a,c*]anthracenes (292b-d), and a methylbenzo[*g*]chrysene (292a); (b) benzo[*ghi*]perylene (276b), anthanthrene (276c), dibenzo[*e,ghi*]fluoranthene (276e), dibenzo[*b,ghi*]fluoranthene (276d), and indeno[1,2,3-*cd*]pyrene (276a). ..... 171
- B13. Yields of C<sub>22</sub>H<sub>12</sub> PAH, and their alkyl derivatives, from supercritical *n*-decane

pyrolysis at 568 °C, 94.6 atm, and 133 sec: (a) benzo[ghi]perylene (276b) and the six methylbenzo[ghi]perylenes (290a-f); (b) indeno[1,2,3- <i>cd</i> ]pyrene (276a), five methylindeno[1,2,3- <i>cd</i> ]pyrenes (290g-k) whose yields increase with doping, three methylindeno[1,2,3- <i>cd</i> ]pyrenes (290o-q) whose yields do not increase with doping, and another methylindeno[1,2,3- <i>cd</i> ]pyrene (290m) co-eluting with an ethylindeno[1,2,3- <i>cd</i> ]pyrene (304a). .....	172
B14. Yields of six-ring C <sub>24</sub> H <sub>14</sub> PAH, and the derivatives of one of these C <sub>24</sub> H <sub>14</sub> PAH, from supercritical <i>n</i> -decane pyrolysis at 568 °C, 94.6 atm, and 133 sec: (a) dibenzo[ <i>a,e</i> ]pyrene (302d), dibenzo[ <i>e,l</i> ]pyrene (302f), dibenzo[ <i>a,l</i> ]pyrene (302g), naphtho[2,1- <i>a</i> ]pyrene (302h), naphtho[2,3- <i>a</i> ]pyrene (302i), naphtho[2,3- <i>e</i> ]pyrene (302j), naphtho[1,2- <i>e</i> ]pyrene (302k), dibenzo[ <i>a,i</i> ]pyrene (302l), and benzo[ <i>b</i> ]perylene (302e); (b) dibenzo[ <i>a,e</i> ]pyrene (302d), two methyl-dibenzo[ <i>a,e</i> ]perylenes (316a and 316b), two ethyl-dibenzo[ <i>a,e</i> ]perylenes (330a and 330b), a dimethyl-dibenzo[ <i>a,e</i> ]pyrene (330c), and two methylene-bridged dibenzo[ <i>a,e</i> ]perylenes (314b and 314c). .....	173
B15. Yields of seven-ring C <sub>26</sub> H <sub>14</sub> PAH, and their methyl derivatives, from supercritical <i>n</i> -decane pyrolysis at 568 °C, 94.6 atm, and 133 sec: (a) dibenzo[ <i>e,ghi</i> ]perylene (326d), dibenzo[ <i>b,ghi</i> ]perylene (326f), naphtho[1,2,3,4- <i>ghi</i> ]perylene (326g), naphtho[8,1,2- <i>bcd</i> ]perylene (326h), dibenzo[ <i>cd,lm</i> ]perylene (326i), three methyl-dibenzo[ <i>e,ghi</i> ]perylenes (340e-g), two methyl-dibenzo[ <i>b,ghi</i> ]perylenes (340a-b), and two methyl-naphtho[1,2,3,4- <i>ghi</i> ]perylenes (340c-d); (b) benz[ <i>l</i> ]indeno[1,2,3- <i>cd</i> ]pyrene (326k), benz[ <i>h</i> ]indeno[1,2,3- <i>cd</i> ]pyrene (326b), benz[ <i>a</i> ]indeno[1,2,3- <i>cd</i> ]pyrene (326c), benz[ <i>i</i> ]indeno[1,2,3- <i>cd</i> ]pyrene (326j), benz[5,6]indeno[1,2,3- <i>cd</i> ]pyrene (326m), fluoreno[1,9- <i>ab</i> ]pyrene (326a), and indeno[1,2,3- <i>cd</i> ]perylene (326e). .....	174
B16. Yields of six- to nine-ring PAH products from supercritical <i>n</i> -decane pyrolysis at 568 °C, 94.6 atm, and 133 sec: (a) benzo[ <i>a</i> ]naphtho[2,3- <i>e</i> ]pyrene (352d), benzo[ <i>e</i> ]naphtho[2,1- <i>a</i> ]pyrene (352b), benzo[ <i>e</i> ]naphtho[2,3- <i>a</i> ]pyrene (352c), tribenzo[ <i>b,j,l</i> ]fluoranthene (352a), naphtho[2,3- <i>b</i> ]fluoranthene (302a), naphtho[1,2- <i>b</i> ]fluoranthene (302b), dibenzo[ <i>b,j</i> ]fluoranthene (302m), dibenzo[ <i>j,l</i> ]fluoranthene (302c), tribenz[ <i>a,c,h</i> ]anthracene (328a), benzo[ <i>c</i> ]pentaphene (328b), and benzo[ <i>h</i> ]pentaphene (328c); (b) benzo[ <i>cd</i> ]naphtho[1,2,3- <i>lm</i> ]perylene (376a), coronene (300a), 1-methylcoronene (314a), benzo[ <i>pqr</i> ]naphtho[8,1,2- <i>bcd</i> ]perylene (350a), benzo[ <i>ghi</i> ]naphtho[8,1,2- <i>bcd</i> ]perylene (350b), benzo[ <i>cd</i> ]naphtho[8,1,2,3- <i>fghi</i> ]perylene (350c) co-eluting with phenanthro[5,4,3,2- <i>efghi</i> ]perylene (350d), benzo[ <i>a</i> ]coronene (350e), and naphtho[8,1,2- <i>abc</i> ]coronene (374a). .....	175
C1. Yields of (a) alkanes (including unreacted fuel <i>n</i> -decane) and (b) C <sub>2</sub> -C <sub>6</sub> alkenes from the supercritical pyrolysis of <i>n</i> -decane at 568 °C, 94.6 atm, and 133 sec. ....	194
C2. Yields of (a) C <sub>7</sub> -C <sub>14</sub> alkenes and (b) dienes from the supercritical pyrolysis of <i>n</i> -decane at 568 °C, 94.6 atm, and 133 sec. ....	195



C3. Yields of (a) C <sub>5</sub> -ring and (b) C <sub>6</sub> -ring cyclic aliphatic products from the supercritical pyrolysis of <i>n</i> -decane at 568 °C, 94.6 atm, and 133 sec. ....	196
C4. Yields of one- and two-ring aromatics from supercritical <i>n</i> -decane pyrolysis at 568 °C, 94.6 atm, and 133 sec: (a) benzene and substituted benzenes; (b) indene (116a), 1-methylindene (130a), 2-methylindene (130b), 3-methylindene (130c), naphthalene (128a), 1-methylnaphthalene (142a), and 2-methylnaphthalene (142b). ....	197
C5. Yields of two- and three-ring aromatics from supercritical <i>n</i> -decane pyrolysis at 568 °C, 94.6 atm, and 133 sec: (a) 1-ethylnaphthalene (156b), 2-ethylnaphthalene (156a), and the ten dimethylnaphthalenes (156c–l); (b) 2-vinylnaphthalene (154a), acenaphthene (154b), acenaphthylene (152a), 1-methylacenaphthylene (166a), phenalene (166d), benz[ <i>f</i> ]indene (166b), and benz[ <i>e</i> ]indene (166c). ....	198
C6. Yields of three- and four-ring PAH from supercritical <i>n</i> -decane pyrolysis at 568 °C, 94.6 atm, and 133 sec: (a) fluorene (166e), the five methylfluorenes (180a–e), dibenzofulvene (178a), 9-ethylfluorene (194a), and 9-ethylidene fluorene (192a); (b) 4 <i>H</i> -cyclopenta[ <i>def</i> ]phenanthrene (190a) and its alkylated derivatives (204a, 218a, and 232a), 4-methylphenanthrene (192f), phenanthrene (178b), the four methylphenanthrenes (192b–e), and 9-ethylphenanthrene (206a). ....	199
C7. Yields of three- and four-ring PAH from supercritical <i>n</i> -decane pyrolysis at 568 °C, 94.6 atm, and 133 sec: (a) phenanthrene (178b), the four methylphenanthrenes (192b–e), and 9-ethylphenanthrene (206a); (b) anthracene (178c), the three methylanthracenes (192g–i), and 7 <i>H</i> -benz[ <i>de</i> ]anthracene (216a). ....	200
C8. Yields of four-ring PAH, and their derivatives, from supercritical <i>n</i> -decane pyrolysis at 568 °C, 94.6 atm, and 133 sec: (a) acephenanthrylene (202b), fluoranthene (202a), the five methylfluoranthenes (216b–f) (one of which co-elutes with benzo[ <i>a</i> ]fluorene (216g) and benzo[ <i>b</i> ]fluorene (216h)), benzo[ <i>c</i> ]fluorene (216i), and a methylbenzo[ <i>c</i> ]fluorene (230a); (b) pyrene (202c), 1-methylpyrene (216j), 2-methylpyrene (216k), 4-methylpyrene (216l), 1-ethylpyrene (230b), 2-vinylpyrene (228d), 3,4-dihydrocyclopenta[ <i>cd</i> ]pyrene (228e), cyclopenta[ <i>cd</i> ]pyrene (226b), 4-methylcyclopenta[ <i>cd</i> ]pyrene (240b), and 6 <i>H</i> -benzo[ <i>cd</i> ]pyrene (240c). ....	201
C9. Yields of four-ring C <sub>18</sub> H <sub>12</sub> , and their alkyl derivatives, from supercritical <i>n</i> -decane pyrolysis at 568 °C, 94.6 atm, and 133 sec: (a) chrysene (228b), 1-methylchrysene (242a), 2-methylchrysene (242g), 3-methylchrysene (242d), 6-methylchrysene (242f), benz[ <i>a</i> ]anthracene (228a), triphenylene (228c), 1-methyltriphenylene (242b), and 2-methyltriphenylene (242c). ....	202
C10. Yields of five-ring C <sub>20</sub> H <sub>12</sub> PAH, their derivatives, and an associated C <sub>18</sub> H <sub>10</sub> PAH product from supercritical <i>n</i> -decane pyrolysis at 568 °C, 94.6 atm, and 133 sec: (a) benzo[ <i>a</i> ]pyrene (252e), benzo[ <i>e</i> ]pyrene (252g), perylene (252f), benzo[ <i>b</i> ]fluoranthene (252b), benzo[ <i>a</i> ]fluoranthene (252a), a methylbenzo[ <i>a</i> ]fluoranthene (266c), benzo[ <i>k</i> ]fluoranthene (252c), benzo[ <i>j</i> ]fluoranthene (252d),	

and benzo[ <i>ghi</i> ]fluoranthene (226a). .....	203
C11. Yields of five-ring C <sub>19</sub> H <sub>12</sub> and C <sub>21</sub> H <sub>14</sub> PAH, and their methyl derivatives, from supercritical <i>n</i> -decane pyrolysis at 568 °C, 94.6 atm, and 133 sec: (a) 4 <i>H</i> -benzo[ <i>cd</i> ]fluoranthene (240a), 4-methyl-4 <i>H</i> -benzo[ <i>cd</i> ]fluoranthene (254a), 1 <i>H</i> -benzo[ <i>cd</i> ]fluoranthene (240e), and 1-methyl-1 <i>H</i> -benzo[ <i>cd</i> ]fluoranthene (254c); (b) dibenzo[ <i>a,c</i> ]fluorene (266a), methyl-dibenzo[ <i>a,c</i> ]fluorene (280a), dibenzo[ <i>a,h</i> ]fluorene (266d), naphtho[1,2- <i>a</i> ]fluorene (266e), naphtho[2,1- <i>a</i> ]fluorene (266f), and naphtho[2,3- <i>a</i> ]fluorene (266g). .....	204
C12. Yields of five-ring C <sub>20</sub> H <sub>12</sub> PAH, and their methyl derivatives, from supercritical <i>n</i> -decane pyrolysis at 568 °C, 94.6 atm, and 133 sec: (a) benzo[ <i>a</i> ]pyrene (252e), 12-methylbenzo[ <i>a</i> ]pyrene (266l), 5-methylbenzo[ <i>a</i> ]pyrene (266m), 11-methylbenzo[ <i>a</i> ]pyrene (266n), 6-methylbenzo[ <i>a</i> ]pyrene (266p), 10-methylbenzo[ <i>a</i> ]pyrene (266o), 7-methylbenzo[ <i>a</i> ]pyrene (266h), 9-methylbenzo[ <i>a</i> ]pyrene (266i), 1-methylbenzo[ <i>a</i> ]pyrene (266q), 4-methylbenzo[ <i>a</i> ]pyrene (266r), 3-methylbenzo[ <i>a</i> ]pyrene (266s), and 2-methylbenzo[ <i>a</i> ]pyrene (266k) co-eluting with 8-methylbenzo[ <i>a</i> ]pyrene (266j); (b) benzo[ <i>e</i> ]pyrene (252g), 3-methylbenzo[ <i>e</i> ]pyrene (266b), 4-methylbenzo[ <i>e</i> ]pyrene (266t), 2-methylbenzo[ <i>e</i> ]pyrene (266u), 1-methylbenzo[ <i>e</i> ]pyrene (266w), 9-methylbenzo[ <i>e</i> ]pyrene (266x), and 10-methylbenzo[ <i>e</i> ]pyrene (266v). .....	205
C13. Yields of five-ring C <sub>22</sub> H <sub>14</sub> PAH, and their methyl derivatives, and six-ring C <sub>22</sub> H <sub>12</sub> PAH from supercritical <i>n</i> -decane pyrolysis at 568 °C, 94.6 atm, and 133 sec: (a) benzo[ <i>b</i> ]chrysene (278a), dibenz[ <i>a,h</i> ]anthracene (278b), dibenz[ <i>a,j</i> ]anthracene (278c), benzo[ <i>a</i> ]naphthacene (278d), pentaphene (278e), picene (278f), benzo[ <i>g</i> ]chrysene (278g), dibenz[ <i>a,c</i> ]anthracene (278h), three methyl-dibenzo[ <i>a,c</i> ]anthracenes (292b-d), and a methylbenzo[ <i>g</i> ]chrysene (292a); (b) indeno[1,2,3- <i>cd</i> ]pyrene (276a), benzo[ <i>ghi</i> ]perylene (276b), and anthanthrene (276c). .....	206
C14. Yields of C <sub>22</sub> H <sub>12</sub> PAH, and their alkyl derivatives, from supercritical <i>n</i> -decane pyrolysis at 568 °C, 94.6 atm, and 133 sec: (a) benzo[ <i>ghi</i> ]perylene (276b) and the six methylbenzo[ <i>ghi</i> ]perylenes (290a-f); (b) indeno[1,2,3- <i>cd</i> ]pyrene (276a), five methylindeno[1,2,3- <i>cd</i> ]perylenes (290g-j, 290q) whose yields increase with doping, three methylindeno[1,2,3- <i>cd</i> ]perylenes (290o-p, 290k) whose yields do not increase with doping, and a methylindeno[1,2,3- <i>cd</i> ]pyrene (290m) co-eluting with an ethylindeno[1,2,3- <i>cd</i> ]pyrene (304a). .....	207
C15. Yields of six-ring C <sub>24</sub> H <sub>14</sub> PAH from supercritical <i>n</i> -decane pyrolysis at 568 °C, 94.6 atm, and 133 sec: (a) dibenzo[ <i>a,e</i> ]pyrene (302d), dibenzo[ <i>e,l</i> ]pyrene (302f), dibenzo[ <i>a,l</i> ]pyrene (302g), naphtho[2,1- <i>a</i> ]pyrene (302h), naphtho[2,3- <i>a</i> ]pyrene (302i), naphtho[2,3- <i>e</i> ]pyrene (302j), naphtho[1,2- <i>e</i> ]pyrene (302k), dibenzo[ <i>a,i</i> ]pyrene (302l), and benzo[ <i>b</i> ]perylene (302e). .....	208
C16. Yields of seven-ring C <sub>26</sub> H <sub>14</sub> PAH, and their methyl derivatives, from supercritical <i>n</i> -decane pyrolysis at 568 °C, 94.6 atm, and 133 sec: (a) dibenzo[ <i>e,ghi</i> ]perylene (326d), dibenzo[ <i>b,ghi</i> ]perylene (326f), naphtho[1,2,3,4- <i>ghi</i> ]perylene (326g), naphtho[8,1,2-	

*bcd*]perylene (326h), dibenzo[*cd,lm*]perylene (326i), three methyldibenzo[*e,ghi*]perylenes (340*e-g*), two methyldibenzo[*b,ghi*]perylenes (340*a-b*), and two methylnaphtho[1,2,3,4-*ghi*]perylenes (340*c-d*); (b) benz[*l*]indeno[1,2,3-*cd*]pyrene (326k), benz[*h*]indeno[1,2,3-*cd*]pyrene (326b), benz[*a*]indeno[1,2,3-*cd*]pyrene (326c), benz[*i*]indeno[1,2,3-*cd*]pyrene (326j), benz[5,6]indeno[1,2,3-*cd*]pyrene (326m), fluoreno[1,9-*ab*]pyrene (326a), and indeno[1,2,3-*cd*]perylene (326e). ..... 209

C17. Yields of six- to nine-ring PAH products from supercritical *n*-decane pyrolysis at 568 °C, 94.6 atm, and 133 sec: (a) benzo[*a*]naphtho[2,3-*e*]pyrene (352d), benzo[*e*]naphtho[2,1-*a*]pyrene (352b), benzo[*e*]naphtho[2,3-*a*]pyrene (352c), tribenzo[*b,j,l*]fluoranthene (352a), naphtho[2,3-*b*]fluoranthene (302a), naphtho[1,2-*b*]fluoranthene (302b), dibenzo[*b,j*]fluoranthene (302m), dibenzo[*j,l*]fluoranthene (302c), tribenz[*a,c,h*]anthracene (328a), benzo[*c*]pentaphene (328b), and benzo[*h*]pentaphene (328c); (b) coronene (300a), 1-methylcoronene (314a), benzo[*pqr*]naphtho[8,1,2-*bcd*]perylene (350a), benzo[*ghi*]naphtho[8,1,2-*bcd*]perylene (350b), benzo[*cd*]naphtho[8,1,2,3-*fghi*]perylene (350c) co-eluting with phenanthro[5,4,3,2-*efghi*]perylene (350d), benzo[*a*]coronene (350e), and naphtho[8,1,2-*abc*]coronene (374a). ..... 210

## Abstract

Prior to its combustion, fuel for future-highspeed aircraft will experience supercritical conditions, causing the fuel to undergo pyrolytic reactions that lead to the formation of polycyclic aromatic hydrocarbons (PAH), precursors to fuel-line solids that hinder aircraft's safe operation. Therefore, understanding the formation pathways of PAH under supercritical conditions is important to preventing formation of these solids.

Previous work from our group has shown that *n*-alkanes are particularly problematic regarding solids formation and that the model fuel *n*-decane produces an abundance of aliphatics and one- to nine-ring aromatics—many of which are methyl-substituted. Some of these methyl-substituted PAH have their methyl group in a bay-region, making them highly reactive. Therefore, to investigate the molecular-growth reactions of bay region methyl-substituted PAH in the supercritical *n*-alkane-pyrolysis environment, we have performed supercritical *n*-decane pyrolysis experiments in an isothermal, isobaric flow reactor at 568 °C, 94.6 atm, and 133 sec, conditions of rapid PAH growth, with two dopants—4-methylchrysene and 4-methylphenanthrene—added in separate experiments. The aliphatics and one- and two-ring aromatics are analyzed by gas chromatography. The complex PAH products are analyzed, isomer-specifically, by a two-dimensional high-pressure liquid-chromatographic technique.

The 4-methylchrysene-doping experiments reveal that the molecular growth of 4-methylchrysene proceeds along two distinctive routes, each starting from its arylmethyl radical's reaction with the aryl carbon across the bay to make a C<sub>19</sub>H<sub>12</sub> PAH and its resonance-stabilized radical. One of these radicals, 4-benzo[*cd*]fluoranthenyl, reacts with *n*-decane's abundant aliphatic species methyl and the C<sub>2</sub>-C<sub>4</sub> 1-alkenes to produce six- and seven-ring PAH with internal 5-membered rings; the other, 4-cyclopenta[*def*]chrysenyl, initiates a series of reactions with these

same aliphatic species to produce *peri*-condensed benzenoid PAH as large as nine-rings. In the supercritical *n*-decane-pyrolysis environment, 4-methylphenanthrene exhibits analogous molecular-growth reactions—substantiating the distinctive growth behaviors of bay-region methyl-substituted PAH.

Previous investigations from our group have revealed that temperature has a strong influence on the supercritical pyrolysis behavior of *n*-decane. To investigate the behavior of *n*-decane at lower temperatures, we have performed additional pyrolysis experiments at 94.6 atm, 133 sec, and four temperatures ranging from 495 to 520 °C. Product analyses have led to the quantification of 62 new products.

# Chapter 1. Introduction

## 1.1. Background and Motivation

Besides their conventional role as propellants, fuels in future high-speed aircraft, prior to their combustion, need to act as coolants to remove excess heat from the engine components.<sup>1-4</sup> Projected requirements indicate that the fuels used for such cooling purposes will be required to sustain, on the order of several minutes, temperatures and pressures as high as 700°C and 130 atm.<sup>1,5</sup> Such extreme conditions are supercritical for jet fuels as well as most hydrocarbons.<sup>6</sup> Under supercritical conditions, the major products produced from endothermic fuel-cracking reactions are the lower-molecular-weight aliphatics, which are ideal because they provide the fuel with the best possible heat sink.<sup>1,7,8</sup> However, a lot of side reactions, lead to the formation of polycyclic aromatic hydrocarbons (PAH), which are undesirable products because they are precursors to carbonaceous solid deposits that block fuel delivery lines, interfere with heat transfer, and decrease engine performance.<sup>1,8-10</sup> Deposit formation of as little as 1 ppm (of the fuel fed), within a matter of a few hours, can hinder the aircraft's safe operation.<sup>1</sup> Therefore, it is extremely important to understand the reaction mechanisms that govern PAH formation and growth in the supercritical fuel-pyrolysis environment.

Jet fuels consist primarily of *n*-paraffins and *iso*-paraffins in addition to cycloparaffins and aromatics.<sup>11,12</sup> Since jet fuels are complex mixtures of a large number of aliphatic and aromatic components, it is difficult to trace the formation of PAH products from initial precursors. Therefore, model fuels,<sup>13-16</sup> representative of components of actual jet fuels, are often utilized because they reduce the number of reactants in the system, which, in turn, reduce the number of reaction pathways. Previous investigations from our own group<sup>17-19</sup> as well other groups<sup>1,5</sup> showed

that the *n*-alkane components of jet fuels are most problematic regarding solids formation in the supercritical fuel pyrolysis environment.

At high-temperatures and low-pressures, Rice and coworkers<sup>20,21</sup> have shown that the pyrolytic reactions of *n*-alkanes proceed by means of a free radical mechanism.<sup>19</sup> Fabuss *et. al.*<sup>14</sup> have performed supercritical pyrolysis experiments with *n*-hexadecane as the model fuel and showed that the free radical mechanisms are prevalent even under supercritical conditions. Moreover, Fabuss *et.al.*<sup>14</sup> pointed out several variations between the reactions taking place in the subcritical and in the supercritical fuel-pyrolysis environment. Consequently, many research groups<sup>13,22-36</sup> have investigated the supercritical pyrolysis of C<sub>7</sub> to C<sub>17</sub> *n*-alkanes, which are the major components of jet fuels.<sup>7,12,37</sup> The major differences between the pyrolysis reactions that occur under supercritical conditions and the reactions that occur under subcritical conditions are detailed below with *n*-decane as an example.<sup>19</sup> The molecular structure of the model fuel *n*-decane<sup>19</sup> and the relevant bond-dissociation energies is illustrated in Figure 1.1.

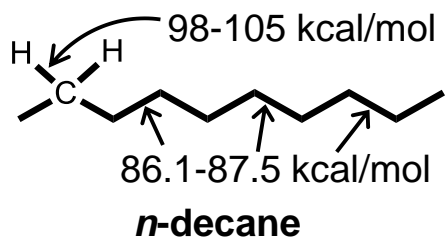
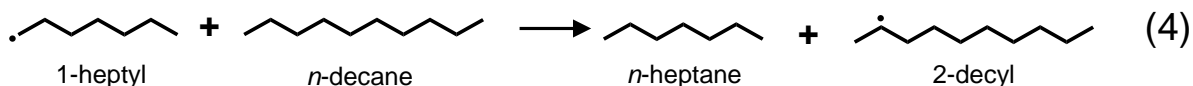
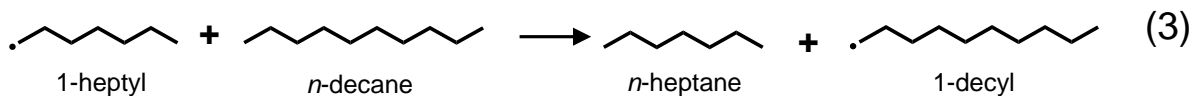
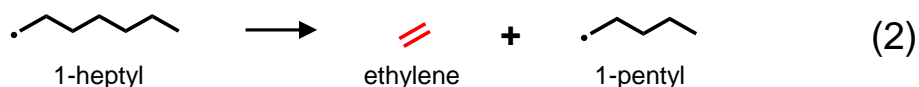


Figure 1.1. Molecular structure and bond-dissociation energies<sup>19,38</sup> for model fuel *n*-decane.

The decomposition of *n*-decane starts with the dissociation of alkyl C-C bonds, which are easiest-to break with bond-dissociation energies of around 86 kcal/mol,<sup>38</sup> to form the 1-alkyl radicals.<sup>19</sup> For example, as shown in Eq. (1), *n*-decane decomposes into 1-heptyl and 1-propyl radicals. These 1-alkyl radicals, once formed, carry the pyrolytic reactions by two main pathways. The first propagation pathway, as illustrated in Eq. (2), is  $\beta$ -scission—a unimolecular

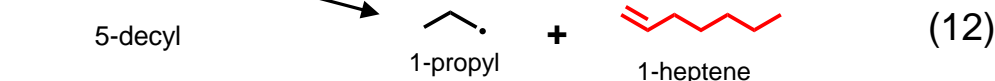
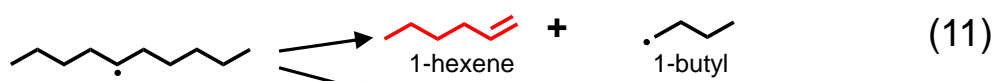
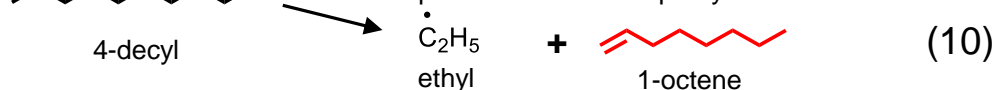
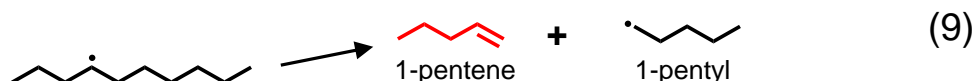
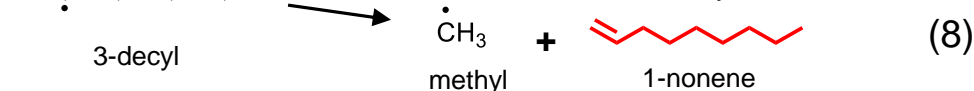
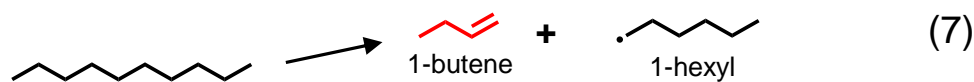
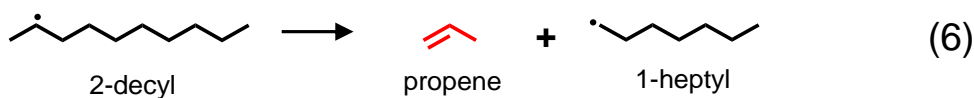
decomposition pathway—where the alkyl C-C bond situated two atoms away from the radical site is broken.<sup>19</sup> This results in the formation of an alkene, in this case, ethylene (shown in red), and a 1-alkyl radical with two fewer carbon atoms, in this case, 1-pentyl. The second propagation pathway is intermolecular hydrogen abstraction, which is a bimolecular reaction.<sup>19</sup> This pathway can proceed by two routes: (a) the 1-alkyl radicals, once formed, can abstract hydrogen from the 1-position of *n*-decane, as shown in Eq. (3), resulting in the formation of the corresponding *n*-alkanes and a primary decyl radical<sup>19</sup> or (b) the 1-alkyl radicals can abstract hydrogen from the 2, 3, 4, or 5 positions of *n*-decane. These hydrogen abstraction reactions result in the formation of the corresponding *n*-alkanes and a secondary decyl radical, an example of one such hydrogen abstraction reaction at *n*-decane's 2-position is illustrated in Eq. (4).



It is well documented that under low-pressure conditions, the 1-alkyl radicals composed of  $\geq 3$  carbons, once formed, readily undergo  $\beta$ -scission reactions to form ethylene and 1-alkyl radicals of two fewer carbons.<sup>27,34,39</sup> However, under high-pressure conditions, hydrogen abstraction reactions are preferred over  $\beta$ -scission reactions, therefore, the formed 1-alkyl radicals abstract hydrogen (from *n*-decane and other molecules in the reaction environment) to form



respective *n*-alkanes.<sup>22,40,41</sup> The 1-alkyl radicals can abstract hydrogen from *n*-decane either at the “1” carbon position of *n*-decane (as shown in Eq. (3)), resulting in a primary decyl radical or at the “2,” “3,” “4,” or “5” carbon positions of *n*-decane, as exemplified by Eq. (4), resulting in secondary decyl radicals. Subsequently, the primary and secondary decyl radicals can decompose via  $\beta$ -scission reactions, as illustrated by Eq. (2) and Eqs. (5)-(12). The net result of the  $\beta$ -scission reactions of the decyl radicals is the production of all the C<sub>2</sub>-C<sub>9</sub> 1-alkenes (shown in red) and C<sub>1</sub>-C<sub>8</sub> 1-alkyl radicals (shown in black), which, subsequently, abstract hydrogen to form their respective *n*-alkanes.<sup>19</sup>



Researchers from other groups,<sup>22-35</sup> while investigating the supercritical pyrolysis of *n*-alkanes (C<sub>7</sub> to C<sub>17</sub>), have only examined the alkane and alkene products. Apart from the previous studies<sup>18,19,51</sup> from our own research group, there are no other supercritical *n*-alkane-pyrolysis studies, which report the yields of individual PAH products of three-aromatic rings or greater.<sup>19</sup>

**Since PAH are precursors to fuel-line solids in the supercritical fuel-pyrolysis environment<sup>1,42-45</sup> and since *n*-alkanes are major components of jet fuels and are known to be particularly problematic regarding solids formation,<sup>1,5</sup> understanding the formation and growth pathways of PAH during supercritical *n*-alkane fuel pyrolysis is the main focus of this dissertation.**

To this end, previous investigations from our group have centered on the model fuel *n*-decane,<sup>46-50</sup> whose supercritical pyrolysis produces an abundance of aliphatic products, particularly *n*-alkanes and 1-alkenes. The supercritical pyrolysis of *n*-decane also produces a lot of one-ring aromatics as well as two- to nine-ring PAH—many of which are methyl-substituted.<sup>46-50</sup>

To elucidate the reaction pathways responsible for the formation and growth of these PAH, Kalpathy *et al.*<sup>49,50</sup> performed supercritical *n*-decane pyrolysis experiments to which lower-ring-number PAH that are representative of *n*-decane's products are added as dopants.<sup>51</sup> These experiments take advantage of our research group's finding<sup>44,49,50</sup> that the temperatures of our experiments ( $\leq 700$  °C) are not high enough to rupture the aromatic carbon-carbon bonds of the fuel reactant or fuel product.<sup>44</sup> Therefore, only aromatic products of the same or higher ring number as the dopant are formed by the dopant, providing a means for understanding that aromatic dopant's growth behaviour.<sup>49,50,51</sup>

Previous *n*-decane experiments by Kalpathy *et al.*<sup>49,50</sup> with the dopants of Figure 1.2—1-methylnaphthalene, 2-methylnaphthalene, and 1-methylphenanthrene—have revealed that molecular growth of these methyl-substituted dopants occurs via reactions of the respective arylmethyl radicals (which are formed by removal of a methyl hydrogen) with principal aliphatic species that are highly abundant in the supercritical *n*-decane pyrolysis environment: methyl,

ethylene, propene, and 1-butene.<sup>51</sup> Additionally, these dopant experiments<sup>17,18</sup> showed that the position of the methyl substituent on the aromatic structure plays a significant role in PAH growth.

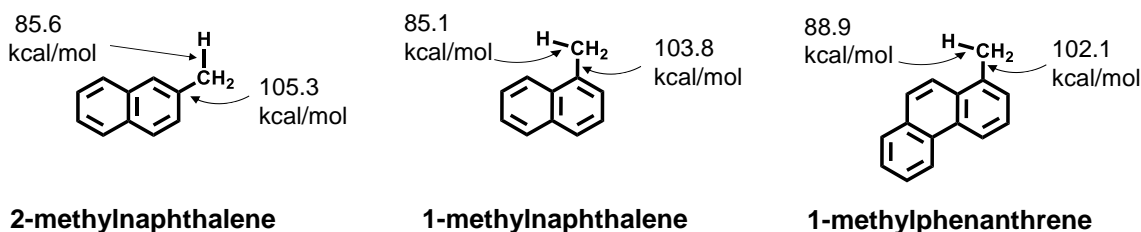


Figure 1.2. Molecular structures of 1-methylnaphthalene, 2-methylnaphthalene, and 1-methylphenanthrene, and relevant bond-dissociation energies.<sup>38</sup> This figure is adapted from Vutukuru *et al.*<sup>51</sup>

2-methylnaphthalene, the first structure of Figure 1.2, has its methyl group located far from a neighboring aromatic-ring. Because of its methyl group's position, 2-methylnaphthalene's molecular growth is limited to the three-ring PAH formed by 2-naphthylmethyl's reactions with ethylene, propene, and 1-butene. However, in case of 1-methylnaphthalene and 1-methylphenanthrene—whose methyl groups are each attached to a carbon adjacent to a “valley” carbon of the aromatic structure—reaction of their arylmethyl radicals with ethylene produces non-fully aromatic PAH, which readily form their resonance-stabilized phenalenyl-type radicals that initiate a sequence of reactions that lead to high-ring-number PAH.<sup>49,50</sup>

## 1.2 Purpose of This Study

Besides the two types of methyl-substituted PAH represented by the dopants of Figure 1.2, the seven product structures of Figure 1.3 show that supercritical *n*-decane pyrolysis<sup>19</sup> also produces a third type of methyl-substituted PAH, whose methyl group is in a bay region of the PAH structure.<sup>51</sup> In the supercritical *n*-decane pyrolysis products, these bay-region methyl-substituted PAH are always the lowest-yield isomers among the methylated derivatives of a given PAH.<sup>51</sup> However, previous investigations<sup>49,50,51</sup> from our research group suggest that this low-

yield status may be a result of their proneness, once formed, to convert to other products. Therefore, the main objective of this work is to understand the growth behaviors of bay-region methyl-substituted PAH in the supercritical *n*-alkane pyrolysis environment. To achieve this goal, our approach is to perform supercritical *n*-decane pyrolysis experiments with and without two bay-region methyl-substituted dopants 4-methylphenanthrene and 4-methylchrysene. The compounds that we are planning to use as dopants—4-methylphenanthrene and 4-methylchrysene—were only available as specially synthesized compounds, so our first dopant experiments have been performed with 4-methylchrysene, the first one of these compounds to become available.<sup>51</sup>

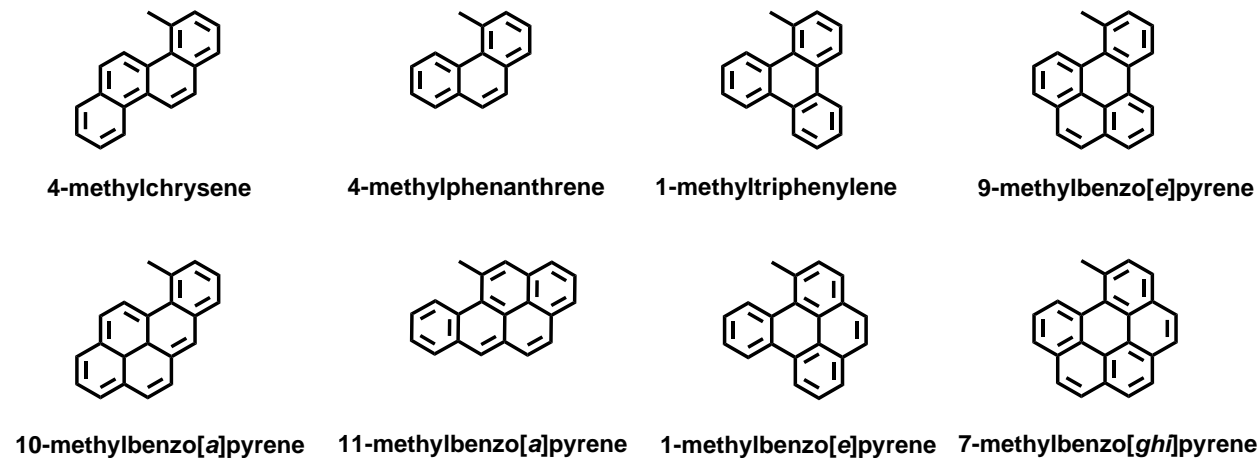


Figure 1.3. Molecular structures of 4-methylchrysene and the three- to six-ring bay-region methyl-substituted PAH products of supercritical *n*-decane pyrolysis at 568 °C, 94.6 atm, and 133 sec: 4-methylphenanthrene, 1-methyltriphenylene, 9-methylbenzo[e]pyrene, 10-methylbenzo[a]pyrene, 11-methylbenzo[a]pyrene, 1-methylbenzo[e]pyrene, and 7-methylbenzo[ghi]perylene.

Just like the non-bay-region-methyl-substituted dopants<sup>49,50</sup> (of Figure 1.2) previously investigated by our group, we would expect the arylmethyl radicals of these bay-region-methyl-substituted dopants to play a significant role in PAH growth. However, the arylmethyl radicals of these bay-region-methyl-substituted dopants have relatively shielded methyl groups that could potentially hinder their ability to react with the principal aliphatic growth species: methyl and the C<sub>2</sub>-C<sub>4</sub> 1-alkenes.<sup>51</sup> Instead, the close proximity of an aryl carbon just across the bay from the

methyl group may open up reaction avenues for bay-region methyl-substituted PAH that are not open to their non-bay-region counterparts.<sup>51</sup> The present work will provide answers to these questions and discuss the growth behaviors of bay-region methyl-substituted PAH in the supercritical *n*-alkane pyrolysis environment.

Since *n*-alkanes are major constituents of jet fuels and are known to be particularly problematic regarding solids formation, Kalpathy *et al.*<sup>48</sup> from our research group performed supercritical pyrolysis experiments with the model fuel *n*-decane (critical temperature, 344.5 °C; critical pressure, 20.7 atm) at a constant pressure of 94.6 atm, a fixed residence time of 133 sec, and at six temperatures ranging from 530 to 570 °C.<sup>48</sup> The strong temperature dependence of the product yields revealed that temperature has a strong influence on the supercritical pyrolysis behavior of *n*-decane.<sup>48</sup> However, Kalpathy *et al.*<sup>48</sup> did not investigate the behavior of *n*-decane at temperatures lower than 530 °C. Therefore, the current work will also focus on the supercritical pyrolysis behavior of *n*-decane at temperatures lower than 530 °C.

It is expected that the findings from the current work will provide a foundation for understanding how bay-region-methyl-substituted PAH grow in the supercritical *n*-alkane-fuel-pyrolysis environment and aid in the design of fuels for next-generation high-speed aircraft.<sup>19</sup>

### **1.3. Structure of the Dissertation**

Chapter 2 presents the reactor system used to perform the supercritical *n*-decane pyrolysis experiments. The analytical techniques used in the identification and quantification of the products resulting from these experiments are also described in detail.

Chapter 3 reports new product identifications of supercritical *n*-decane pyrolysis. The supercritical *n*-decane pyrolysis experiments produce a multitude of products both in the gas-phase as well as the liquid-phase. The aliphatic and one- and two-ring aromatic products are separated

by gas chromatography.<sup>18,19</sup> The highly complex PAH product mixture is separated by a two-dimensional high-pressure liquid chromatographic technique, and the PAH products are subsequently characterized by ultraviolet-visible (UV) diode-array detection and mass spectrometry (MS).<sup>18,19</sup> Chapter 3 will provide a list of newly identified products of the following structural classes: (a) *n*-alkanes, 1-alkenes, and dienes, (b) C<sub>5</sub>-ring and C<sub>6</sub>-ring cyclic aliphatics, (c) one-ring aromatics, and (4) polycyclic aromatic hydrocarbons (PAH). This chapter will also provide ultraviolet-visible (UV) spectral and mass spectral (MS) evidence for the newly identified PAH.

Chapter 4 presents the effects of temperature on the yields of the major products (including 58 newly identified aliphatic and one-ring aromatic products) produced from the supercritical *n*-decane pyrolysis experiments conducted at 94.6 atm, 133 sec, and ten temperatures: 495, 500, 515, 520, 530, 540, 550, 560, 565, and 570 °C. Furthermore, the reaction mechanisms responsible for the formation of aliphatic products and one- to nine-ring aromatic products are also discussed.

Chapter 5 reports the findings from an experimental work undertaken to investigate the growth reactions of bay-region methyl-substituted PAH in the supercritical *n*-alkane fuel pyrolysis environment. Supercritical pyrolysis experiments have been performed with the model fuel *n*-decane, to which 4-methylchrysene has been added as a dopant. These experiments have been performed at 568 °C, 94.6 atm, and 133 sec, conditions of rapid PAH growth.<sup>51</sup> The chosen dopant, 4-methylchrysene, is a four-ring PAH whose structure, as shown in Figure 1.3, is representative of *n*-decane's three- to six-ring bay-region methyl-substituted PAH products.<sup>51</sup> The chosen dopant allows us to investigate not only the roles of arylmethyl radicals of bay-region methyl-substituted PAH, but also any effects of the position of the methyl group on the aromatic structure.

The experimental work reported in chapter 5 has been published as a journal article in the *Proceedings of the Combustion Institute*.<sup>54</sup>

Results from the supercritical *n*-decane pyrolysis experiments with 4-methylchrysene<sup>51</sup> as dopant have revealed that this bay-region-methyl-substituted dopant exhibits several behaviors that are different from those of the non-bay-region-methyl-substituted dopants<sup>49,50</sup> previously investigated by our research group. To substantiate the distinctive growth behaviors of bay-region methyl-substituted PAH, as exhibited by 4-methylchrysene, we have performed supercritical *n*-decane pyrolysis experiments to which 4-methylphenanthrene (second methyl-substituted PAH shown in Figure 1.3), *n*-decane's highest-yield bay-region methyl-substituted PAH product, has been added as a dopant. These experiments have been performed at 568 °C, 94.6 atm, and 133 sec, conditions of rapid PAH growth. Chapter 6 reports the results of 4-methylphenanthrene-doped experiments.

Chapter 7 outlines the conclusions drawn from the results reported in the current work and highlights any significant findings. Chapter 7 also provides recommendations for future work in supercritical fuel-pyrolysis research.

## Chapter 2. Experimental Equipment and Analytical Techniques

### 2.1. Introduction

To understand the formation and growth mechanisms of polycyclic aromatic hydrocarbons (PAH) in the supercritical *n*-alkane pyrolysis environment, experiments have been performed with the model fuel *n*-decane (critical temperature, 345 °C; critical pressure, 20.8 atm), an alkane component of jet fuels.<sup>18,19,51</sup> These supercritical pyrolysis experiments have been performed in an isothermal, isobaric plug-flow reactor that replicates the conditions experienced by fuels in the pre-combustion environment of next-generation hypersonic aircraft. This chapter will give a detailed description of the reactor system and the procedure used to perform the supercritical pyrolysis experiments.<sup>19,61</sup> The analytical techniques (developed by Bagley and Wornat)<sup>46,47</sup> used for the identification and quantification of the products of supercritical *n*-decane pyrolysis will also be presented.

### 2.2. Supercritical Fuel Pyrolysis Reactor System

The supercritical pyrolysis experiments are performed in an isothermal and isobaric tubular flow reactor system designed by Davis.<sup>55</sup> This reactor system was previously used by Stewart,<sup>15,56</sup> Ledesma *et al.*,<sup>57</sup> McClaine *et al.*,<sup>60</sup> Somers *et al.*,<sup>44</sup> Bagley *et al.*,<sup>18,46,47</sup> Nguyen,<sup>58</sup> Grubb,<sup>59</sup> Kalpathy *et al.*,<sup>48-50</sup>, and Hurst *et al.*<sup>54,61</sup> to simulate the conditions experienced by jet fuels in the pre-combustion environment of future high-speed aircraft.

The reactor system, as illustrated in Figure 2.1, consists of three components: a high-pressure fuel delivery pump, a heated reaction zone, and a product collection apparatus. Before starting an experiment, the *n*-decane fuel ( $\geq 99$  % pure, from Sigma-Aldrich Corporation) is sparged with ultra-high purity nitrogen for three hours to remove any dissolved oxygen that could cause auto-oxidative effects in the supercritical reaction environment.<sup>62</sup> The sparged fuel is then



introduced into a high-pressure syringe pump (Teledyne ISCO 500D Syringe Pump) which continuously delivers the fuel to the reactor.<sup>19,61</sup>

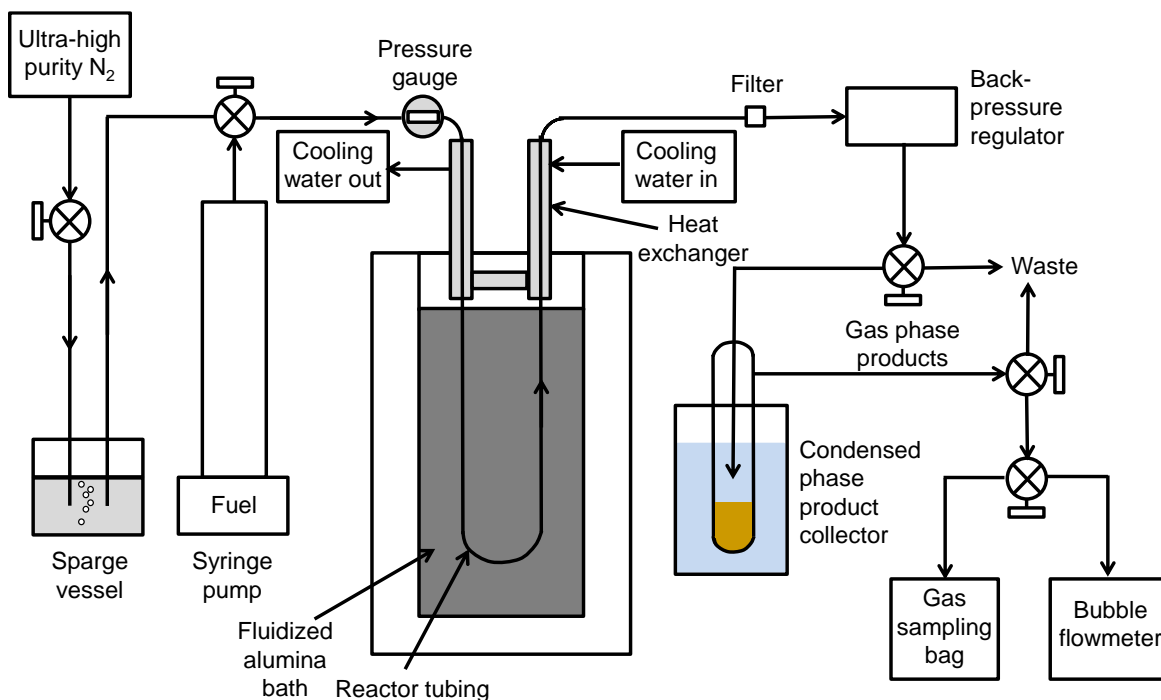


Figure 2.1. Schematic of the supercritical fuel pyrolysis reactor system.<sup>19</sup>

The reactor consists of a silica-lined stainless-steel tube (length, 53cm; outer diameter, 3.17 mm; inner diameter, 2.16mm) placed in a temperature-controlled fluidized alumina bath (Techn Model FB-08) that ensures isothermal condition throughout the length of the reactor.<sup>19</sup> The silica lining on the reactor tube prevents any possible wall-catalyzed reactions.<sup>15,56</sup>

To control the thermal history for the reactants, during each experiment, the entrance and the exit lines of the reactor tube pass through a water-cooled shell-and-tube heat exchanger maintained at 25 °C.<sup>19,61</sup> The quenched reaction products, as well as the unreacted fuel, pass through a filter (10 µm hole) to remove any carbonaceous solid deposits that are formed during an experiment and then pass through a dome-loaded back-pressure regulator (connected to an EQUILIBAR Model

3000 pressure controller) that maintains constant pressure inside the reactor. The experimental pressure is measured with a pressure gauge (ASHCROFT Model 2000) upstream of the reactor. Subsequently, the liquid-phase and gas-phase products along with the unreacted fuel pass through a product collection apparatus where they are collected by phase for further analysis. The gas-phase products are collected in a Teflon gas sampling bag, and the liquid-phase products are collected in a 50-ml collection flask that is immersed in an ice bath. The supercritical pyrolysis reactor system can operate at temperatures of up to 700 °C (controlled to within  $\pm 1$  °C), pressures of up to 110 atm (controlled to within  $\pm 0.2$  atm), and residence times of up to several minutes.<sup>19,61</sup>

By utilizing the reactor system shown in Figure 2.1, the following sets of supercritical *n*-decane pyrolysis experiments have been performed to better understand the formation and growth pathways of polycyclic aromatic hydrocarbons (PAH) in the supercritical *n*-alkane pyrolysis environment.<sup>19</sup>

- (1) To understand the behavior of *n*-decane at lower temperatures, supercritical pyrolysis experiments have been performed at a constant pressure of 94.6 atm, a fixed residence time of 133 sec, and at four temperatures of 495, 500, 515, and 520 °C. The findings from these experiments are reported in chapter 4.
- (2) To understand the growth behaviors of bay-region methyl-substituted PAH in the supercritical *n*-alkane pyrolysis environment, we have performed supercritical *n*-decane pyrolysis experiments to which 4-methylchrysene, a bay-region methyl-substituted PAH, has been added as a dopant at a concentration of 0.684 mg/g *n*-decane.<sup>51</sup> The experiments are conducted at 568 °C, 94.6 atm, and 133 sec, conditions of rapid PAH growth.<sup>51</sup> The results from these experiments are reported in chapter 5.

(3) To substantiate the growth behaviors of bay-region methyl-substituted PAH, as exhibited by 4-methylchrysene, we have performed supercritical *n*-decane pyrolysis experiments to which 4-methylphenanthrene, *n*-decane's highest-yield bay-region methyl-substituted PAH product, has been added as a dopant at a concentration of 0.685 mg/g *n*-decane, which is same as that used in the experiments with 4-methylchrysene.<sup>51</sup> These experiments are also conducted at 568 °C, 94.6 atm, and 133 sec, conditions of rapid PAH growth. The results from these experiments are discussed in chapter 6.

### 2.3. Product Analysis

As shown in Figure 2.1, the quenched reaction products and the unreacted fuel pass through a product collection apparatus where the products are separated by phase. The gas-phase products consist of C<sub>1</sub>-C<sub>6</sub> aliphatics and one-ring aromatics which are analyzed by gas chromatography (GC) coupled with flame-ionization detection (FID).<sup>19,61</sup> The details of the analysis method are discussed in section 2.3.1. The liquid-phase products consist of  $\geq$  C<sub>3</sub> aliphatic products, one- and two-ring aromatics, and three- to nine-ring PAH. The liquid-phase products are collected in a 50 ml flask which is placed in an ice bath to prevent the loss of products that are volatile from the sample.<sup>19</sup> Next, the liquid-phase products are transferred to an amber vial for storage and subsequent analyses.<sup>19,61</sup> The aliphatic and one- and two-ring aromatic products are analyzed by GC coupled to FID and mass spectrometry (MS).<sup>18,19</sup> The complex PAH product mixture is separated by a two-dimensional high-pressure liquid chromatographic technique, and the PAH products are subsequently characterized by ultraviolet-visible diode-array detection (UV-DAD) and mass spectrometry (MS).<sup>18,19</sup> The details of the liquid-phase product analysis are reported in section 2.3.2.

### 2.3.1. Analysis of Gas-Phase Products

The gas-phase products collected in a Teflon gas bag are diluted with nitrogen before being injected on an Agilent model 6890 gas chromatograph with flame ionization detection (GC/FID).<sup>19</sup> A GS GasPro fused silica capillary column (length, 30 m; inside diameter, 0.32 mm; manufactured by J&W Scientific) is used to separate the gas-phase products. The carrier gas is Helium (flow rate of 5 mL/min). The sample is injected at a volume of 0.5 mL and the split flow ratio is 5:1.<sup>19</sup> Initially, the oven temperature is maintained at 35 °C for 2 min, then increased to 240 °C at a rate of 10 °C/min, and subsequently held constant at 240 °C for 10 min.<sup>19,61</sup> Products are identified by matching retention times and mass spectra with those of known reference standards. Quantification is achieved by multiplying the areas from the FID peaks with corresponding response factors, which are calculated by injecting a reference standard of each identified gas-phase product at several known concentrations onto the GC/FID.<sup>18,19,61</sup> The GC/FID response factors used for the quantification of gas-phase products can be found in Table A1 in Appendix A.

### 2.3.2. Analysis of Liquid-Phase Products

The liquid-phase product mixtures of supercritical *n*-decane pyrolysis experiments consist of aliphatics (alkanes, alkenes, and cyclic aliphatics) as well as unsubstituted and alkylated aromatics. To handle these various sorts of products and their wide range of yields in the liquid-phase sample produced during the supercritical *n*-decane pyrolysis experiment, a five-sequence analysis scheme (as illustrated in Figure 2.2) is employed.<sup>19,61</sup> Each of these sequences is designated by a circled number, and classified by the analytical techniques used for the following products: (1) C<sub>3</sub>-C<sub>6</sub> aliphatics; (2) C<sub>6</sub>-C<sub>14</sub> aliphatics and one-ring aromatics; (3) two-ring aromatics; (4) two- to six-ring PAH; and (5) five- to nine-ring PAH.

### 2.3.2.1. Analysis of Aliphatic and One-Ring Aromatic Products

The identification and quantification of the aliphatics and one-ring aromatics, as well as the calculation of *n*-decane's conversion, are achieved by sequences 1 and 2 in Figure 2.2. The liquid-phase products from first three sequences are analyzed on an Agilent model 7890B GC/FID in conjunction with an Agilent model 5977B mass spectrometer (MS). A HP-5MSi fused silica capillary column (length 30 m; inner diameter 0.25 mm; film thickness 0.1 μm; made by J&W Scientific) is used to separate the samples.<sup>19,61</sup>

For the analysis of the C<sub>3</sub>-C<sub>6</sub> aliphatics, since dichloromethane (solvent) masks the peaks of some of these hydrocarbons, a new method with a higher split ratio (175:1) was developed for this work, where the sample is shot neat on both the GC/FID and MS.<sup>54,61</sup> The injection volume is 2 μL for both detectors (as illustrated by sequence 1 of Figure 2.2.), and the carrier gas is helium with a flowrate of 350 mL/min. The temperature of the oven is set to 40 °C for 3 min, then increased to 280 °C at 10 °C/min, and finally held constant at 280 °C for a period of 30 min.<sup>54,61</sup>

The products are identified by evaluating their mass spectra and by comparing their elution times to those of reference standards.<sup>19,61</sup> Quantification is achieved by multiplying the FID peak areas with the response factor of 1-pentene (obtained from shooting 1-pentene at different concentrations) reported in Table A2 in Appendix A.

For the analysis of the C<sub>6</sub>-C<sub>14</sub> aliphatics and one-ring aromatics, as well as the calculation of *n*-decane's conversion, a small amount of sample (100 μL) is first diluted in dichloromethane (solvent) before being shot on the GC/FID/MS. The injection volume is 2 μL for the FID and 4 μL for the MS.<sup>19,61</sup> As shown in sequence 2 of Figure 2.2, if any of the products' FID peak areas are outside the linear range, an even smaller amount of the sample is diluted in dichloromethane and a second injection is made on the GC/FID/MS.<sup>19,61</sup>

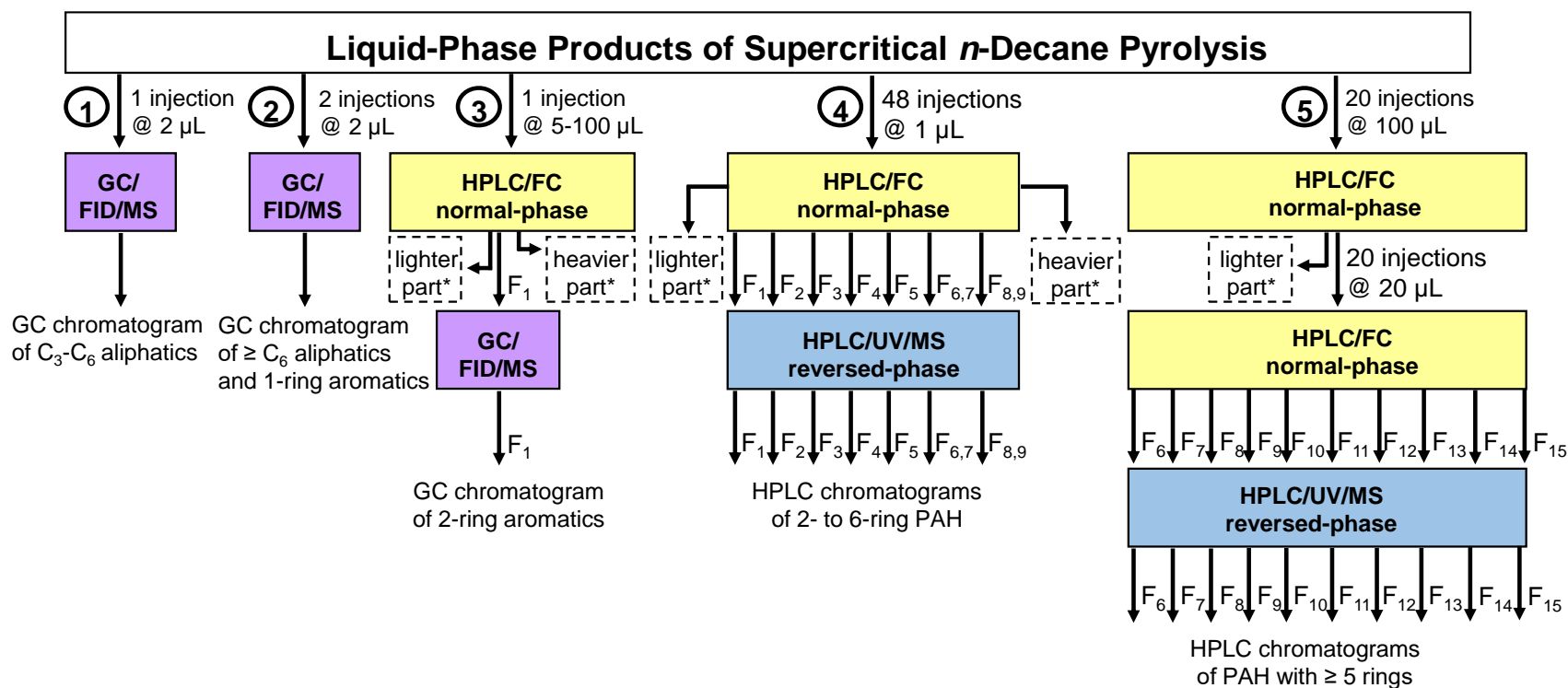


Figure 2.2. Analyses scheme for the fractionation of the liquid-phase products from the supercritical pyrolysis of *n*-decane. “F<sub>x</sub>” denotes the fraction number. Note that there are five analysis or fractionation/analysis sequences. An exit stream marked “lighter part” or “heavier part” from an HPLC/FC fractionation step in one of the sequences contains material whose analysis is covered in one of the other analysis sequences, tailored to that material. This figure is adapted from Hurst *et al.*<sup>61</sup>

The split flow ratio is set to 5:1, and helium is used as the carrier gas. The temperature of oven is set to 40 °C for 3 min, then increased to 280 °C at 4 °C/min, and finally held constant at 280 °C for 30 min.<sup>19,61</sup>

The C<sub>6</sub>-C<sub>14</sub> aliphatic and one-ring aromatic products are identified by matching retention times and mass spectra with those of known reference standards.<sup>19,61</sup> Quantification is achieved by multiplying the areas from the FID peaks with corresponding response factors, which are determined by injecting reference standards onto the GC/FID at several known concentrations.<sup>19,61</sup> The response factors used for the analysis of these products can be found in Table A2 in Appendix A. Due to the abundance of compounds, in some cases, the response factors of compounds with similar molecular weight and structure were used, and this list of surrogate compounds can be found in Table A3 in Appendix A.

The subsequent sections will describe the analytical techniques utilized to analyze the two- to nine-ring PAH products formed during the supercritical pyrolysis of *n*-decane. These analytical techniques (as shown by sequences 3-5 of Figure 2.2) were developed by Bagley and Wornat<sup>46,47</sup> and later modified by Kalpathy<sup>19</sup> to achieve the best possible resolution for the identification and quantification of two- to nine-ring PAH products.

Bagley and Wornat<sup>46,47</sup> showed that liquid-phase products from the supercritical *n*-decane pyrolysis contain an abundance of highly alkylated PAH in addition to aliphatics and unsubstituted aromatics.<sup>19</sup> Furthermore, it was reported that these highly alkylated PAH product mixtures exhibit low resolution when separated only by reversed-phase HPLC columns, which otherwise, exhibit good resolution for product mixtures containing only unalkylated PAH.<sup>44,45,61</sup> Therefore, these complex PAH products are subjected to a combination of normal-phase fractionation along with reversed-phase HPLC. Based on a method originally established by Wise *et al.*<sup>63</sup>, Bagley and

Wornat<sup>46,47</sup> (later modified by Kalpathy<sup>19</sup>) developed a normal-phase HPLC fractionation technique to separate the liquid-phase products of supercritical *n*-decane pyrolysis into 15 fractions based on aromatic ring number. Each fraction corresponds to PAH of a common ring number or isomer group, along with alkylated derivatives of those PAH.<sup>19</sup> Table 2.1 presents the PAH isomer classes, which can be found in each of the fifteen fractions obtained. The fractions include the “primary constituents” which are the unsubstituted parent PAH. The alkylated derivatives of these “primary constituents” are also collected in each fraction. On a mass basis, these alkylated PAH dominate the PAH product distribution.<sup>19</sup> After this step, the products from each fraction are analyzed by GC/FID/MS or reversed-phase HPLC with diode-array ultraviolet–visible (UV) absorbance and mass-spectrometric detection, for isomer-specific product identification and quantification, after calibrating the instruments with reference standards.<sup>19,46,47</sup>

The normal-phase HPLC fractionation steps shown in sequences 3-5 of Figure 2.2 are performed by injecting a neat experimental sample into an Agilent Model 1200 HPLC with a diode-array ultra-violet (UV) absorbance detector and a fraction collector (FC). For separation, the HPLC/FC instrument is equipped with two Restek Pinnacle II Cyano columns (each with a diameter of 46 mm, length of 250 mm, and particle size of 5 µm) in series.<sup>19,46,47</sup>

In order to identify when individual PAH products or PAH isomer groups of the first nine fractions eluted from the normal-phase Cyano HPLC column, a PAH 16 standard containing a mixture of unsubstituted PAH that represents the different isomer groups of PAH is shot on the normal-phase Cyano columns, and the fractions are cut based on the elution times of the standards.<sup>19,46,47</sup> To determine the division of the Fractions 10-14, the Cyano columns are mounted on the HPLC/UV/MS, and a sample from the *n*-decane experiments at the condition of incipient solids formation (570 °C, 94.6 atm, and 133 sec) is shot repeatedly on the Cyano columns.<sup>19,46,47</sup>



Table 2.1. Constituents of the 15 normal-phase HPLC fractions of an *n*-decane product mixture.<sup>19</sup>

Fraction Number	Primary Constituents
1	2-ring, C <sub>8</sub> H <sub>10</sub>
2	3-ring, C <sub>13</sub> H <sub>10</sub>
3	3-ring, C <sub>14</sub> H <sub>10</sub>
4	4-ring, C <sub>16</sub> H <sub>10</sub>
5	4-ring, C <sub>18</sub> H <sub>12</sub>
6	5-ring, C <sub>20</sub> H <sub>12</sub>
7	5-ring, C <sub>20</sub> H <sub>12</sub> and C <sub>21</sub> H <sub>14</sub>
8	6-ring, C <sub>22</sub> H <sub>12</sub>
9	5-ring, C <sub>22</sub> H <sub>14</sub> and 7-ring, C <sub>24</sub> H <sub>12</sub>
10	6-ring, C <sub>24</sub> H <sub>14</sub>
11	7-ring, C <sub>26</sub> H <sub>14</sub>
12	8-ring, C <sub>28</sub> H <sub>14</sub>
13	9-ring, C <sub>30</sub> H <sub>14</sub>
14	8-ring, C <sub>30</sub> H <sub>16</sub>
15	10-ring, C <sub>32</sub> H <sub>14</sub>

After this step, single ion monitoring on the mass spectrometer (MS) is used with the various molecular masses monitored as the following: 302 for Fraction 10, 326 for Fraction 11, 350 for Fraction 12, 374 for Fraction 13, and 376 for Fraction 14.<sup>19,61</sup> The same process is used to establish the demarcation time for Fractions 10-14 as it is for Fractions 1-9, except that a given molecular weight represents a whole isomer group rather than one or a few PAH products. The procedure for collecting Fraction 15 will be explained in Section 2.3.2.3.

### 2.3.2.2. Analysis of Two-Ring Aromatic Products

As illustrated by sequence 3 in Figure 2.2, the two-ring aromatic products are first separated from the lighter and heavier products by shooting a small volume (5-100  $\mu$ L) of experimental sample on a normal-phase HPLC (Agilent Model 1200) with a fraction collector (FC). After separation, the two-ring aromatics are collected in hexanes (designated as Fraction 1),

and 2  $\mu\text{L}$  and 4  $\mu\text{L}$  are injected on the FID and MS of the GC, respectively.<sup>19</sup> The oven temperature is set to 60 °C for 3 minutes, then increased to 220 °C at a rate of 4 °C/min, and finally ramped to 280 °C at a rate 15 °C/min with a final hold of 10 min.<sup>19</sup> The carrier gas is helium with a flow rate of 5 mL/min, and the split flow ratio is 5:1. The two-ring aromatic products are identified by matching retention times and mass spectra with those of known reference standards. Quantification is achieved by multiplying the areas from the FID peaks with corresponding response factors, which are determined by injecting known concentrations of reference standards onto the GC/FID. The response factors utilized for the quantification of two-ring aromatic products can be found in Table A2 in Appendix A. Fraction 1 is also analyzed by the reversed-phase HPLC coupled with diode-array ultraviolet–visible (UV) absorbance and mass-spectrometric (MS) detection.

### **2.3.2.3. Analysis of Two- to Ten-Ring PAH**

Sequences 4 and 5 in Figure 2.2 illustrate the analysis and fractionation steps used for the analysis of two- to ten-ring PAH products. Sequence 4 is used to analyze two- to six-ring PAH and sequence 5 for PAH  $\geq$  5 rings. Analysis of two- to six-ring PAH compounds begins with a normal-phase fractionation step, which separates the products into seven fractions based on their aromatic structure, as shown in sequence 4, which is regarded the "less-involved" fractionation (both in terms of time and solvent consumption).<sup>19,46,47,61</sup> To obtain better resolution of products and to collect enough material for each of the seven fractions, 48 separate 1- $\mu\text{L}$  injections of the pyrolysis product mixture are shot on the normal phase HPLC/FC. Each run lasts 30 min, and hexane is the mobile phase solvent which is pumped through the Cyano columns (maintained at 11 °C) at a rate of 1 mL/min. Each of these normal-phase HPLC fractions are concentrated down

utilizing a Kuderna Danish apparatus and then analyzed on the reversed-phase HPLC coupled with diode-array ultraviolet–visible (UV) absorbance and mass-spectrometric (MS) detection.<sup>19,46,47</sup>

Note that sequence 5's first four fractions overlap with sequence 4's last two fractions. Because the concentrations of the 5- to 9-ring PAH products are orders of magnitude lower than those of the smaller-ring-number aromatics, two fractionation steps are required to produce enough material for analysis of these large PAH.<sup>19,46,47</sup> This fractionation procedure is “more-involved” in terms of both time and solvent consumption. To isolate the 5- to 9-ring PAH from the lower-ring-PAH products, the liquid-phase products are injected into the HPLC/FC in twenty injections of 100- $\mu$ L volume as seen in the first step of sequence 5 of Figure 2.2. The Cyano columns are maintained at a temperature of 25 °C, and pure hexane is initially sent through the columns at 1 mL/min for 40 min. Next, the mobile phase solvent (hexane) is ramped to 90/10 hexane/dichloromethane (DCM) in 1 min and held constant for 9 minutes. The material in the first step is collected as two separate fractions: (1) the material collected in hexane that contains 5- to 9-ring PAH (Fractions 6-14); and (2) the material collected in 90/10 hexane/DCM that consists of 10-ring PAH (Fraction 10). Then, the material collected in hexane that contains 5- to 9-ring PAH is concentrated in a Kuderna-Danish apparatus and exchanged into 200  $\mu$ L of *n*-decane.<sup>19,46,47</sup> In the second step of “more-involved” fractionation, around twenty-five 20- $\mu$ L injections of the concentrated sample are injected onto the Cyano columns (maintained at 11 °C), and the 5- to 9-ring products are separated according to ring number and isomer group into Fractions 6-14. The heavy PAH material collected in Fraction 15 tend to fall out of solution when this material is being exchanged in *n*-decane.<sup>19</sup> As a result, Fraction 15 is spared the second fractionation stage. As illustrated in the third step of sequence 5 in Figure 2.2, the final step of “more-involved” fractionation is to concentrate each fraction down, including Fraction 15, using a Kuderna Danish

apparatus and analyze the 5- to 10-ring PAH products by reversed-phase HPLC/UV/MS. Each fraction is subsequently prepared for reversed-phase analysis as described below and analyzed by HPLC/UV/MS.<sup>19</sup>

To achieve individual component resolution, each of the normal-phase HPLC fractions of the liquid-phase product mixture are concentrated in a Kuderna-Danish apparatus, and subsequently, Fraction 1 is exchanged in 100  $\mu\text{L}$  of dimethyl sulfoxide (DMSO) while all the other Fractions 2-15 are exchanged in 45  $\mu\text{L}$  of DMSO. DMSO is chosen because it is compatible with the solvents used in the reversed-phase analyses.<sup>19</sup> A small amount (1 to 20  $\mu\text{L}$ ) of each fraction is then injected onto an Agilent Model 1290 HPLC/UV system coupled to a 6120 APPI-MS, which tracks mass-to-charge ratios of up to 700 by employing atmospheric-pressure photoionization. A dopant delivery system has been installed downstream of the UV detector, which introduces benzene as a dopant into the spray-chamber of the APPI-MS. Benzene enhances the ionization of the PAH products, thus giving stronger mass signals, which is critical to analyze the yields of the lower-yield-PAH products. The details of the dopant delivery system are documented elsewhere.<sup>64</sup>

For separation of the PAH products, a Restek Pinnacle II PAH octadecylsilica column (C18) (inner diameter, 2.1 mm; length, 250 mm; particle size, 4  $\mu\text{m}$ ) is employed. The solvent compositions of methods used for the reversed-phase HPLC analysis of PAH products produced from the supercritical pyrolysis of *n*-decane are presented in Table 2.2. These solvent methods consist of either pure acetonitrile (ACN), pure dichloromethane (DCM), or a mixture of ACN/water. The exact details of the solvent sequences used for the analysis of each fraction are presented elsewhere.<sup>46,47</sup>

Figure 2.3 shows the reversed-phase HPLC chromatogram of Fraction 6, which was obtained from separating the liquid-phase products of a supercritical *n*-decane pyrolysis

experiment (570 °C, 94.6 atm, and 133 sec) by using HPLC/UV/MS. This fraction mainly contains benzo[*a*]pyrene, benzo[*e*]pyrene, and their alkylated derivatives. The black structures represent unsubstituted PAH; the red structures represent singly methylated PAH; and the blue structures represent dimethylated or ethylated PAH.<sup>46,47</sup>

Table 2.2. Solvent methods used for the reversed-phase HPLC analysis of PAH products produced from the supercritical pyrolysis of *n*-decane.<sup>19,46,47,61</sup>

Method	Sequence	Column Temperature (° C)	Used for Fraction
1	Mobile phase is 50/50 H <sub>2</sub> O/ACN held for 70 min	40	F <sub>2</sub>
2	Mobile phase is 35/65 H <sub>2</sub> O/ACN held for 30 min	40	F <sub>3</sub>
3	Mobile phase is 35/65 H <sub>2</sub> O/ACN held for 40 min	40	F <sub>4</sub>
4	Mobile phase is 40/60 H <sub>2</sub> O/ACN held for 50 min	50	F <sub>5</sub>
5	Mobile phase is 35/65 H <sub>2</sub> O/ACN held for 60 min	50	F <sub>6,7</sub>
6	Mobile phase is initially 15/85 H <sub>2</sub> O/ACN and then ramped at a constant gradient for 80 min to pure ACN and held for 100 min	30	F <sub>6</sub> , F <sub>7</sub> , F <sub>8</sub> , and F <sub>8,9</sub>
7	Mobile phase is initially 60/40 H <sub>2</sub> O/ACN, then ramped at a constant gradient for 60 min to pure ACN and held for 30 min, and then ramped at a constant gradient for 60 min to pure DCM and held for 30 min	30	F <sub>10</sub>
8	Mobile phase is initially 50/50 H <sub>2</sub> O/ACN, then ramped at a constant gradient for 40 min to pure ACN and held for 30 min, and then ramped at a constant gradient for 120 min to pure DCM and held for 30 min	30	F <sub>11</sub>
9	Mobile phase is initially 50/50 H <sub>2</sub> O/ACN, then ramped at a constant gradient for 40 min to pure ACN and held for 30 min, and then ramped at a constant gradient for 90 min to pure DCM and held for 30 min	30	F <sub>12</sub> , F <sub>13</sub> , F <sub>14</sub> , and F <sub>15</sub>

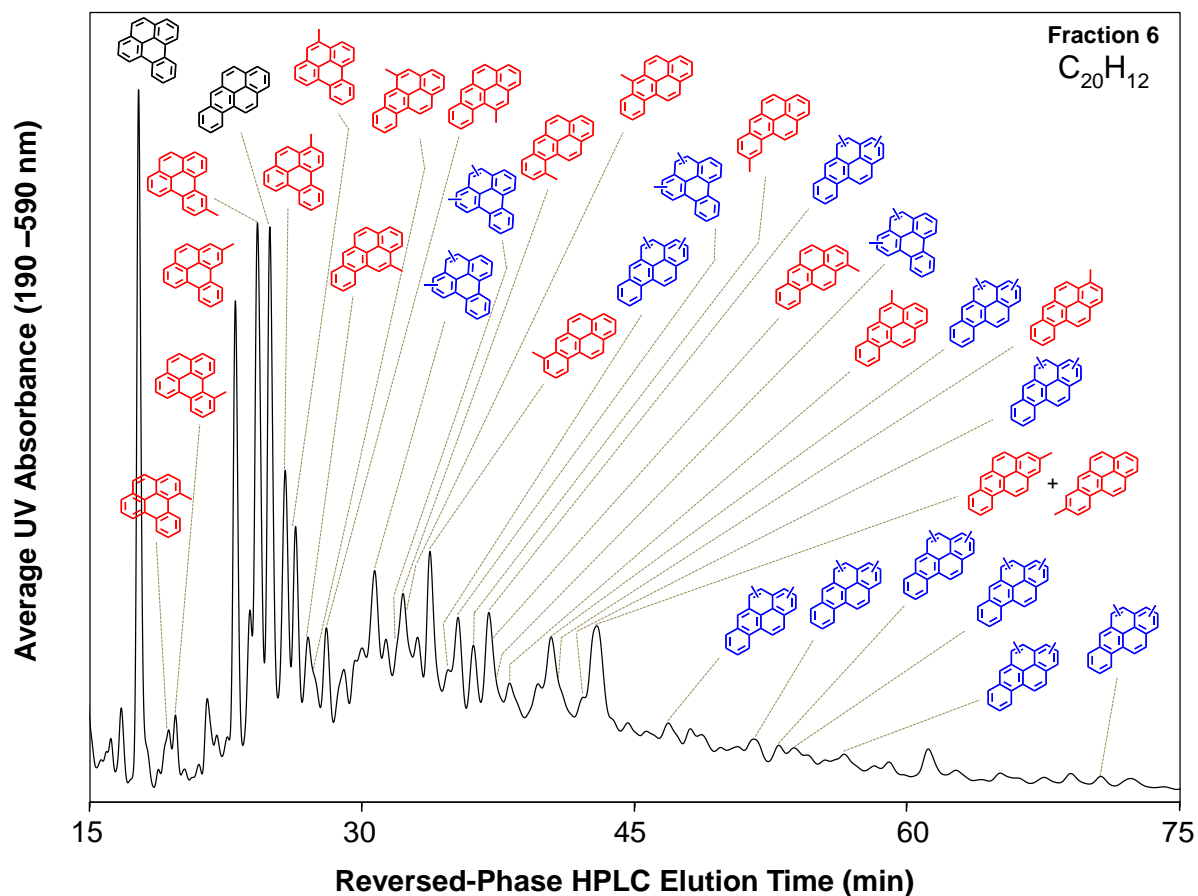


Figure 2.3. Reversed-phase HPLC chromatogram of five-ring  $C_{20}H_{12}$  PAH and their alkylated derivatives from the supercritical pyrolysis of *n*-decane at 570 °C, 94.6 atm, and 133 sec.<sup>19,46,47</sup> The black structures represent unsubstituted PAH; the red structures represent singly methylated PAH; and the blue structures represent dimethylated or ethylated PAH.

A UV absorption spectrum and mass spectrum of each resolved product is obtained by the HPLC/UV/MS. A UV absorption spectrum is unique to each PAH; therefore, the product is unequivocally identified by matching its spectrum with that of the appropriate reference standard.<sup>19,46,47,49</sup> In the absence of reference standards, product identities are established by comparing their UV spectra with those published in the literature. Panels a and b of Figure 2.4 provide an example of the isomer-specific identification of two unsubstituted PAH, benzo[*a*]pyrene and benzo[*e*]pyrene. Figure 2.4 reveals that there is extremely good agreement

between the products' UV spectra (shown in black) and the reference standards' UV spectra (shown in red). The APPI mass spectrum (shown in the insets of Figure 2.4) establishes the molecular mass of the PAH, its  $C_xH_y$  formula, and whether the aromatic structure contains any substituent groups such as methyl. The mass spectrum presented in the inset of panel a of Figure 2.4 indicates that the *n*-decane pyrolysis product has a molecular weight of 252, corresponding to a  $C_xH_y$  formula of  $C_{20}H_{12}$ , thus establishing benzo[*a*]pyrene as having no alkyl substituents on its aromatic structure. Similarly, in the inset of panel c of Figure 2.4, the molecular weight is 252, corresponding to a  $C_xH_y$  formula of  $C_{20}H_{12}$ , thus establishing benzo[*e*]pyrene as having no alkyl substituents on its aromatic structure.

While unsubstituted PAH products are identified in the above manner, reference spectra are less readily available for alkylated PAH. Therefore, the alkylated PAH are identified by a combination of UV and mass spectra. The UV spectrum of an alkylated PAH looks almost exactly like that of the parent PAH, only shifted by a few nanometers towards higher wavelengths, with the position(s) and length(s) of the substituent group(s) dictating the details of the shift.<sup>46,47,67</sup> Thus the UV spectrum establishes the aromatic structure of an alkylated PAH. The APPI mass spectrum establishes the molecular mass of the PAH, its  $C_xH_y$  formula, and whether the aromatic structure contains any substituent groups such as methyl. For example, the mass spectrum presented in the inset of panel b of Figure 2.4 shows that the *n*-decane pyrolysis product is a methyl-substituted derivative of benzo[*a*]pyrene. The good agreement between the UV spectra of the pyrolysis product/reference standard pair (in panel b of Figure 2.4) unequivocally establishes the unknown product as 8-methylbenzo[*a*]pyrene. In a similar way, the mass spectrum presented in the inset of panel d of Figure 2.4 shows that the *n*-decane pyrolysis product is a methyl-substituted of

benzo[*e*]pyrene, and the good match between the UV spectra of the pyrolysis product/reference standard combination unequivocally establishes the unknown product as 2-methylbenzo[*e*]pyrene.

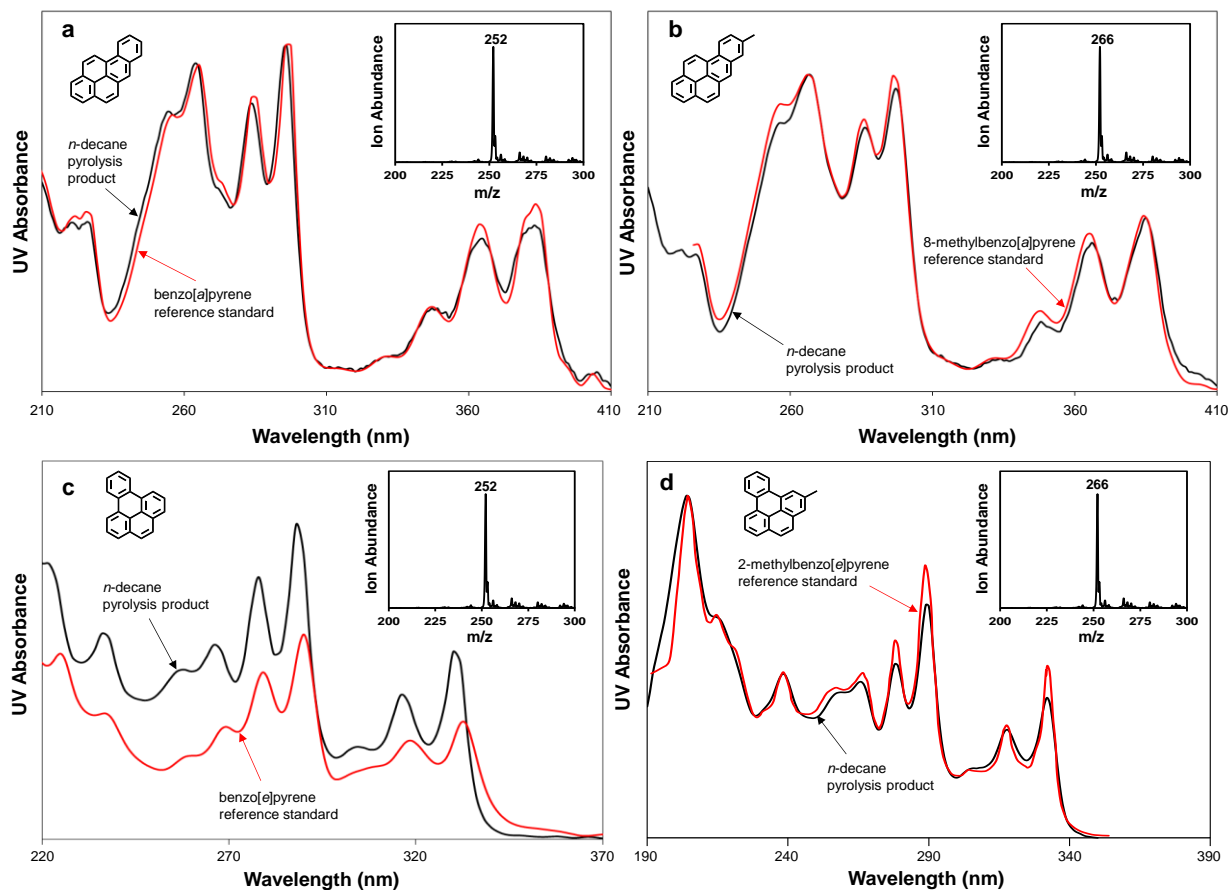


Figure 2.4. The black line is the UV spectrum of a PAH product from the supercritical pyrolysis of *n*-decane overlaid with the red line, which is the UV spectrum of a reference standard. The inset shows the mass spectrum of the compound and establishes its  $C_xH_y$  formula. By matching the UV spectrum of the unknown to that of a known reference standard, the compounds can unequivocally be identified as follows: (a) benzo[*a*]pyrene, (b) 8-methylbenzo[*a*]pyrene, (c) benzo[*e*]pyrene, and (d) 2-methylbenzo[*e*]pyrene.

Quantification is achieved by multiplying the peak areas with appropriate response factors.<sup>19,61</sup> The HPLC/UV/MS is first calibrated with a PAH 16 reference standard, and the determined response factors are used for the quantification of PAH. The response factors employed for PAH product quantification are reported in Table A4 in Appendix A. The supercritical *n*-decane pyrolysis experiments produce a large variety of PAH. Therefore, it is



impossible to determine the response factor for each individual PAH. Table A5 in Appendix A lists such product components along with the surrogate compounds whose response factors were utilized to quantify them. However, according to prior work by Lafleur *et al.*,<sup>65</sup> when UV absorbance is integrated over the complete range of wavelengths over which a PAH absorbs, the integrated UV absorbance per mass varies very little from one PAH to the next. As a result, when we did not have a reference standard for a PAH product, we used the response factor of a structurally similar PAH or a PAH with a similar molecular weight for which a response factor was available.<sup>19,61</sup> In case of alkylated PAH, the response factors of parent PAH were multiplied by the ratio of the molecular weight of the alkylated PAH to the molecular weight of the parent PAH.<sup>19,61</sup> Because the number of possible PAH structures grows exponentially with ring number,<sup>66</sup> this HPLC/UV/MS approach is particularly suited for analyzing the large PAH molecules that are precursors to fuel-line solid deposits.

#### **2.4. Concluding Remarks**

The reactor setup utilized to perform the supercritical *n*-decane pyrolysis experiments, as well as the analytical techniques used to identify and quantify the products produced by these experiments, are explained in length in this chapter. The subsequent chapters will show the ability of these analytical techniques in elucidating the reaction mechanisms of PAH growth in the supercritical *n*-decane pyrolysis environment.

## Chapter 3. New Identifications of Aliphatic and Aromatic Products

### 3.1. Introduction

This chapter presents 62 new identifications of aliphatic and aromatic products of supercritical *n*-decane pyrolysis. The aliphatic and one-ring aromatic products, as described in section 2.3.2.1, are analyzed on an Agilent model 7890B GC/FID in conjunction with an Agilent model 5977B mass spectrometer (MS). The products are identified by analyzing their mass spectra and by comparing their elution times with those of reference standards. Quantification is achieved by multiplying the FID peak areas with appropriate response factors. The highly complex PAH products, as described in section 2.3.2.3, are separated by a two-dimensional high-pressure liquid chromatographic (HPLC) technique.<sup>19,61</sup> In the first stage of separation, using a normal-phase HPLC, the PAH product mixture is separated into 15 fractions based on aromatic ring number.<sup>19,61</sup> After this step, the PAH products from each fraction are individually separated by reversed-phase HPLC. The separated PAH products are subsequently characterized by ultraviolet-visible diode-array detection (UV) and mass spectrometry (MS).<sup>19,61</sup> The UV absorbance and mass spectral data establishing the identities of the newly identified PAH products will be discussed in detail.

The subsequent sections will list the newly identified aliphatic and aromatic products of supercritical *n*-decane pyrolysis based on the following structural classes: (1) *n*-alkanes, alkenes, and dienes, (2) cyclic aliphatics, (3) one-ring aromatics, and (4) polycyclic aromatic hydrocarbons (most of these newly identified products have already been identified as products of supercritical 1-octene pyrolysis by Hurst *et al.*<sup>54</sup>).

### 3.2. Identification of *n*-Alkanes, Alkenes, and Dienes

The newly identified *n*-alkanes, alkenes, and dienes of supercritical *n*-decane pyrolysis along with their chemical formulas, molecular weights, and chemical structures are listed in Table

3.1. Except for 2-undecene and 2-dodecene, all the products are identified by shooting a reference standard on the GC/FID/MS and matching the elution time and mass spectrum.

Table 3.1. Newly identified *n*-alkanes, alkenes, and dienes of supercritical *n*-decane pyrolysis.<sup>51,61</sup>

Product	Chemical Formula	Molecular Mass	Structure
1,3-pentadiene	C <sub>5</sub> H <sub>8</sub>	68	
1,4-pentadiene	C <sub>5</sub> H <sub>8</sub>	68	
2-hexane	C <sub>6</sub> H <sub>12</sub>	84	
3-hexene	C <sub>6</sub> H <sub>12</sub>	84	
1,3-hexadiene	C <sub>6</sub> H <sub>10</sub>	82	
1,5-hexadiene	C <sub>6</sub> H <sub>10</sub>	82	
2-heptene	C <sub>7</sub> H <sub>14</sub>	98	
3-heptene	C <sub>7</sub> H <sub>14</sub>	98	
3-octene	C <sub>8</sub> H <sub>16</sub>	112	
4-octene	C <sub>8</sub> H <sub>16</sub>	112	
2-nonene	C <sub>9</sub> H <sub>18</sub>	126	
3-nonene	C <sub>9</sub> H <sub>18</sub>	126	
4-nonene	C <sub>9</sub> H <sub>18</sub>	126	
2-decene	C <sub>10</sub> H <sub>20</sub>	140	
1-undecene	C <sub>11</sub> H <sub>22</sub>	154	
2-undecene	C <sub>11</sub> H <sub>22</sub>	154	
1-dodecene	C <sub>12</sub> H <sub>24</sub>	168	
2-dodecene	C <sub>12</sub> H <sub>24</sub>	168	
1-tridecene	C <sub>13</sub> H <sub>26</sub>	182	
1-tetradecene	C <sub>14</sub> H <sub>28</sub>	196	
<i>n</i> -pentadecane	C <sub>15</sub> H <sub>32</sub>	212	
<i>n</i> -hexadecane	C <sub>16</sub> H <sub>34</sub>	226	

The two products, 2-undecene and 2-dodecene, are tentatively identified based on their elution behavior and mass spectral evidence. For the products listed in Table 3.1, the identification and quantification of the alkenes and dienes includes both the cis and trans isomers. Furthermore, the products 1,3-pentadiene and 1,5-hexadiene exist both in the gas and liquid phases.

### 3.3. Identification of Cyclic Aliphatic Products

The supercritical *n*-decane pyrolysis experiments produce an abundance of cyclic aliphatic products, which consist of either a five-membered ring or a six-membered ring. The newly identified C<sub>5</sub>-ring cyclic aliphatic products along with their chemical formulas, molecular masses, and chemical structures are listed in Table 3.2. Among the C<sub>5</sub>-ring cyclic aliphatic products, cyclopentene and cyclopentadiene are present in both the gas and liquid phases. The newly identified C<sub>6</sub>-ring cyclic aliphatic products along with their chemical formulas, molecular masses, and chemical structures are listed in Table 3.3. These aliphatic products are analyzed by a gas chromatograph coupled with a mass spectrometer. Subsequently, the products are identified by analyzing their mass spectra and by comparing their elution times to those of reference standards.

### 3.4. Identification of One-Ring Aromatic Products

The one-ring aromatic products of supercritical *n*-decane pyrolysis are analyzed by a gas chromatograph coupled with a mass spectrometer. Most of the one-ring aromatic products of supercritical *n*-decane pyrolysis have been previously identified by Kalpathy *et al.*<sup>19</sup> However, because of lack of reference standards, the one-ring aromatic products with substituents containing three and four carbons were tentatively identified and their exact chemical structures were unknown. After obtaining reference standards and shooting them on the GC/FID/MS, all three possible trimethylbenzenes, *n*-propylbenzene, *n*-butylbenzene, and *n*-pentylbenzene are identified as products of supercritical *n*-decane pyrolysis. Based on the analytical evidence, two ethylmethylbenzenes and two C<sub>4</sub>-substituted one-ring aromatics are also identified as products of supercritical *n*-decane pyrolysis. However, due to a lack of reference standards, we could not determine the exact locations of the methyl, ethyl, and propyl groups on the aromatic structure. Table 3.4 lists the newly identified one-ring aromatic products.

Table 3.2. Newly identified C<sub>5</sub>-ring aliphatic products of supercritical *n*-decane pyrolysis.<sup>51,61</sup>




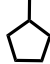
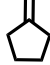
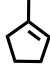
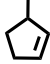
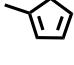


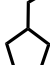
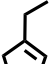
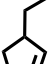
Product	Chemical Formula	Molecular Mass	Structure
cyclopentane	C <sub>5</sub> H <sub>10</sub>	70	
cyclopentene	C <sub>5</sub> H <sub>8</sub>	68	
cyclopentadiene	C <sub>5</sub> H <sub>6</sub>	66	
methylcyclopentane	C <sub>6</sub> H <sub>12</sub>	84	
methylenecyclopentane	C <sub>6</sub> H <sub>10</sub>	82	
1-methylcyclopentene	C <sub>6</sub> H <sub>10</sub>	82	
3-methylcyclopentene	C <sub>6</sub> H <sub>10</sub>	82	
1-methylcyclopentadiene	C <sub>6</sub> H <sub>8</sub>	80	
2-methylcyclopentadiene	C <sub>6</sub> H <sub>8</sub>	80	
5-methylcyclopentadiene	C <sub>6</sub> H <sub>8</sub>	80	
ethylcyclopentane	C <sub>7</sub> H <sub>14</sub>	98	
1-ethylcyclopentene	C <sub>7</sub> H <sub>12</sub>	96	
3-ethylcyclopentene	C <sub>7</sub> H <sub>12</sub>	96	

Table 3.3. Newly identified C<sub>6</sub>-ring aliphatic products of supercritical *n*-decane pyrolysis.<sup>51,61</sup>

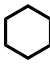

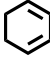
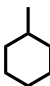
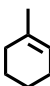
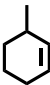
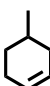
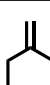
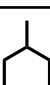
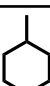
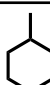
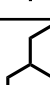
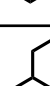
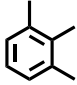
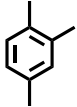
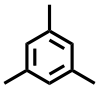
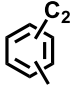
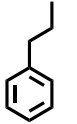
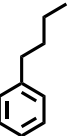
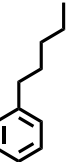
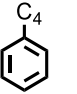
Product	Chemical Formula	Molecular Mass	Structure
cyclohexane	C <sub>6</sub> H <sub>12</sub>	84	
cyclohexene	C <sub>6</sub> H <sub>10</sub>	82	
1,3-cyclohexadiene	C <sub>6</sub> H <sub>8</sub>	80	
methylcyclohexane	C <sub>7</sub> H <sub>14</sub>	98	
1-methylcyclohexene	C <sub>7</sub> H <sub>12</sub>	96	
3-methylcyclohexene	C <sub>7</sub> H <sub>12</sub>	96	
4-methylcyclohexene	C <sub>7</sub> H <sub>12</sub>	96	
methylenecyclohexane	C <sub>7</sub> H <sub>12</sub>	96	
1,2-dimethylcyclohexane	C <sub>8</sub> H <sub>16</sub>	112	
1,3-dimethylcyclohexane	C <sub>8</sub> H <sub>16</sub>	112	
1,4-dimethylcyclohexane	C <sub>8</sub> H <sub>16</sub>	112	
ethylcyclohexane	C <sub>8</sub> H <sub>16</sub>	112	
4-ethylcyclohexene	C <sub>8</sub> H <sub>14</sub>	110	

Table 3.4. Newly identified one-ring aromatic products of supercritical *n*-decane pyrolysis.<sup>51,61</sup>

Product	Chemical Formula	Molecular Mass	Structure
1,2,3-trimethylbenzene	C <sub>9</sub> H <sub>12</sub>	120	
1,2,4-trimethylbenzene	C <sub>9</sub> H <sub>12</sub>	120	
1,3,5-trimethylbenzene	C <sub>9</sub> H <sub>12</sub>	120	
ethylmethylbenzene	C <sub>9</sub> H <sub>12</sub>	120	
<i>n</i> -propylbenzene	C <sub>9</sub> H <sub>12</sub>	120	
<i>n</i> -butylbenzene	C <sub>10</sub> H <sub>14</sub>	134	
<i>n</i> -pentylbenzene	C <sub>11</sub> H <sub>16</sub>	148	
C <sub>4</sub> -alkylbenzene	C <sub>10</sub> H <sub>14</sub>	134	

### 3.5. Identification of PAH Products

The supercritical *n*-decane pyrolysis experiments produce an abundance of two- to nine-ring PAH. As described in section 2.3.2.3, the highly complex PAH product mixture is separated by using a two-dimensional high-pressure liquid chromatographic (HPLC) technique. The

separated PAH products are analyzed, isomer-specifically, by ultraviolet-visible (UV) diode-array detection and mass spectrometry (MS) detection. By using these analyses, we have identified four new PAH products from the supercritical pyrolysis of *n*-decane and four new PAH products from the supercritical pyrolysis of *n*-decane doped with 4-methylchrysene. Tables 3.5 and 3.6 list the newly identified PAH along with their chemical formulas, molecular masses, and chemical structures. The UV absorbance and mass spectral data establishing the identities of these PAH products are presented in Figures 3.1 and 3.2.

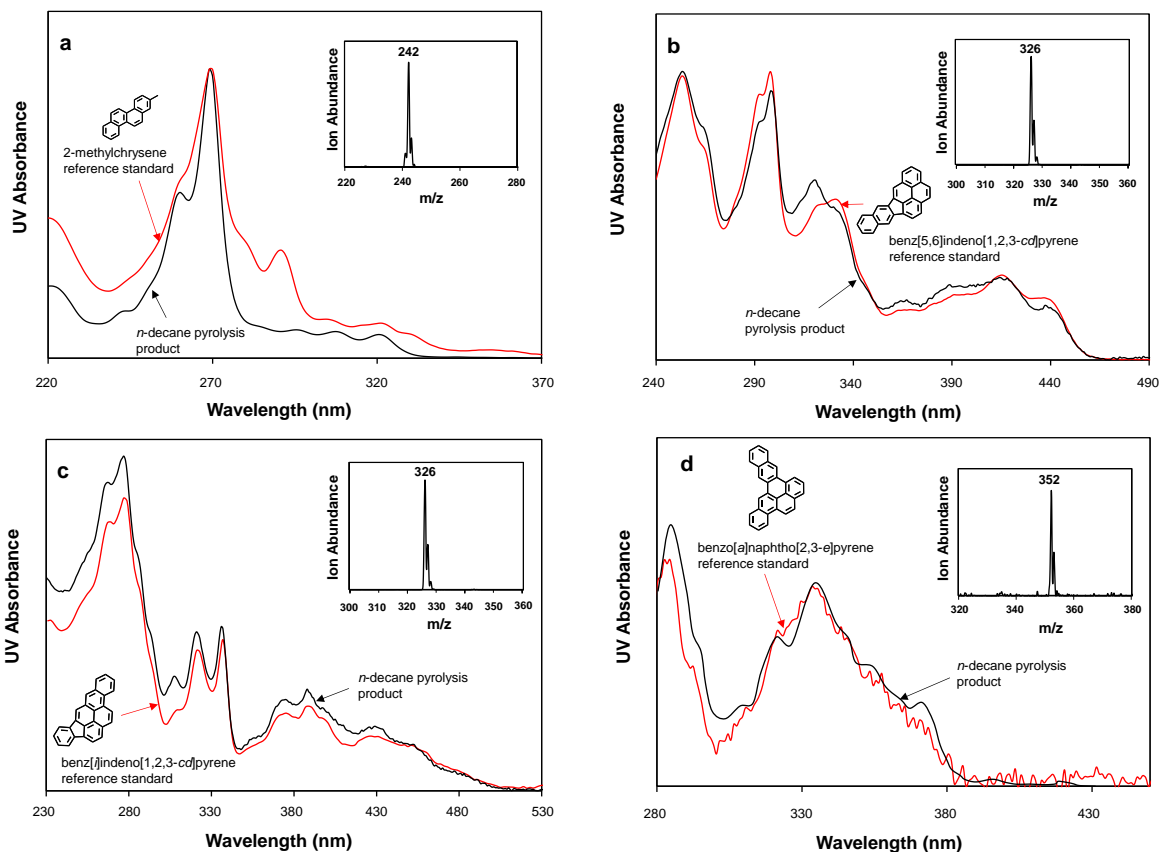


Figure 3.1. The black line is the UV spectrum of a PAH product from the supercritical pyrolysis of *n*-decane overlaid with the red line, which is the UV spectrum of a reference standard. The inset shows the mass spectrum of the compound and establishes its  $C_xH_y$  formula. By matching the UV spectrum of the unknown to that of a known reference standard, the compounds can unequivocally be identified as follows: (a) 2-methylchrysene, (b) benz[5,6]indeno[1,2,3-*cd*]pyrene, (c) benz[*i*]indeno[1,2,3-*cd*]pyrene, and (d) benzo[*a*]naphtho[2,3-*e*]pyrene.



Table 3.5. Newly identified PAH products of supercritical *n*-decane pyrolysis.<sup>51</sup>

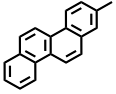
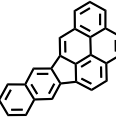
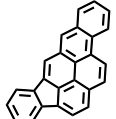
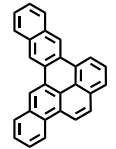
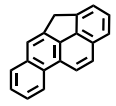
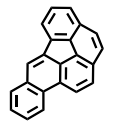
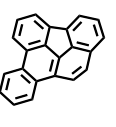
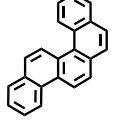
Product	Chemical Formula	Molecular Mass	Structure
2-methylchrysene	C <sub>19</sub> H <sub>14</sub>	242	
benz[5,6]indeno[1,2,3- <i>cd</i> ]pyrene	C <sub>26</sub> H <sub>14</sub>	326	
benz[ <i>i</i> ]indeno[1,2,3- <i>cd</i> ]pyrene	C <sub>26</sub> H <sub>14</sub>	326	
benzo[ <i>a</i> ]naphtho[2,3- <i>e</i> ]pyrene	C <sub>28</sub> H <sub>16</sub>	352	

Table 3.6. Newly identified PAH products from the supercritical pyrolysis of *n*-decane to which 4-methylchrysene has been added as a dopant.<sup>51</sup>

Product	Chemical Formula	Molecular Mass	Structure
4 <i>H</i> -cyclopenta[ <i>def</i> ]chrysene	C <sub>19</sub> H <sub>12</sub>	240	
dibenzo[ <i>b,ghi</i> ]fluoranthene	C <sub>22</sub> H <sub>12</sub>	276	
dibenzo[ <i>e,ghi</i> ]fluoranthene	C <sub>22</sub> H <sub>12</sub>	276	
benzo[ <i>c</i> ]chrysene	C <sub>22</sub> H <sub>14</sub>	278	

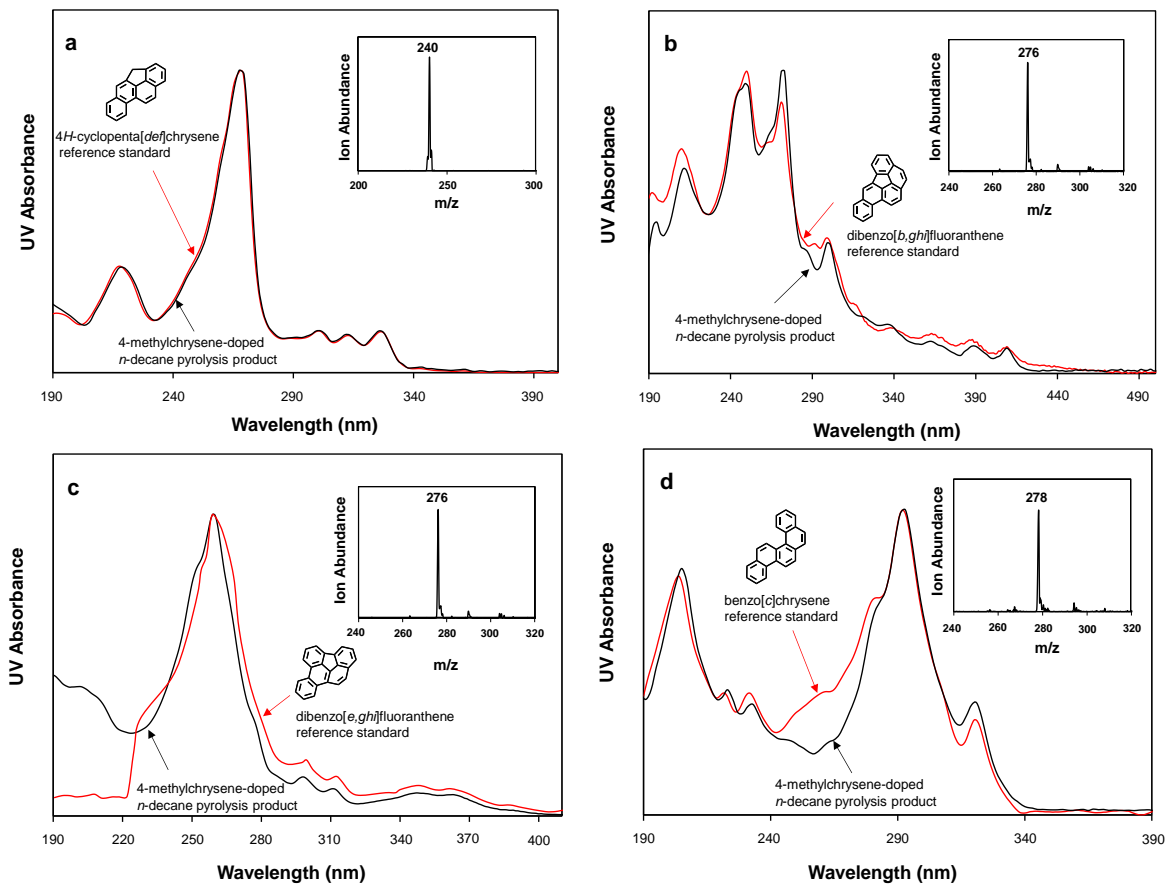


Figure 3.2. Comparisons of the UV spectra of 4-methylchrysene-doped *n*-decane pyrolysis products (black lines) to reference spectra (red lines). The inset shows the mass spectrum of the compound and establishes its  $C_xH_y$  formula. By matching the UV spectrum of the unknown to that of a known reference standard, the compounds can unequivocally be identified as follows: (a) 4*H*-cyclopenta[*def*]chrysene, (b) dibenzo[*b,ghi*]fluoranthene, (c) dibenzo[*e,ghi*]fluoranthene, and (d) benzo[*c*]chrysene.

### 3.6. Concluding Remarks

In this chapter, 62 new identifications of aliphatic and aromatic products produced from the supercritical pyrolysis of *n*-decane have been provided. The details of how these products are formed and how temperature affects their yields will be discussed in the next chapter.

## Chapter 4. Effects of Temperature on the Yields of Aliphatic and Aromatic Products

### 4.1. Introduction

It is well documented that the *n*-alkane components of jet fuels are most problematic regarding solids formation in the supercritical fuel-pyrolysis environment.<sup>1,5</sup> Therefore, Kalpathy *et al.*<sup>48</sup> from our research group performed supercritical pyrolysis experiments with the model fuel *n*-decane (critical temperature, 344.5 °C; critical pressure, 20.7 atm). These experiments<sup>48</sup> were carried out in a silica-lined stainless-steel tubular reactor at a constant pressure of 94.6 atm, a fixed residence time of 133 sec, and at six different temperatures ranging from 530 to 570 °C. The strong temperature dependence of the product yields revealed that temperature has a strong influence on the supercritical pyrolysis behavior of *n*-decane.<sup>19,48</sup>

To gain a better understanding of the behavior of *n*-decane at lower temperatures, we have performed additional supercritical *n*-decane pyrolysis experiments.<sup>54</sup> These experiments<sup>54</sup> have been performed in the same silica-lined stainless-steel tubular reactor at 94.6 atm, 133 sec, and at four different temperatures in the range of 495-520 °C. As detailed in chapter 2, the aliphatic and one- and two-ring aromatic products are analyzed by gas chromatography coupled with mass spectrometry.<sup>18,19,61</sup> The highly complex PAH product mixture is separated by a two-dimensional high-pressure liquid chromatographic technique, and the PAH products are subsequently characterized by ultraviolet-visible diode-array detection and mass spectrometry.<sup>18,19,61</sup>

This chapter will present the effects of temperature on the yields of the major products (including 58 newly identified aliphatic and one-ring aromatic products) produced from the supercritical *n*-decane pyrolysis experiments performed at 94.6 atm, 133 sec, and ten temperatures: 495, 500, 515, 520, 530, 540, 550, 560, 565, and 570 °C. Additionally, the reaction mechanisms

responsible for the formation of aliphatic products and one- to nine-ring aromatic products are also presented. The lowest temperature (495 °C) corresponds to the minimum temperature at which appreciable fuel conversion (21.2%) takes place. The highest temperature (570 °C) corresponds to incipient solids formation where the fuel conversion is 92%. Above this temperature, solids are formed so profusely that the reactor clogs, and the pyrolysis experiments must be stopped.<sup>18,19</sup>

The subsequent sections will present the yield-vs.-temperature plots of the major products. Based on the structural classes, these plots are separated into the following groups: (1) *n*-alkanes, alkenes, and dienes, (2) cyclic aliphatics, (3) one-ring and two-ring aromatics, and (4) polycyclic aromatic hydrocarbons (PAH). In these yield-vs.-temperature graphs, all plotted symbols represent experimentally measured yields. For *n*-decane data from 530-570 °C, the open symbols represent the yields of the products quantified by Kalpathy *et. al.*,<sup>48</sup> and the semi-solid symbols represent the yields of the products quantified by Vutukuru. For *n*-decane data from 495-520 °C, the solid symbols represent the yields of the products quantified by Vutukuru.

#### **4.2. Effects of Temperature on the Yields of Major Straight-Chain Aliphatic Products**

Figures 4.1 and 4.2 present the yields, as functions of temperature, of the major straight-chain aliphatic products (*n*-alkanes, alkenes, and dienes) of *n*-decane pyrolysis. In Figures 4.1 and 4.2, the black symbols represent the yields of the product *n*-alkanes; the red symbols, the 1-alkenes; the blue symbols, the 2-alkenes; the green symbols, the 3- and/or 4-alkenes; and the pink symbols, the dienes. The yields of acetylene are not reported here because no acetylene or any other triple-bonded species are produced in our supercritical *n*-decane pyrolysis experiments.<sup>19</sup>

Figures 4.1 and 4.2 reveal that C<sub>1</sub>-C<sub>9</sub> *n*-alkanes and C<sub>2</sub>-C<sub>9</sub> 1-alkenes are the highest-yield products of supercritical *n*-decane pyrolysis at all the temperatures (495-570 °C) investigated.<sup>19</sup>

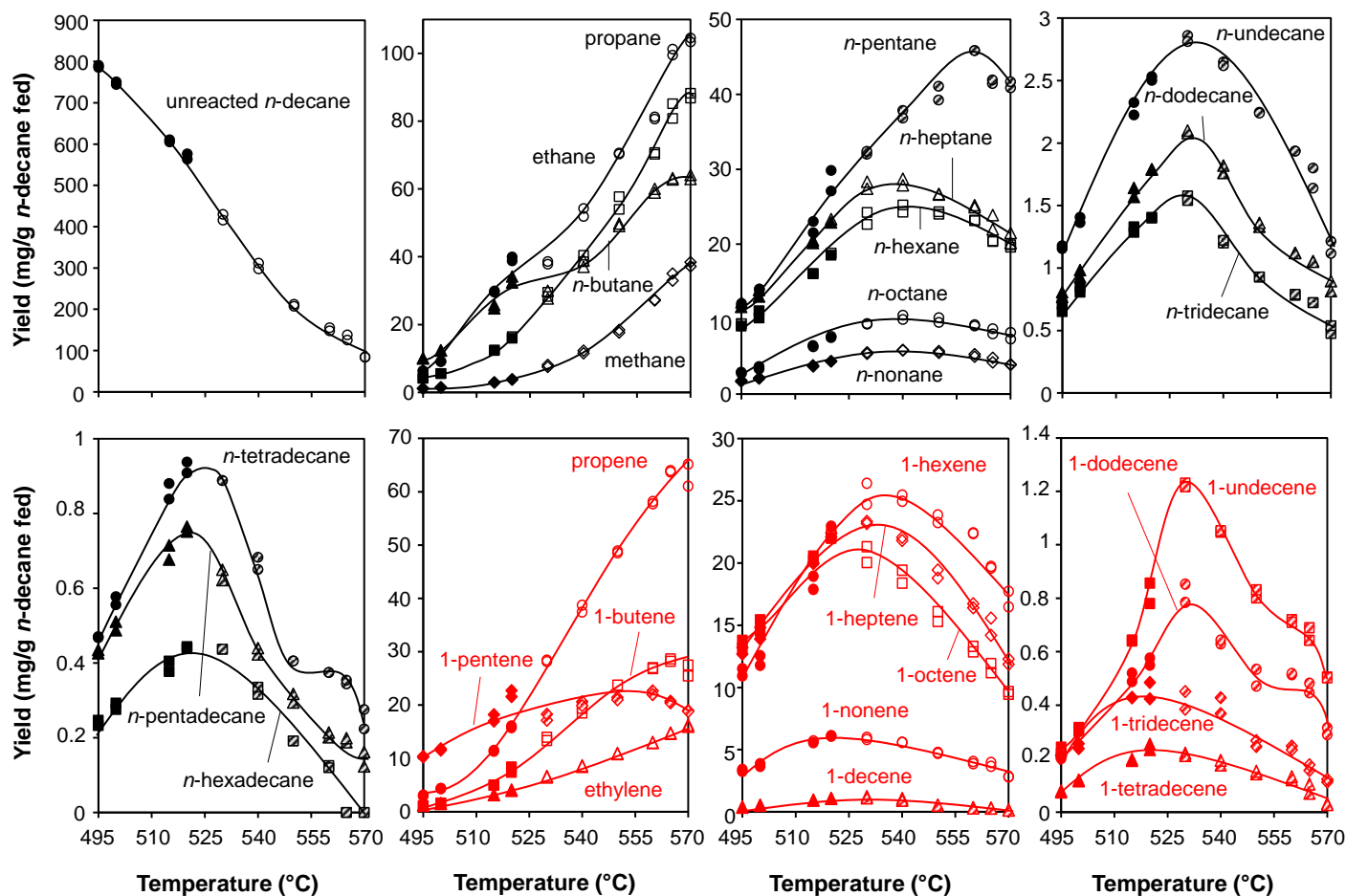


Figure 4.1 Yields, as functions of temperature, of the major straight-chain *n*-alkanes and 1-alkenes of supercritical *n*-decane pyrolysis at 94.6 atm and 133 sec. All plotted symbols are experimentally measured yields. In each panel, the black symbols represent the yields of the product *n*-alkanes; the red symbols, the 1-alkenes. *n*-Decane data from 530-570 °C comes from Kalpathy *et. al.*,<sup>19,48</sup> and *n*-decane data from 495-520 °C comes from the current work. For *n*-decane data from 530-570 °C, the open symbols represent the yields of the products quantified by Kalpathy *et. al.*,<sup>48</sup> and the semi-solid symbols represent the yields of the products quantified by Vutukuru. For *n*-decane data from 495-520 °C, the solid symbols represent the yields of the products quantified by Vutukuru.

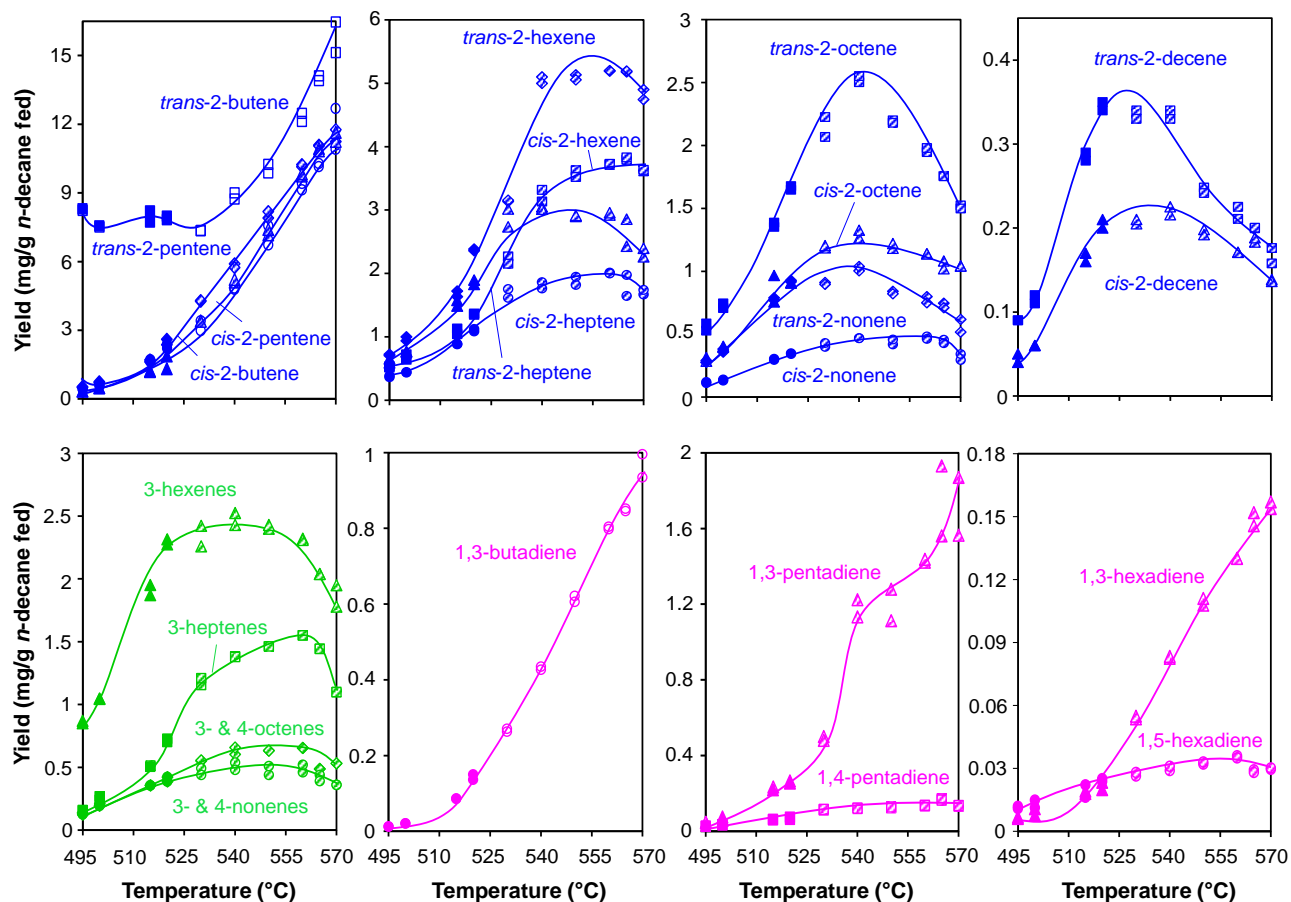


Figure 4.2. Yields, as functions of temperature, of the major straight-chain 2-alkenes, 3- & 4-alkenes, and dienes of supercritical *n*-decane pyrolysis at 94.6 atm and 133 sec. All plotted symbols are experimentally measured yields. In each panel, the blue symbols represent the yields of the product 2-alkenes; the green symbols, the 3- and/or 4-alkenes; and the pink symbols, the dienes. *n*-Decane data from 530-570 °C comes from Kalpathy *et al.*,<sup>19,48</sup> and *n*-decane data from 495-520 °C comes from the current work. For *n*-decane data from 530-570 °C, the open symbols represent the yields of the products quantified by Kalpathy *et al.*,<sup>48</sup> and the semi-solid symbols represent the yields of the products quantified by Vutukuru. For *n*-decane data from 495-520 °C, the solid symbols represent the yields of the products quantified by Vutukuru.

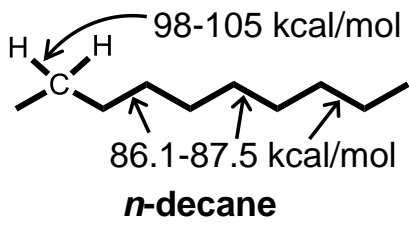
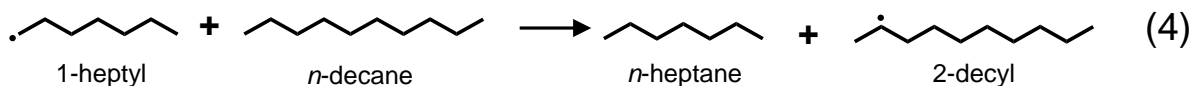
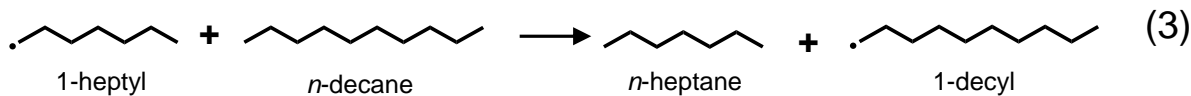
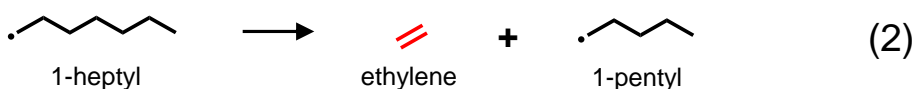


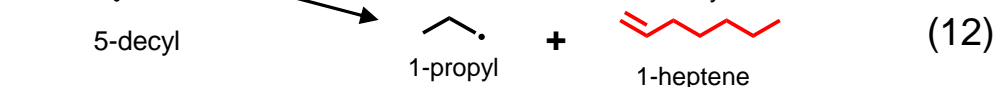
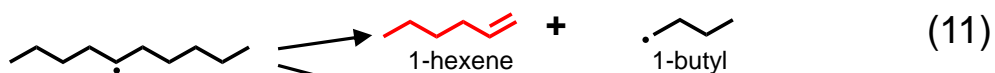
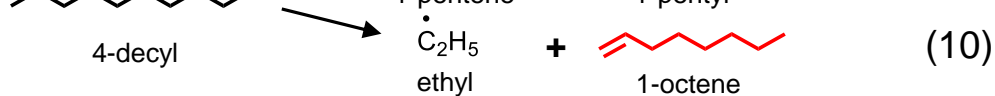
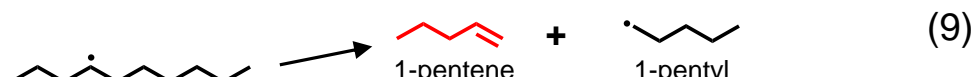
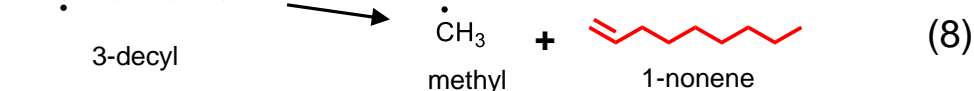
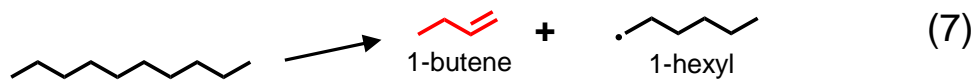
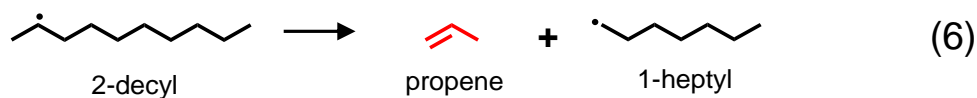
Figure 4.3. Molecular structure of *n*-decane and relevant bond-dissociation energies.<sup>38</sup>

The first step to the formation of these C<sub>1</sub>-C<sub>9</sub> *n*-alkanes and C<sub>2</sub>-C<sub>9</sub> 1-alkenes is the decomposition of *n*-decane. The structure of *n*-decane, as well as the relevant bond-dissociation energies, is shown in Figure 4.3, which reveals that the bond-dissociation energy of *n*-decane's alkyl C-C bond (86 kcal/mole<sup>38</sup>) is much lower than any of the C-H bonds. Therefore, as illustrated in Eq. (1), the dissociation of *n*-decane starts with the breaking of alkyl C-C bonds to form the corresponding 1-alkyl radicals.<sup>18,19</sup>



As discussed in chapter 1, these 1-alkyl radicals carry the pyrolytic reactions via two main pathways. The first propagation pathway, as illustrated in Eq. (2), is  $\beta$ -scission—a unimolecular decomposition pathway—in which the alkyl C-C bond situated two atoms away from the radical site is broken. This results in the formation of an olefin (as shown in red) and a 1-alkyl radical with two fewer carbon atoms (1-pentyl in this case). The second propagation pathway is intermolecular hydrogen abstraction, which is a bimolecular reaction. This pathway can proceed

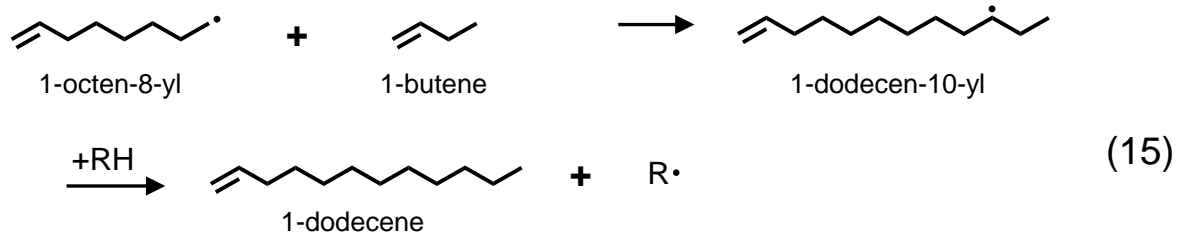
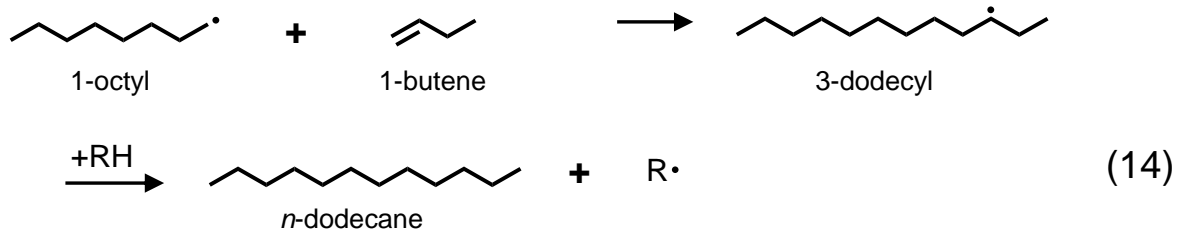
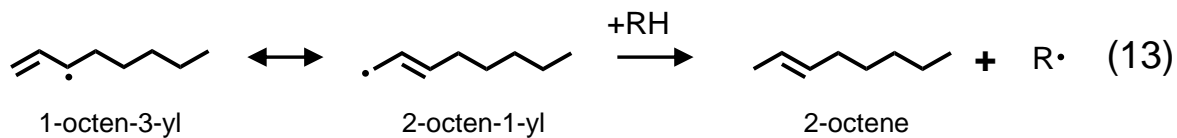
by two routes: (1) the 1-alkyl radicals, once formed, can abstract hydrogen from the 1-position of *n*-decane, as shown in Eq. (3), resulting in the formation of the corresponding *n*-alkanes and a primary decyl radical or (2) the 1-alkyl radicals can also abstract hydrogen from the 2, 3, 4, or 5 positions of *n*-decane, as exemplified by Eq. (4), resulting in the formation of the corresponding *n*-alkanes and a secondary decyl radical. Subsequently, the primary and secondary decyl radicals decompose via  $\beta$ -scission reactions, as illustrated by Eqs. (5)-(12). These  $\beta$ -scission reactions result in the production of all the C<sub>2</sub>-C<sub>9</sub> 1-alkenes (shown in red) as well as C<sub>1</sub>-C<sub>8</sub> 1-alkyl radicals (shown in black), which can further abstract hydrogen to form their respective *n*-alkanes.<sup>18,19</sup>



In addition to the C<sub>1</sub>-C<sub>9</sub> *n*-alkanes and C<sub>2</sub>-C<sub>9</sub> 1-alkenes, the supercritical *n*-decane pyrolysis experiments also produce appreciable amounts of 2-alkenes as well as *n*-alkanes and 1-alkenes of carbon number greater than ten. Since 1-alkenes are major products of *n*-decane fuel pyrolysis, Hurst *et al.*<sup>54</sup> from our research group have performed supercritical pyrolysis experiments with 1-octene as the model fuel. These experiments have revealed that 2-alkenes, as illustrated in Eq.



(13), result from the isomerization reactions of 1-alkenes.<sup>54</sup> The supercritical 1-octene pyrolysis experiments have also revealed that larger-carbon-number *n*-alkanes and 1-alkenes, as shown in Eqs. (14)-(15), result from the addition reactions between the parent alkyl radicals and 1-alkenes.

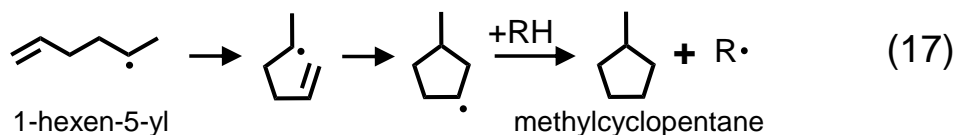
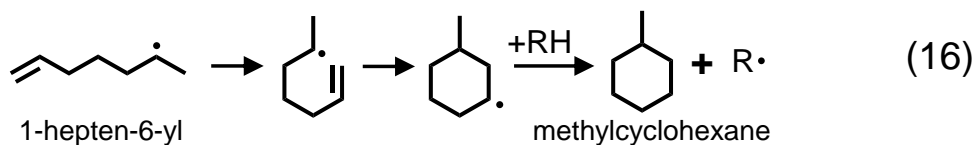


Figures 4.1 and 4.2 reveal that as temperature rises, the aliphatic-product distribution shifts from one rich in the higher-carbon-number ( $\geq C_6$ ) *n*-alkanes and 1-alkenes to one progressively rich in the lower-carbon-number ( $\leq C_4$ ) *n*-alkanes and 1-alkenes.<sup>19,54</sup> These results clearly suggest that temperature has a major role in dictating pyrolysis behavior.<sup>19</sup> The subsequent section will present the yields of the cyclic aliphatic products versus temperature and discuss the roles of these  $C_1$ - $C_9$  *n*-alkanes and  $C_2$ - $C_9$  1-alkenes in cyclic aliphatics formation.

### 4.3. Effects of Temperature on the Yields of Cyclic Aliphatic Products

Figures 4.4 and 4.5 present the yields, as functions of temperature, of newly identified cyclic aliphatic products with  $C_6$ -rings and  $C_5$ -rings, respectively. In Figures 4.4 and 4.5, all plotted symbols represent experimentally measured yields; the black symbols correspond to the

unsubstituted cyclic aliphatic products whose structures also are in black; the red symbols and structures correspond to methyl-substitute derivatives; and the blue symbols and structures correspond to ethylated or dimethylated derivatives. These cyclic aliphatic products, as reported in the literature, can be formed from the cyclization reactions of radicals of straight-chain alkenes<sup>54,68</sup> and dienes<sup>54,69</sup> as well as from addition reactions of allyl or methylallyl radicals with C<sub>2</sub>-C<sub>4</sub> alkenes or dienes.<sup>54,70</sup> In our supercritical *n*-decane pyrolysis environment, we believe that both types of reactions take place. For instance, as shown in Eq. (16), cyclization of the 1-hepten-6-yl radical in which the radical at the “6” carbon attacks the double-bond carbon at the “1” position would result in methylcyclohexane, one of the highest-yield products in Figure 4.4 at all temperatures. Analogous to Eq. (16), the cyclization of 1-hexen-5-yl radical in which the radical at the “5” carbon attacks the double-bond carbon at the “1” position, as shown in Eq. (17), would result in methylcyclopentane whose yields are presented in Figure 4.5.



The cyclization reactions of radicals of dienes<sup>54,69</sup> can result in cyclic aliphatic products that contain a double-bond within the ring. For example, as shown in the first step of Eq. (18), 1,5-hexadiene loses its hydrogen to form 1,5-hexadien-4-yl radical, which readily converts to its resonance structure, 1,4-hexadien-6-yl. This radical, as illustrated in Eq. (18), subsequently undergoes cyclization reaction and H abstraction reaction to form cyclohexene.<sup>54,70</sup>

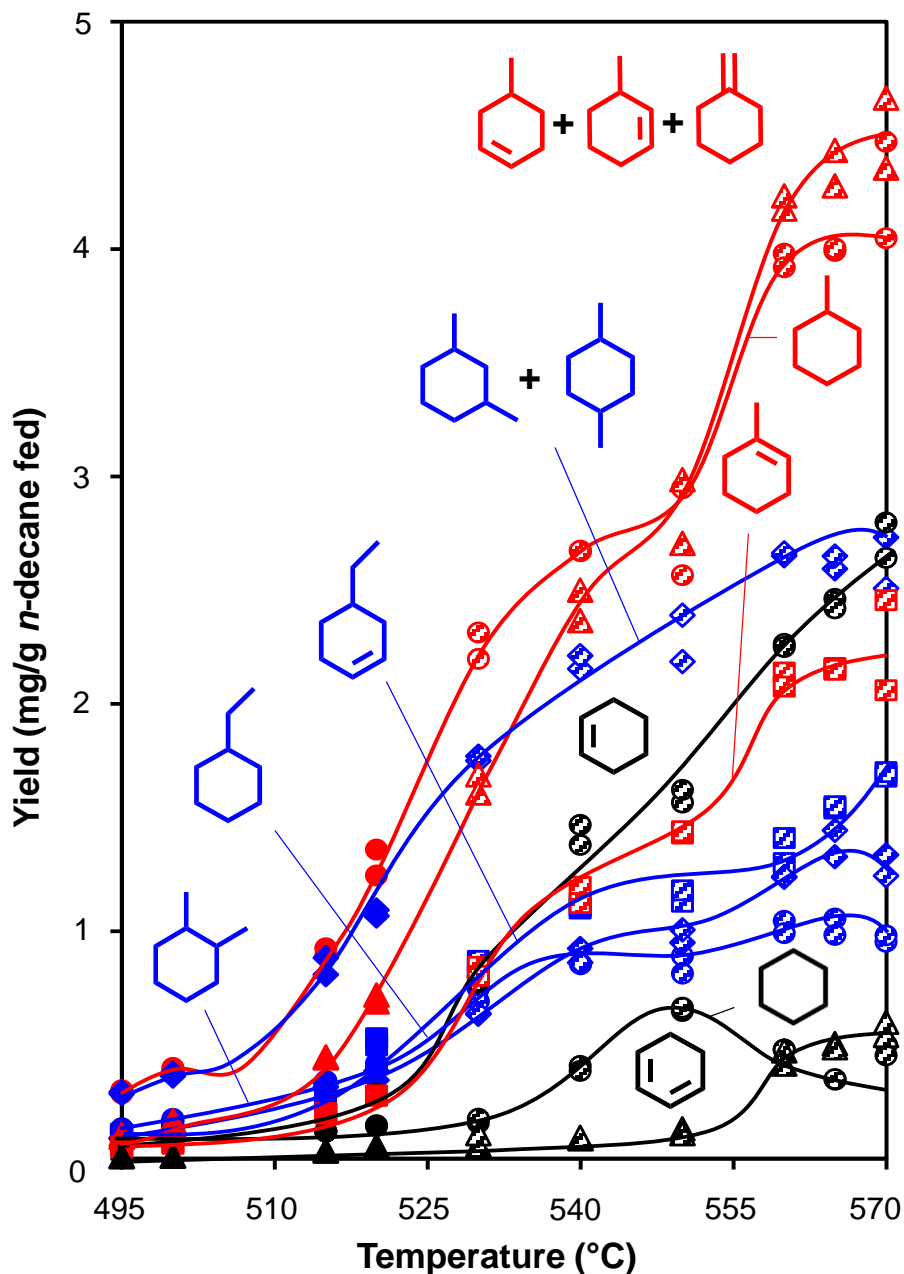


Figure 4.4. Yields, as functions of temperature, of the major C<sub>6</sub>-ring cyclic aliphatic products of supercritical *n*-decane pyrolysis at 94.6 atm and 133 sec. All plotted symbols are experimentally measured yields. The black symbols correspond to the unsubstituted cyclic aliphatic products whose structures also are in black; the red symbols and structures correspond to methyl-substituted derivatives; and the blue symbols and structures correspond to ethylated or dimethylated derivatives. *n*-Decane data from 530-570 °C comes from Kalpathy *et. al.*,<sup>19,48</sup> and *n*-decane data from 495-520 °C comes from the current work. For *n*-decane data from 530-570 °C, the open symbols represent the yields of the products quantified by Kalpathy *et. al.*,<sup>48</sup> and the semi-solid symbols represent the yields of the products quantified by Vutukuru. For *n*-decane data from 495-520 °C, the solid symbols represent the yields of the products quantified by Vutukuru.

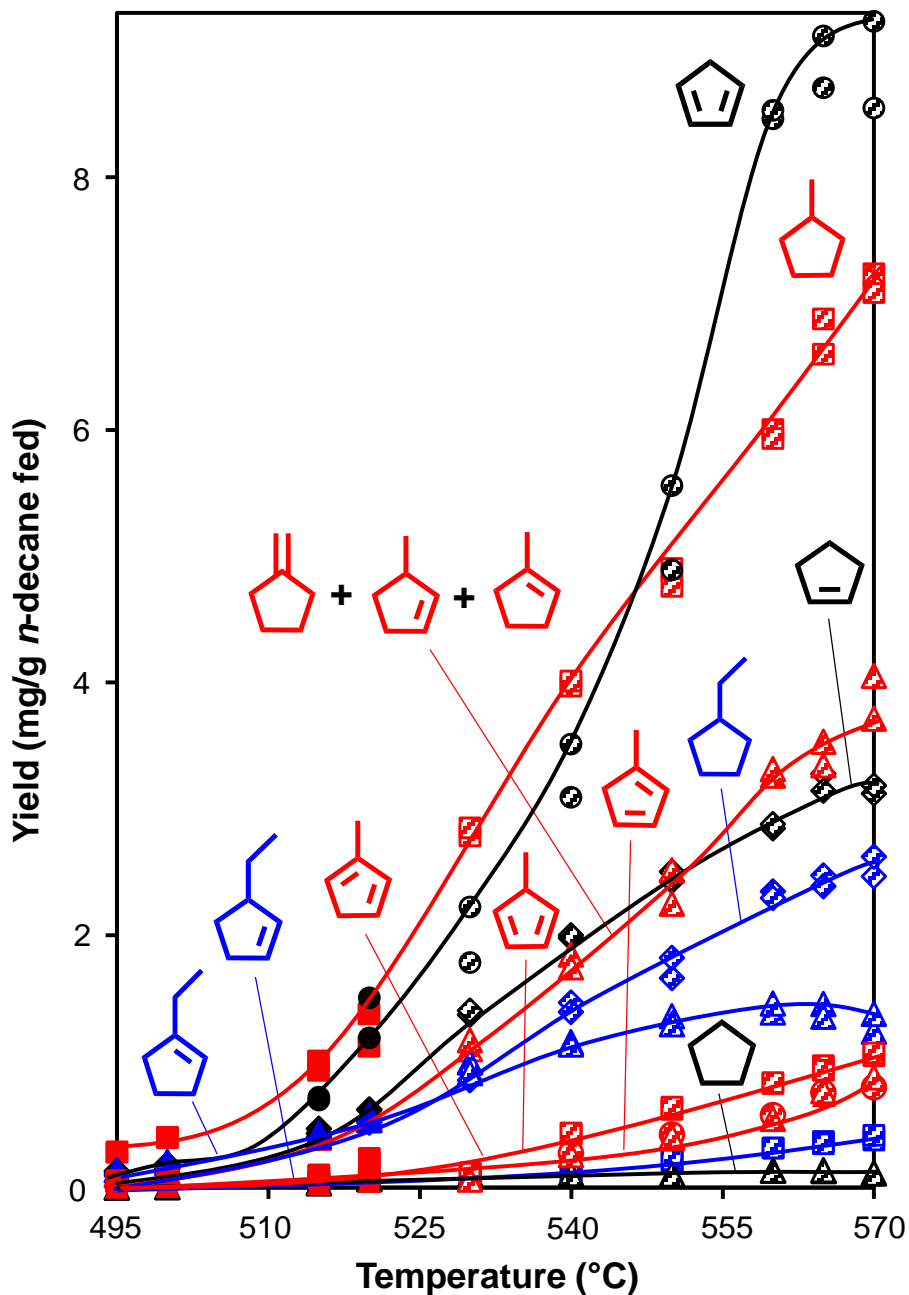
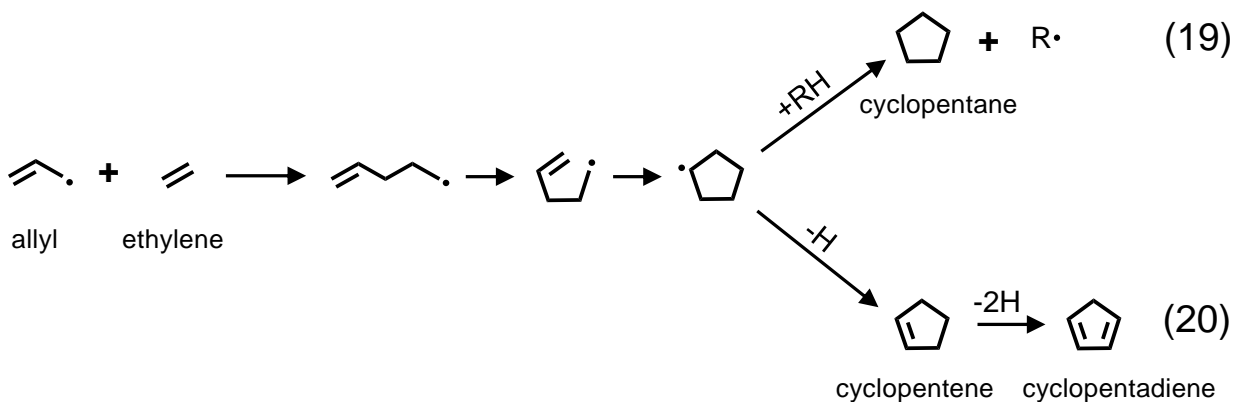
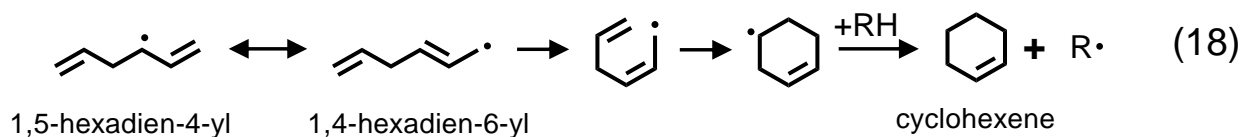


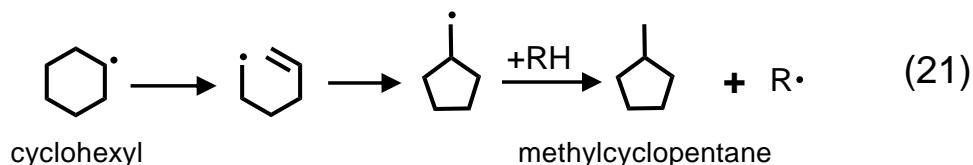
Figure 4.5. Yields, as functions of temperature, of the major C<sub>5</sub>-ring cyclic aliphatic products of supercritical *n*-decane pyrolysis at 94.6 atm and 133 sec. All plotted symbols are experimentally measured yields. The black symbols correspond to the unsubstituted cyclic aliphatic products whose structures also are in black; the red symbols and structures correspond to methyl-substituted derivatives; and the blue symbols and structures correspond to ethylated or dimethylated derivatives. *n*-Decane data from 530-570 °C comes from Kalpathy *et al.*,<sup>19,48</sup> and *n*-decane data from 495-520 °C comes from the current work. For *n*-decane data from 530-570 °C, the open symbols represent the yields of the products quantified by Kalpathy *et al.*,<sup>48</sup> and the semi-solid symbols represent the yields of the products quantified by Vutukuru. For *n*-decane data from 495-520 °C, the solid symbols represent the yields of the products quantified by Vutukuru.

The reactions of allyl and methylallyl with the smaller alkenes,<sup>54,70</sup> which are highly abundant in the supercritical *n*-decane pyrolysis environment, can also result in many of the C<sub>5</sub>-ring products in Figure 4.5. For instance, the recombination of allyl with ethylene produces a cyclopentyl radical, which can either abstract H to form cyclopentane, illustrated in Eq. (19), or can undergo dehydrogenation to form cyclopentene.<sup>54,70</sup> As illustrated in Eq. (20), cyclopentene, once formed, can further undergo dehydrogenation to form cyclopentadiene, which is one of the highest-yield products in Figure 4.5 at all temperatures. If, in Eq. (20), propene and 1-butene react with allyl, then methylcyclopentane and ethylcyclopentane would be formed, respectively. The addition reactions of allyl with propene and 1-butene<sup>70</sup> can also form cyclohexane and methylcyclohexane, respectively.



The decomposition reactions of the C<sub>6</sub>-ring cyclic aliphatics such as cyclohexane and methylcyclohexane can also contribute to methylcyclopentane and ethylcyclopentane production.<sup>54,71</sup> As illustrated in Eq. (21), cyclohexane undergoes H abstraction to form cyclohexyl,  $\beta$ -scission of this radical leads to 1-hexen-6-yl, which attacks the double-bond carbon at the

“2” position, followed by H abstraction, to form methylcyclopentane.<sup>54,71</sup> If, in Eq. (21), the starting reactant is methylcyclohexane, then ethylcyclopentane would be formed.



The supercritical *n*-decane pyrolysis experiments produce an abundance of cyclic aliphatic products. The main importance of these cyclic aliphatic products is that they can act as sources for one-ring aromatic products. The next section will present the yields, as functions of temperature, of aromatic products. The reaction mechanisms that lead to the formation of aromatic products will also be discussed.

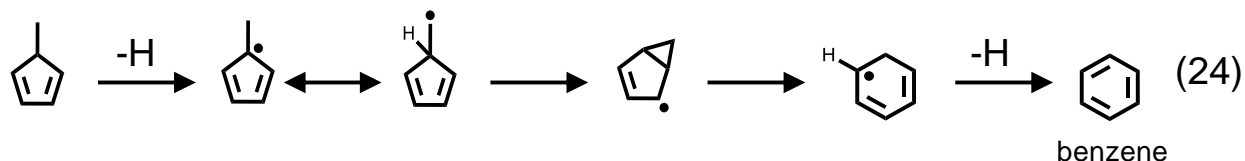
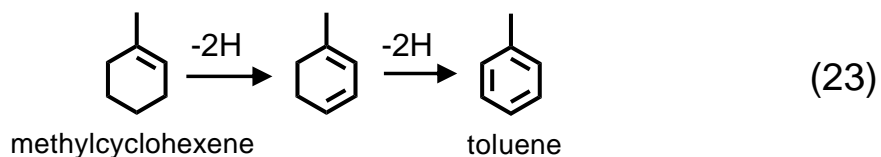
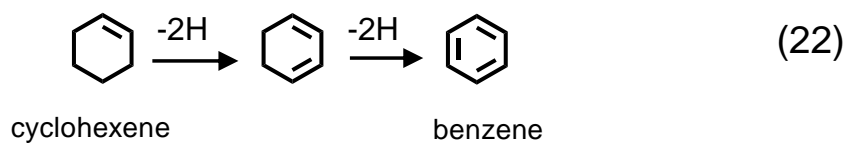
#### 4.4. Effects of Temperature on the Yields of Aromatic Products

In addition to the aliphatic products, the supercritical *n*-decane pyrolysis experiments also produce an abundance of aromatics. The names, molecular formulas, and chemical structures of the 230 quantified aromatic products are listed in Table B1 in Appendix B, along with their associated number/letter codes. Our research group<sup>19,46,47,51</sup> have identified 188 three- to nine-ring PAH and 186 of these PAH have never previously been identified as products of *n*-decane pyrolysis or combustion. Before analyzing the effects of temperature on the yields of aromatic products, it is important to note (from Table B1) that, on a mass basis, the unsubstituted PAH and their singly-methylated derivatives dominate the PAH product distribution. Table B1 further shows that highly condensed benzenoid PAH have a strong preference over isomers having internal five-membered rings, such as fluoranthene and its benzologues.<sup>19,51</sup> Having made these important observations, we will first focus on the one-ring aromatic products and their role in aromatic growth. Subsequently, the yields, as functions of temperature, of two- to nine-PAH will also be examined along with their primary routes of formation.

#### 4.4.1. Effects of Temperature on the Yields of One- and Two-Ring Aromatic Products

Figures 4.6 and 4.7 present the yields, as functions of temperature, of the one-ring aromatic products and the two-ring aromatic products, respectively. In Figures 4.6 and 4.7, all plotted symbols represent experimentally measured yields; the black symbols correspond to the unsubstituted aromatic products whose structures and number/letter codes also are in black; the red, blue, green, pink, turquoise blue, and purple symbols, number/letter codes, and structures correspond, respectively, to methyl-, ethyl- or dimethyl-, propyl- or trimethyl-, vinyl-, butyl-, and pentyl-substituted derivatives. These figures reveal that as temperatures increase, the yields of one- and two-ring aromatic products also increase.

The one-ring aromatics can be formed either from H-abstraction reactions of C<sub>6</sub>-ring cyclicaliphatics<sup>54,68,71</sup> or from ring-expansion reactions<sup>54,70</sup> of methylcyclopentadiene and dimethylcyclopentadiene. For example, as shown in Eqs. (22)-(23), cyclohexene and methylcyclohexene can undergo H abstraction to form benzene and toluene, respectively. Benzene, as illustrated in Eq. (24), can also be formed via ring expansion reaction of 5-methylcyclopentadiene.



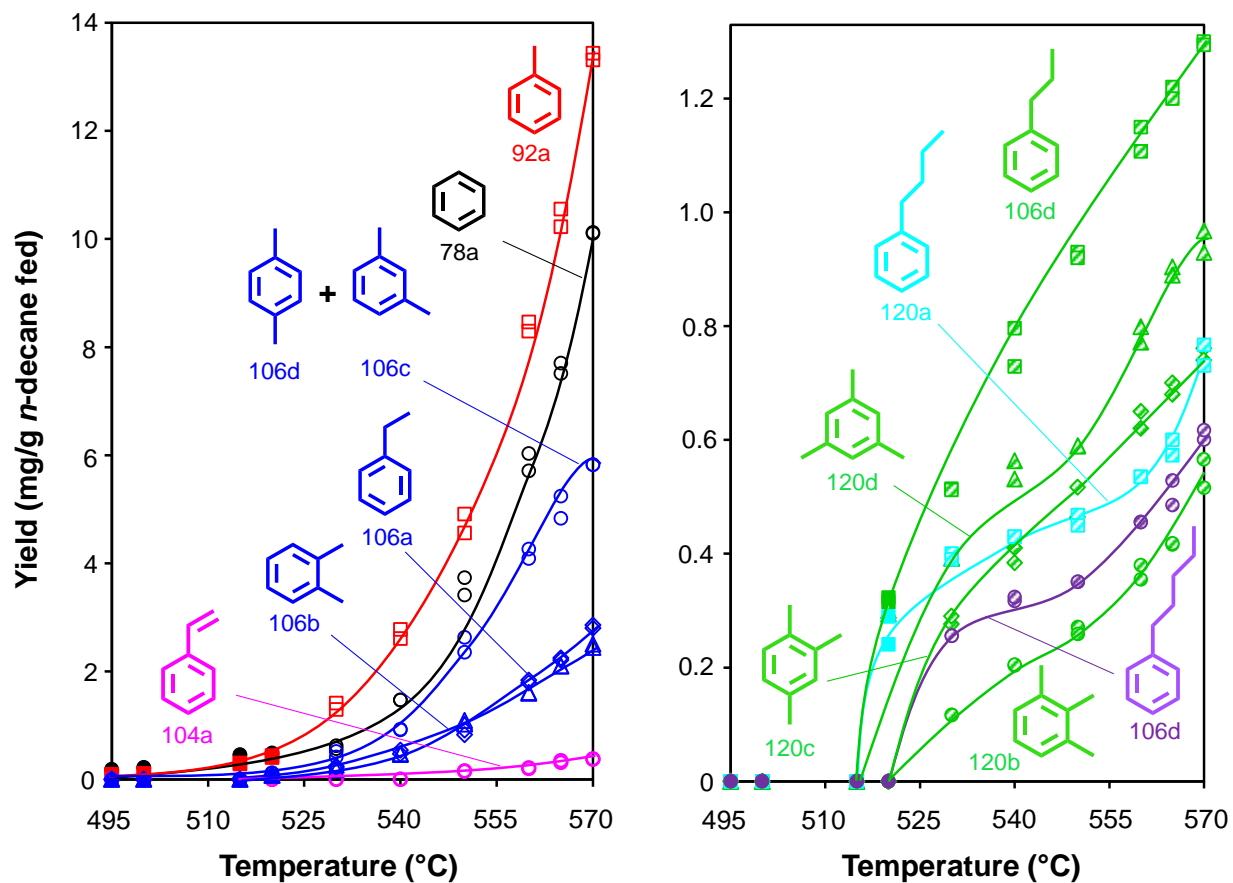


Figure 4.6. Yields, as functions of temperature, of the major one-ring aromatic products of supercritical *n*-decane pyrolysis at 94.6 atm and 133 sec. All plotted symbols are experimentally measured yields. The black symbols correspond to the unsubstituted aromatic products whose structures and number/letter codes also are in black; the red, blue, green, pink, turquoise blue, and purple symbols, number/letter codes, and structures correspond, respectively, to methyl-, ethyl- or dimethyl-, propyl- or trimethyl-, vinyl-, butyl-, and pentyl-substituted derivatives. *n*-Decane data from 530-570 °C comes from Kalpathy *et. al.*,<sup>19,48</sup> and *n*-decane data from 495-520 °C comes from the current work. For *n*-decane data from 530-570 °C, the open symbols represent the yields of the products quantified by Kalpathy *et. al.*,<sup>48</sup> and the semi-solid symbols represent the yields of the products quantified by Vutukuru. For *n*-decane data from 495-520 °C, the solid symbols represent the yields of the products quantified by Vutukuru.



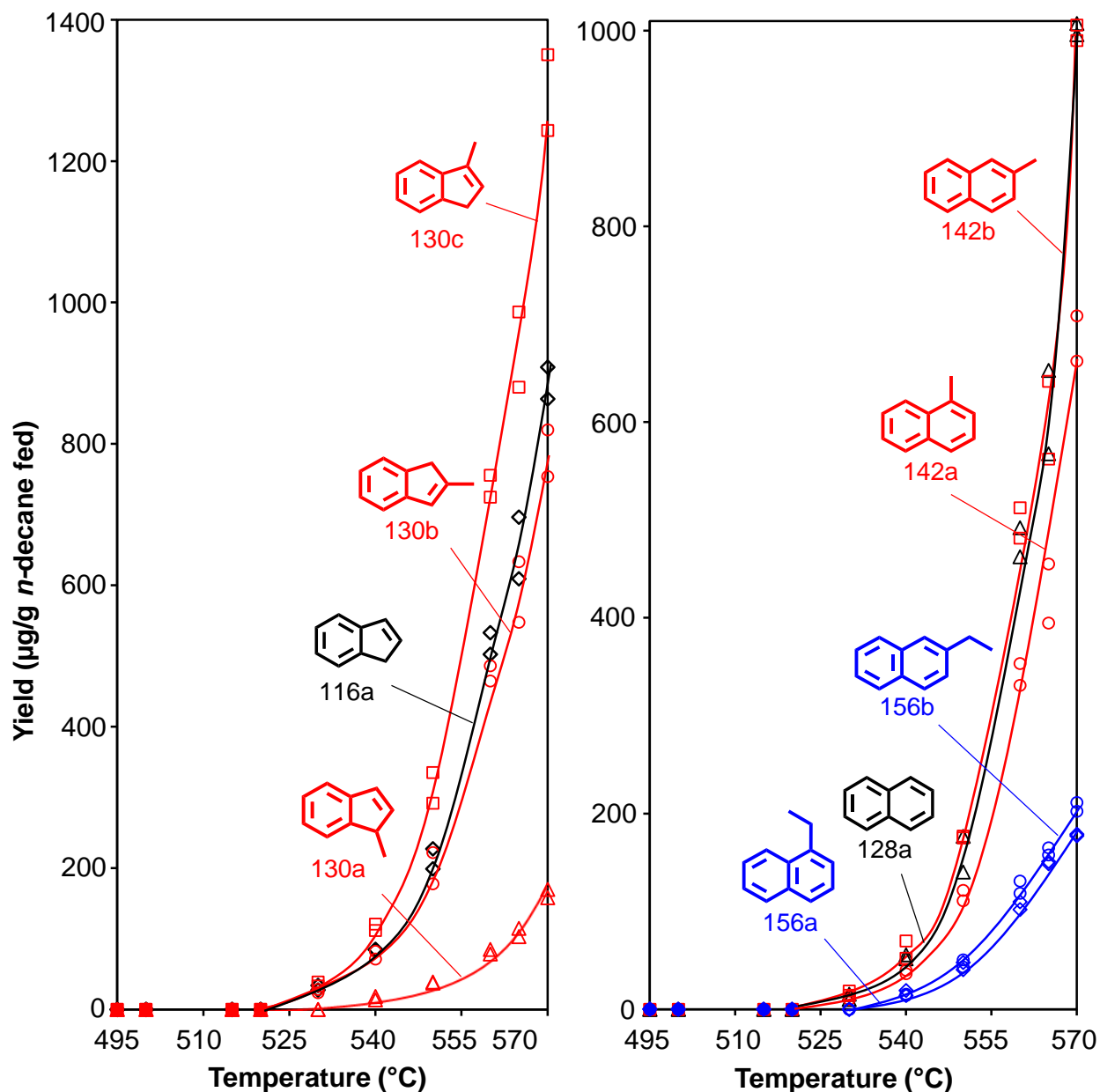
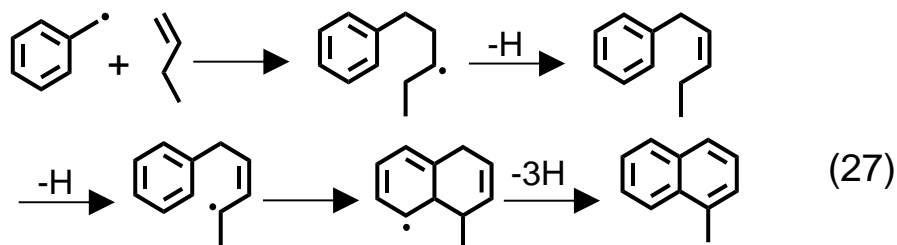
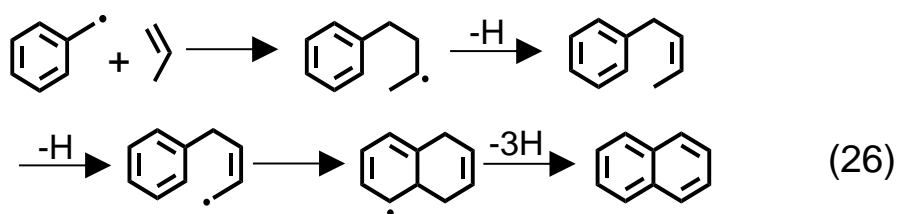
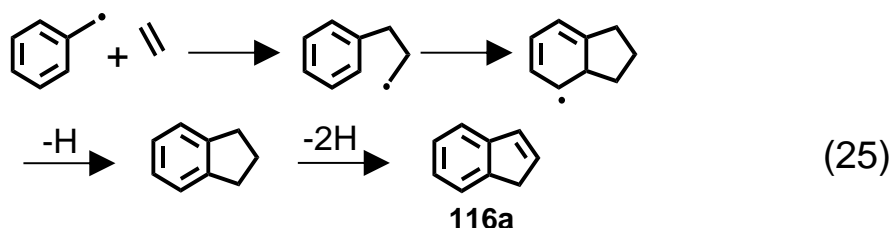


Figure 4.7. Yields, as functions of temperature, of the major two-ring aromatic products of supercritical *n*-decane pyrolysis at 94.6 atm and 133 sec. All plotted symbols are experimentally measured yields. The black symbols correspond to the unsubstituted aromatic products whose structures and number/letter codes also are in black; the red symbols, number/letter codes, and structures correspond to methylated derivatives; and the blue symbols, number/letter codes, and structures correspond to ethylated or dimethylated derivatives. *n*-Decane data from 530-570 °C comes from Kalpathy *et al.*,<sup>19,48</sup> and *n*-decane data from 495-520 °C comes from the current work. For *n*-decane data from 530-570 °C, the open symbols represent the yields of the products quantified by Kalpathy *et al.*,<sup>48</sup> and the semi-solid symbols represent the yields of the products quantified by Vutukuru. For *n*-decane data from 495-520 °C, the solid symbols represent the yields of the products quantified by Vutukuru.

The one-ring aromatic<sup>54,68-71</sup> products of supercritical *n*-decane pyrolysis can also be formed from the cyclization reactions of radicals of straight-chain alkenes as well as from addition reactions of allyl or methylallyl radicals with C<sub>2</sub>-C<sub>4</sub> 1-alkenes.<sup>70</sup>

The one-ring aromatic products, once formed, act as a jumping off point for PAH growth by producing resonantly stabilized radicals.<sup>61</sup> The benzylic C—H bond dissociation energy for toluene is around 88 kcal/mol,<sup>38</sup> and the benzylic C—C bond dissociation energies for *n*-alkylbenzenes are around 75 kcal/mol.<sup>38</sup> Therefore, the facile scission of the benzylic C—H bond or C—C bonds leads to the formation of the resonance-stabilized benzyl radical. The benzyl radical, as shown in Eqs (25)-(27), can readily react with C<sub>2</sub>-C<sub>4</sub> 1-alkenes, which are highly abundant in the supercritical *n*-decane pyrolysis environment, to form two-ring aromatics.<sup>59</sup>



To investigate the growth behaviors of two-ring aromatics in the supercritical pyrolysis *n*-alkane pyrolysis environment, Kalpathy *et al.*<sup>49</sup> from our research group have performed supercritical pyrolysis experiments with the model fuel *n*-decane, to which 2-methylnaphthalene and 1-methylnaphthalene, two two-ring products of *n*-decane pyrolysis, were added, in separate experiments, as dopants. These methyl-aromatic dopant experiments revealed the primary routes for PAH growth,<sup>49</sup> which will be explained in the subsequent section.

#### 4.4.2. Effects of Temperature on the Yields of Polycyclic Aromatic Hydrocarbons (PAH)

Figure 4.8 presents the yields, as functions of temperature, of selected benzenoid aromatic products produced from the supercritical *n*-decane pyrolysis experiments conducted at 94.6 atm and 133 sec: 3-ring PAH, in Figure 4.8a; 4-ring PAH, in Figure 4.8b; 5-ring PAH, in Figure 4.8c; 5-ring C<sub>22</sub>H<sub>14</sub> PAH, in Figure 4.8d; 6-ring PAH, in Figure 4.8e; 7-ring PAH, in Figure 4.8f; 8-ring PAH, in Figure 4.8g; and 9-ring PAH, in Figure 4.8h. Figure 4.8 shows that only the lowest-ring-number aromatic products are present at the lowest pyrolysis temperatures, with the formation of the highest-ring-number PAH becoming substantial only at the highest temperatures.<sup>48</sup> Figure 4.8 further shows that the slopes of the yield-vs-temperature plots rise as the number of aromatic rings increases. All of these observations indicate that, in the supercritical *n*-decane pyrolysis environment, the PAH growth occurs through a series of addition reactions.<sup>48</sup>

To elucidate the reaction mechanisms responsible for the formation and growth of PAH in the supercritical pyrolysis *n*-alkane pyrolysis environment, Kalpathy *et al.*<sup>49,50</sup> have conducted supercritical *n*-decane pyrolysis experiments with and without the methylnaphthalene and methylphenanthrene dopants. These methyl-aromatic dopant experiments<sup>49,50</sup> have revealed that, in supercritical *n*-decane-pyrolysis environment, aromatic-ring growth is mostly accomplished through a series of reactions involving C<sub>2</sub>-C<sub>4</sub> 1-alkene additions to resonance-stabilized arylmethyl

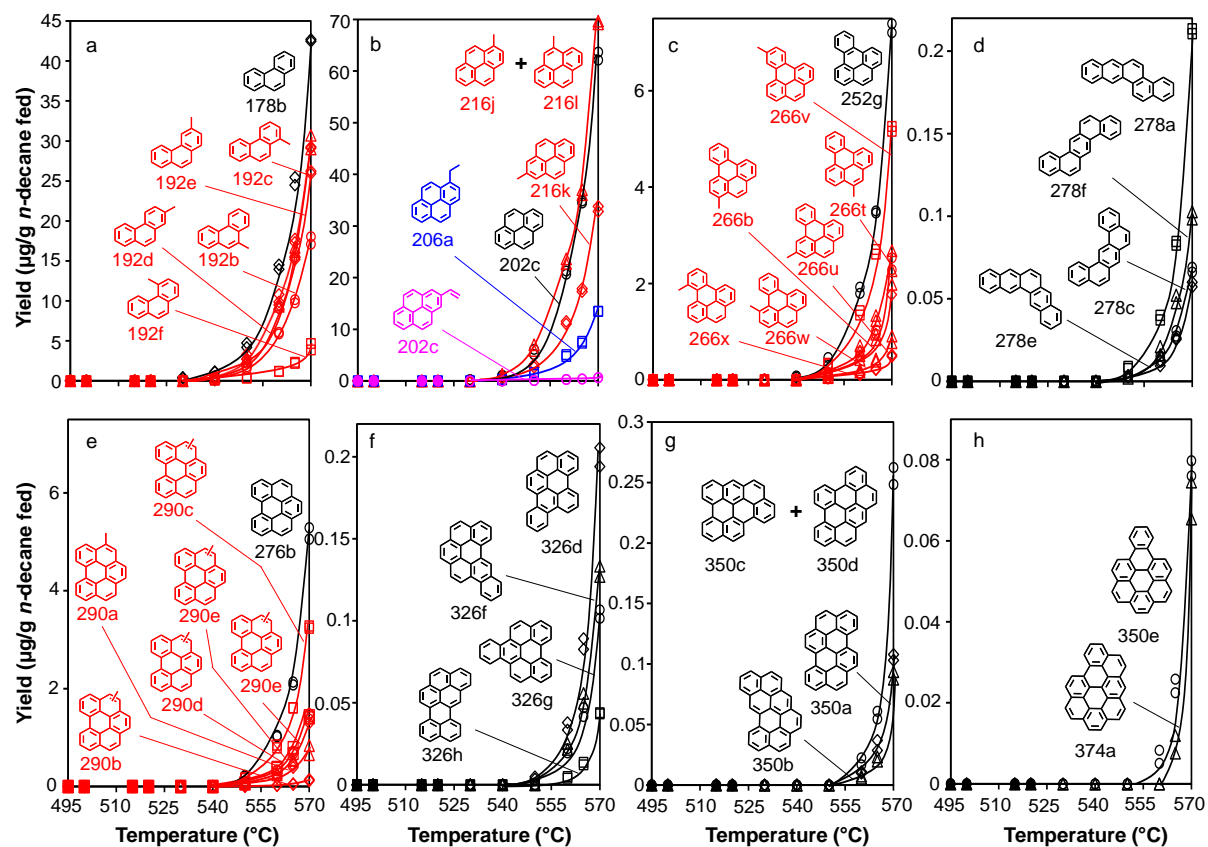


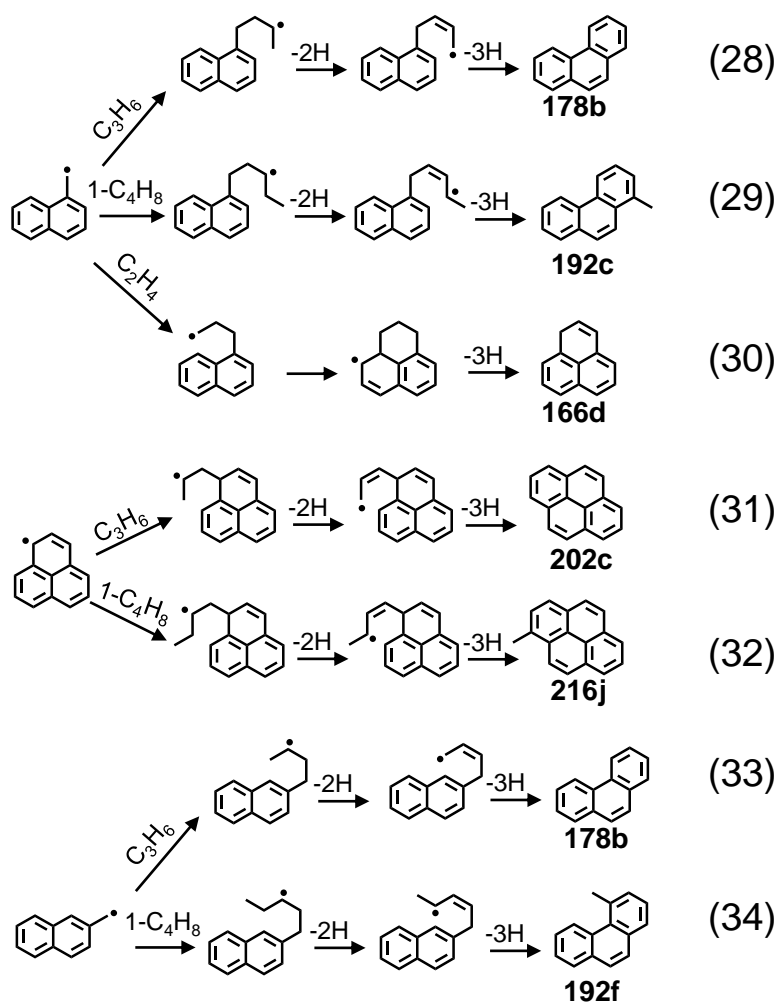
Figure 4.8. Yields, as functions of temperature, of selected benzenoid PAH products produced from the supercritical *n*-decane pyrolysis experiments conducted at 94.6 atm and 133 sec: (a) 3-ring PAH; (b) 4-ring PAH; (c) 5-ring PAH; (d) 5-ring C<sub>22</sub>H<sub>14</sub> PAH; (e) 6-ring PAH; (f) 7-ring PAH; (g) 8-ring PAH; and (h) 9-ring PAH. All plotted symbols are experimentally measured yields. The black symbols correspond to the unsubstituted aromatic products whose structures and number/letter codes also are in black; the red, blue, and pink symbols, number/letter codes, and structures correspond, respectively, to methyl-, ethyl- or dimethyl-, and vinyl-substituted derivatives. *n*-Decane data from 530-570 °C comes from Kalpathy *et al.*,<sup>19,48</sup> and *n*-decane data from 495-520 °C comes from the current work. For *n*-decane data from 530-570 °C, the open symbols represent the yields of the products quantified by Kalpathy *et al.*,<sup>48</sup> and the semi-solid symbols represent the yields of the products quantified by Vutukuru. For *n*-decane data from 495-520 °C, the solid symbols represent the yields of the products quantified by Vutukuru.

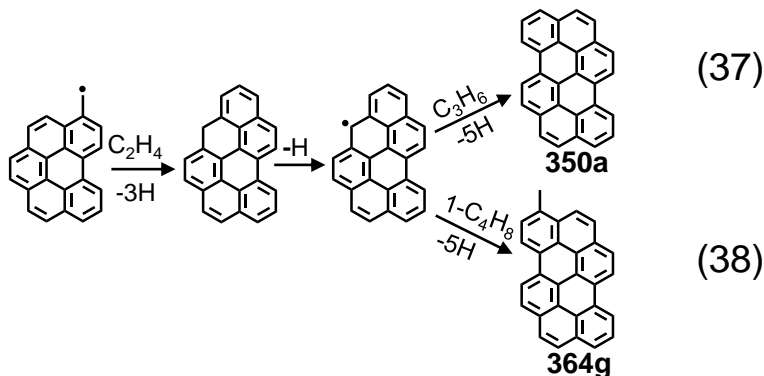
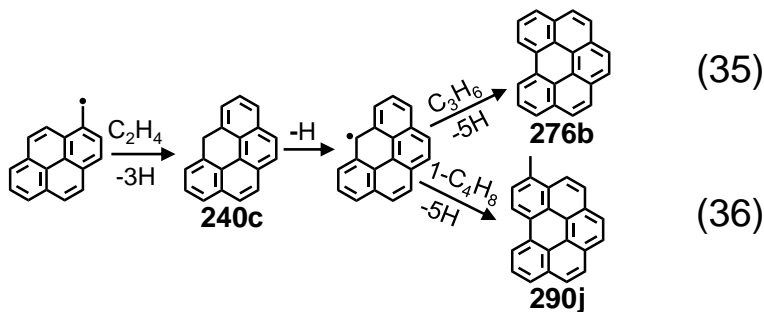
radicals and phenalenyl-type radicals.<sup>19</sup> This arylmethyl/phenalenyl/1-alkene mechanism accounts for most of the favored three- to eight-ring benzenoid PAH products of supercritical *n*-decane pyrolysis.<sup>19</sup> As a result, the main arylmethyl/1-alkene and phenalenyl/1-alkene reactions will be investigated separately.<sup>54</sup>

Equations (28)-(30) show that 1-naphthylmethyl, the resonance-stabilized arylmethyl radical of 1-methylnaphthalene (142a), reacts with propene, 1-butene, and ethylene, respectively, to make phenanthrene (178b), 1-methylphenanthrene (192c), and phenalene (166d). Phenalene (166d), once formed, readily loses its hydrogen at the methylene carbon (C-H bond-dissociation energy, 74 kcal/mole<sup>38</sup>) and forms resonance-stabilized phenalenyl radical. Eqs. (31) and (32) show that phenalene's resonance-stabilized radical phenalenyl reacts with propene and 1-butene to make pyrene (202c) and 1-methylpyrene (216j), respectively. Equations (33)-(34) show that 2-naphthylmethyl, the resonance-stabilized arylmethyl radical of 2-methylnaphthalene (142b), reacts with propene and 1-butene to form phenanthrene (178b) and 4-methylphenanthrene (192f), respectively. However, due to the position of its methyl group, 2-methylnaphthalene<sup>49</sup> does not form phenalene. Therefore, 2-methylnaphthalene's growth virtually terminates with the formation of phenanthrene, which is a stable three-ring PAH.

As illustrated in Eqs. (35)-(36), 1-pyrenylmethyl, the resonance-stabilized arylmethyl radical of 1-methylpyrene (216j), reacts with ethylene to form 6*H*-benzo[*cd*]pyrene (240c), whose resonance-stabilized phenalenyl-type radical reacts with propene and 1-butene, respectively, to make benzo[*ghi*]perylene (276b) and 5-methylbenzo[*ghi*]perylene (290d).<sup>54</sup> The resonance-stabilized arylmethyl radical of 5-methylbenzo[*ghi*]perylene then goes through a similar sequence in Eqs. (37) and (38) to form benzo[*pqr*]naphtho[8,1,2-*bcd*]perylene (350a) and its methylated derivative, 3-methylbenzo[*pqr*]naphtho[8,1,2-*bcd*]perylene (364g). Some of the 5- and 7-ring

PAH products of Figure 4.8—benzo[*e*]pyrene (252g), 3-methylbenzo[*e*]pyrene (266b), and dibenzo[*e,ghi*]perylene (326d)—result from an analogous sequence<sup>49,50</sup> of reactions, which starts with 1-phenanthrylmethyl, the arylmethyl radical of 1-methylphenanthrene (methyl-aromatic-dopant previously investigated by our research group).<sup>54</sup> This reaction sequence<sup>49,50</sup> involves the phenalenyl-type radical of 7*H*-benz[*de*]anthracene (216b). Reactions of arylmethyl radicals<sup>49,50</sup> with other arylmethyl radicals and methyl-aromatic molecules account for most of the remaining minor four- to seven-ring benzenoid PAH products such as 5-ring C<sub>22</sub>H<sub>14</sub> PAH (as illustrated in Figure 4.8d).





#### 4.5. Concluding Remarks

To better understand the reaction pathways that govern PAH formation and growth in the supercritical fuel pyrolysis environment, Kalpathy *et al.*<sup>48</sup> from our research group performed supercritical pyrolysis experiments in a silica-lined stainless-steel tubular flow reactor with the model fuel *n*-decane (critical temperature, 344.5 °C; critical pressure 20.7 atm), an *n*-alkane component of jet fuels,<sup>18,19</sup> at a constant pressure of 94.6 atm, a fixed residence time of 133 sec, and at six temperatures ranging from 530 to 570 °C.<sup>48</sup> Since *n*-alkanes are major components of jet fuels and are known to be particularly problematic regarding solids formation, Kalpathy *et al.*<sup>48</sup> chose to investigate an *n*-alkane. The strong temperature dependence of the product yields revealed that temperature has a strong influence on the supercritical pyrolysis behavior of *n*-decane.<sup>48</sup> Therefore, to complement the previous *n*-decane pyrolysis work at 94.6 atm, 133 sec, and at six temperatures in the range of 530-570 °C, we have performed additional supercritical *n*-decane pyrolysis experiments<sup>54</sup> at lower temperatures. These experiments have been performed

in the same silica-lined stainless-steel tubular reactor at 94.6 atm, 133 sec, and at four temperatures: 495, 500, 515, 520 °C. The lowest temperature (495 °C) corresponds to the minimum temperature at which appreciable fuel conversion (21%) takes place.

The supercritical *n*-decane pyrolysis experiments produce a multitude of products both in the gas-phase as well as the liquid-phase. The aliphatic and one- and two-ring aromatic products are analyzed by gas chromatography (GC) coupled with mass spectrometry (MS).<sup>18,19,61</sup> The PAH products are a highly complex mixture of unsubstituted and alkylated PAH. So, the highly complex PAH product mixture is separated by a two-dimensional high-pressure liquid chromatographic (HPLC) technique, and the PAH products are subsequently characterized, isomer specifically, by ultraviolet-visible (UV) diode-array detection (DAD) and mass spectrometry (MS).<sup>19,46,47</sup> Reaction product analyses have led to the identification and quantification of 62 new products, which include 22 straight-chain aliphatics, 26 cyclic aliphatics, 10 one-ring aromatics, and 4 PAH from four- to seven-rings.

The yields of the major products, including newly identified aliphatic and one-ring aromatic products, have been plotted as functions of temperature. These plots reveal that C<sub>1</sub>-C<sub>9</sub> *n*-alkanes and C<sub>2</sub>-C<sub>9</sub> 1-alkenes are the highest-yield products of supercritical *n*-decane pyrolysis at all temperatures investigated; 2-alkenes as well as *n*-alkanes and 1-alkenes of carbon number greater than ten are also produced in appreciable amounts.<sup>48,54</sup> These plots also reveal that as temperature rises, the aliphatic-product distribution shifts from one rich in the higher-carbon-number ( $\geq$  C<sub>6</sub>) *n*-alkanes and 1-alkenes to one progressively rich in the lower-carbon-number ( $\leq$  C<sub>4</sub>) *n*-alkanes and 1-alkenes.<sup>19,48,54</sup>

The first step to the formation of these C<sub>1</sub>-C<sub>9</sub> *n*-alkanes and C<sub>2</sub>-C<sub>9</sub> 1-alkenes is the decomposition of *n*-decane. The bond-dissociation energy of *n*-decane's alkyl C-C bond (86



kcal/mole<sup>38</sup>) is much lower than any of the C-H bonds. Therefore, the dissociation of *n*-decane starts with the breaking of alkyl C-C bonds to form the corresponding C<sub>1</sub> to C<sub>9</sub> 1-alkyl radicals. Each of these 1-alkyl radicals carry the pyrolytic reactions by abstracting hydrogen from *n*-decane to produce corresponding *n*-alkanes and primary or secondary decyl radicals.<sup>19</sup> The decyl radicals, as well as other straight-chain alkyl radicals with more than three carbon atoms, undergo  $\beta$ -scission reactions to produce C<sub>2</sub> to C<sub>9</sub> 1-alkenes.<sup>19</sup> The isomerization reactions of 1-alkenes<sup>54,61</sup> result in the formation of 2-alkenes. Larger-carbon-number *n*-alkanes and 1-alkenes can be produced by the addition reactions between the parent alkyl radicals and 1-alkenes.<sup>19,54,61</sup>

The supercritical *n*-decane pyrolysis experiments also produce an abundance of cyclic aliphatic products with C<sub>5</sub>-rings and C<sub>6</sub>-rings. These cyclic aliphatic products can be formed from the cyclization reactions of radicals of straight-chain alkenes<sup>54,61,69</sup> as well as from addition reactions of allyl or methylallyl radicals with C<sub>2</sub>-C<sub>4</sub> 1-alkenes.<sup>54,61,70</sup>

Besides the aliphatic products, the supercritical *n*-decane pyrolysis experiments also produce an abundance of one-ring aromatics as well as two- to nine-ring PAH—many of which are methyl-substituted. At all temperatures investigated, GC-MS analysis of the reaction products reveal that benzene and toluene are the main one-ring aromatic products. The two-ring aromatic products are formed only at temperatures greater than 530 °C. Analyses of reaction products reveal that indene, methyl-substituted indenenes, naphthalene, and methylated naphthalenes are the dominant two-ring aromatic products.<sup>19</sup>

The one-ring aromatics can be formed from the cyclization reactions of radicals of straight-chain alkenes<sup>54,69</sup> as well as from addition reactions of allyl or methylallyl radicals with C<sub>2</sub>-C<sub>4</sub> alkenes.<sup>54,70</sup> One-ring aromatics can also be formed either from ring-expansion reactions of C<sub>5</sub>-cyclic aliphatics or from H-abstraction reactions of C<sub>6</sub>-cyclic aliphatics. The one-ring aromatic

products, once formed, act as a jumping-off point for PAH growth by producing resonantly stabilized radicals,<sup>61</sup> which readily react with C<sub>2</sub>-C<sub>4</sub> 1-alkenes to form two-ring aromatics.<sup>59</sup>

Due to an abundance of methyl-substituted PAH, the arylmethyl radicals are predicted to be plentiful in the supercritical *n*-decane pyrolysis environment.<sup>19</sup> To understand the potential role of arylmethyl radicals in the supercritical *n*-alkane pyrolysis environment, Kalpathy *et al.*<sup>49,50</sup> performed supercritical *n*-decane pyrolysis experiments with three methyl-aromatic dopants: 1-methylnaphthalene, 2-methylnaphthalene, and 1-methylphenanthrene.

Previous *n*-decane experiments by Kalpathy *et al.*<sup>49,50</sup> with the methyl-aromatic dopants—1-methylnaphthalene, 2-methylnaphthalene, and 1-methylphenanthrene—showed that, in the supercritical-*n*-decane-pyrolysis environment, aromatic-ring growth occurs primarily through a series of reactions involving C<sub>2</sub>-C<sub>4</sub> 1-alkene additions to resonance-stabilized arylmethyl radicals and phenalenyl-type radicals.<sup>19,61</sup> Most of the three- to eight-ring benzenoid PAH products of supercritical *n*-decane pyrolysis are accounted for by this arylmethyl/phenalenyl/1-alkene pathway.<sup>19</sup>

The dopant experiments of Kalpathy *et al.*<sup>49,50</sup> also showed that the position of the methyl substituent on the aromatic structure plays a significant role in PAH growth.<sup>49,50,51</sup> Specifically, the arylmethyl radicals resulting from methylaromatics<sup>19,49,50</sup> in which the methyl group is attached to a carbon adjacent to a “valley” carbon (for example 1-methylnaphthalene and 1-methylphenanthrene) are particularly effective in promoting PAH growth. Contrary to this, arylmethyl radicals formed by methylaromatics in which the methyl group is not attached to a carbon adjacent to a “valley” carbon (2-methylnaphthalene) are not nearly as effective as PAH growth agents.<sup>19</sup>

Besides the two types of methyl-substituted PAH exemplified by the dopants—1-methylnaphthalene, 2-methylnaphthalene, and 1-methylphenanthrene—the supercritical *n*-decane pyrolysis also forms a third type of methyl-substituted PAH, whose methyl group is in a bay region of the PAH structure.<sup>51</sup> The subsequent chapters will report the growth reactions of bay-region methyl-substituted PAH in the supercritical *n*-decane fuel-pyrolysis environment.

## Chapter 5. Reaction Pathways of Molecular Growth for Bay-Region Methyl-Substituted Polycyclic Aromatic Hydrocarbons During Supercritical Pyrolysis of *n*-Decane, as Determined from Experiments with 4-Methylchrysene Dopant

### 5.1. Introduction

In addition to their role as propellants, fuels in future high-speed aircraft will need to serve as cooling agents for the aircraft—experiencing, in the fuel lines, temperatures and pressures predicted to be as high as 700 °C and 130 atm<sup>1,5</sup> for times on the order of minutes. Such conditions, supercritical for most hydrocarbons, cause the fuel to undergo pyrolytic reactions<sup>1,8</sup> that can lead to polycyclic aromatic hydrocarbons (PAH) and eventually carbonaceous solids, which can clog fuel lines and nozzles, threatening aircraft operation. Critical to the design of fuel-delivery systems that avoid this threat is an understanding of the chemical-reaction mechanisms responsible for PAH formation and growth in the supercritical fuel-pyrolysis environment.

Of the many components in jet fuels, *n*-alkanes are particularly problematic with regard to solids formation under supercritical pyrolysis conditions.<sup>1</sup> Several of our investigations<sup>18,19</sup> therefore have focused on the model fuel *n*-decane, whose supercritical pyrolysis produces an abundance of aliphatics, particularly *n*-alkanes and 1-alkenes, as well as one-ring aromatics and two- to nine-ring PAH—many of which are methyl-substituted.

To investigate the mechanisms responsible for the formation and growth of these PAH, Kalpathy *et al.*<sup>49,50</sup> have conducted supercritical *n*-decane pyrolysis experiments to which lower-ring-number PAH that are representative of *n*-decane's aromatic products are added as dopants. These doping experiments performed by Kalpathy *et al.*<sup>49,50</sup> have revealed that at the temperatures of our experiments ( $\leq 700$  °C), the aromatic carbon-carbon bond does not break, so only aromatic

---

This chapter originally appeared as K. Vutukuru, A.R. Mali, and M.J. Wornat “*Proceedings of the Combustion Institute*” 38 (2021), 1355-1364.

products of the same or higher ring number as the dopant are formed by the dopant, providing a means for discerning the pathways for that specific aromatic dopant's growth.<sup>49,50</sup>

Previous *n*-decane experiments by Kalpathy *et al.*<sup>49,50</sup> with the first three dopants of Figure 5.1—1-methylnaphthalene, 2-methylnaphthalene, and 1-methylphenanthrene—have revealed<sup>49,50</sup> that the molecular growth of these methyl-substituted PAH occurs principally through the reactions of the respective arylmethyl radicals (formed by removal of a methyl hydrogen) with four aliphatic species abundantly present in the supercritical *n*-decane pyrolysis environment: methyl, ethylene, propene, and 1-butene.

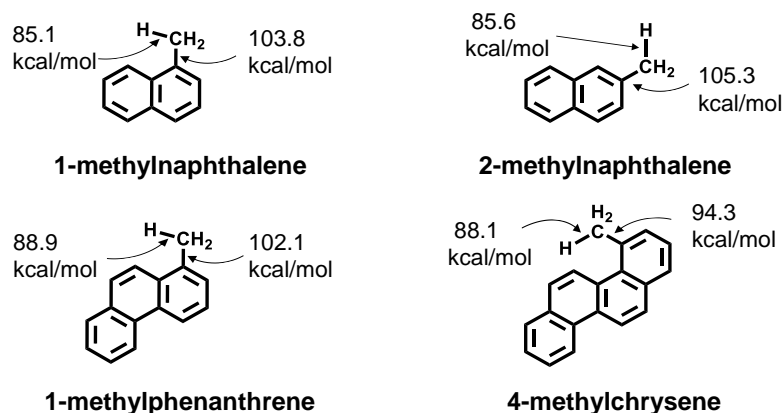


Figure 5.1. Molecular structures of 1-methylnaphthalene, 2-methylnaphthalene, 1-methylphenanthrene, and 4-methylchrysene and relevant bond-dissociation energies.<sup>38,52</sup>

Those doping experiments<sup>49,50</sup> have also shown that the position of the methyl substituent on the aromatic structure plays a major role in PAH growth. For 2-methylnaphthalene, whose methyl group is located far from a neighboring ring, molecular growth is virtually limited to the three-ring PAH formed by 2-naphthylmethyl's reactions with methyl and the C<sub>2</sub>-C<sub>4</sub> 1-alkenes. However, for 1-methylnaphthalene and 1-methylphenanthrene—whose methyl groups are each attached to a carbon adjacent to a “valley” carbon of the aromatic structure—reaction of their arylmethyl radicals with ethylene produces non-fully aromatic PAH whose readily-formed, resonance-stabilized phenalenyl-type radicals initiate chain reactions that lead to high-ring-

number PAH.<sup>49,50</sup> In addition to the two types of methyl-PAH exemplified by the first three dopants of Figure 5.1, the seven product structures of Figure 5.2 reveal that supercritical *n*-decane pyrolysis also produces a third type of methyl-PAH, whose methyl group is in a bay region of the PAH structure. In the *n*-decane products, these bay-region methyl-substituted PAH are always the lowest-yield isomers among the methyl derivatives of a given PAH, but evidence suggests<sup>49,50</sup> that this low-yield status may be a result of their proneness, once formed, to convert to other products.

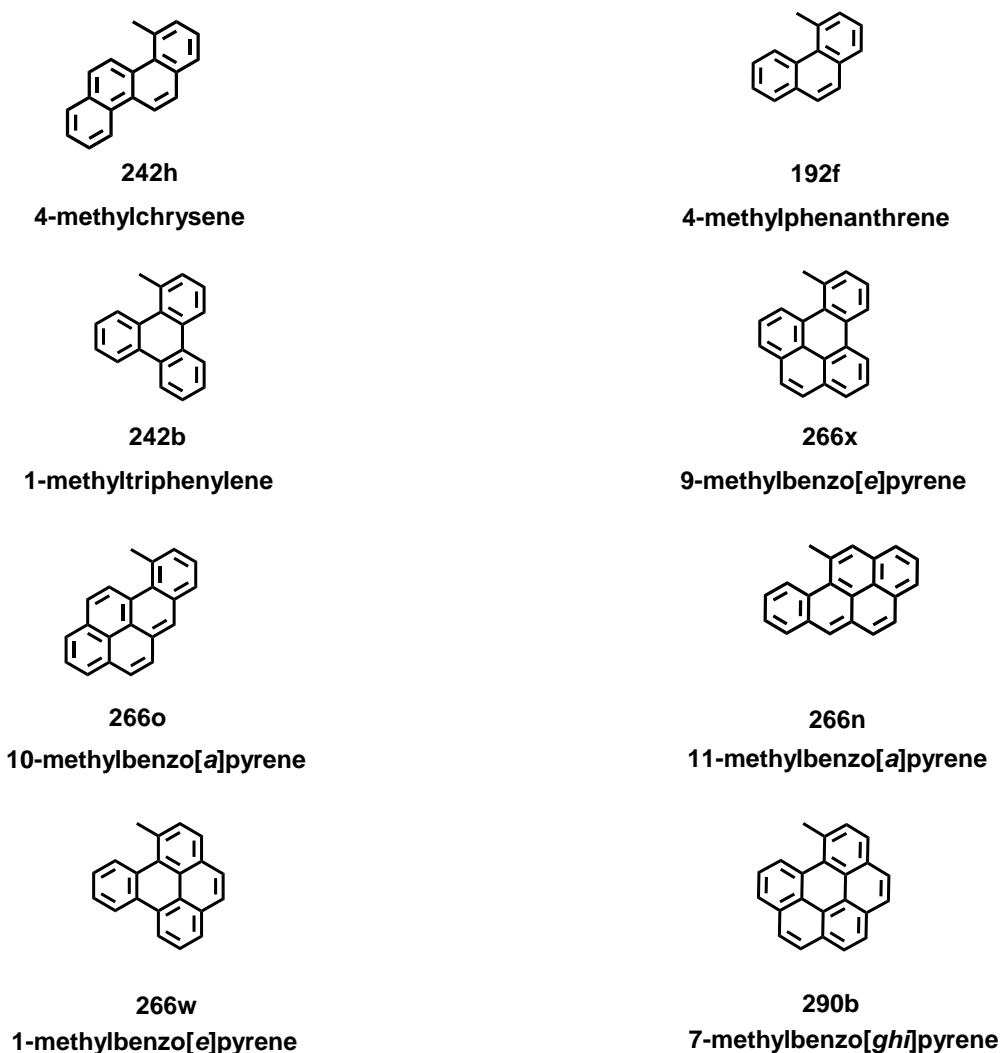


Figure 5.2. Molecular structures of 4-methylchrysene (242h) and seven three- to six-ring bay-region methyl-substituted PAH products of supercritical *n*-decane pyrolysis at 568 °C, 94.6 atm, and 133 sec: 4-methylphenanthrene (192f), 1-methyltriphenylene (242b), 9-methylbenzo[e]pyrene (266x), 10-methylbenzo[a]pyrene (266o), 11-methylbenzo[a]pyrene (266n), 1-methylbenzo[e]pyrene (266w), and 7-methylbenzo[ghi]perylene (290b).

To investigate the growth reactions of bay-region methyl-substituted PAH in the supercritical *n*-alkane pyrolysis environment, we have performed supercritical *n*-decane experiments with the fourth methyl-PAH dopant illustrated in Figure 5.1: 4-methylchrysene, a four-ring PAH whose structure, as shown in Figure 5.2, is representative of *n*-decane's three- to six-ring bay-region methyl-substituted PAH products.

The experiments are conducted at 568 °C, 94.6 atm, and 133 sec, conditions of rapid PAH growth. As with the other methyl-PAH dopants of Figure 5.1, we would expect 4-methylchrysene's arylmethyl radical to play a role in its reactions of molecular growth, but the relatively shielded location of 4-chrysenylmethyl's methyl group could potentially hinder its accessibility and ability to react with the aliphatic growth species methyl and the C<sub>2</sub>-C<sub>4</sub> 1-alkenes. On the other hand, the close proximity of an aryl carbon just across the bay from the methyl group may open up reaction avenues for bay-region methyl-substituted PAH that are not open to their non-bay-region counterparts. Exploring these questions, we report here the results of our supercritical *n*-decane pyrolysis experiments with the bay-region methyl-substituted PAH dopant 4-methylchrysene and discuss the mechanisms responsible for its growth to PAH as large as nine rings in this reaction environment.

## 5.2. Experimental Equipment and Procedures

Two sets of supercritical *n*-decane pyrolysis experiments have been performed in an isothermal, silica-lined stainless-steel flow reactor at 568 °C, 94.6 atm, and 133 sec, conditions of rapid PAH growth. The reactor design and procedures for the experiments have been described in chapter 2. In the Set-1 experiments, the fuel is neat *n*-decane (99.5% pure; critical temperature, 344.5 °C; critical pressure, 20.7 atm). In the Set-2 experiments, the fuel is *n*-decane to which 4-

methylchrysene (>99% pure; synthesized by the Biochemical Institute for Environmental Carcinogens) has been added as a dopant at a concentration of 0.684 mg/g *n*-decane.

The chosen dopant concentration—corresponding to 400-800 times the yields of the individual methylchrysenes produced by *n*-decane in undoped *n*-decane pyrolysis experiments at the same conditions—is high enough to bring about observable effects on the pyrolysis-product yields but too low to influence the physical properties of the reaction environment.

For each of the pyrolysis experiments, the products exiting the reactor are quenched to room temperature and collected as previously described in chapter 2 of this thesis. The aliphatic products and one-ring aromatics are analyzed by gas chromatography with flame-ionization and mass-spectrometric detection. Because of their high degree of methylation, the PAH products are first fractionated by normal-phase high-pressure liquid chromatography (HPLC)—the higher-yield PAH requiring one fractionation procedure; the lower-yield, higher-ring-number PAH requiring a particularly involved fractionation procedure.<sup>19,46,47</sup> Each PAH-product fraction is then analyzed by reversed-phase HPLC with diode-array ultraviolet-visible (UV) absorbance and mass-spectrometric detection, for isomer-specific product identification and quantification, after extensive calibration with reference standards.<sup>19,46,47</sup> The UV and mass spectra establishing the identities of the PAH products reported here are documented elsewhere.<sup>46,47</sup>

### **5.3. Results and Discussion**

The two sets of supercritical *n*-decane pyrolysis experiments—Set 1, ten identical experiments without dopant; Set 2, three identical experiments with 4-methylchrysene dopant—have been conducted at 568 °C, 94.6 atm, and 133 sec, and the yields of the 320 individually quantified products appear in Figures B1-B16, in Appendix B. The names, molecular formulas, and chemical structures of the 230 quantified aromatic products appear in Table B1 in Appendix B, along with



their assigned number/letter codes. The structures and yields of the 41 PAH products whose yields are affected most by the 4-methylchrysene dopant are presented in Figure 5.3.

In all cases, the yields from the Set-1 *n*-decane-only experiments are plotted as the green bars; the yields from the Set-2 *n*-decane experiments with 4-methylchrysene dopant are plotted as the blue bars. Because analysis of most of the PAH products of five or more rings requires the more-involved (in terms of time and solvent consumption) fractionation procedure, the products from only three of the ten undoped experiments undergo that analysis; hence, in Figures 5.3 and B8-B16 (Appendix B), there are only three green bars for each of those products' yields from the undoped experiments. For the eleven PAH of Figure 5.3 that are produced in the Set-2 *n*-decane pyrolysis experiments with dopant—but are not produced in detectable amounts in the Set-1 *n*-decane-only experiments—only blue bars appear in Figure 5.3 for these products. Before examining Figure 5.3 and the products whose yields are affected by the 4-methylchrysene dopant, we first note, from Figures B1-B7 of Appendix B, that the dopant has no effect on: (1) the level of *n*-decane conversion, which remains constant at  $89.9 \pm 0.3\%$  for all experiments; (2) the yields of *n*-decane's aliphatic products, of which the C<sub>1</sub>-C<sub>9</sub> *n*-alkanes and the C<sub>2</sub>-C<sub>9</sub> 1-alkenes are dominant components (No acetylene or any hydrocarbon with a C-C triple bond is formed in these experiments.); or (3) the yields of *n*-decane's aromatic products of ring number lower than that of the dopant (so there is no evidence of aromatic-ring rupture). All of these findings from the 4-methylchrysene-doped *n*-decane experiments are consistent with our findings<sup>49,50</sup> from the *n*-decane pyrolysis experiments with the other methylaromatic dopants of Figure 5.1.

The yields and structures of the products in Figure 5.3a, however, reveal that 4-methylchrysene exhibits several behaviors that are different from those of the other methylaromatic dopants we previously examined. First, the blue bars for 4-methylchrysene

(242h), at the right-most end of Figure 5.3a, show that the yield of unreacted 4-methylchrysene dopant from the Set-2 *n*-decane pyrolysis experiments is 325+16  $\mu\text{g/g}$  *n*-decane fed, which corresponds to 47.5+2.3% of the 4-methylchrysene fed to the reactor, or a dopant conversion of 52.5+2.3%—an order of magnitude higher than those of Figure 5.1's other dopants.<sup>49,50</sup> Second, the first two sets of bars in Figure 5.3a reveal that in the 4-methylchrysene-doped *n*-decane pyrolysis experiments (blue bars), the yields of chrysene (228b) and 3-methylchrysene (242d) are, respectively, five times and six times higher than in the undoped *n*-decane pyrolysis experiments (green bars). 4-Methylchrysene's unique growth behavior to produce its unsubstituted parent PAH (chrysene) and its neighbor isomer (3-methylchrysene) is not exhibited by the other methylaromatic dopants of previously investigated by our research group.<sup>49,50</sup>

4-Methylchrysene's ability to produce its unsubstituted parent PAH (chrysene) and its neighbor isomer (3-methylchrysene)—behavior not exhibited by the other methylaromatic dopants of Figure 5.1—is almost certainly linked to its methyl group being in a bay region, where it experiences steric repulsive forces in close proximity to the H across the bay. Due to these forces, the methyl-C/aryl-C bond-dissociation energy for 4-methylchrysene (94.3 kcal/mole<sup>52</sup>), as depicted in Figure 5.1, is 7.8 to 11.0 kcal/mole lower than the corresponding values for the dopants whose methyl groups are not in bay regions—apparently allowing homolytic scission of 4-methylchrysene's methyl-C/aryl-C bond. As shown in the first step of Eq. (1), scission of this bond forms 4-chrysenyl radical, which can add H, as in Eq. (2), to form chrysene (228b), or—as indicated by the 4-methylchrysene-induced enhancement of 3-methylchrysene's yield—proceed with the H shift<sup>53</sup> of Eq. (1) to form 3-chrysenyl, whose combination with methyl forms 3-methylchrysene (242d). Any H shift in some of the 3-chrysenyl to make 2-chrysenyl, or some of that 2-chrysenyl to make 1-chrysenyl would, after reaction with methyl, as shown in Eqs. (3)-(4),

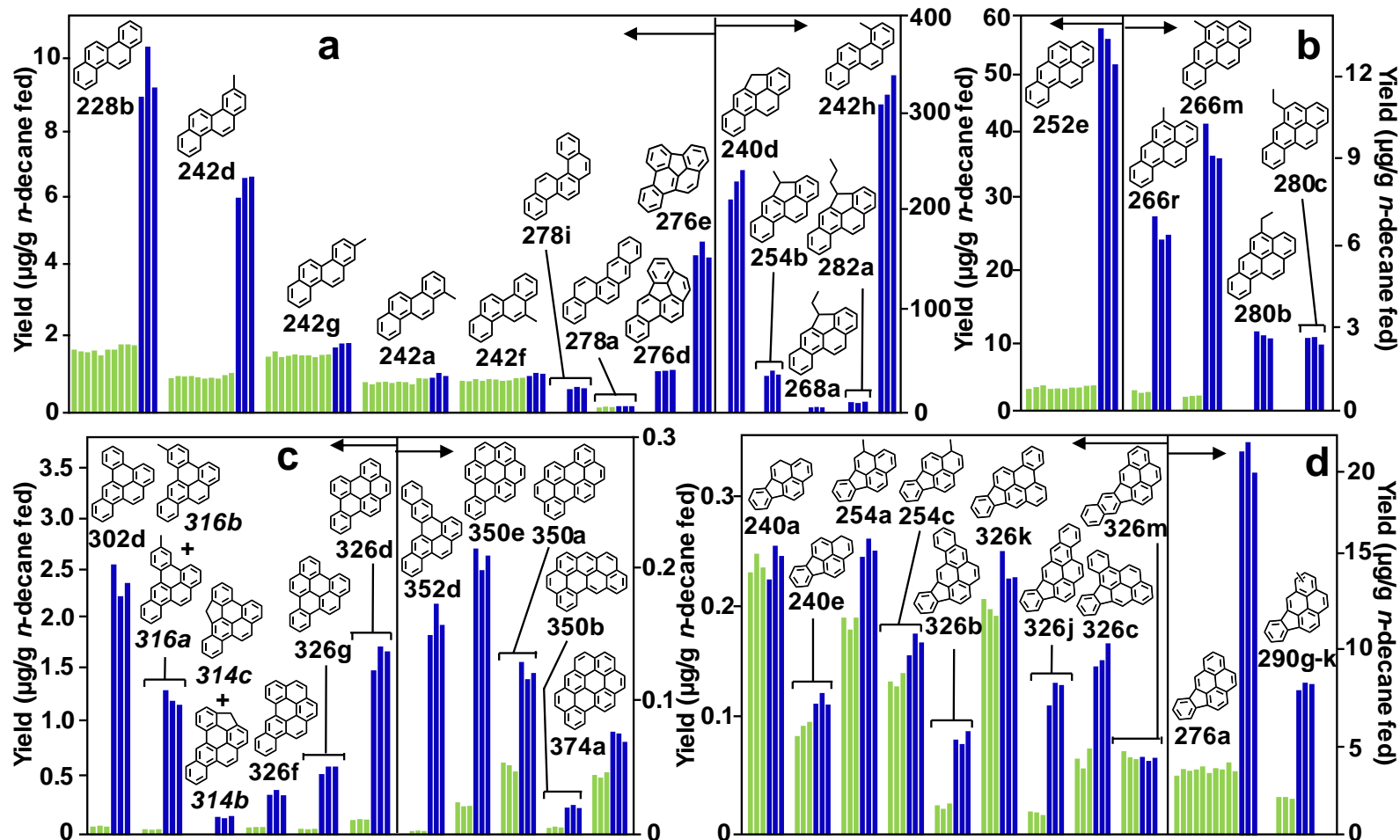
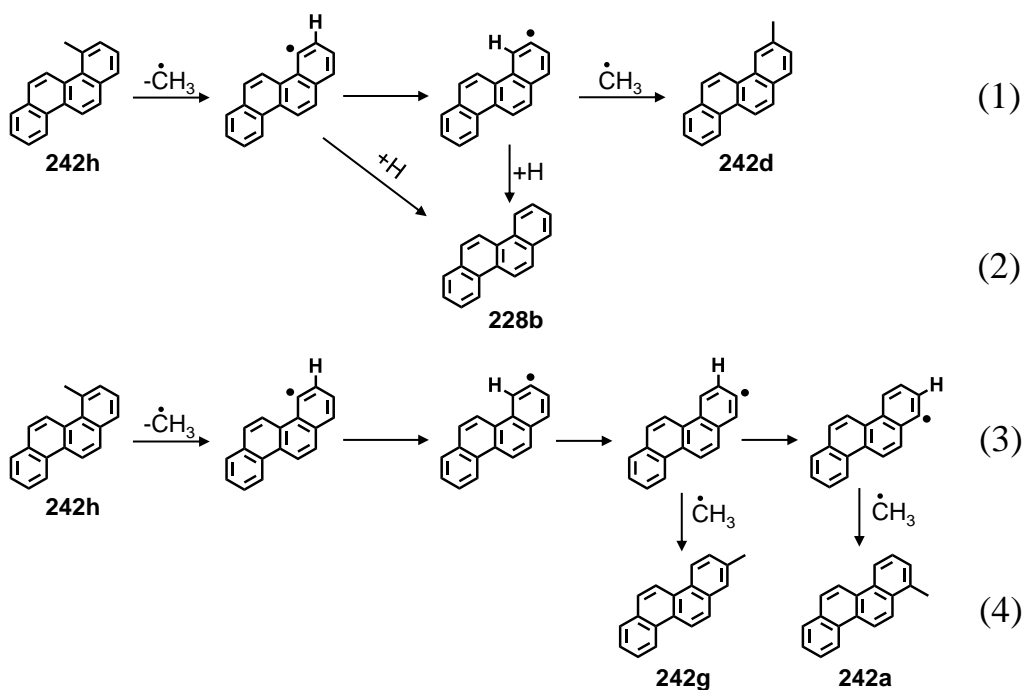


Figure 5.3. Yields of selected PAH products of supercritical *n*-decane pyrolysis at 568 °C, 94.6 atm, and 133 sec: (a) four- to six-ring PAH, (b) benzo[*a*]pyrene and alkyl derivatives, (c) six- to nine-ring benzenoid PAH and derivatives, and (d) five- to seven-ring PAH with internal five-membered rings. Experiments: (■) without dopant; (■) with 4-methylchrysene dopant. All product names, structures, and number/letter codes are listed in Table B1 in Appendix B. Analysis of most high-ring-number PAH requires a very lengthy, highly solvent-consuming fractionation procedure, so the products from only three of the ten undoped experiments undergo that analysis. Hence, there are only three green bars for these products' yields from the undoped experiments.

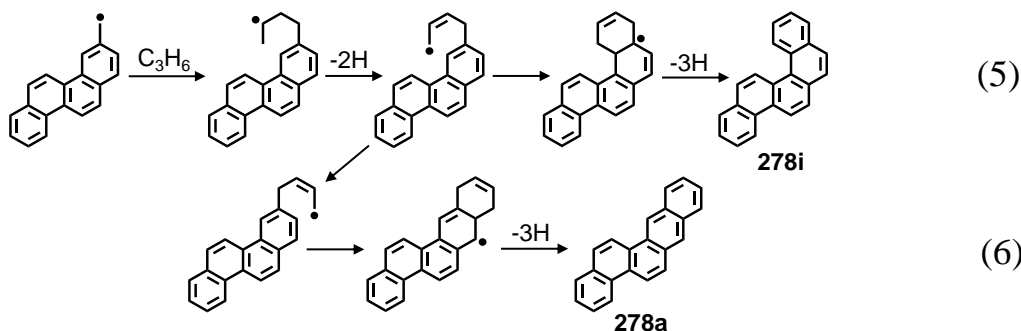
account for the small and successively lower dopant-induced increases in the yields of 2-methylchrysene (242g) and 1-methylchrysene (242a), the third and fourth products of Figure 5.3a. The yield of 6-methylchrysene (242f), the fifth product of Figure 5.3a, is only minimally affected by the dopant, if at all.



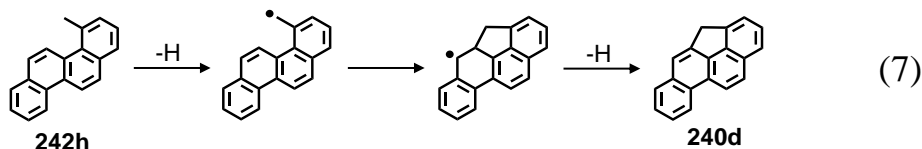
The mechanism of Eq. (1)—which, in the supercritical *n*-decane pyrolysis environment, apparently only applies to bay-region methyl-substituted PAH—accounts not only for our findings in Figure 5.3a for the methylchrysenes, but it also explains why in our other doping experiments<sup>49,50</sup>, PAH-growth reactions that would have led exclusively to the bay-region methyl-substituted PAH 4-methylphenanthrene and 1-methyltriphenylene produced not only these isomers but also their non-bay-region neighbor isomers, 3-methylphenanthrene and 2-methyltriphenylene, respectively.

A consequence of the 4-methylchrysene-dopant-induced increase in 3-methylchrysene's yield is an elevated level of 3-chrysenylmethyl, which, as illustrated in Eqs. (5)-(6), reacts with propene,

*n*-decane's most abundant alkene product, to produce benzo[*c*]chrysene (278i) and, to a lesser extent, benzo[*b*]chrysene (278a), the sixth and seventh products in Figure 5.3a and the only C<sub>22</sub>H<sub>14</sub> PAH in Figure 5.4 to exhibit 4-methylchrysene-dopant-induced increases in yield.



The high blue bars of the tenth product in Figure 5.3a reveal that 4*H*-cyclopenta[*def*]chrysene (240d) is the favored product of 4-methylchrysene, accounting for 65% of the 4-methylchrysene that converts. As illustrated in Eq. (7), loss of H from 4-methylchrysene's methyl carbon (C-H bond-dissociation energy, 88.5 kcal/mole<sup>52</sup>), either by H abstraction or homolytic scission, forms the arylmethyl radical 4-chrysenylmethyl, which then attacks the nearby carbon across the bay at chrysene's "5" position; subsequent dehydrogenation results in 4*H*-cyclopenta[*def*]chrysene (240d). The immediate availability of a self-provided reaction partner just across the bay—an advantage unique to arylmethyl radicals whose methyl is in a bay region—accounts for 4-methylchrysene's high conversion, relative to that of the other methylaromatic dopants of Figure 5.1, as well as its high selectivity for 4*H*-cyclopenta[*def*]chrysene (240d).



We see from Figure 5.5 that the nineteen-carbon structure of 4*H*-cyclopenta[*def*]chrysene contains the thirteen-carbon structure of fluorene, a three-ring PAH that was previously

investigated by Kalpathy *et al.*<sup>50</sup> as a dopant in supercritical *n*-decane pyrolysis experiments. As illustrated in Figure 5.5, both contain a five-membered ring whose CH<sub>2</sub> methylene bridge has a relatively low C-H bond-dissociation energy of ~82.0 kcal/mole.<sup>38,50</sup> As shown in the first step of Eq. (8), abstraction of H at 4*H*-cyclopenta[*def*]chrysene's methylene carbon makes the resonantly stabilized 9-fluorenyl-type radical 4-cyclopenta[*def*]chrysenyl, which is then readily available to react with the C<sub>1</sub>-C<sub>3</sub> aliphatic species most abundant in the supercritical *n*-decane pyrolysis environment.

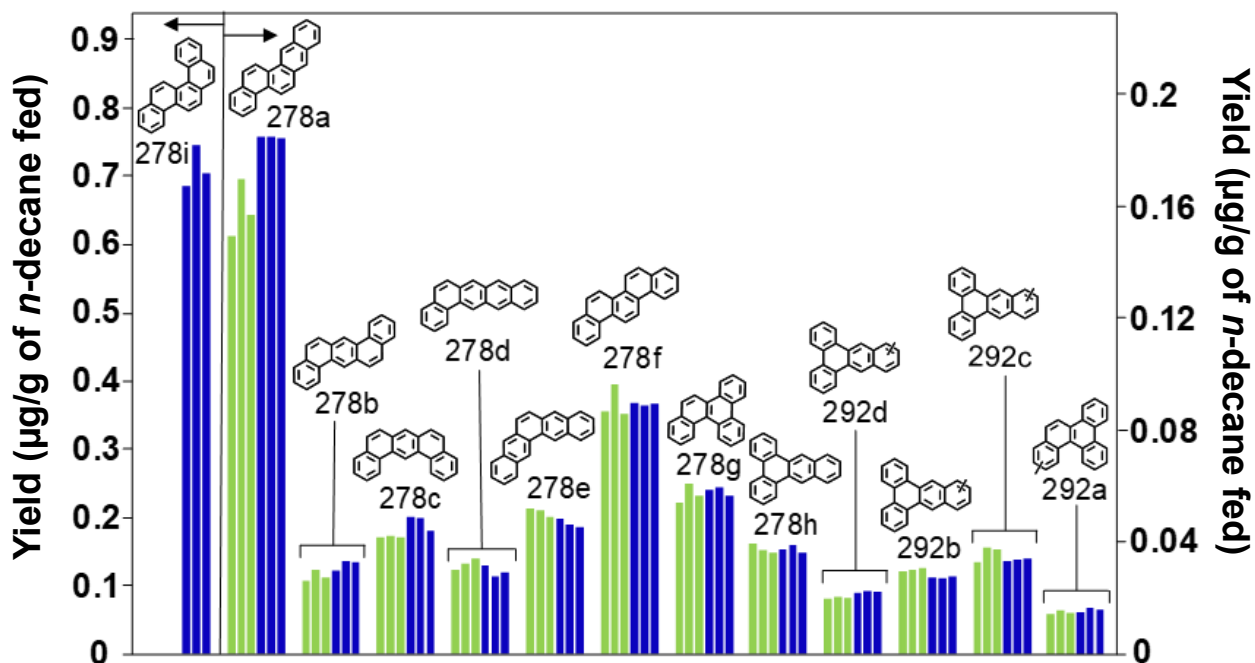


Figure 5.4. Yields of five-ring C<sub>22</sub>H<sub>14</sub> PAH and their methyl derivatives from supercritical *n*-decane pyrolysis at 568 °C, 94.6 atm, and 133 sec: benzo[*c*]chrysene (278i), benzo[*b*]chrysene (278a), dibenz[*a,h*]anthracene (278b), dibenz[*a,j*]anthracene (278c), benzo[*a*]naphthacene (278d), pentaphene (278e), picene (278f), benzo[*g*]chrysene (278g), dibenz[*a,c*]anthracene (278h), three methyl dibenz[*a,c*]anthracenes (292b-d), and a methyl benzo[*g*]chrysene (292a). Experiments: (■) without dopant and (■) with 4-methylchrysene dopant (684 µg 4-methylchrysene / g *n*-decane fed).

As indicated in the second step of Eq. (8), 4-cyclopenta[*def*]chrysenyl's combination with methyl produces 4-methyl-4*H*-cyclopenta[*def*]chrysene (254b), the eleventh product in Figure

5.3a. Equation (9) shows that reaction of 4-cyclopenta[*def*]chrysenyl with ethylene leads to 4-ethyl-4*H*-cyclopenta[*def*]chrysene (268a), the twelfth product in Figure 5.3a; the analogous reaction with propene would give the thirteenth product, 4-propyl-4*H*-cyclopenta[*def*]chrysene (282a). The remaining two products of Figure 5.3a, the non-fully planar dibenzo[*b,ghi*]fluoranthene (276d) and dibenzo[*e,ghi*]fluoranthene (276e), result from alternative reactions of 4-cyclopenta[*def*]chrysenyl with propene, in Eqs. (10)-(11).

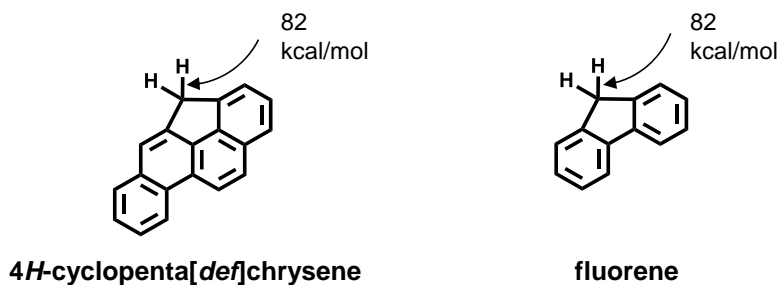
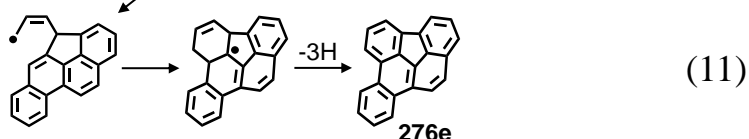
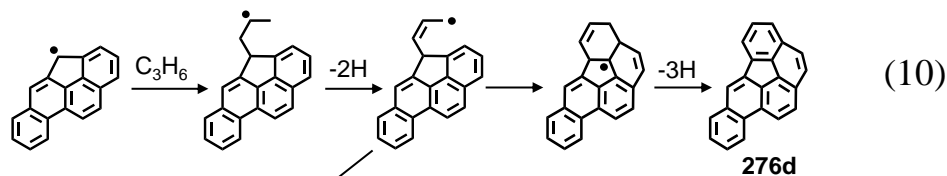
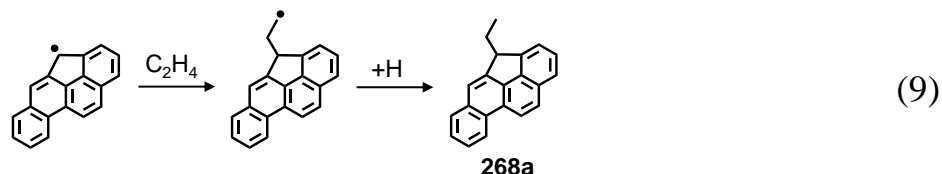
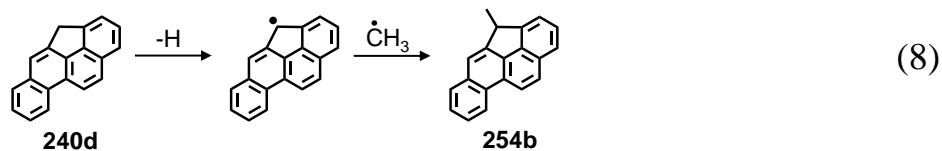


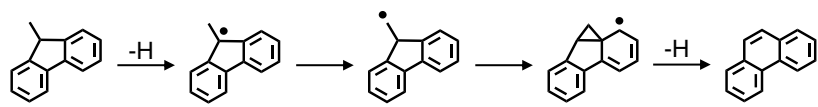
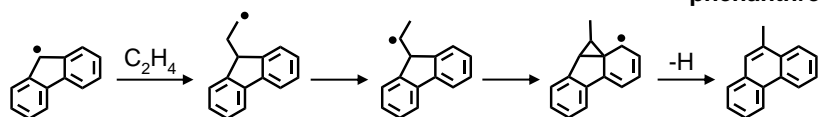
Figure 5.5. Molecular structures of 4*H*-cyclopenta[*def*]chrysene and fluorene and relevant bond-dissociation energies.<sup>38</sup>



Turning to Figure 5.3b and referring to Figure 5.6, we see that 4-methylchrysene doping brings about a fifteen-fold increase in the yield of one C<sub>20</sub>H<sub>12</sub> PAH, benzo[*a*]pyrene (252e), but

has no effect on the yields of any of the other six C<sub>20</sub>H<sub>12</sub> PAH products of supercritical *n*-decane pyrolysis. This high selectivity is further exhibited in Figure 5.7 for benzo[*a*]pyrene's methyl derivatives: of the twelve different methylbenzo[*a*]pyrene products of *n*-decane, only two, 4-methylbenzo[*a*]pyrene (266r) and 5-methylbenzo[*a*]pyrene (266m), experience dopant-induced increases in yield—nine-fold and sixteen-fold, respectively, as evident in Figure 5.3b. The other two products in Figure 5.3b, 4-ethylbenzo[*a*]pyrene (280b) and 5-ethylbenzo[*a*]pyrene (280c), experience 4-methylchrysene-dopant-enhanced production as well. Even though benzo[*a*]pyrene and its 4- and 5- methyl and ethyl derivatives contain only six-membered rings, we do not believe that they result directly from reactions with 4-chrysenylmethyl—which does not even combine with methyl, as no 4-ethylchrysene is observed in our products—but rather from reactions of 4-cyclopenta[*def*]chrysenyl with the principal aliphatic reactants methyl, ethylene. We note that the doping experiments with fluorene demonstrated<sup>50</sup> that 9-methylfluorene underwent ring expansion to form the benzenoid PAH phenanthrene, and 9-fluorenyl reacted with ethylene and propene in ring-expansion reactions to yield exclusively 9-methylphenanthrene and 9-ethylphenanthrene, respectively. These reactions are presented as Eqs. (12)-(13) in Table 5.1.

Table 5.1. Ring-expansion reactions of 9-methylfluorene and of 9-fluorenyl (with ethylene), as determined from supercritical *n*-decane pyrolysis experiments<sup>50</sup> with the dopant fluorene.

Reaction	Equation
 <p style="text-align: center;"><b>178b</b> phenanthrene</p>	(12)
 <p style="text-align: center;"><b>192b</b> 9-methylphenanthrene</p>	(13)



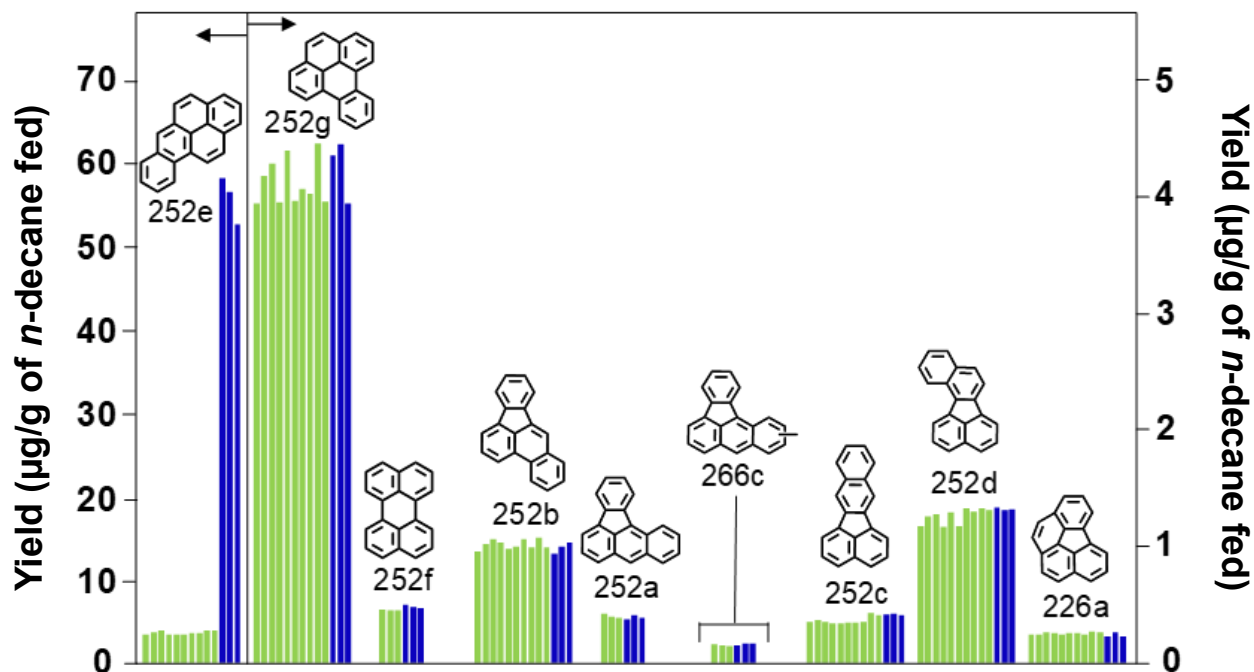


Figure 5.6. Yields of five-ring  $C_{20}H_{12}$  PAH, their derivatives, and an associated  $C_{18}H_{10}$  PAH product from supercritical *n*-decane pyrolysis at 568 °C, 94.6 atm, and 133 sec: benzo[*a*]pyrene (252e), benzo[*e*]pyrene (252g), perylene (252f), benzo[*b*]fluoranthene (252b), benzo[*a*]fluoranthene (252a), a methylbenzo[*a*]fluoranthene (266c), benzo[*k*]fluoranthene (252c), benzo[*j*]fluoranthene (252d), and benzo[*ghi*]fluoranthene (226a). Experiments: (■) without dopant and (■) with 4-methylchrysene dopant (684 µg 4-methylchrysene / g *n*-decane fed).

Analogous to Eq. (12), for the production of phenanthrene from 9-methylfluorene, is Eq. (14), for the production of benzo[*a*]pyrene from 4-methyl-4*H*-cyclopenta[*def*]chrysene. Analogous to Eq. (13), for the production of 9-methylphenanthrene from 9-fluorenyl (and ethylene), are Eqs. (15)-(16) for the production of 4- and 5-methylbenzo[*a*]pyrene from 4-cyclopenta[*def*]chrysenyl (and ethylene). If, as shown in Eqs. (17)-(18), propene were the reactant alkene instead of ethylene, the resulting products would be 4-ethylbenzo[*a*]pyrene and 5-ethylbenzo[*a*]pyrene, the fourth and fifth products of Figure 5.3b. We note that the ring-expansion reaction sequences in Eqs. (14)-(16) account for the observed high selectivity in the production of benzo[*a*]pyrene and its 4- and 5- methyl and ethyl derivatives.

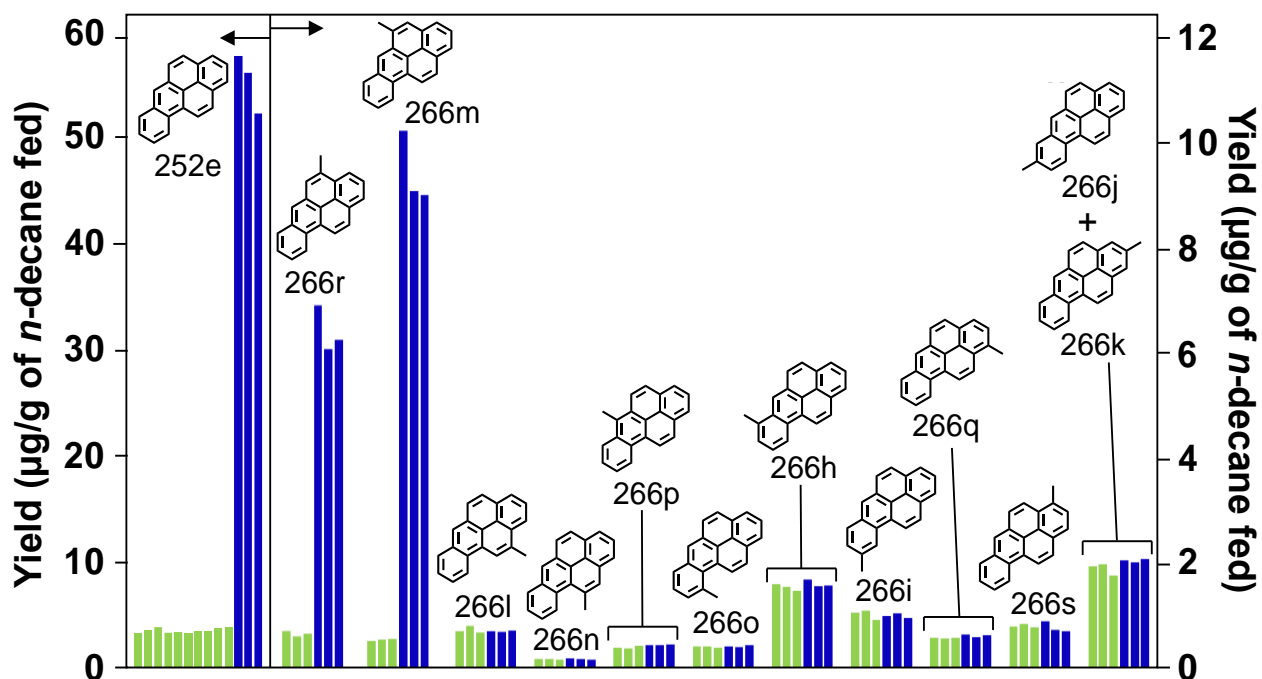
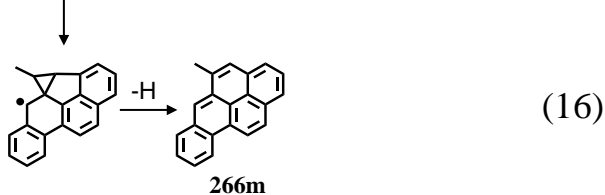
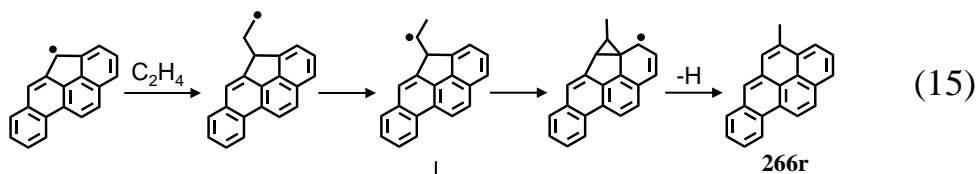
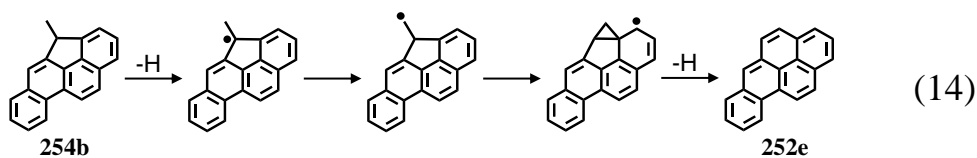
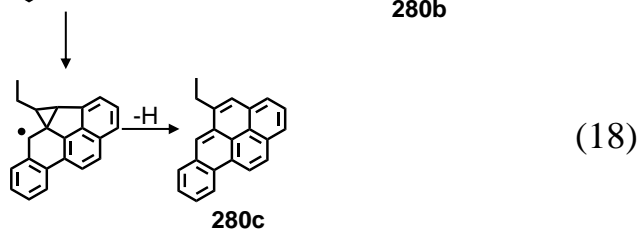
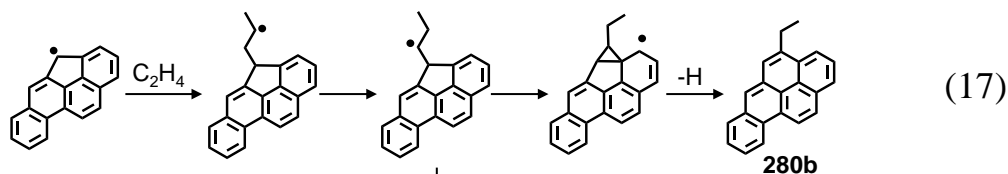


Figure 5.7. Yields of five-ring  $C_{20}H_{12}$  PAH, and their methyl derivatives, from supercritical *n*-decane pyrolysis at 568 °C, 94.6 atm, and 133 sec: benzo[*a*]pyrene (252e), 4-methylbenzo[*a*]pyrene (266r), 5-methylbenzo[*a*]pyrene (266m), 12-methylbenzo[*a*]pyrene (266l), 11-methylbenzo[*a*]pyrene (266n), 6-methylbenzo[*a*]pyrene (266p), 10-methylbenzo[*a*]pyrene (266o), 7-methylbenzo[*a*]pyrene (266h), 9-methylbenzo[*a*]pyrene (266i), 1-methylbenzo[*a*]pyrene (266q), 3-methylbenzo[*a*]pyrene (266s), and 2-methylbenzo[*a*]pyrene (266k) co-eluting with 8-methylbenzo[*a*]pyrene (266j). Experiments: (■) without dopant and (■) with 4-methylchrysene dopant (684 µg 4-methylchrysene / g *n*-decane fed).





We see then, from the results of Figures 5.3a and 5.3b, that there are two major routes for bay-region methyl-substituted PAH, such as 4-methylchrysene, to grow by one ring number. In the first route, exemplified by Eqs. (1), (5), and (6), the bay-region methyl-substituted PAH converts to its neighbor isomer, whose arylmethyl radical then reacts with propene to form a benzenoid PAH of one higher ring number. In the second route, exemplified by the Eq.-(7)-(8)-(14) sequence, the arylmethyl radical of the bay-region methyl-substituted PAH reacts with the aryl carbon across the bay to form a methylene-bridged PAH, whose 9-fluorenyl-type radical combines with methyl; subsequent ring expansion yields a benzenoid PAH of one higher ring number. When that 9-fluorenyl-type radical instead reacts with ethylene or propene in ring-expansion reactions such as Eqs. (15)-(16), however, the products are methyl- and ethyl-substituted benzenoid PAH—exemplified here by the 4- and 5- methyl- and ethylbenzo[*a*]pyrenes, whose alkyl-substituent positions render them sources of arylmethyl radicals of the same type as 1-naphthylmethyl and 1-phenanthrylmethyl—opening the door to PAH growth by more than one ring number. As demonstrated in our doping experiments with 1-methylnaphthalene<sup>49</sup> and 1-methylphenanthrene<sup>50</sup> and as illustrated in Figure 5.8, each one of these arylmethyl radicals react with propene, 1-butene, and ethylene exclusively at the arylmethyl radical's methyl site.

The reactions of arylmethyl radicals with propene, 1-butene, and ethylene exclusively at the arylmethyl radical's methyl site, produces, respectively, a particular benzenoid PAH of one ring more; one of that benzenoid PAH's methyl derivatives; and a phenalene-type PAH, whose low C-H bond-dissociation energy at the saturated carbon (74 kcal/mole<sup>38</sup>) permits the facile formation of resonance-stabilized phenalenyl-type radicals (shown in green in Figure 5.8).

These radicals in turn react with propene and 1-butene to selectively produce particular unsubstituted and methyl-substituted *peri*-condensed benzenoid PAH of two rings more than the initial arylmethyl radical.

To see how the growth reactions of 4-benzo[*a*]pyrenylmethyl and 5-benzo[*a*]pyrenylmethyl play out in the supercritical *n*-decane pyrolysis environment, we turn to Figure 5.3c, which presents the yields of six- to nine-ring *peri*-condensed benzenoid PAH products and their methyl derivatives, and to Figure 5.9, which shows how these product PAH are formed via reactions with the principal aliphatic reactants methyl, ethylene, propene, and 1-butene.

The enlarged black structures in the middle of the top row in Figure 5.9 are the 5-benzo[*a*]pyrenylmethyl radical (on the left) and the 4-benzo[*a*]pyrenylmethyl radical (on the right). In accordance with the colors used in Figure 5.8, the phenalenyl-type radicals associated with each benzo[*a*]pyrenylmethyl radical are shown in green in Figure 5.9, and products of propene's reaction with either a phenalenyl-type radical or an arylmethyl radical are shown in blue. Because a number of the reactions in Figure 5.9 produce bay-region methyl-substituted PAH, we take advantage of our findings from the 4-methylchrysene-doping experiments.

In cases where the bay-region methyl-substituted PAH converts, as in Eq. (1), to the neighbor isomer, we show the structure of the product neighbor isomer in purple. In cases where

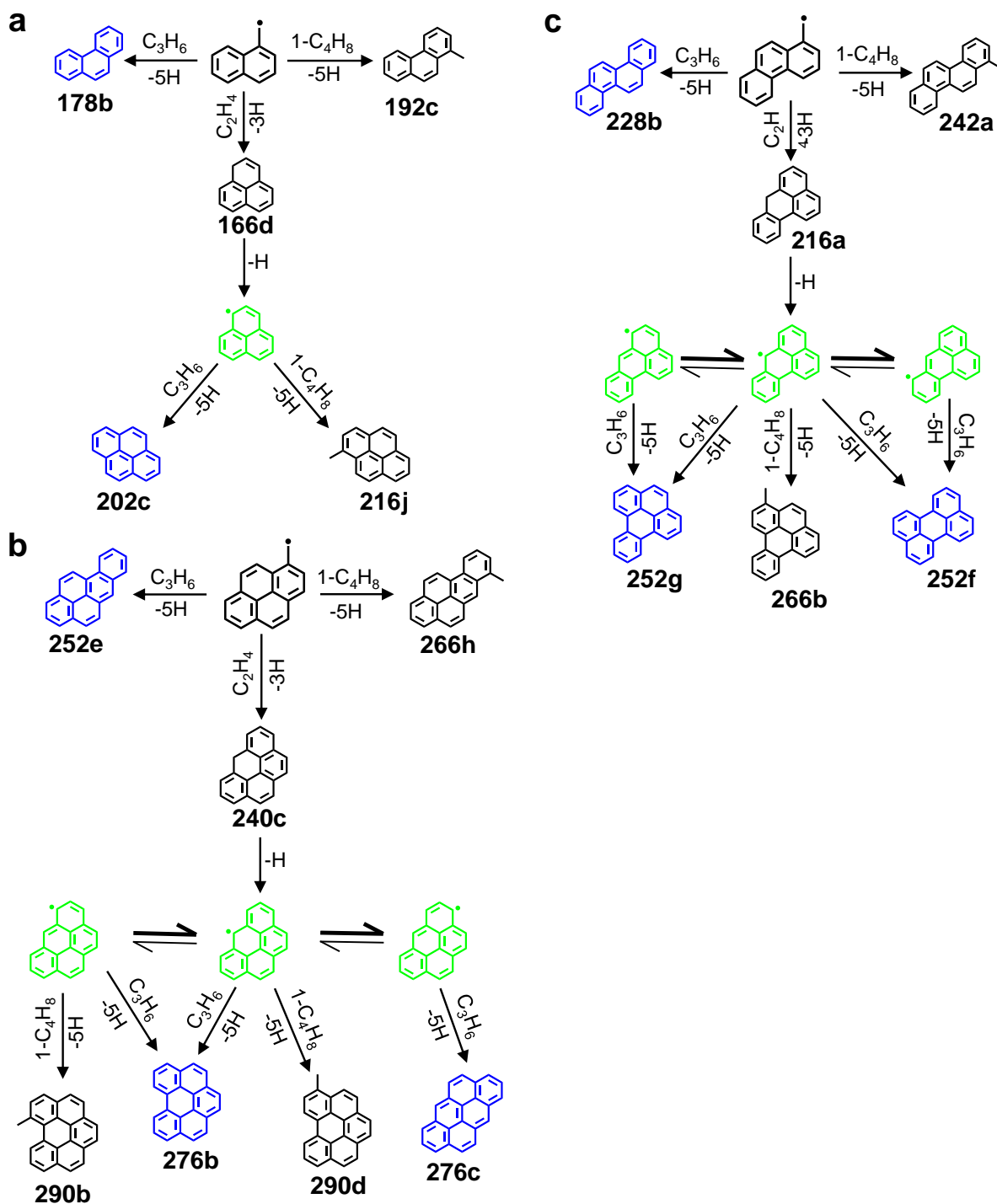


Figure 5.8. PAH growth reactions—as determined from supercritical *n*-decane pyrolysis experiments with 1-methylnaphthalene<sup>49</sup> and 1-methylphenanthrene<sup>50</sup> as dopants—of (a) 1-naphthylmethyl, (b) 1-pyrenylmethyl, and (c) 1-phenanthrylmethyl and their respective phenalenyl-type radicals with *n*-decane’s highest-yield alkenes: ethylene, propene, and 1-butene. Blue structures: products of reactions with propene. Green structures: phenalenyl-type radicals. Tables B2-B4 in Appendix B provide the detailed reactions.

the bay-region methyl-substituted PAH undergoes the Eq.-(7)-(8)-(14) methylene-bridge/methyl-addition/ring-expansion sequence to produce a benzenoid PAH, we show the product PAH in red. Throughout Figure 5.9, all structures with number/letter codes correspond to unequivocally identified products whose yields, by experiment, are increased by the 4-methylchrysene dopant. For the six purple structures with italicized number/letter codes, the positions of the methyl substituents have been deduced, as noted in Table B1 in Appendix B.

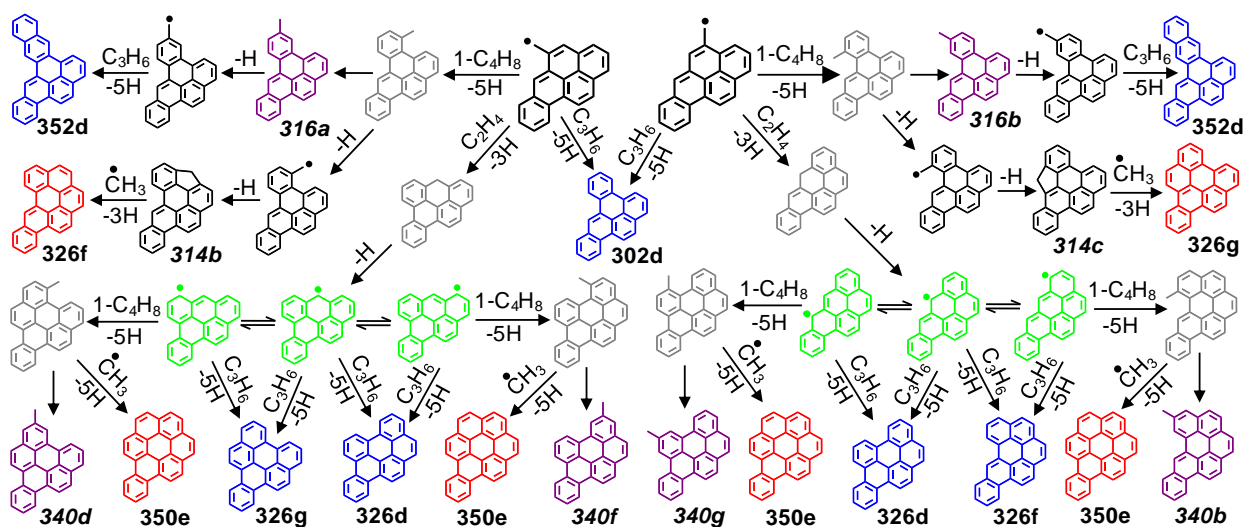


Figure 5.9. Reaction pathways, stemming from the 5-benzo[*a*]pyrenylmethyl and 4-benzo[*a*]pyrenylmethyl radicals, for PAH growth in the supercritical *n*-decane pyrolysis environment. Blue structures: products of reactions with propene. Red structures: products of an Eqn-(7)-(8)-(14)-type methylene-bridge/methyl-addition/ring-expansion sequence. Purple structures: non-bay-region methyl-substituted PAH resulting from the Eq.-(1)-type conversion of bay-region methyl-substituted PAH. Grey structures: hypothetical products whose presence is not verified. Green structures: phenalenyl-type radicals.

As illustrated at the top center of Figure 5.9, reaction of propene with either 5-benzo[*a*]pyrenylmethyl or 4-benzo[*a*]pyrenylmethyl results in dibenzo[*a,e*]pyrene (302d), shown in blue, the only one of *n*-decane's thirteen  $C_{24}H_{14}$  PAH products in Figure 5.10 to exhibit a 4-methylchrysene-dopant-induced increase in yield—twenty-eight-fold, as portrayed by the first set of bars in Figure 5.3c. As shown to the left of 5-benzo[*a*]pyrenylmethyl and to the right of 4-benzo[*a*]pyrenylmethyl in Figure 5.9, each of these arylmethyl radicals reacts with 1-butene to

produce a bay-region methyl-substituted dibenzo[*a,e*]pyrene, neither of which we experimentally observe (hence, the grey structures) because they, like 4-methylchrysene, each readily convert to: (1) their neighbor isomers (methyl-dibenzo[*a,e*]pyrenes *316a* and *316b*, shown in purple on the top row of Figure 5.9), whose summed yields compose the second set of bars in Figure 5.3c, and (2) their methylene-bridged derivatives (*314b* and *314c* on the second row of Figure 5.9), whose summed yields make up the third set of bars in Figure 5.3c.

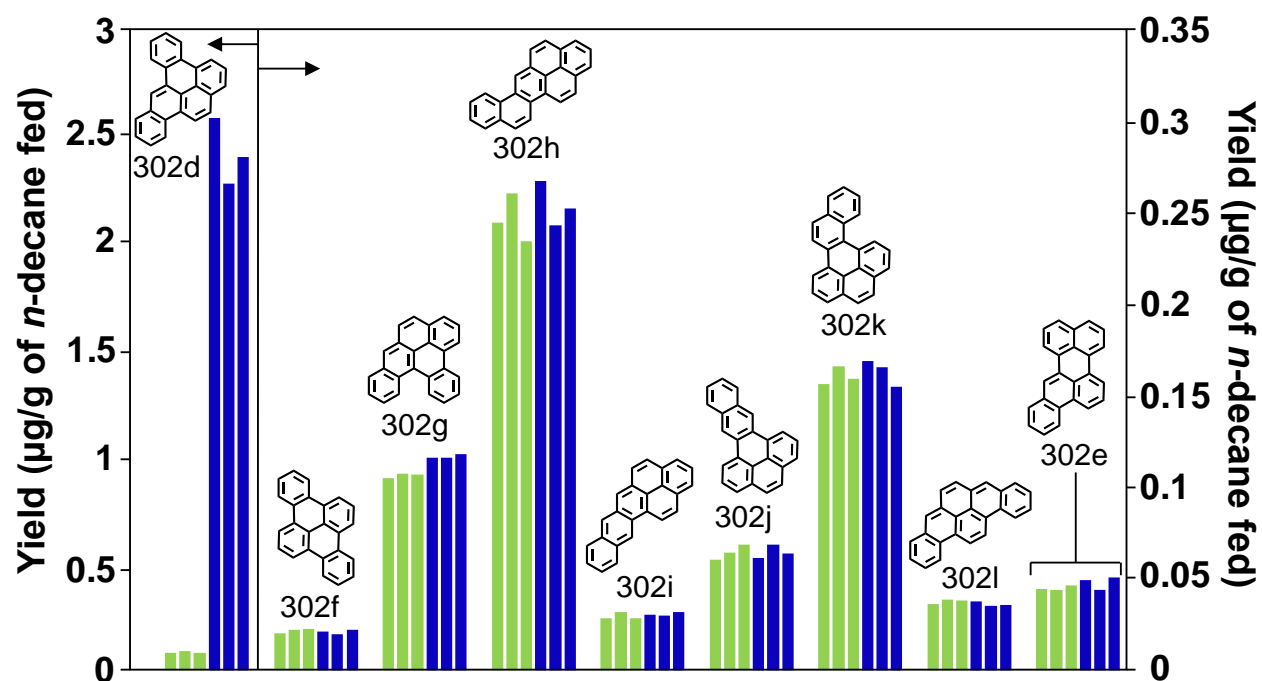


Figure 5.10. Yields of six-ring  $C_{24}H_{14}$  PAH from supercritical *n*-decane pyrolysis at 568 °C, 94.6 atm, and 133 sec: dibenzo[*a,e*]pyrene (302d), dibenzo[*e,l*]pyrene (302f), dibenzo[*a,l*]pyrene (302g), naphtho[2,1-*a*]pyrene (302h), naphtho[2,3-*a*]pyrene (302i), naphtho[2,3-*e*]pyrene (302j), naphtho[1,2-*e*]pyrene (302k), dibenzo[*a,i*]pyrene (302l), benzo[*b*]perylene (302m), naphtho[2,3-*b*]fluoranthene (302n), naphtho[1,2-*b*]fluoranthene (302o), dibenzo[*b,j*]fluoranthene (302p), and dibenzo[*j,l*]fluoranthene (302q). Experiments: (■) without dopant and (■) with 4-methylchrysene dopant (684 µg 4-methylchrysene / g *n*-decane fed).

As portrayed at the left and right ends of Figure 5.9's top row, the arylmethyl radicals of the two methyl-dibenzo[*a,e*]pyrene neighbor isomers (*316a* and *316b*) each react with propene to yield the  $C_{28}H_{16}$  product benzo[*a*]naphtho[2,3-*e*]pyrene (352d), whose yield, in Figure 5.3c,

exhibits a dramatic forty-eight-fold increase with 4-methylchrysene doping. As shown at the left and right ends of Figure 5.9's second row, the two methylene-bridged dibenzo[*a,e*]pyrenes (314*b* and 314*c*) undergo the Eq.-(8)-(14)-type methyl-addition/ring-expansion sequence to produce two C<sub>26</sub>H<sub>14</sub> PAH shown in red: dibenzo[*b,ghi*]perylene (326*f*) and naphtho[1,2,3,4-*ghi*]perylene (326*g*), whose yields, in Figure 5.3c, exhibit dopant-induced increases that are five-fold and ten-fold, respectively.

To account for the remaining products in Figure 5.3c, we consider 5-benzo[*a*]pyrenylmethyl's and 4-benzo[*a*]pyrenylmethyl's reactions with ethylene. By analogy to our findings in Figure 5.8 for 1-naphthylmethyl, 1-phenanthrylmethyl, and 1-pyrenylmethyl—ethylene addition to 5-benzo[*a*]pyrenylmethyl and 4-benzo[*a*]pyrenylmethyl would yield, respectively, 4*H*-dibenzo[*a,cd*]pyrene and 6*H*-dibenzo[*a,fg*]pyrene, the two six-ring C<sub>23</sub>H<sub>14</sub> PAH shown in grey on the second row of Figure 5.9. Loss of H at the saturated carbon of each of these phenalene-type PAH would give the respective phenalenyl-type radicals—three resonance structures of each appearing in green in Figure 5.9. As indicated by the four blue structures at the bottom of Figure 5.9, these radicals react with propene to form the three C<sub>26</sub>H<sub>14</sub> PAH whose yields, in Figure 5.3c, increase with doping: dibenzo[*b,ghi*]perylene (326*f*), naphtho[1,2,3,4-*ghi*]perylene (326*g*), and dibenzo[*e,ghi*]perylene (326*d*)—the isomer with the highest number of aromatic sextets, dibenzo[*e,ghi*]perylene, being the favored product.

Just as the phenalenyl-type radicals' reactions with propene yield the unsubstituted naphtho- and dibenzo-perylenes of Figure 5.3c, their reactions with 1-butene yield particular methyl-substituted derivatives of these C<sub>26</sub>H<sub>14</sub> PAH, as fully outlined in Figure 5.11. The four grey structures of Figure 5.9's third row show that 1-butene's reactions with four of the resonance structures of the phenalenyl-type radicals yield bay-region methyl-substituted C<sub>26</sub>H<sub>14</sub> PAH, which



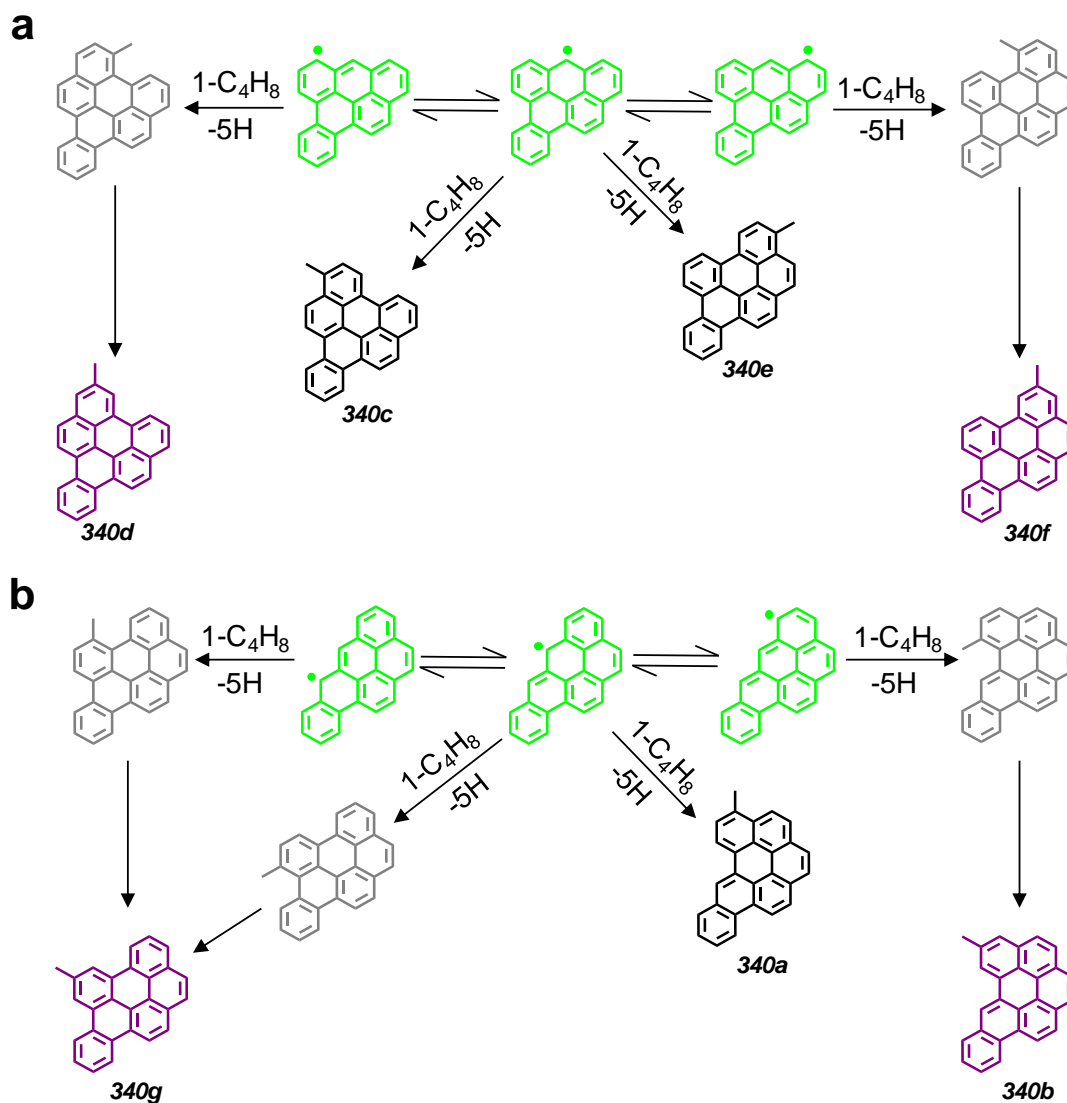


Figure 5.11. Reactions of 1-butene with the phenalenyl-type radicals (green structures) (a) dibenz[*a,cd*]pyrenyl and (b) dibenz[*a,fg*]pyrenyl of Figure 5.9 to produce the seven methyl-substituted C<sub>26</sub>H<sub>14</sub> PAH products (black and purple structures) whose yields are plotted in Figure 5.12. For the three cases in which the reactions lead to non-bay-region methyl-substituted PAH, the product structures—1-methylnaphtho[1,2,3,4-*ghi*]perylene (340c), 3-methyldibenzo[*e,ghi*]perylene (340e), and 5-methyldibenzo[*b,ghi*]perylene (340a)—are shown in black. For the five cases in which the reactions lead to bay-region methyl-substituted PAH, the hypothetical product structures are shown in grey and the non-bay-region methyl-substituted PAH (neighbor isomers) that are the products of their Eq.-(1)-type conversion are shown in purple: 2-methylnaphtho[1,2,3,4-*ghi*]perylene (340d), 4-methyldibenzo[*e,ghi*]perylene (340f), 7-methyldibenzo[*e,ghi*]perylene (340g), and 6-methyldibenzo[*b,ghi*]perylene (340b). Note that among the seven black and purple product structures, there are three methyldibenzo[*e,ghi*]perylenes, two methyldibenzo[*b,ghi*]perylenes, and two methylnaphtho[1,2,3,4-*ghi*]perylenes—exactly the numbers of each of these isomer groups whose yields exhibit 4-methylchrysene-dopant-induced increases in Figure 5.12.

—like their bay-region methyl-substituted dibenzo[*a,e*]pyrene counterparts at the top of Figure 5.9—(1) convert to their neighbor isomers (four purple structures on Figure 5.9’s bottom row), whose yields, as shown in Figure 5.12, increase with 4-methylchrysene doping, and (2) undergo the Eq.-(7)-(8)-(14) methylene-bridge/methyl-addition/ring-expansion sequence to produce, in all four cases, benzo[*a*]coronene (350e; red structures on the bottom row of Figure 5.9), whose yield, in Figure 5.3c, increases with doping.

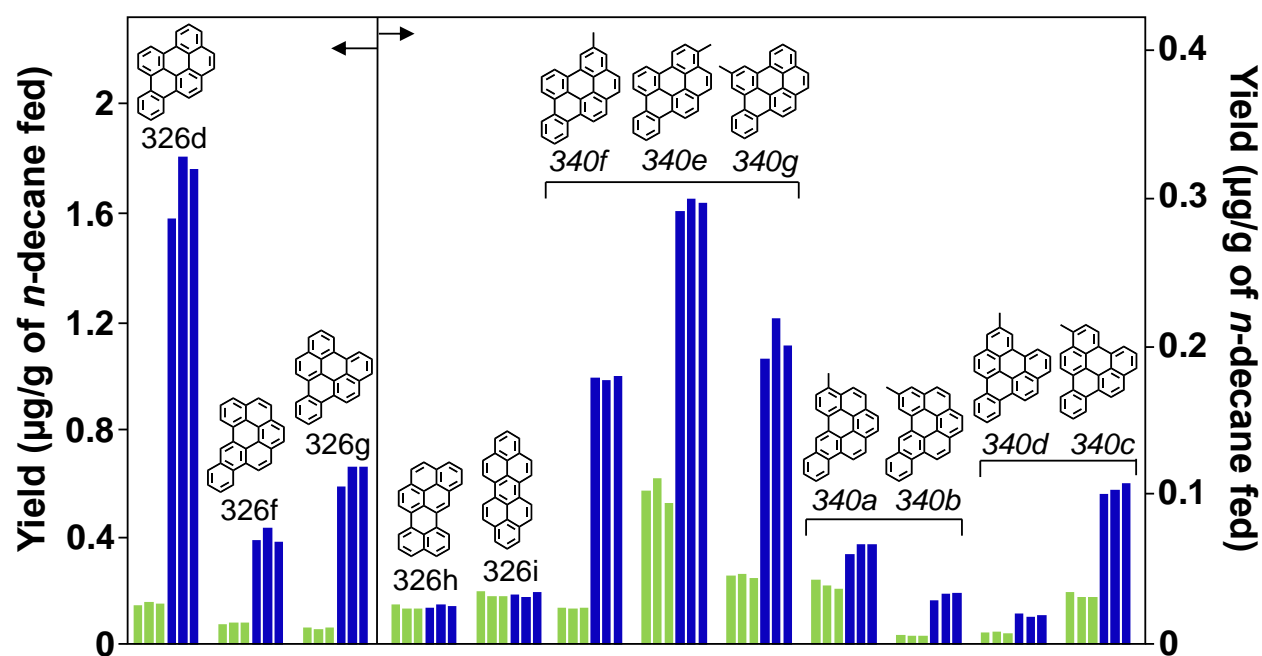


Figure 5.12. Yields of seven-ring  $C_{26}H_{14}$  PAH, and their methyl derivatives, from supercritical *n*-decane pyrolysis at 568 °C, 94.6 atm, and 133 sec: dibenzo[*e,ghi*]perylene (326d), dibenzo[*b,ghi*]perylene (326f), naphtho[1,2,3,4-*ghi*]perylene (326g), naphtho[8,1,2-*bcd*]perylene (326h), dibenzo[*cd,lm*]perylene (326i), three methyl-dibenzo[*e,ghi*]perylenes (340e-g), two methyl-dibenzo[*b,ghi*]perylenes (340a-b), and two methyl-naphtho[1,2,3,4-*ghi*]perylenes (340c-d). Experiments: (■) without dopant and (■) with 4-methylchrysene dopant (684 µg 4-methylchrysene / g *n*-decane fed). The positions of the methyl substituents on the dibenzo[*e,ghi*]perylene, dibenzo[*b,ghi*]perylene, and naphtho[1,2,3,4-*ghi*]perylene structures have been deduced, as noted in Table B1 in Appendix B and Figure 5.11.

Table B5 in Appendix B presents the multistep reaction sequences—involving the phenalenyl-type radicals of Figure 5.9, *n*-decane’s principal aliphatic reactants, and ring expansion—that account for formation of the three remaining peri-condensed benzenoid PAH in

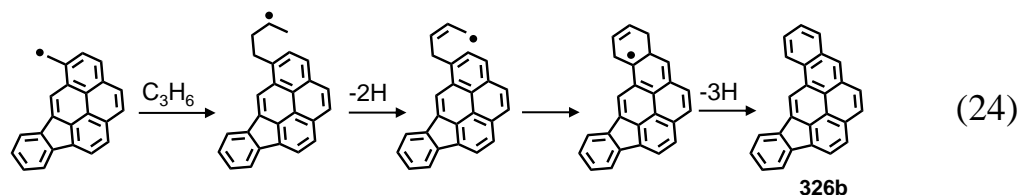
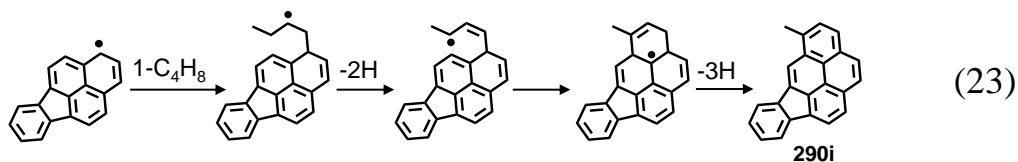
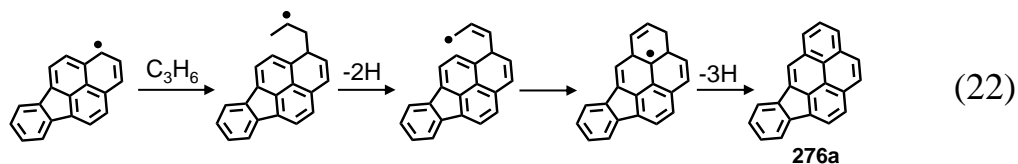
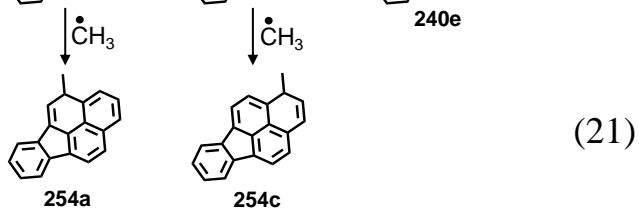
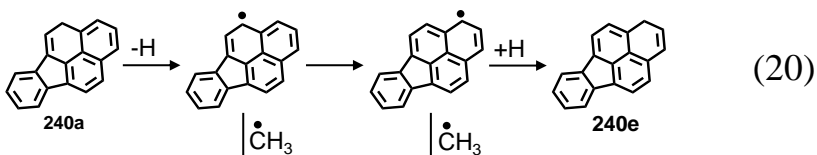
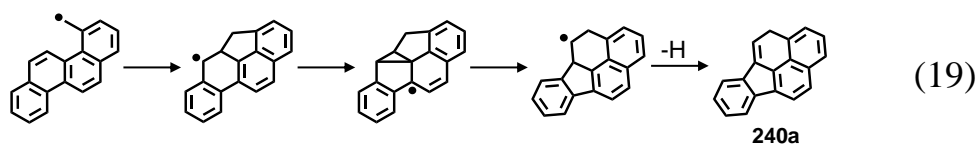
Figure 5.3c whose yields increase with 4-methylchrysene doping: the eight-ring benzo[*pqr*]naphtho[8,1,2-*bcd*]perylene (350a) and benzo[*ghi*]naphtho[8,1,2-*bcd*]perylene (350b) and the nine-ring naphtho[8,1,2-*abc*]coronene (374a).

Turning to Figure 5.3d, we notice that—unlike the products in Figures 5.3a-5.3c, whose structures each preserve the four-ring chrysene structure of the 4-methylchrysene dopant—the structures of the products in Figure 5.3d reveal that their formation has been accompanied by the conversion of one of 4-methylchrysene's six-membered rings into a five-membered ring. To account for these products, we propose Eq. (19), for the formation of 4*H*-benzo[*cd*]fluoranthene (240a), the first product of Figure 5.3d, and Eqs. (20)-(24), for the products stemming from this C<sub>19</sub>H<sub>12</sub> PAH. In Eq. (19), the 4-chrysenylmethyl radical attacks the aryl carbon across the bay to make the same intermediate as in Eq. (7). However, rather than losing H to form the major C<sub>19</sub>H<sub>12</sub> product 4*H*-cyclopenta[*def*]chrysene (240d) as in Eq. (7), this radical, in Eq. (19), attacks an internal carbon, forming a strained intermediate whose strain is relieved by a type of ring expansion that effectively reconfigures a six-membered-ring/five-membered-ring unit into a five-membered-ring/six-membered-ring unit. Subsequent dehydrogenation results in the C<sub>19</sub>H<sub>12</sub> product 4*H*-benzo[*cd*]fluoranthene (240a).

As a phenalene-type compound, 4*H*-benzo[*cd*]fluoranthene, as illustrated in Eq. (20), readily loses H at its saturated carbon, forming the resonance-stabilized phenalenyl-type radical 4-benzo[*cd*]fluoranthenyl. This radical can combine with methyl, as in Eq. (21), to give 4-methyl-4*H*-benzo[*cd*]fluoranthene (254a), whose yield, in Figure 5.3d, experiences a 34% dopant-induced increase—or it can convert, as in Eq. (20), to the other preferred resonance structure of the radical, 1-benzo[*cd*]fluoranthenyl. As illustrated in the rest of Eqs. (20)-(21), 1-benzo[*cd*]fluoranthenyl can itself combine with H and methyl to make, respectively, 1*H*-benzo[*cd*]fluoranthene (240e) and

1-methyl-1*H*-benzo[*cd*]fluoranthene (254c), whose yields, in Figure 5.3d, exhibit dopant-induced increases of ~25%.

Just as the phenalenyl-type radicals of Figure 5.9 react with *n*-decane's highest-yield alkene products propene and 1-butene, so do the benzo[*cd*]fluoranthenyl radicals of Eq. (20). Their reaction with propene, as exemplified by Eq. (22) for 1-benzo[*cd*]fluoranthenyl, produces indeno[1,2,3-*cd*]pyrene (276a), the highest-yield PAH of  $\geq 6$  rings in Figure 5.3, exhibiting, in Figure 5.3d, a five-fold increase in yield with 4-methylchrysene doping. A four-fold increase is exhibited by the last set of bars in Figure 5.3d, which corresponds to the summed yields of the five methylindeno[1,2,3-*cd*]pyrenes (among the nine we observe in Figure B13 in Appendix B) whose yields increase with 4-methylchrysene doping.



We do not have reference standards of all twelve possible methylindeno[1,2,3-*cd*]pyrene isomers, so we cannot tell exactly which ones are affected by the 4-methylchrysene doping and which are not. However, we believe that each of the five isomers whose yields increase are ones whose methyl group is on the four-ring “pyrene” unit of the indeno[1,2,3-*cd*]pyrene structure.

Our reasons are two-fold: First, as depicted in Figure 5.13 and exemplified by Eq. (23) for 1-benzo[*cd*]fluoranthenyl, the reactions of 1-benzo[*cd*]fluoranthenyl and 4-benzo[*cd*]fluoranthenyl with 1-butene give two such methylindeno[1,2,3-*cd*]pyrenes; two others result from propene’s reactions with the radicals of 4-methyl-4*H*-benzo[*cd*]fluoranthene (254a) and 1-methyl-1*H*-benzo[*cd*]fluoranthene (254c), Figure 5.3d’s third and fourth products. Second, as exemplified by Eq. (24), reaction of propene with the arylmethyl radical of each such “pyrene-unit-associated” methyl-substituted indeno[1,2,3-*cd*]pyrene gives a benzindeno[1,2,3-*cd*]pyrene in which the “benz” ring is fused to the pyrene unit of the indeno[1,2,3-*cd*]pyrene structure—a characteristic shared by the four benzindeno[1,2,3-*cd*]pyrene products (326b, 326k, 326j, 326c) of Figure 5.3d whose yields increase with doping. The isomer (326m) whose “benz” ring is not fused to the pyrene unit of the indeno[1,2,3-*cd*]pyrene structure is the one whose yield, in Figure 5.3d, does not increase with 4-methylchrysene doping.

We see then that in the supercritical *n*-decane pyrolysis environment, molecular growth of 4-methylchrysene proceeds along two major routes, each starting from 4-chrysenylmethyl’s reaction with the aryl carbon across the bay to make a C<sub>19</sub>H<sub>12</sub> PAH and its resonance-stabilized radical. One of these radicals, 4-benzo[*cd*]fluoranthenyl, reacts with *n*-decane’s abundant aliphatic species methyl and the C<sub>2</sub>-C<sub>4</sub> 1-alkenes to produce six- and seven-ring PAH with internal five-membered rings; while the other, 4-cyclopenta[*def*]chrysenyl, initiates a series of reactions with these same aliphatic species to produce *peri*-condensed benzenoid PAH as large as nine rings—

testifying to the efficacy of bay-region methyl-substituted PAH in contributing to the high-ring-number PAH that are precursors to carbonaceous solids.

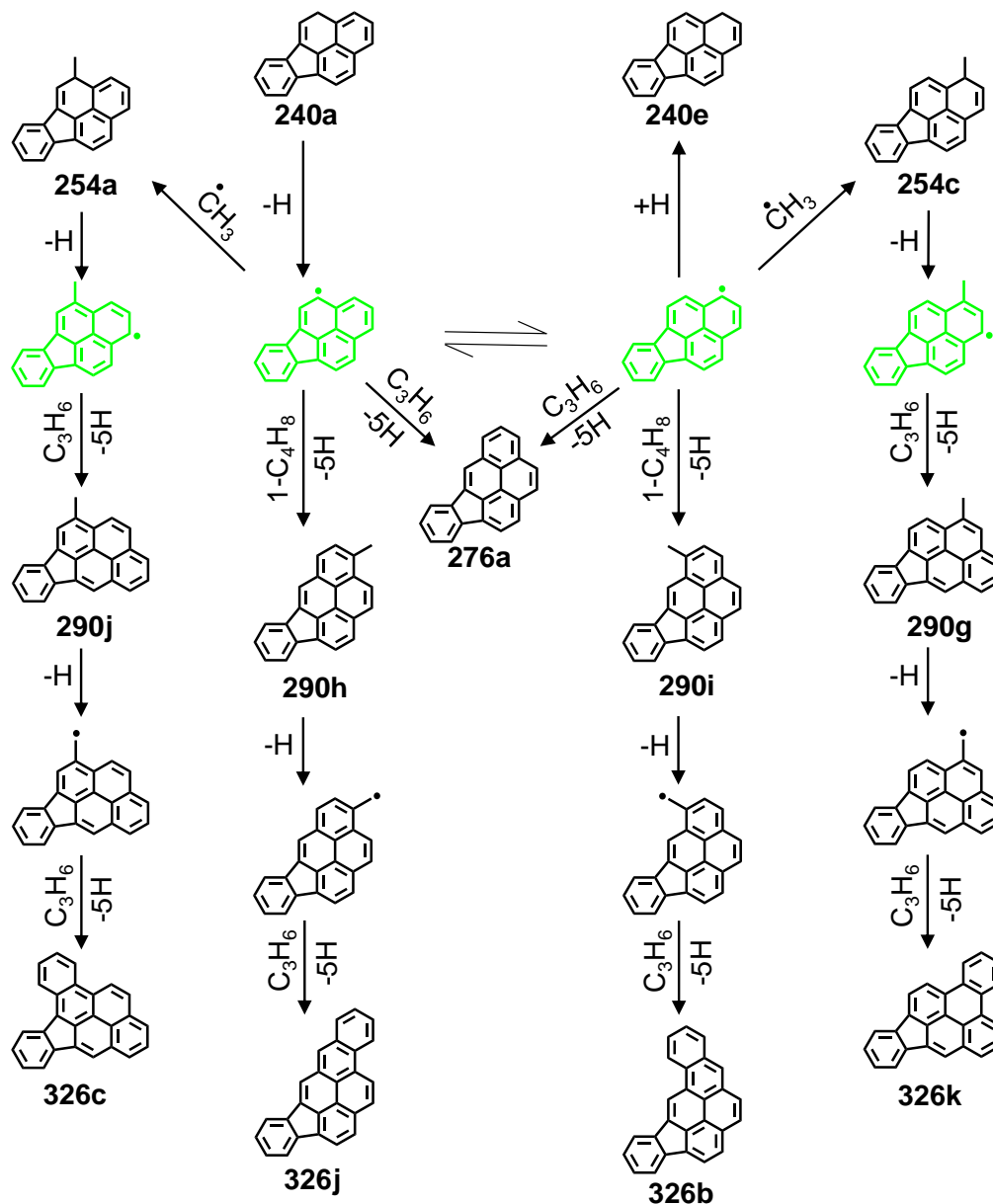


Figure 5.13. Reaction pathways of 4H-benzo[cd]fluoranthene (240a), 1H-benzo[cd]fluoranthene (240e), 4-methyl-4H-benzo[cd]fluoranthene (254a), and 1-methyl-1H-benzo[cd]fluoranthene (254c)—via their phenalenyl-type radicals (green structures)—to produce indeno[1,2,3-cd]pyrene (276a), 12-methylindeno[1,2,3-cd]pyrene (290j), 3-methylindeno[1,2,3-cd]pyrene (290h), 5-methylindeno[1,2,3-cd]pyrene (290i), 1-methylindeno[1,2,3-cd]pyrene (290g), benz[a]indeno[1,2,3-cd]pyrene (326c), benz[i]indeno[1,2,3-cd]pyrene (326j), benz[h]indeno[1,2,3-cd]pyrene (326b), and benz[l]indeno[1,2,3-cd]pyrene (326k).

## 5.4. Concluding Remarks

The supercritical *n*-decane pyrolysis experiments with the bay-region methyl-substituted PAH dopant 4-methylchrysene reveal that 4-methylchrysene exhibits several behaviors in this reaction environment that non-bay-region methyl-substituted PAH<sup>49,50</sup> dopants—*e.g.*, 1-methylnaphthalene, 2-methylnaphthalene, and 1-methylphenanthrene—do not: high dopant conversion and the ability to form the dopant's unsubstituted parent PAH and neighbor methyl-PAH isomer. More significant, however, are the differences in their pathways of molecular growth. For non-bay-region methyl-substituted PAH, molecular growth proceeds<sup>49,50</sup> with the respective arylmethyl radical—*e.g.*, 1-naphthylmethyl, 2-naphthylmethyl, or 1-phenanthrylmethyl—reacting with the principal aliphatic reactants that are most abundant in the supercritical *n*-decane pyrolysis environment: methyl, ethylene, propene, and 1-butene. Our experiments with the bay-region methyl-substituted dopant 4-methylchrysene, however, reveal that its arylmethyl radical, 4-chrysenylmethyl, does not react directly with any of these aliphatic species.

Instead, 4-methylchrysene's growth occurs chiefly through two routes, both of which take advantage of the bay-region position of 4-methylchrysene's methyl substituent. In the first route, 4-methylchrysene's resonance-stabilized arylmethyl radical 4-chrysenylmethyl attacks the aryl carbon just across the bay of 4-methylchrysene's structure to form the C<sub>19</sub>H<sub>12</sub> methylene-bridged PAH 4*H*-cyclopenta[*def*]chrysene, whose resonance-stabilized radical 4-cyclopenta[*def*]chrysenyl reacts with methyl and ethylene in ring-expansion reactions that selectively produce the five-ring C<sub>20</sub>H<sub>12</sub> benzo[*a*]pyrene and its derivatives 4- and 5-methylbenzo[*a*]pyrene. The arylmethyl radicals 4- and 5-benzo[*a*]pyrenylmethyl then undergo a series of reactions with *n*-decane's high-

yield C<sub>2</sub>-C<sub>4</sub> 1-alkenes to selectively produce particular six- to nine-ring *peri*-condensed benzenoid PAH, whose yields all increase dramatically with 4-methylchrysene doping.

In 4-methylchrysene's second major route of molecular growth, 4-chrysenylmethyl's attack of the aryl carbon across the bay is followed by an intramolecular rearrangement that produces the non-fully aromatic C<sub>19</sub>H<sub>12</sub> PAH 4*H*-benzo[*cd*]fluoranthene; reactions of its resonance-stabilized radicals with methyl, propene, and 1-butene selectively produce particular six- and seven-ring PAH with internal five-membered rings.

In both of 4-methylchrysene's principal routes of molecular growth, all of the reactions take place in the three-ring area that composes the methyl-substituted bay-region part of the 4-methylchrysene structure; 4-methylchrysene's fourth aromatic ring stays completely untouched throughout the growth processes. Therefore, the mechanisms determined here for the molecular growth of 4-methylchrysene would apply to any bay-region methyl-substituted PAH in the supercritical *n*-decane pyrolysis environment.

To substantiate the distinctive growth behaviors of bay-region methyl-substituted PAH, as exhibited by 4-methylchrysene, we have performed supercritical *n*-decane pyrolysis experiments to which 4-methylphenanthrene, *n*-decane's highest-yield bay-region methyl-substituted PAH product, has been added as a dopant. The next chapter will present the results of 4-methylphenanthrene-doping experiments.



## Chapter 6. Reaction Pathways of Molecular Growth for Bay-Region Methyl-Substituted Polycyclic Aromatic Hydrocarbons During Supercritical Pyrolysis of *n*-Decane, as Determined from Experiments with 4-Methylphenanthrene Dopant

### 6.1. Introduction

In its pre-combustion role as coolant, fuel in future high-speed aircraft will be expected to sustain temperatures and pressures as high as 700 °C and 130 atm<sup>1,5</sup> for times on the order of minutes. These conditions, supercritical for most hydrocarbons, will cause the fuel to undergo pyrolytic reactions that may lead to polycyclic aromatic hydrocarbons (PAH), which are precursors to fuel-line solids that can hinder the aircraft's safe operation. Therefore, understanding the formation pathways of PAH under supercritical conditions is important to prevent the formation of these solids.<sup>1,18,19,51</sup>

It is well documented that, of the many components in jet fuels, *n*-alkanes are particularly problematic with regard to solids formation under supercritical pyrolysis conditions.<sup>1</sup> Therefore, previous investigations from our group have focused on the model fuel *n*-decane,<sup>18,19,51</sup> whose supercritical pyrolysis produces an abundance of aliphatics, particularly *n*-alkanes and 1-alkenes, as well as one-ring aromatics and two- to nine-ring PAH—many of which are methyl-substituted.<sup>19,51</sup> To determine the reaction pathways of formation and growth of these PAH, Kalpathy *et al.*<sup>49,50</sup> from our research group have performed supercritical *n*-decane pyrolysis experiments to which lower-ring-number PAH that are representative of *n*-decane's aromatic products are added as dopants. These doping experiments have revealed<sup>49,50</sup> that at the temperatures of our experiments ( $\leq 700$  °C), the aromatic carbon-carbon bond does not break. Hence, only aromatic products of the same or higher ring number as the dopant are formed by the dopant, providing a way for discerning the pathways for that particular aromatic dopant's growth.<sup>49,50</sup>

Kalpathy *et al.*<sup>49,50</sup> have performed supercritical *n*-decane pyrolysis experiments with the dopants of Figure 6.1—1-methylnaphthalene, 2-methylnaphthalene, and 1-methylphenanthrene. These experiments<sup>49,50</sup> have revealed that the molecular growth of these methylaromatics occurs mainly through the reactions of the respective arylmethyl radicals (formed by removal of a methyl hydrogen) with four principal aliphatic species (methyl, ethylene, propene, and 1-butene) present in the supercritical *n*-decane pyrolysis environment. These doping experiments<sup>49,50</sup> have also shown that the position of the methyl substituent on the aromatic structure plays a crucial role in the formation and growth of PAH.

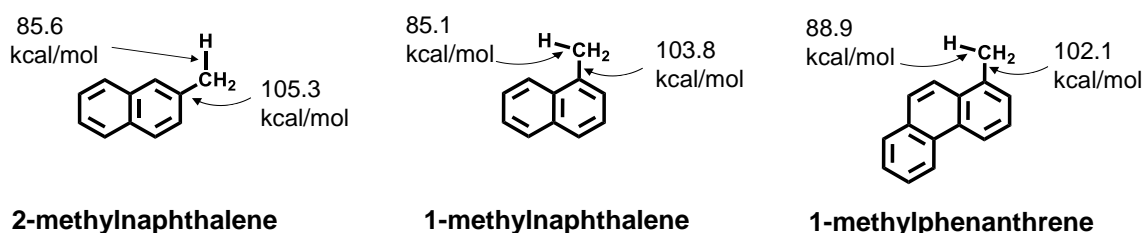


Figure 6.1. Molecular structures of 2-methylnaphthalene, 1-methylnaphthalene, and 1-methylphenanthrene and relevant bond-dissociation energies.<sup>38,52</sup> This figure is adapted from Vutukuru *et al.*<sup>51</sup>

Besides the two types of methyl-substituted PAH exemplified by the dopants of Figure 6.1, the supercritical *n*-decane pyrolysis also produces a third type of methyl-substituted PAH, whose methyl group is in a bay region of the PAH structure.<sup>49-51</sup> It has been observed that, in the supercritical *n*-decane pyrolysis products, these bay-region methyl-substituted PAH are always the lowest-yield isomers among the methyl derivatives of a given PAH.<sup>49,50</sup> However, experimental evidence<sup>49,50</sup> suggests that the low-yield status of these bay-region methyl-substituted PAH may be a result of their tendency, once formed, to convert to other products. To investigate the growth reactions of bay-region methyl-substituted PAH in the supercritical *n*-alkane pyrolysis environment, in our earlier paper,<sup>51</sup> we have performed supercritical *n*-decane experiments with

the first methyl-substituted PAH dopant illustrated in Figure 6.2: 4-methylchrysene, a four-ring PAH whose structure is representative of *n*-decane's three- to six-ring bay-region methyl-substituted PAH products.

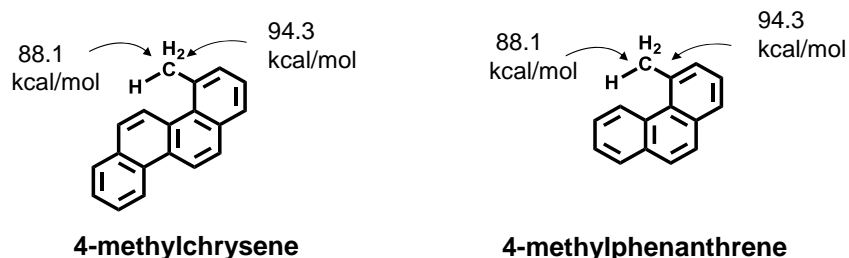


Figure 6.2. Molecular structures of 4-methylchrysene and 4-methylphenanthrene and relevant bond-dissociation energies.<sup>38,52</sup>

The supercritical *n*-decane pyrolysis experiments doped with 4-methylchrysene were performed at conditions of rapid PAH growth (568 °C, 94.6 atm, and 133 sec). Results from these supercritical *n*-decane pyrolysis experiments with 4-methylchrysene<sup>51</sup> as dopant have revealed that this bay-region-methyl-substituted dopant exhibits several behaviors that are different from those of the non-bay-region-methyl-substituted dopants<sup>49,50</sup> previously investigated by our research group. These behaviors are as follows: (a) 4-methylchrysene's dopant conversion (52.5±2.3%) is an order of magnitude higher than those of the non-bay-region-methyl-substituted dopants<sup>49,50</sup> previously investigated; (b) because of its methyl group being in a bay region, 4-methylchrysene<sup>51</sup> has a special ability to produce its unsubstituted parent PAH (chrysene) and its neighbor isomer (3-methylchrysene)—behavior not exhibited by the previously investigated non-bay-region-methyl-substituted dopants<sup>49,50</sup> of Figure 6.1; (c) 4-methylchrysene's resonance-stabilized arylmethyl radical 4-chrysenylmethyl, due to its configuration, has the ability to attack the aryl carbon just across the bay to form two resonance-stabilized C<sub>19</sub>H<sub>11</sub> radicals—one, 4-benzo[*cd*]fluoranthenyl, which reacts with *n*-decane's abundant aliphatic species methyl and the C<sub>2</sub>-C<sub>4</sub> 1-alkenes to produce six- and seven-ring PAH with internal five-membered rings; and the

other, 4-cyclopenta[*def*]chrysenyl, which initiates a series of reactions with these same aliphatic species to produce *peri*-condensed benzenoid PAH as large as nine rings.<sup>51</sup>

To substantiate the distinctive growth behaviors of bay-region methyl-substituted PAH, as exhibited by 4-methylchrysene, we have performed supercritical *n*-decane pyrolysis experiments to which 4-methylphenanthrene (second methyl-substituted PAH dopant shown in Figure 6.2), *n*-decane's highest-yield bay-region methyl-substituted PAH product, has been added as a dopant at a concentration of 0.685 mg/g *n*-decane, which is same as that used in the experiments with 4-methylchrysene.<sup>51</sup>

## 6.2. Experimental Equipment and Procedures

We have performed two sets of supercritical *n*-decane pyrolysis experiments in an isothermal, silica-lined stainless-steel flow reactor at 568 °C, 94.6 atm, and 133 sec, which are conditions of rapid PAH growth. The reactor design and procedures for the experiments have been described in chapter 2.

In Set 1, ten identical experiments have been performed with neat *n*-decane (99.5% pure; critical temperature, 344.5 C; critical pressure, 20.7 atm) as fuel; in Set 2, three identical experiments are carried out with the fuel *n*-decane to which 4-methylphenanthrene (99.3% pure; synthesized by the Biochemical Institute for Environmental Carcinogens, Germany) has been added as a dopant at a concentration of 0.685 mg/g *n*-decane. The chosen dopant concentration is high enough to bring about observable effects on the pyrolysis-product yields. However, this dopant is too low to influence the physical properties of the reaction environment.<sup>51</sup>

For each of the pyrolysis experiments, the products exiting the reactor are quenched to room temperature and collected as described in chapter 2 of this thesis. The aliphatic and one- and two-ring aromatic products are analyzed by gas chromatography (GC) coupled with flame-

ionization detection (FID) and mass-spectrometric (MS) detection. The highly complex PAH product mixtures are separated by a two-dimensional high-pressure liquid chromatographic technique.<sup>19,46,47,51</sup> In the first stage of separation, the PAH products are fractionated by using a normal-phase high-pressure liquid chromatography (HPLC)—the higher-yield PAH requiring one fractionation procedure; the lower-yield, higher-ring-number PAH requiring a particularly involved (in terms of time and solvent consumption) fractionation procedure.<sup>19,51</sup> Subsequently, isomer-specific product identification and quantification is achieved by analyzing each PAH-product fraction by reversed-phase HPLC with diode-array ultraviolet-visible (UV) absorbance and mass-spectrometric (MS) detection, after extensive calibration with reference standards.<sup>19,46,47,51</sup> The UV and mass spectra establishing the identities of the PAH products reported in this chapter are documented elsewhere.<sup>46,47</sup>

### **6.3. Results and Discussion**

Two sets of supercritical *n*-decane pyrolysis experiments have been conducted at 568 °C, 94.6 atm, and 133 sec, which are conditions of rapid PAH growth. In Set 1, ten identical experiments have been performed with neat *n*-decane (99.5% pure; critical temperature, 344.5 C; critical pressure, 20.7 atm) as fuel; in Set 2, three identical experiments are carried out with the fuel *n*-decane to which 4-methylphenanthrene (99.3% pure) has been added as a dopant at a concentration of 0.685 mg/g *n*-decane, which is same as that used in the experiments with 4-methylchrysene.<sup>51</sup> For each pyrolysis experiment, a total of 320 products (90 aliphatic products and 230 aromatic products) have been quantified. The names, molecular formulas, number/letter codes, and chemical structures of the 230 quantified aromatic products appear in Table C1 in Appendix C.

The structures and yields of the 36 PAH products whose yields are significantly affected by the 4-methylphenanthrene dopant are presented in Figure 6.3, where the yields from the Set-1 *n*-decane-only experiments are plotted as the green bars, and the yields from the Set-2 *n*-decane experiments doped with 4-methylphenanthrene are plotted as the red bars. Analysis of most of the PAH products of five or more rings requires the more-involved (in terms of time and solvent consumption) fractionation, so the products from only three of the ten undoped experiments undergo that analysis. Therefore, there are only three green bars in Figure 6.3 for each of those products' yields from the undoped experiments. For the three PAH of Figure 6.3 that are produced in the *n*-decane pyrolysis experiments with dopant—but are not produced in detectable amounts in the *n*-decane-only experiments—only red bars appear in Figure 6.3 for these products.

Before analyzing the products whose yields are affected by the 4-methylphenanthrene dopant, it is important to bear in mind, from the yields of the products in Figures C1-C5 of Appendix C, that the dopant has no measurable effects on: (a) the level of *n*-decane conversion, which remains constant at  $90 \pm 0.3\%$  for all the thirteen experiments; (b) the yields of *n*-decane's aliphatic products, which primarily consist of the C<sub>1</sub>-C<sub>9</sub> *n*-alkanes as well as the C<sub>2</sub>-C<sub>9</sub> 1-alkenes; or (c) the yields of *n*-decane's aromatic products of ring number lower than that of the dopant (there is no evidence of aromatic-ring rupture). It is also important to note that, in our supercritical *n*-decane pyrolysis experiments, there is no evidence of acetylene or any hydrocarbon with a C-C triple bond. All of these observations from the 4-methylphenanthrene-doped *n*-decane experiments are consistent with our research groups' previous findings<sup>49,50</sup> from the *n*-decane pyrolysis experiments with the non-bay-region-methyl-substituted dopants of Figure 6.1.

A close look at Figure 6.2 reveals that the molecular structure of 4-methylphenanthrene, except for one less aromatic-ring, is the same as that of the other bay-region methyl-substituted

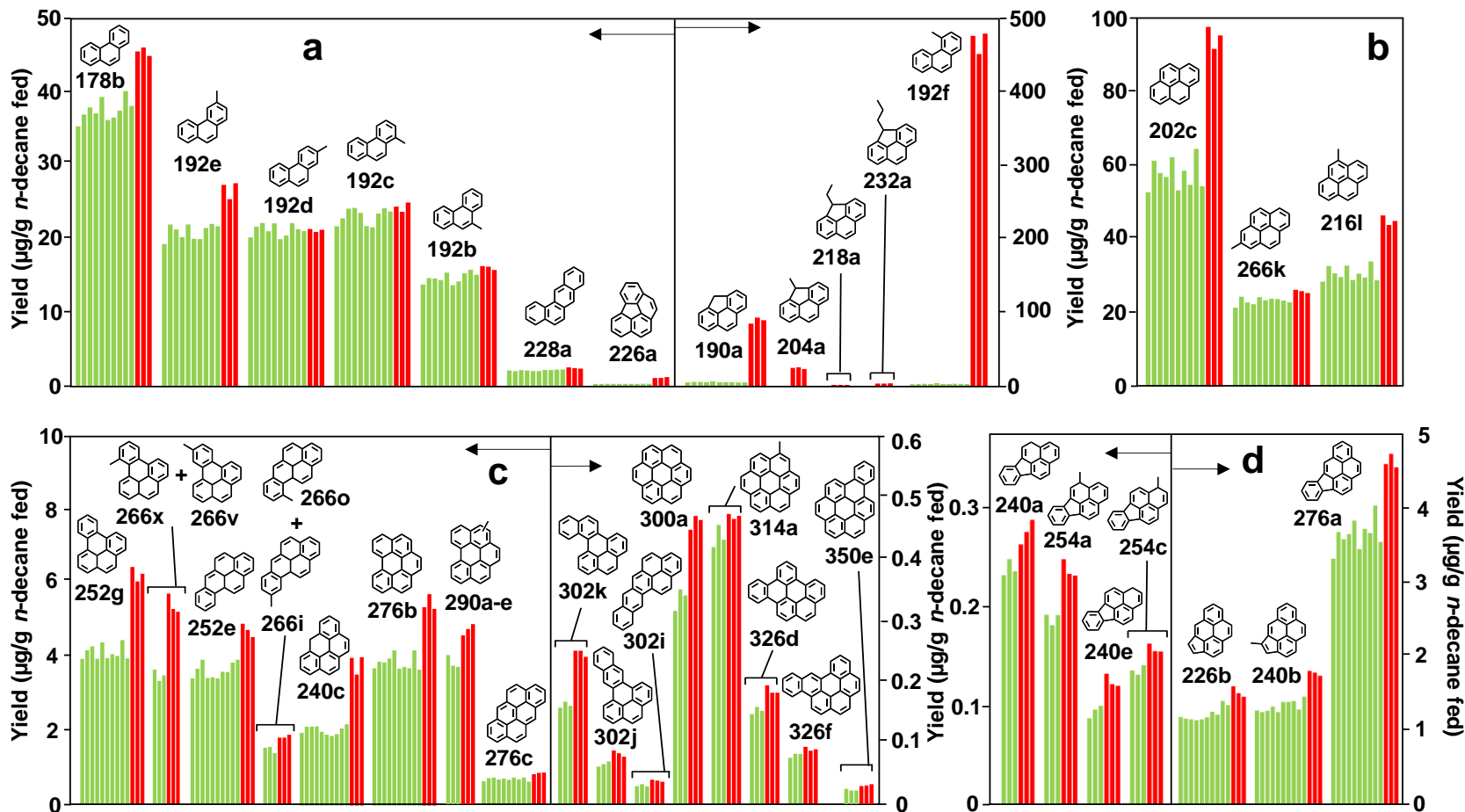


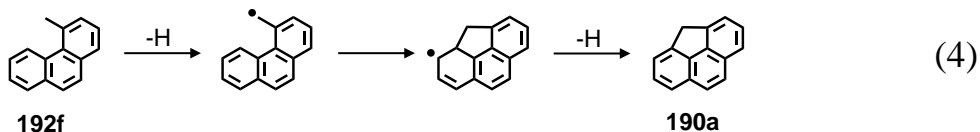
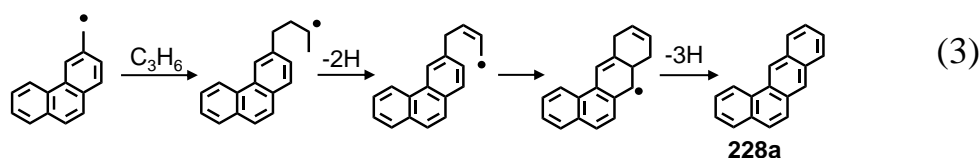
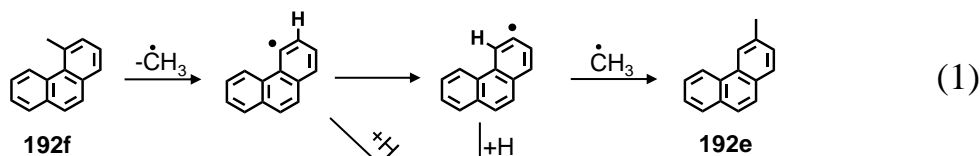
Figure 6.3. Yields of selected PAH products of supercritical *n*-decane pyrolysis at 568 °C, 94.6 atm, and 133 sec: (a) three- to five-ring PAH, (b) pyrene and its methyl derivatives, (c) five- to eight-ring benzenoid PAH and derivatives, and (d) five- and six-ring PAH with internal five-membered rings. Experiments: (■) without dopant; (■) with 4-methylphenanthrene dopant. All product names, structures, and number/letter codes are listed in Table C1 in Appendix C. Analysis of most high-ring-number PAH requires a very lengthy, highly solvent-consuming fractionation procedure, so the products from only three of the ten undoped experiments undergo that analysis; hence there are only three green bars for these products' yields from the undoped experiments.

dopant, 4-methylchrysene. Hence, we believe that both the bay-region methyl-substituted dopants, 4-methylphenanthrene and 4-methylchrysene,<sup>51</sup> will have similar growth reactions in the supercritical *n*-decane pyrolysis environment. First, the 4-methylphenanthrene dopant, just like 4-methylchrysene, has no effects on: (a) the level of *n*-decane conversion; (b) the yields of *n*-decane's aliphatic products; and (c) the yields of *n*-decane's aromatic products of ring number lower than that of the dopant. Second, the red bars for 4-methylphenanthrene (192f), at the end of Figure 6.3a, reveal that the yield of unreacted dopant from the second set of *n*-decane pyrolysis experiments is 466±15 µg/g *n*-decane fed, which corresponds to a dopant conversion of 31.9±2.2%. This dopant conversion, similar to 4-methylchrysene's conversion, is also an order of magnitude higher than those of Figure 6.1's other dopants.<sup>49,50</sup>

Next, the red bars for the first product, phenanthrene (178b), reveal that this product's yield is 22% higher in the 4-methylphenanthrene-doping experiments than in the *n*-decane only experiments (green bars). Similarly, the second product of Figure 6.3a, 3-methylphenanthrene (192e) experiences a 28% dopant-induced increase in its yield. However, as shown in Figure 6.3a, none of the other methylphenanthrenes show this dopant-induced increase in their yields. This unique growth behavior of 4-methylphenanthrene to produce its unsubstituted parent PAH (phenanthrene) and its neighbor isomer (3-methylphenanthrene)—like 4-methylchrysene—is mostly linked to its methyl group being in a bay region, where it experiences steric repulsive forces near the H across the bay. Because of these forces, the methyl-C/aryl-C bond-dissociation energy for 4-methylphenanthrene (94.3 kcal/mole<sup>51,52</sup>), as shown in Figures 6.1 and 6.2, is 7.8 to 11.0 kcal/mole lower than the corresponding values for the dopants whose methyl groups are not in bay regions—allowing homolytic scission of 4-methylphenanthrene's methyl-C/aryl-C bond to form 4-phenanthryl radical, as shown in the first step of Eq. (1). 4-phenanthryl radical can add H, as



shown in Eq. (2), to form phenanthrene (178b), or—as indicated by the 4-methylphenanthrene-induced enhancement of 3-methylphenanthrene’s yield—proceed with the H shift<sup>51,53</sup> of Eq. (1) to form 3-phenanthryl radical, whose reaction with methyl forms 3-methylphenanthrene (192e).



A consequence of the 4-methylphenanthrene-induced increase in 3-methylphenanthrene’s yield is an elevated level of 3-phenanthrylmethyl radical, which, as illustrated in Eq. (3), reacts with propene to produce benz[*a*]anthracene (228a), the sixth product in Figure 6.3a and the only C<sub>18</sub>H<sub>12</sub> PAH in Figure 6.4 to exhibit dopant-induced increase in yield.

The high red bars of the eighth, ninth, tenth, and eleventh products in Figure 6.3a reveal that 4*H*-cyclopenta[*def*] phenanthrene(190a) and its alkylated derivatives are the most favored products of 4-methylphenanthrene. As shown in Eq. (4), loss of H from 4-methylphenanthrene’s methyl carbon forms the resonance-stabilized arylmethyl radical 4-phenanthrylmethyl, which later attacks the carbon across the bay at phenanthrene’s “5” position, and subsequent dehydrogenation reaction results in the formation of 4*H*-cyclopenta[*def*]phenanthrene (190a). This special ability of the arylmethyl radicals whose methyl group is in a bay region position, undoubtedly accounts for 4-

methylphenanthrene's high conversion, relative to that of the other methyl-substituted dopants of Figure 6.1, as well as its high selectivity for 4*H*-cylopenta[*def*]phenanthrene (190a).

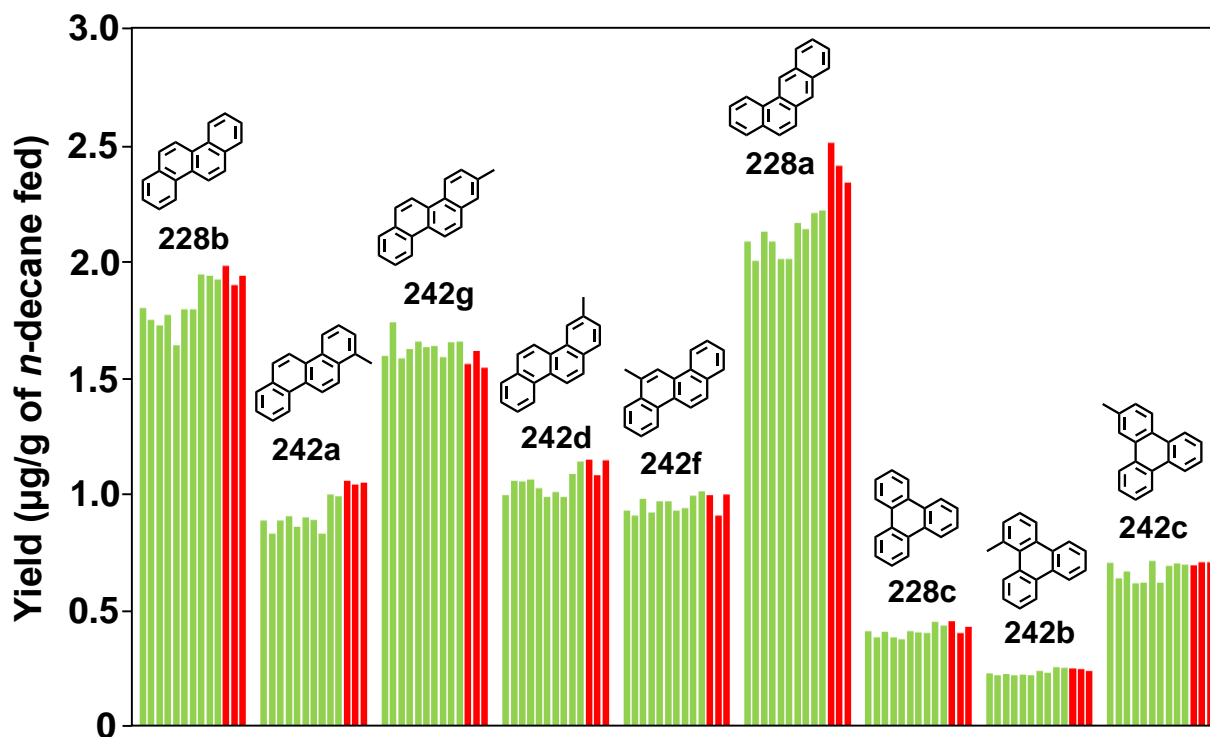


Figure 6.4. Yields of four-ring  $C_{18}H_{12}$  PAH, and their alkyl derivatives, from supercritical *n*-decane pyrolysis at 568 °C, 94.6 atm, and 133 sec: (a) chrysene (228b), 1-methylchrysene (242a), 2-methylchrysene (242g), 3-methylchrysene (242d), 6-methylchrysene (242f), benz[*a*]anthracene (228a), triphenylene (228c), 1-methyltriphenylene (242b), and 2-methyltriphenylene (242c). Experiments: (■) without dopant and (■) with 4-methylphenanthrene dopant (685 µg 4-methylphenanthrene / g *n*-decane fed).

Figure 6.5 reveals that the fifteen-carbon structure of 4*H*-cylopenta[*def*]phenanthrene contains the structure of fluorene, a three-ring PAH that was previously investigated<sup>50</sup> as a dopant in supercritical *n*-decane pyrolysis experiments. As shown in Figure 6.5, both the structures contain a five-membered ring whose  $CH_2$  methylene bridge has a relatively low C-H bond-dissociation energy of around 82.0 kcal/mole.<sup>38,50</sup> Therefore, as shown in the first step of Eq. (5), 4*H*-cylopenta[*def*] phenanthrene can readily form its resonantly stabilized 9-fluorenyl-type radical

4-cyclopenta[*def*]phenanthryl, which subsequently reacts with the most abundant aliphatic species in the supercritical *n*-decane pyrolysis environment.

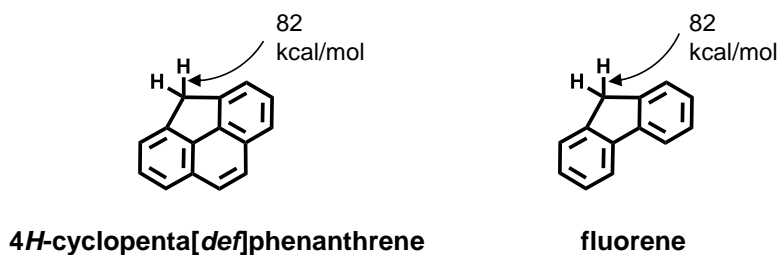
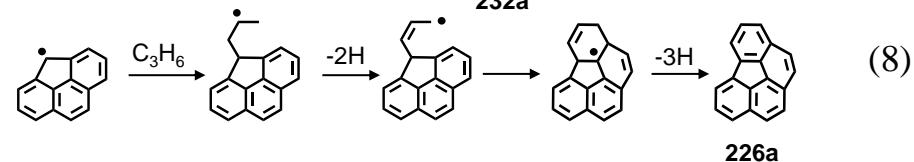
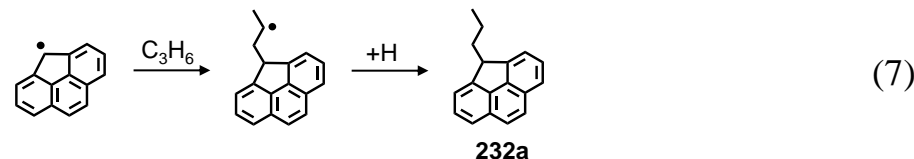
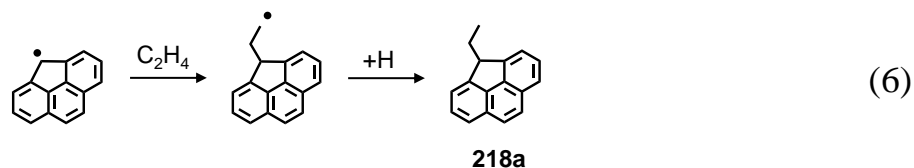
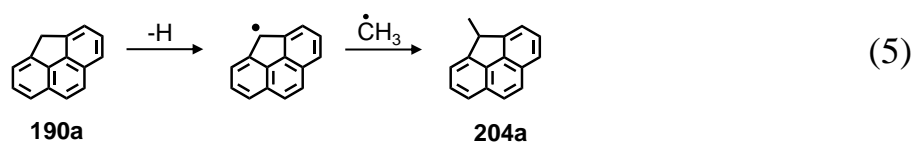


Figure 6.5. Molecular structures of 4H-cyclopenta[*def*]phenanthrene and fluorene and relevant bond-dissociation energies.<sup>38,50</sup>

As illustrated in the second step of Eq. (5), 4-cyclopenta[*def*]phenanthryl reacts with methyl to form 4-methyl-4H-cyclopenta[*def*]phenanthrene (204a), the ninth product in Figure 6.3a. Equation (6) shows that the reaction of 4-cyclopenta[*def*]phenanthryl with ethylene forms 4-ethyl-4H-cyclopenta[*def*]phenanthrene (218a), the tenth product in Figure 6.3a. Similarly, Eq. (7) shows that the reaction of 4-cyclopenta[*def*]phenanthryl with propene forms 4-propyl-4H-cyclopenta[*def*]phenanthrene (232a), the eleventh product in Figure 6.3a.



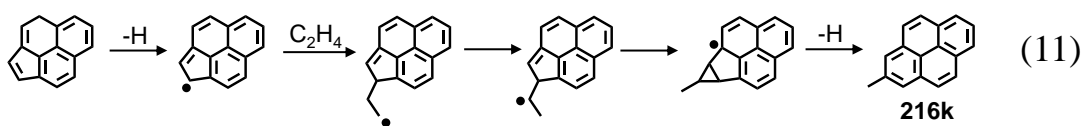
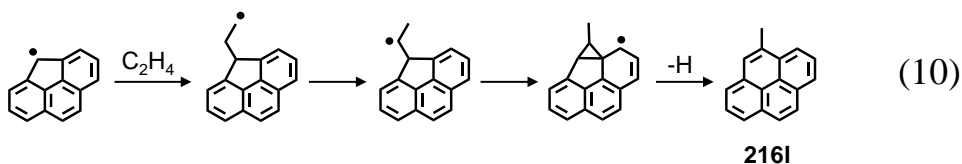
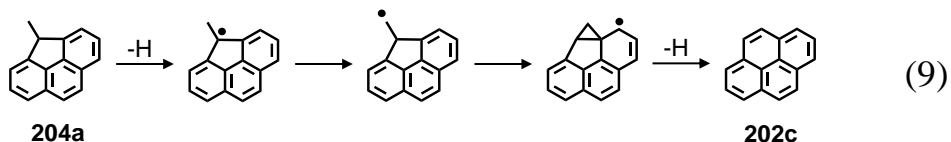
This unique growth behavior of 4-methylphenanthrene to form 4*H*-cyclopenta[*def*]phenanthrene (190a) and its alkylated derivatives is similar to that of the other bay-region methyl-substituted dopant, 4-methylchrysene (242h). The remaining product of Figure 6.3a, benzo[*ghi*]fluoranthene (226a) results from alternative reaction of 4-cyclopenta[*def*]phenanthryl with propene, as shown in Eq. (8).

Now let's shift our attention to Figure 6.3b and referring to Figures 6.6a and 6.6b, we see that 4-methylphenanthrene doping brings about a 64% increase in the yield of one C<sub>16</sub>H<sub>10</sub> PAH, pyrene (202c), but has no effect on the yields of any of the other two C<sub>16</sub>H<sub>10</sub> PAH products of supercritical *n*-decane pyrolysis. This selectivity is further seen in Figure 6.6b for pyrene's methyl derivatives: of the three different methylpyrenes of *n*-decane, only two, 2-methylpyrene (216k) and 4-methylpyrene (216l), experience dopant-induced increases of 17% and 47%, respectively, as evident in Figure 6.3b.

Although pyrene and its 2- and 4- methyl derivatives contain only six-membered rings, experimental evidence suggests that they do not result directly from reactions with 4-phenanthrylmethyl—which does not even combine with methyl, as no 4-ethylphenanthrene is observed in our products. The doping experiments with fluorene demonstrated<sup>50</sup> that 9-methylfluorene underwent ring expansion to form the benzenoid PAH phenanthrene (178b), and 9-fluorenyl reacted with ethylene in ring-expansion reaction to yield exclusively 9-methylphenanthrene (192b). We believe that the analogous ring-expansion reactions happen even in the case of 4-methylphenanthrene-doping experiments.

The ring-expansion reaction of 4-methyl-4*H*-cyclopenta[*def*]phenanthrene (204a) would form pyrene (202c), as illustrated in Eq. (9). Similarly, the ring-expansion reaction of 4-cyclopenta[*def*]phenanthryl with ethylene would form 4-methylpyrene (216l), as shown in Eq.

(10). 2-methylpyrene (216k) results from a different type of ring-expansion reaction, as shown in Eq. (11), which will be discussed at a later stage.



The results of Figures 6.3a and 6.3b reveal that there are two major routes for bay-region methyl-substituted PAH, such as 4-methylphenanthrene, to grow by one ring number. In the first route, as shown by Eqs. (1) and (3), the bay-region methyl-substituted PAH converts to its neighbor isomer; the arylmethyl radical of this neighbor isomer subsequently reacts with propene to form a benzenoid PAH of one higher ring number. Whereas in the second route, shown by the Eq.-(4)-(5)-(9) sequence, the arylmethyl radical of the bay-region-substituted PAH reacts with the aryl carbon across the bay to form a methylene-bridged PAH. This methylene-bridged PAH readily loses H to form its resonance-stabilized 9-fluorenyl-type radical that combines with methyl and subsequently undergoes a ring-expansion reaction to form a benzenoid PAH of one higher ring number. Instead of reacting with methyl, if this 9-fluorenyl-type radical reacts with ethylene in ring-expansion reaction such as Eq. (10), the product is a methyl-substituted benzenoid PAH—4-methylpyrene in this case. All of these growth behaviors are consistent with the other bay-region methyl-substituted dopant, 4-methylchrysene.<sup>51</sup>

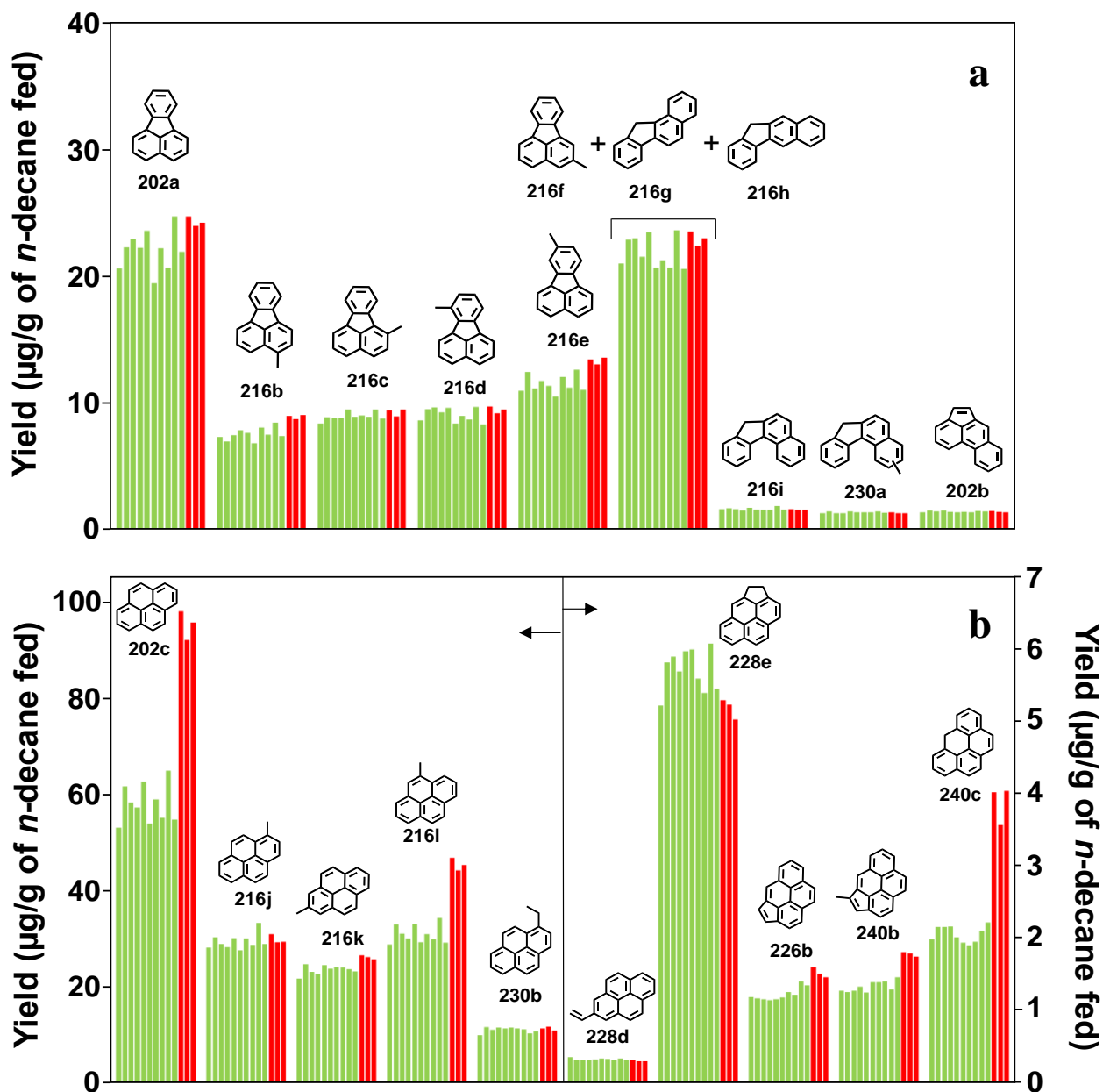


Figure 6.6. Yields of four-ring PAH, and their derivatives, from supercritical *n*-decane pyrolysis at 568 °C, 94.6 atm, and 133 sec: (a) acephenanthrylene (202b), fluoranthene (202a), the five methylfluoranthenes (216b-f) (one of which co-elutes with benzo[*a*]fluorene (216g) and benzo[*b*]fluorene (216h)), benzo[*c*]fluorene (216i), and a methylbenzo[*c*]fluorene (230a); (b) pyrene (202c), 1-methylpyrene (216j), 2-methylpyrene (216k), 4-methylpyrene (216l), 1-ethylpyrene (230b), 2-vinylpyrene (228d), 3,4-dihydrocyclopenta[*cd*]pyrene (228e), cyclopenta[*cd*]pyrene (226b), 4-methylcyclopenta[*cd*]pyrene (240b), and 6*H*-benzo[*cd*]pyrene (240c). Experiments: (■) without dopant and (■) with 4-methylphenanthrene dopant (685 µg 4-methylphenanthrene / g *n*-decane fed). The yield reported in (b) for 1-ethylpyrene might include contributions from co-eluting ethylpyrenes or dimethylpyrenes; hence it is a maximum possible 1-ethylpyrene yield.

We have seen that 4-methylphenanthrene doping increases the yields of 2-methylpyrene (216k) and 4-methylpyrene (216l). Both of these methyl-substituted PAH, once formed, can readily form their resonance-stabilized arylmethyl radicals (4-pyrenylmethyl and 2-pyrenylmethyl)—opening the door to PAH growth by more than one ring number. To understand the role of 4-pyrenylmethyl and 2-pyrenylmethyl in our reaction environment, we look at Figure 6.3c, which presents the yields of selected five- to eight-ring *peri*-condensed benzenoid PAH products and their methyl-substituted derivatives, and observe Figure 6.7, which shows how these products are formed via reactions with the highly abundant aliphatic reactants: methyl, ethylene, propene, and 1-butene.

To begin with, the large black structures in the middle of the top row in Figure 6.7 represent the 4-pyrenylmethyl radical (on the left) and the 2-pyrenylmethyl radical (on the right). In Figure 6.7, the phenalenyl-type radicals are shown in green, and blue structures represent the products of reactions with propene. Analogous to 4-methylchrysene-doping experiments,<sup>51</sup> in cases where the bay-region methyl-substituted PAH converts, as shown in Eq. (1), to the neighbor isomer, we show the structure of the product neighbor isomer in purple. In cases where the bay-region methyl-substituted PAH undergoes the Eq.-(4)-(5)-(9) methylene-bridge/methyl-addition/ring-expansion sequence to produce a benzenoid PAH, we show the product PAH in red.<sup>51</sup> Similarly, if the bay-region methyl-substituted PAH undergoes the Eq.-(4)-(6)-(10) methylene-bridge/ethylene-addition/ring-expansion sequence to produce a methyl-substituted benzenoid PAH, we show that PAH in red. In Figure 6.7, all structures with number/letter codes correspond to unequivocally identified products which experience dopant-induced increases in their yields.

4-methylphenanthrene doping brings about 30% and 50% increases in the yields of two C<sub>20</sub>H<sub>12</sub> PAH, benzo[*a*]pyrene (252e) and benzo[*e*]pyrene (252g), respectively. However, as shown





in Figure C10 of Appendix C, the same dopant has no effect on the yields of any of the other five C<sub>20</sub>H<sub>12</sub> PAH products of supercritical *n*-decane pyrolysis. This high selectivity is further seen in case of methyl derivatives of benzo[*e*]pyrene and benzo[*a*]pyrene. As shown in Figure 6.8a and 6.8b, out of the twelve different methylbenzo[*a*]pyrene products of *n*-decane, only two, 9-methylbenzo[*a*]pyrene (266i) and 10-methylbenzo[*a*]pyrene (266o), experience dopant-induced increases in yield; and in case of benzo[*e*]pyrene's methyl derivatives: of the six different methylbenzo[*e*]pyrene products, only two, 9-methylbenzo[*e*]pyrene (266x) and 10-methylbenzo[*e*]pyrene (266v), exhibit dopant-induced increases in yield. As shown at the top of Figure 6.7, reaction of propene with 4-pyrenylmethyl and 2-pyrenylmethyl results, respectively, in benzo[*e*]pyrene (252g) and benzo[*a*]pyrene (252e), as shown in blue. As shown to the left of 4-pyrenylmethyl and to the right of 2-pyrenylmethyl in Figure 6.7, each of these arylmethyl radicals react with 1-butene to produce two bay-region methyl-substituted PAH, 9-methylbenzo[*e*]pyrene (266x) and 10-methylbenzo[*a*]pyrene (266o), whose yields show dopant-induced increases in Figure 6.3c. Both of these bay-region methyl-substituted PAH, like 4-methylchrysene,<sup>51</sup> each readily convert to: (1) their neighbor isomers (10-methylbenzo[*e*]pyrene (266v) and 9-methylbenzo[*a*]pyrene (266i), shown in purple on the top row of Figure 6.7), whose yields increase with 4-methylphenanthrene-doping, and (2) their methylene-bridged derivatives (shown in grey because we do not observe them experimentally).

Next, as shown at the left and right ends of Figure 6.7's top row, the arylmethyl radicals of 10-methylbenzo[*e*]pyrene (266v) and 9-methylbenzo[*a*]pyrene (266i) each react with propene to form, respectively, naphtho[1,2-*e*]pyrene (302k), and naphtho[2,3-*a*]pyrene (302i). Both of these PAH, as shown in Figure 6.3c, exhibit dopant-induced increases in their yields. The arylmethyl radical of 10-methylbenzo[*e*]pyrene (266v) can react with propene to form, alternatively,

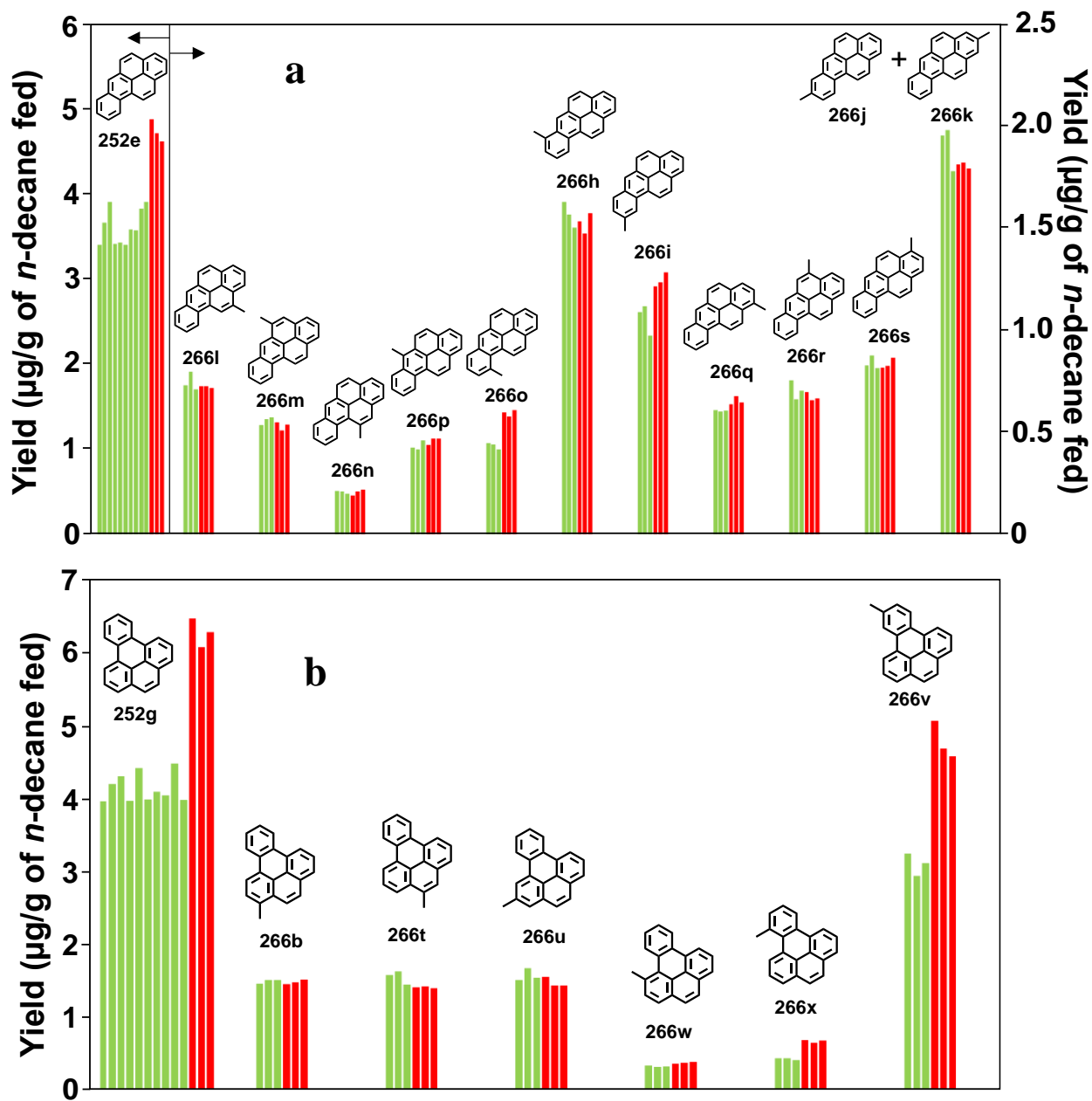


Figure 6.8. Yields of five-ring  $C_{20}H_{12}$  PAH, and their methyl derivatives, from supercritical *n*-decane pyrolysis at 568 °C, 94.6 atm, and 133 sec: (a) benzo[*a*]pyrene (252e), 12-methylbenzo[*a*]pyrene (266l), 5-methylbenzo[*a*]pyrene (266m), 11-methylbenzo[*a*]pyrene (266n), 6-methylbenzo[*a*]pyrene (266p), 10-methylbenzo[*a*]pyrene (266o), 7-methylbenzo[*a*]pyrene (266h), 9-methylbenzo[*a*]pyrene (266i), 1-methylbenzo[*a*]pyrene (266q), 4-methylbenzo[*a*]pyrene (266r), 3-methylbenzo[*a*]pyrene (266s), and 2-methylbenzo[*a*]pyrene (266k) co-eluting with 8-methylbenzo[*a*]pyrene (266j); (b) benzo[*e*]pyrene (252g), 3-methylbenzo[*e*]pyrene (266b), 4-methylbenzo[*e*]pyrene (266t), 2-methylbenzo[*e*]pyrene (266u), 1-methylbenzo[*e*]pyrene (266w), 9-methylbenzo[*e*]pyrene (266x), and 10-methylbenzo[*e*]pyrene (266v). Experiments: (■) without dopant and (■) with 4-methylphenanthrene dopant (685 µg 4-methylphenanthrene / g *n*-decane fed).

naphtho[2,3-*e*]pyrene (302j), whose yields compose the tenth set of bars in Figure 6.3c. As shown at the left and right ends of Figure 6.7's second row, the two methylene-bridged derivatives (shown in grey) undergo the Eq.-(5)-(9)-type methyl-addition/ring-expansion sequence to produce two C<sub>22</sub>H<sub>12</sub> PAH shown in red: benzo[*ghi*]perylene (276b) and anthanthrene (276c), whose yields, as shown in Figure 6.3c, exhibit dopant-induced increases of 42% and 24%, respectively. Additionally, the methylene bridged derivative of benzo[*e*]pyrene can also undergo the Eq.-(6)-(10)-type ethylene-addition/ring-expansion sequence to produce two methyl-substituted PAH shown in red: 4-methylbenzo[*ghi*]perylene (290a) and 3-methylbenzo[*ghi*]perylene (290e), whose yields, as shown in Figure 6.9, exhibit dopant-induced increases. As shown at the left end of Figure 6.7's fourth row, the two methylated derivatives of benzo[*ghi*]perylene react with propene to produce a C<sub>26</sub>H<sub>14</sub> PAH shown in blue: dibenzo[*e,ghi*]perylene (326d), whose yield, as shown in Figure 6.3c, experiences a 22% dopant-induced increase.

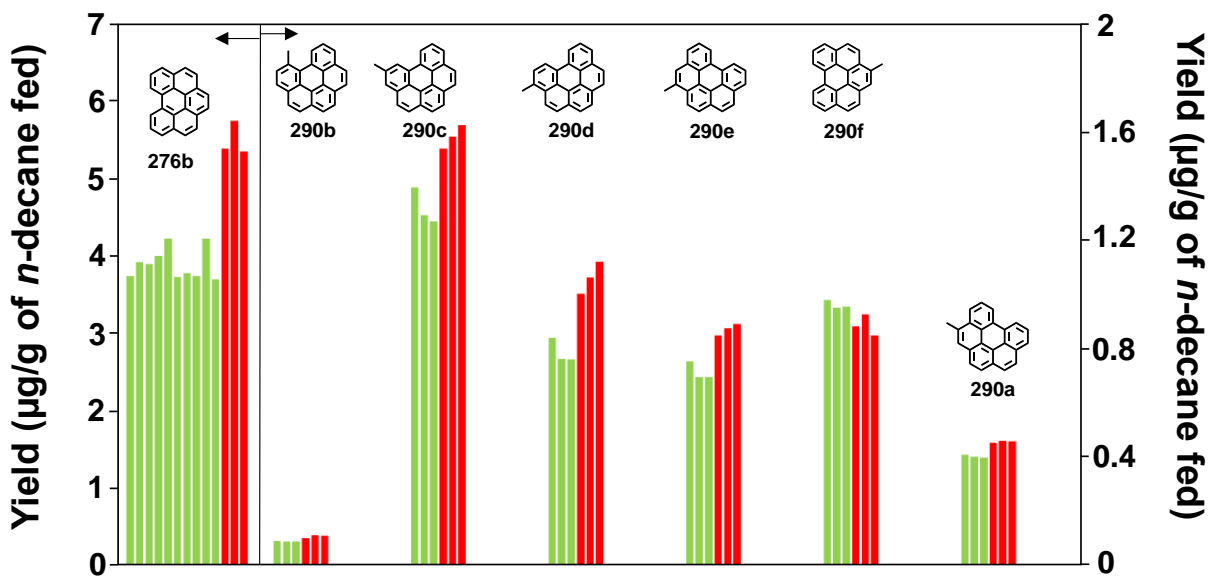


Figure 6.9. Yields of benzo[*ghi*]perylene (276b) and the six methylbenzo[*ghi*]perylenes (290a-f), from supercritical *n*-decane pyrolysis at 568 °C, 94.6 atm, and 133 sec. Experiments: (■) without dopant and (■) with 4-methylphenanthrene dopant (685 µg 4-methylphenanthrene / g *n*-decane fed). Among the sets of bars associated with the six methylbenzo[*ghi*]perylene products, the set for 4-methylbenzo[*ghi*]perylene (290a) is assigned to that isomer since we have a reference standard for that isomer; a lack of reference standards for the other five methylbenzo[*ghi*]perylene isomers prevents assigning the other sets of bars to particular isomers.

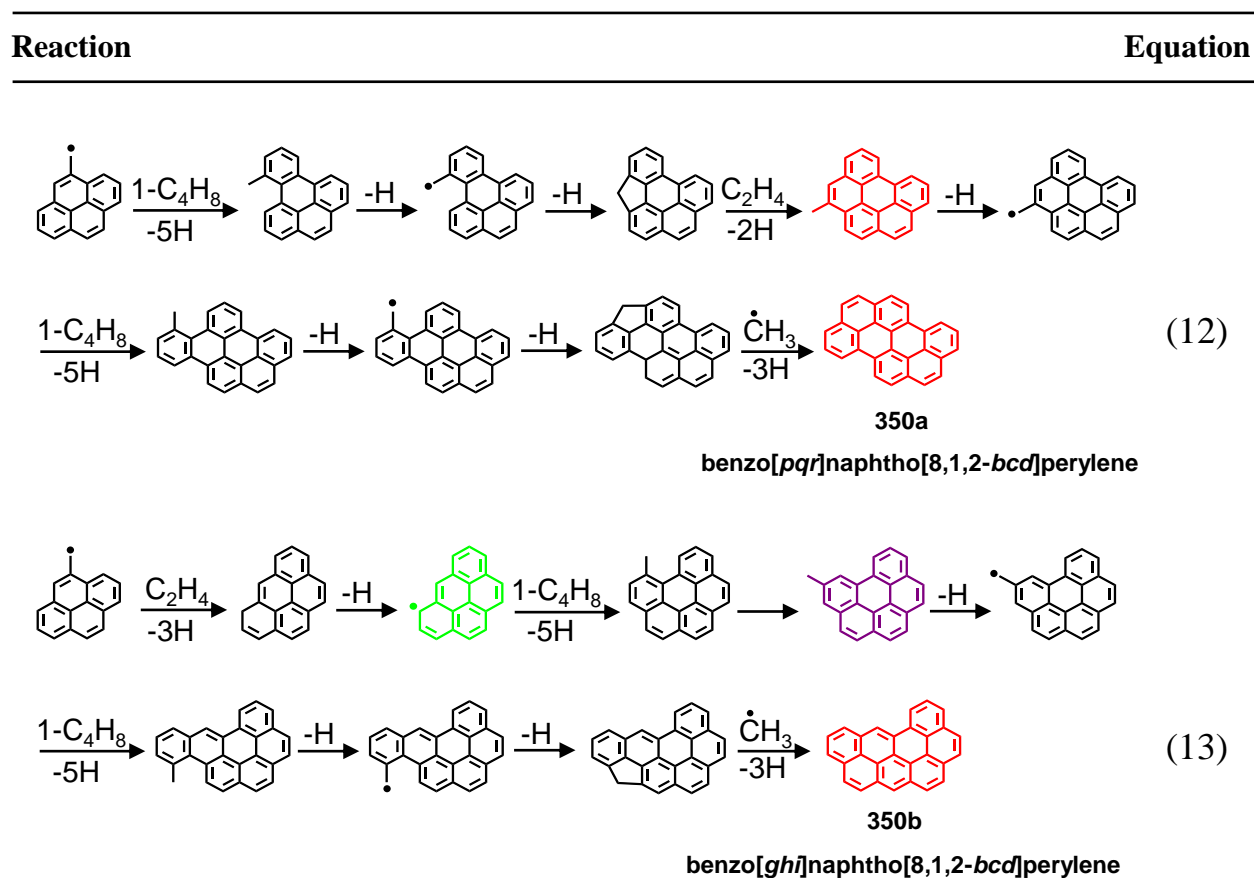
A close look at the structure of 4-pyrenylmethyl shows that it is of the same type as 1-naphthylmethyl and 1-phenanthrylmethyl. Therefore, as demonstrated by Kalpathy *et al.*<sup>49,50</sup> in our previous doping experiments with 1-methylnaphthalene and 1-methylphenanthrene, 4-pyrenylmethyl can also react with ethylene to form 6*H*-dibenzo[*cd*]pyrene (240c), whose yield, as shown by the fifth set of bars in Figure 6.3c, experiences a 42% dopant-induced increase. The 6*H*-dibenzo[*cd*]pyrene, once formed, can readily lose its H at the saturated carbon and form the respective phenalenyl-type radicals—whose resonance structures are shown in green in Figure 6.7. As indicated by the two blue structures in the sixth row of Figure 6.7, these phenalenyl-type radicals react with propene to form dibenzo[*b,ghi*]perylene (326f), whose yield, as shown in Figure 6.3c, increases with doping (~15%). The phenalenyl-type radicals' reactions with 1-butene results in the formation of two methyl-substituted PAH: 7-methylbenzo[*ghi*]perylene (290b) and 5-methylbenzo[*ghi*]perylene (290d), whose yields, as shown in Figure 6.9, exhibit dopant-induced increases.

A close look at the structure of 7-methylbenzo[*ghi*]perylene (290b) reveals that its methyl-group is in a bay-region position. Therefore, 7-methylbenzo[*ghi*]perylene (290b)—like its bay-region methyl-substituted counterparts at the top of Figure 6.7—(a) converts to its neighbor isomer 6-methylbenzo[*ghi*]perylene (shown in purple on Figure 6.7's seventh row), whose yield, as shown in Figure 6.9, increases with doping, (b) undergoes the Eq.-(4)-(5)-(9) methylene-bridge/methyl-addition/ring-expansion sequence to produce coronene (300a), whose yield, as shown in Figure 6.3c, exhibits a dopant-induced increase, and (c) undergoes the Eq.-(4)-(6)-(10) methylene-bridge/ethylene-addition/ring-expansion sequence to produce 1-methylcoronene (314a), whose yield, as illustrated in Figure 6.3c, also exhibits a dopant-induced increase. Finally, both the methyl-substituted benzo[*ghi*]perylene (290c and 290d) react with propene to form

dibenzo[*b,ghi*]perylene (326f), whose yield, as shown in Figure 6.3c, increases with doping. In a similar way, 1-methylcoronene (314a) also reacts with propene to form benzo[*a*]coronene (350e), whose yield, as shown in Figure 6.3c, exhibits a dopant-induced increase.

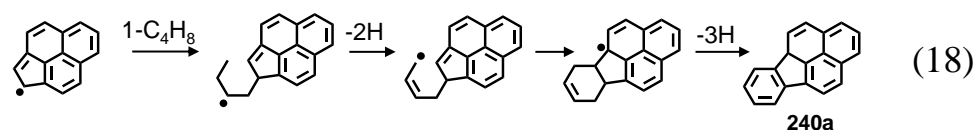
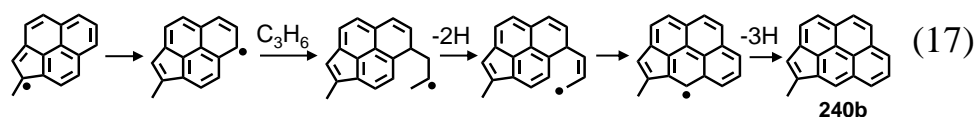
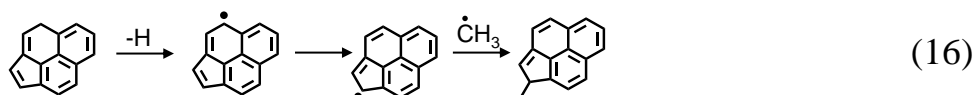
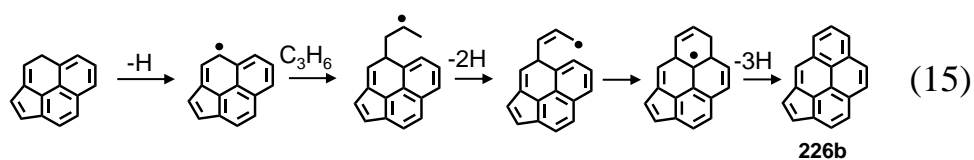
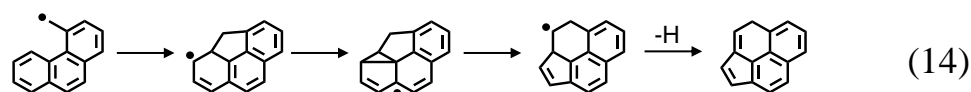
Table 6.1 presents the reaction sequences—involving the phenalenyl-type radicals of Figure 6.7, *n*-decane's principal aliphatic reactants, and ring expansion—that account for formation of the two remaining peri-condensed benzenoid PAH in Figure C17 (Appendix C) whose yields increase with 4-methylphenanthrene doping: the eight-ring benzo[*pqr*]naphtho[8,1,2-*bcd*]perylene (350a) and benzo[*ghi*]naphtho[8,1,2-*bcd*]perylene (350b).

Table 6.1. Proposed pathways for the formation of benzo[*pqr*]naphtho[8,1,2-*bcd*]perylene and benzo[*ghi*]naphtho[8,1,2-*bcd*]perylene from reactions of 4-pyrenylmethyl with the principal aliphatic growth species—methyl, ethylene, and 1-butene—in the supercritical *n*-decane pyrolysis environment.



Now let's try to focus our attention to the products in Figure 6.3d. First, we observe that—unlike the products in Figures 6.3a-6.3c, whose structures each preserve the three-ring 'phenanthrene' structure of the 4-methylphenanthrene dopant—the structures of the products in Figure 6.3d clearly show that their formation has been accompanied by the conversion of one of 4-methylphenanthrene's six-membered rings into a five-membered ring. We believe that all of these products with internal five-membered rings result from 4*H*-cyclopenta[*cd*]phenalene, a phenalene-type compound, whose formation pathway is shown in Eq. (14). We do not observe this product because it is highly reactive and readily forms its resonance-stabilized phenalenyl-type radical 4-cyclopenta[*cd*]phenalenyl. This radical, as shown in Eq. (15), reacts with propene to form cyclopenta[*cd*]pyrene (226b), whose yield, as shown in Figure 6.3d, experiences a 25% dopant-induced increase—or it can convert, as illustrated in Eq. (16), to the other phenalenyl-type resonance structure of the radical, 1-cyclopenta[*cd*]phenalenyl.

As shown in Eq. (16), 1-cyclopenta[*cd*]phenalenyl can readily combine with methyl to make, 1-methyl-1*H*-cyclopenta[*cd*]phenalene. We do not observe this product experimentally because it, as shown in Eq. (17), readily forms its resonance-stabilized phenalenyl-type radical that subsequently converts to the other preferred resonance structure of the radical. This resonance-stabilized phenalenyl-type radical, as illustrated in the second step of Eq. (17), reacts with propene to form 4-methylcyclopenta[*cd*]pyrene (240b), whose yield, as shown in Figure 6.3d, exhibits a 35% dopant-induced increase. As shown in Eq. (11), 1-cyclopenta[*cd*]phenalenyl can react with ethylene in ring-expansion reaction to form 2-methylpyrene (216k), whose yield, as shown in Figure 6.3b, increases with 4-methylphenanthrene-doping. As illustrated in Eq. (18), 1-cyclopenta[*cd*]phenalenyl radical can also react with 1-butene to form 4*H*-benzo[*cd*]fluoranthene (240a), whose yield, as shown in Figure 6.3d, increases with 4-methylphenanthrene-doping.



4-methylchrysene-doping experiments<sup>51</sup> have revealed that 4*H*-benzo[*cd*]fluoranthene (240a), once formed, continues PAH growth. To understand the role of 4*H*-benzo[*cd*]fluoranthene in the supercritical *n*-decane pyrolysis environment, we turn to Figure 6.10, which shows how the remaining products in Fig. 3d are formed from 4*H*-benzo[*cd*]fluoranthene. In Figure 6.10, the phenalenyl-type radicals are shown in green. First, as illustrated at the top of Figure 6.10, 4*H*-benzo[*cd*]fluoranthene readily loses its H at the saturated carbon, forming the resonance-stabilized phenalenyl-type radical 4-benzo[*cd*]fluoranthenyl. This radical reacts with methyl, as illustrated at the left end of Figure 6.10's top row, to form 4-methyl-4*H*-benzo[*cd*]fluoranthene (254a), whose yield, as illustrated by the second set of bars in Figure 6.3d, exhibits a 16% dopant-induced increase—or it can convert, as illustrated at the top center of Figure 6.10, to the other preferred resonance structure of the radical, 1-benzo[*cd*]fluoranthenyl. The resonance-stabilized

phenalenyl-type radical 1-benzo[*cd*]fluoranthenyl, as illustrated at the right end of Figure 6.10's top row, can react with H and methyl to form, respectively, 1*H*-benzo[*cd*]fluoranthene (240e) and 1-methyl-1*H*-benzo[*cd*]fluoranthene (254c), whose yields, as shown in Figure 6.3d, experience dopant-induced increases of 30% and 16%, respectively.

Both the phenalenyl-type benzo[*cd*]fluoranthenyl radicals (green structures) of Figure 6.10 react with *n*-decane's highest-yield alkene products propene and 1-butene. Their reaction with propene, as shown at the center of Figure 6.10, forms indeno[1,2,3-*cd*]pyrene (276a), whose yield, as illustrated by the last set of bars in Figure 6.3d, exhibits a 26% dopant-induced increase. Out of the nine methylindeno[1,2,3-*cd*]pyrenes we observe in Figure C14 of Appendix C, five methylindeno[1,2,3-*cd*]pyrenes exhibit dopant-induced increases in their yields.

Although we do not have reference standards for all the twelve possible methylindeno[1,2,3-*cd*]pyrene isomers, we believe that each of the five isomers whose yields increase are the following ones: 12-methylindeno[1,2,3-*cd*]pyrene (290j), 3-methylindeno[1,2,3-*cd*]pyrene (290h), 5-methylindeno[1,2,3-*cd*]pyrene (290i), 1-methylindeno[1,2,3-*cd*]pyrene (290g), and 10-methylindeno[1,2,3-*cd*]pyrene (290q).

We have the following two mechanistic reasons: first, as shown in the last row of Figure 6.10, the reactions of 1-benzo[*cd*]fluoranthenyl and 4-benzo[*cd*]fluoranthenyl (resonance-stabilized phenalenyl-type radicals, green structures) with 1-butene give two of these methylindeno[1,2,3-*cd*]pyrenes (290h and 290i). As shown in the last row of Figure 6.10, the other two methylindeno[1,2,3-*cd*]pyrene isomers result from propene's reactions with the radicals of 4-methyl-4*H*-benzo[*cd*]fluoranthene (254a) and 1-methyl-1*H*-benzo[*cd*]fluoranthene (254c), the second and fourth set of bars in Figure 6.3d.



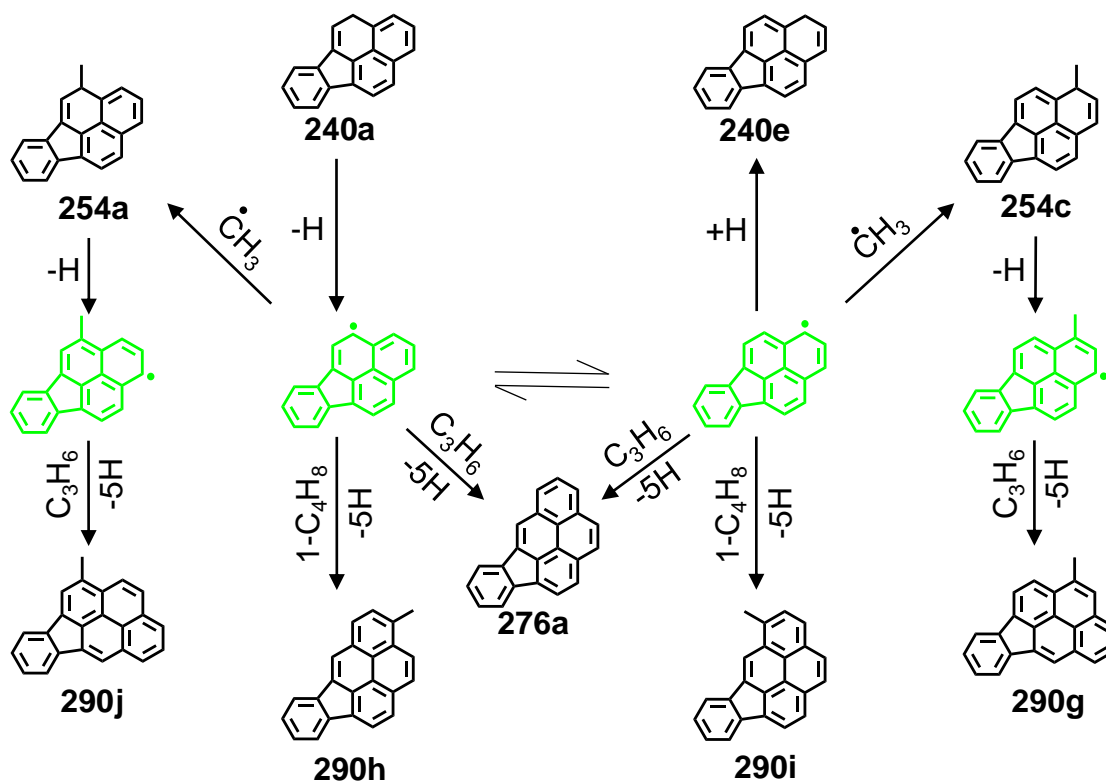
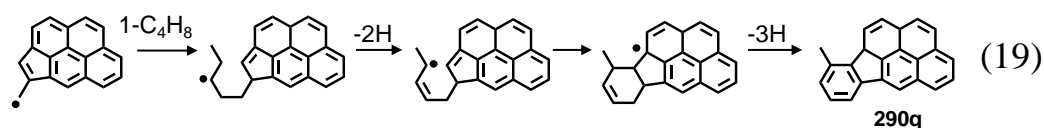


Figure 6.10. Reaction pathways of 4*H*-benzo[*cd*]fluoranthene (240a), 1*H*-benzo[*cd*]fluoranthene (240e), 4-methyl-4*H*-benzo[*cd*]fluoranthene (254a), and 1-methyl-1*H*-benzo[*cd*]fluoranthene (254c)—via their phenalenyl-type radicals (green structures)—to produce indeno[1,2,3-*cd*]pyrene (276a), 12-methylindeno[1,2,3-*cd*]pyrene (290j), 3-methylindeno[1,2,3-*cd*]pyrene (290h), 5-methylindeno[1,2,3-*cd*]pyrene (290i), and 1-methylindeno[1,2,3-*cd*]pyrene (290g). This figure is adapted from Vutukuru *et al.*<sup>51</sup>

Second, we have seen that 4-methylphenanthrene-doping brings about a 35% increase in the yield of 4-methylcyclopenta[*cd*]pyrene (240b). As shown in Eq. (19), the reaction of 1-butene with the arylmethyl radical of 4-methylcyclopenta[*cd*]pyrene forms 10-methylindeno[1,2,3-*cd*]pyrene (290q), the fifth isomer of methylindeno[1,2,3-*cd*]pyrene whose yield increased with 4-methylphenanthrene-doping.



## 6.4. Concluding Remarks

Results from our supercritical *n*-decane pyrolysis experiments with 4-methylphenanthrene as dopant have revealed that this bay-region-methyl-substituted dopant exhibits several behaviors that are different from those of the non-bay-region-methyl-substituted dopants<sup>49,50</sup> previously investigated by our research group. These behaviors are as follows: (1) 4-methylphenanthrene's dopant conversion (31.9+2.2%) is almost an order of magnitude higher than those of the non-bay-region-methyl-substituted dopants<sup>49,50</sup> previously investigated; (2) due to its methyl group being in a bay-region position, 4-methylphenanthrene has a special ability to produce its unsubstituted parent PAH (phenanthrene) as well as its neighbor isomer (3-methylphenanthrene); (3) 4-methylphenanthrene's resonance-stabilized arylmethyl radical 4-phenanthrylmethyl, due to its structure, has the ability to attack the aryl carbon just across the bay to form two resonance-stabilized C<sub>15</sub>H<sub>9</sub> radicals—one, 4-cyclopenta[*cd*]phenalenyl, which reacts with *n*-decane's principal aliphatic species methyl and the C<sub>2</sub>-C<sub>4</sub> 1-alkenes to form five- and six-ring PAH with internal five-membered rings; and the other, 4-cyclopenta[*def*]phenanthryl, which initiates a series of reactions with these same aliphatic species to produce *peri*-condensed benzenoid PAH as large as nine rings. All of these findings from the 4-methylphenanthrene-doped *n*-decane experiments are consistent with our findings<sup>51</sup> from the *n*-decane pyrolysis experiments with the other bay-region-methyl-substituted dopant 4-methylchrysene.

Similar to 4-methylchrysene,<sup>51</sup> all of the growth reactions of 4-methylphenanthrene take place only in the three-ring area that composes the methyl-substituted bay-region part of the 4-methylphenanthrene structure—substantiating the distinctive growth behaviors of bay-region methyl-substituted PAH.

## Chapter 7. Conclusions and Recommendations

### 7.1. Summary

The purpose of the research conducted for this dissertation is to gain more insight into the formation pathways of polycyclic aromatic hydrocarbons (PAH), which are precursors to fuel-line carbonaceous solid deposits, in the pre-combustion environment of next-generation hypersonic aircraft, where the fuel is expected to sustain supercritical conditions. These carbonaceous solid deposits, which are formed when hydrocarbon fuels undergo pyrolytic reactions, can clog fuel delivery lines and hamper aircraft's safety.<sup>1</sup> Deposit formation of as little as 1 ppm (of the fuel fed), within a matter of a few hours, can hinder the aircraft's safe operation.<sup>1</sup> Therefore, it is extremely important to understand the reaction mechanisms that govern PAH formation and growth in the supercritical fuel pyrolysis environment.

To better understand these reaction pathways, Kalpathy *et al.*<sup>48</sup> from our research group performed supercritical pyrolysis experiments in a silica-lined stainless-steel tubular flow reactor with the model fuel *n*-decane (critical temperature, 344.5 °C; critical pressure 20.7 atm), an *n*-alkane component of jet fuels,<sup>18,19</sup> at a constant pressure of 94.6 atm, a fixed residence time of 133 sec, and at six temperatures ranging from 530 to 570 °C.<sup>48</sup> Since *n*-alkanes are major components of jet fuels and are known to be particularly problematic regarding solids formation, Kalpathy *et al.*<sup>48</sup> chose to investigate an *n*-alkane. The strong temperature dependence of the product yields revealed that temperature has a strong influence on the supercritical pyrolysis behavior of *n*-decane.<sup>48</sup> Therefore, to complement the previous *n*-decane pyrolysis work at 94.6 atm, 133 sec, and at six temperatures in the range of 530-570 °C, we have performed additional supercritical *n*-decane pyrolysis experiments<sup>54</sup> at lower temperatures. The findings from these supercritical *n*-decane pyrolysis experiments at lower temperatures are presented in section 7.2.

The supercritical *n*-decane pyrolysis experiments produce an abundance of aliphatics as well as one-ring aromatics and two- to nine-ring PAH—many of which are methyl-substituted. These methyl-substituted PAH are ready sources of the resonance stabilized arylmethyl radicals.<sup>19</sup> Therefore, to understand the potential role of arylmethyl radicals in the supercritical *n*-alkane pyrolysis environment, Kalpathy *et al.*<sup>49,50</sup> from our research group performed supercritical *n*-decane pyrolysis experiments with three methyl-aromatic dopants: 1-methylnaphthalene, 2-methylnaphthalene, and 1-methylphenanthrene. These experiments were carried out in a silica-lined stainless-steel tubular reactor at 570 °C, 94.6 atm, and 133 sec, conditions of incipient solids formation for *n*-decane.

The dopant experiments of Kalpathy *et al.*<sup>49,50</sup> showed that the position of the methyl substituent on the aromatic structure plays a significant role in PAH growth.<sup>49,50,51</sup> Besides the two types of methyl-PAH exemplified by the dopants—1-methylnaphthalene, 2-methylnaphthalene, and 1-methylphenanthrene—the supercritical *n*-decane pyrolysis also produces a third type of methyl-PAH, whose methyl group is in a bay region of the PAH structure.<sup>51</sup> The role of these bay-region methyl-substituted PAH in the supercritical *n*-alkane pyrolysis environment till now has been unknown. Hence, to understand the molecular-growth reactions of bay-region methyl-substituted PAH in the supercritical *n*-alkane pyrolysis environment, we have performed supercritical *n*-decane pyrolysis experiments with two bay-region methyl-substituted dopants—4-methylphenanthrene and 4-methylchrysene—added in separate experiments. The mechanistic findings from these bay-region methyl-substituted-dopant experiments are presented in section 7.3.

## 7.2. Supercritical Pyrolysis of *n*-Decane at Low Temperatures

To gain a better understanding of the behavior of *n*-decane at low temperatures, we have performed additional supercritical *n*-decane pyrolysis experiments. These experiments have been performed in the same silica-lined stainless-steel tubular reactor at 94.6 atm, 133 sec, and at four temperatures: 495, 500, 515, 520 °C. The lowest temperature (495 °C) corresponds to the minimum temperature at which appreciable fuel conversion (21%) occurs.

The supercritical *n*-decane pyrolysis experiments produce a multitude of products both in the gas-phase as well as the liquid-phase. The aliphatic and one- and two-ring aromatic products are analyzed by gas chromatography (GC) coupled with mass spectrometry (MS).<sup>18,19,61</sup> The PAH products are a highly complex mixture of unsubstituted and alkylated PAH. So, the highly complex PAH product mixture is separated by a two-dimensional high-pressure liquid chromatographic (HPLC) technique, and the PAH products are subsequently characterized, isomer specifically, by ultraviolet-visible (UV) diode-array detection (DAD) and mass spectrometry (MS).<sup>19,46,47</sup> Reaction product analyses have led to the identification and quantification of 62 new products, which include 22 straight-chain aliphatics, 26 cyclic aliphatics, 10 one-ring aromatics, and 4 PAH from four- to seven-rings.

The yields of the major products, including newly identified aliphatic and one-ring aromatic products, have been plotted as functions of temperature. These plots reveal that C<sub>1</sub>-C<sub>9</sub> *n*-alkanes and C<sub>2</sub>-C<sub>9</sub> 1-alkenes are the highest-yield products of supercritical *n*-decane pyrolysis at all temperatures investigated; 2-alkenes as well as *n*-alkanes and 1-alkenes of carbon number greater than ten are also produced in appreciable amounts.<sup>48,54</sup> These plots also reveal that as the temperature rises, the aliphatic-product distribution shifts from one rich in the higher-carbon-

number ( $\geq C_6$ ) *n*-alkanes and 1-alkenes to one progressively rich in the lower-carbon-number ( $\leq C_4$ ) *n*-alkanes and 1-alkenes.<sup>19,48,54</sup>

The first step to the formation of these  $C_1$ - $C_9$  *n*-alkanes and  $C_2$ - $C_9$  1-alkenes is the decomposition of *n*-decane. The bond-dissociation energy of *n*-decane's alkyl C-C bond (86 kcal/mole<sup>38</sup>) is much lower than any of the C-H bonds. Therefore, the dissociation of *n*-decane starts with the breaking of alkyl C-C bonds to form the corresponding  $C_1$  to  $C_9$  1-alkyl radicals. Each of these 1-alkyl radicals carry the pyrolytic reactions by abstracting hydrogen from *n*-decane to produce corresponding *n*-alkanes and primary or secondary decyl radicals.<sup>19</sup> The decyl radicals, as well as other straight-chain alkyl radicals with more than three carbon atoms, undergo  $\beta$ -scission reactions to produce  $C_2$  to  $C_9$  1-alkenes.<sup>19</sup> The isomerization reactions of 1-alkenes<sup>54,61</sup> result in the formation of 2-alkenes. Larger-carbon-number *n*-alkanes and 1-alkenes can be produced by the addition reactions between the parent alkyl radicals and 1-alkenes.<sup>19,54,61</sup>

The supercritical *n*-decane pyrolysis experiments also produce an abundance of cyclic aliphatic products with  $C_5$ -rings and  $C_6$ -rings. These cyclic aliphatic products can be formed from the cyclization reactions of radicals of straight-chain alkenes<sup>54,61,69</sup> as well as from addition reactions of allyl or methylallyl radicals with  $C_2$ - $C_4$  1-alkenes.<sup>54,61,70</sup>

Besides the aliphatic products, the supercritical *n*-decane pyrolysis experiments also produce an abundance of one-ring aromatics as well as two- to nine-ring PAH—many of which are methyl-substituted. At all temperatures investigated, GC-MS analysis of the reaction products reveal that benzene and toluene are the main one-ring aromatic products. The two-ring aromatic products are formed only at temperatures greater than 530 °C. Analyses of reaction products reveal that indene, methyl-substituted indenenes, naphthalene, and methylated naphthalenes are the dominant two-ring aromatic products.<sup>19</sup>

The one-ring aromatics can be formed from the cyclization reactions of radicals of straight-chain alkenes<sup>54,69</sup> as well as from addition reactions of allyl or methylallyl radicals with C<sub>2</sub>-C<sub>4</sub> alkenes.<sup>54,70</sup> One-ring aromatics can also be formed either from ring-expansion reactions of C<sub>5</sub>-cyclic aliphatics or from H-abstraction reactions of C<sub>6</sub>-cyclic aliphatics. The one-ring aromatic products, once formed, act as a jumping-off point for PAH growth by producing resonantly stabilized radicals,<sup>61</sup> which readily react with C<sub>2</sub>-C<sub>4</sub> 1-alkenes to form two-ring aromatics.<sup>59</sup>

Due to an abundance of methyl-substituted PAH, the arylmethyl radicals are predicted to be plentiful in the supercritical *n*-decane pyrolysis environment.<sup>19</sup> To understand the potential role of arylmethyl radicals in the supercritical *n*-alkane pyrolysis environment, Kalpathy *et al.*<sup>49,50</sup> performed supercritical *n*-decane pyrolysis experiments with three methyl-aromatic dopants: 1-methylnaphthalene, 2-methylnaphthalene, and 1-methylphenanthrene.

Previous *n*-decane experiments by Kalpathy *et al.*<sup>49,50</sup> with the methyl-aromatic dopants—1-methylnaphthalene, 2-methylnaphthalene, and 1-methylphenanthrene—showed that, in the supercritical-*n*-decane-pyrolysis environment, aromatic-ring growth occurs primarily through a series of reactions involving C<sub>2</sub>-C<sub>4</sub> 1-alkene additions to resonance-stabilized arylmethyl radicals and phenalenyl-type radicals.<sup>19,61</sup> Most of the three- to eight-ring benzenoid PAH products of supercritical *n*-decane pyrolysis are accounted for by this arylmethyl/phenalenyl/1-alkene pathway.<sup>19</sup>

### **7.3. Mechanistic Findings from Dopant Experiments with Bay-Region Methyl-Substituted PAH**

To investigate the molecular-growth reactions of bay-region methyl-substituted PAH in the supercritical *n*-alkane pyrolysis environment, we have performed supercritical *n*-decane pyrolysis experiments with two bay-region methyl-substituted dopants—4-methylphenanthrene and 4-methylchrysene—added in separate experiments. The compounds that we have used as dopants—

4-methylphenanthrene and 4-methylchrysene—are only available as specially synthesized compounds, so our first dopant experiments<sup>51</sup> have been performed with 4-methylchrysene, the first one of these compounds to become available. The chosen dopant, 4-methylchrysene, is a four-ring PAH whose structure is representative of *n*-decane's three- to six-ring bay-region methyl-substituted PAH products. The chosen dopant allows us to investigate not only the roles of arylmethyl radicals of bay-region methyl-substituted PAH but also any effects of the position of the methyl group, with respect to the aromatic structure.<sup>19,51</sup>

The 4-methylchrysene-doping experiments<sup>51</sup> have been performed at 568 °C, 94.6 atm, and 133 sec, conditions of rapid PAH growth. In these experiments, 4-methylchrysene has been added as a dopant at a concentration of 0.684 mg/g *n*-decane.<sup>51</sup> This dopant concentration—corresponding to 400-800 times the yields of the individual methylchrysenes produced by *n*-decane in undoped *n*-decane pyrolysis experiments at the same conditions—is high enough to bring about observable effects on the pyrolysis-product yields but too low to influence the physical properties of the reaction environment.<sup>51</sup>

The supercritical *n*-decane pyrolysis experiments with the bay-region methyl-substituted PAH dopant 4-methylchrysene reveal that 4-methylchrysene exhibits several behaviors in this reaction environment that non-bay-region methyl-substituted PAH<sup>49,50</sup> dopants—*e.g.*, 1-methylnaphthalene, 2-methylnaphthalene, and 1-methylphenanthrene—do not: high dopant conversion and the ability to form the dopant's unsubstituted parent PAH and neighbor methyl-PAH isomer.<sup>51</sup> More significant, however, are the differences in their pathways of molecular growth. For non-bay-region methyl-substituted PAH, molecular growth proceeds<sup>49,50</sup> with the respective arylmethyl radical—*e.g.*, 1-naphthylmethyl, 2-naphthylmethyl, or 1-phenanthrylmethyl—reacting with the principal aliphatic reactants that are most abundant in the



supercritical *n*-decane pyrolysis environment: methyl, ethylene, propene, and 1-butene.<sup>51</sup> Our experiments with the bay-region methyl-substituted dopant 4-methylchrysene, however, reveal that its arylmethyl radical, 4-chrysenylmethyl, does not react directly with any of these aliphatic species.<sup>51</sup>

Instead, molecular growth of the four-ring 4-methylchrysene occurs mainly by two routes, both of which take advantage of the bay-region position of 4-methylchrysene's methyl substituent.<sup>51</sup> In the first route, 4-methylchrysene's resonance-stabilized arylmethyl radical 4-chrysenylmethyl attacks the aryl carbon just across the bay of 4-methylchrysene's structure to form the C<sub>19</sub>H<sub>12</sub> methylene-bridged PAH 4*H*-cyclopenta[*def*]chrysene, whose resonance-stabilized radical 4-cyclopenta[*def*]chrysenyl reacts with methyl and ethylene in ring-expansion reactions that selectively produce the five-ring C<sub>20</sub>H<sub>12</sub> benzo[*a*]pyrene and its derivatives 4- and 5-methylbenzo[*a*]pyrene.<sup>51</sup> The arylmethyl radicals 4- and 5-benzo[*a*]pyrenylmethyl then undergo a series of reactions with *n*-decane's high-yield C<sub>2</sub>-C<sub>4</sub> 1-alkenes to selectively produce particular six- to nine-ring *peri*-condensed benzenoid PAH, whose yields all increase dramatically with 4-methylchrysene doping.<sup>51</sup>

In 4-methylchrysene's second major route of molecular growth, 4-chrysenylmethyl's attack of the aryl carbon across the bay is followed by an intramolecular rearrangement that produces the non-fully aromatic C<sub>19</sub>H<sub>12</sub> PAH 4*H*-benzo[*cd*]fluoranthene; reactions of its resonance-stabilized radicals with methyl, propene, and 1-butene selectively produce particular six- and seven-ring PAH with internal five-membered rings.<sup>51</sup>

To substantiate the distinctive growth behaviors of bay-region methyl-substituted PAH, as exhibited by 4-methylchrysene,<sup>51</sup> we have performed supercritical *n*-decane pyrolysis experiments to which 4-methylphenanthrene, *n*-decane's highest-yield bay-region methyl-substituted PAH

product, has been added as a dopant at a concentration of 0.685 mg/g *n*-decane, which is same as that used in the experiments with 4-methylchrysene. Just like 4-methylchrysene-doping experiments,<sup>51</sup> 4-methylphenanthrene-doping experiments have been performed at 568 °C, 94.6 atm, and 133 sec, which are conditions of rapid PAH growth.

Results from our supercritical *n*-decane pyrolysis experiments with 4-methylphenanthrene as dopant have revealed that this bay-region-methyl-substituted dopant—just like 4-methylchrysene—exhibits several behaviors that non-bay-region-methyl-substituted dopants<sup>49,50</sup> do not: high dopant conversion and the ability to form the dopant's unsubstituted parent PAH and neighbor methyl-PAH isomer.<sup>51</sup> More significant, however, are the differences in their pathways of molecular growth. Previous *n*-decane experiments by Kalpathy *et al.*<sup>49,50</sup> with the non-bay-region methyl-substituted dopants—1-methylnaphthalene, 2-methylnaphthalene, and 1-methylphenanthrene—have revealed that molecular growth of these PAH occurs via reactions of the respective arylmethyl radicals with four principal aliphatic species that are highly abundant in the supercritical *n*-decane pyrolysis environment: methyl, ethylene, propene, and 1-butene.<sup>51</sup>

Results from our supercritical *n*-decane pyrolysis experiments with 4-methylphenanthrene as dopant have revealed that its arylmethyl radical, 4-phenanthrylmethyl, does not react directly with any of the principal aliphatic species. In case of 4-methylphenanthrene, molecular growth occurs mainly by two routes, both of which take advantage of the bay-region position of 4-methylphenanthrene's methyl substituent. In the first route, 4-methylphenanthrene's resonance-stabilized arylmethyl radical 4-phenanthrylmethyl, due to its structure, attacks the aryl carbon just across the bay to form the C<sub>15</sub>H<sub>10</sub> methylene-bridged PAH 4*H*-cyclopenta[*def*]phenanthrene, whose resonance-stabilized radical 4-cylopenta[*def*]phenanthryl reacts with methyl and ethylene in ring-expansion reactions that selectively produce pyrene and 4-methylpyrene. The arylmethyl

radical of 4-methylpyrene, 4-pyrenylmethyl, then undergo a series of reactions with methyl and C<sub>2</sub>-C<sub>4</sub> 1-alkenes to selectively produce particular five- to nine-ring *peri*-condensed benzenoid PAH, whose yields all increase with 4-methylphenanthrene-doping.

In 4-methylphenanthrene's second major route of molecular growth, 4-methylphenanthrene's resonance-stabilized arylmethyl radical, 4-phenanthrylmethyl, attacks the aryl carbon just across the bay. This step is followed by an intramolecular rearrangement that produces the non-fully aromatic C<sub>15</sub>H<sub>10</sub> PAH 4*H*-cyclopenta[*cd*]phenalene; reactions of its resonance-stabilized radicals with methyl and the C<sub>2</sub>-C<sub>4</sub> 1-alkenes (*n*-decane's key aliphatic species) selectively produce particular five- and six-ring PAH with internal five-membered rings. All of these findings from the 4-methylphenanthrene-doped *n*-decane experiments are consistent with our findings<sup>51</sup> from the *n*-decane pyrolysis experiments with the other bay-region-methyl-substituted dopant 4-methylchrysene.

In both of 4-methylchrysene's principal routes of molecular growth, all of the reactions take place in the three-ring area that composes the methyl-substituted bay-region part of the 4-methylchrysene structure; 4-methylchrysene's fourth aromatic ring stays completely untouched throughout the growth processes.<sup>51</sup> Similarly, all of the growth reactions of 4-methylphenanthrene take place only in the three-ring area that composes the methyl-substituted bay-region part of the 4-methylphenanthrene structure. Therefore, the reaction mechanisms determined here for the molecular growth of 4-methylphenanthrene and 4-methylchrysene would apply to any other bay-region methyl-substituted PAH in the supercritical *n*-decane pyrolysis environment.<sup>51</sup> These mechanisms, along with the complementary ones we determined previously<sup>49,50</sup> for non-bay-region methyl-substituted PAH, provide a framework for understanding not only how methyl-

substituted PAH grow in the supercritical *n*-alkane-fuel-pyrolysis environment but also the importance of the methyl group's position, relative to the base aromatic structure, in that growth.<sup>51</sup>

#### **7.4. Recommendations for Future Work**

The current work has shown the ability of our fuel pyrolysis reactor system to produce consistent data and has highlighted the power of our analytical techniques in elucidating reaction mechanisms for PAH formation and growth. Experimental studies with *n*-decane<sup>18,19,51</sup> as the model fuel have elucidated PAH formation mechanisms from *n*-alkane components of jet fuels. Jet fuels, on the other hand, contain additional hydrocarbon components, such as cycloalkanes. Other than the previous work of Stewart *et al.*,<sup>56</sup> there is no study that reports PAH formation from cycloalkanes. Hence, an experimental study of the efficacy of cycloalkanes at producing PAH in a supercritical pyrolysis environment will be a good choice.<sup>19</sup> The results of such an investigation, when combined with our present knowledge of PAH growth mechanism, could help us get closer to tackling the problem of fuel-line solids formation in the pre-combustion environment of next-generation high-speed aircraft.

## Appendix A. Supporting Information for Chapter 2

Table A1. GC retention times and response factors for C<sub>1</sub>-C<sub>6</sub> hydrocarbons.

Compound	Retention Time (min)	GC Response Factor (ppm/area)
methane	0.95	3.200
ethane	1.33	1.643
ethylene	1.67	1.634
propane	3.51	1.052
propene	6.57	1.099
<i>iso</i> -butane	8.02	0.825
<i>n</i> -butane	8.80	0.825
1-butene	12.67	0.825
1,3-butadiene	13.55	0.849
<i>trans</i> -2-butene	13.74	0.849
<i>iso</i> -butene	13.98	0.829
<i>cis</i> -2-butene	14.23	0.829
benzene	26.12	0.536
toluene*	31.78	0.553

\*Note that a reference standard for toluene was unavailable, so its response factor was calculated by multiplying by a correction factor that considers the extra mass of the methyl group.

Table A2. GC retention times and responses factor for the Agilent model 7890B GC/FID.

<b>Compound</b>	<b>Retention Time (min)</b>	<b>GC Response Factor ((mg/ml)/area)</b>
1-pentene*	2.80	2.447E-07
1-octene	7.73	7.305E-09
<i>n</i> -heptane	5.26	8.370E-09
<i>n</i> -octane	8.01	7.305E-09
<i>n</i> -nonane	11.63	6.990E-09
<i>n</i> -decane	15.76	6.775E-09
toluene	7.07	6.566E-09
ethylbenzene	10.23	6.238E-09
<i>m</i> -xylene	10.52	6.240E-09
<i>o</i> -xylene	11.41	6.280E-09
Indene*	12.64	6.680E-09
Naphthalene*	17.69	6.062E-09
1-methylnaphthalene*	21.95	6.144E-09
2-methylnaphthalene*	21.42	6.009E-09

\*Note that the response factors of 1-pentene, indene, naphthalene, 1-methylnaphthalene, and 2-methylnaphthalene were calculated using their respective methods on the GC.

Table A3. Surrogate compounds for GC calibration.

<b>Compound</b>	<b>GC Response Factor Used</b>
propane	1-pentene
propene	1-pentene
<i>n</i> -butane	1-pentene
1- and 2-butenes	1-pentene
<i>iso</i> -butane	1-pentene
<i>n</i> -pentane	1-pentene
2-pentene	1-pentene
1,3-pentadiene	1-pentene
1,4-pentadiene	1-pentene
1,3-hexadiene	1-pentene
1,5-hexadiene	1-pentene
cyclopentane	1-pentene
cyclopentene	1-pentene
cyclopentadiene	1-pentene
methylcyclopentane	1-pentene
3-methylcyclopentene	1-pentene
<i>n</i> -hexane	<i>n</i> -heptane
1-, 2-, and 3-hexenes	<i>n</i> -heptane
1-, 2-, and 3-heptenes	<i>n</i> -heptane
1-methylcyclopentene	<i>n</i> -heptane
1-methylcyclopentadiene	<i>n</i> -heptane
2-methylcyclopentadiene	<i>n</i> -heptane
5-methylcyclopentadiene	<i>n</i> -heptane
ethylcyclopentane	<i>n</i> -heptane
3-ethylcyclopentene & 1-ethylcyclopentene	<i>n</i> -heptane
cyclohexane	<i>n</i> -heptane
cyclohexene	<i>n</i> -heptane
1,3-cyclohexadiene	<i>n</i> -heptane

(Table cont'd)

<b>Compound</b>	<b>GC Response Factor Used</b>
methylcyclohexane	<i>n</i> -heptane
1-methylcyclohexene	<i>n</i> -heptane
3-methylcyclohexene	<i>n</i> -heptane
4-methylcyclohexene	<i>n</i> -heptane
2-, 3-, and 4-octenes	1-octene
1,2-dimethylcyclohexane	<i>n</i> -octane
1,3-dimethylcyclohexane	<i>n</i> -octane
1,4-dimethylcyclohexane	<i>n</i> -octane
ethylcyclohexane	<i>n</i> -octane
4-ethylcyclohexene	<i>n</i> -octane
1-, 2-, 3-, and 4-nonenes	<i>n</i> -nonane
1- and 2-decene	<i>n</i> -decane
<i>n</i> -undecane	<i>n</i> -decane
1- and 2-undecene	<i>n</i> -decane
<i>n</i> -dodecane	<i>n</i> -decane
1- and 2-dodecene	<i>n</i> -decane
<i>n</i> -tridecane	<i>n</i> -decane
1-tridecene	<i>n</i> -decane
<i>n</i> -tetradecane	<i>n</i> -decane
1-tetradecene	<i>n</i> -decane
<i>n</i> -pentadecane	<i>n</i> -decane
<i>n</i> -hexadecane	<i>n</i> -decane
methylenecyclopentane	<i>n</i> -heptane
methylenecyclohexane	<i>n</i> -heptane
<i>p</i> -xylene	<i>m</i> -xylene
1,2,3-trimethylbenzene	toluene
1,2,4-trimethylbenzene	toluene
1,3,5-trimethylbenzene	toluene

(Table cont'd)



<b>Compound</b>	<b>GC Response Factor Used</b>
ethylmethylbenzene	toluene
alkylbenzenes	toluene
1-, 2-, and 3-methylindenes	indene
ethylnaphthalenes and dimethylnaphthalenes	naphthalene

Table A4. HPLC elution times and response factors for polycyclic aromatic hydrocarbons.

<b>Compound</b>	<b>Retention Time (min)</b>	<b>HPLC Response Factor ((mg/ml)/area)</b>
naphthalene	24.9	1.637E-04
acenaphthylene	28	1.607E-04
acenaphthene	32.2	1.907E-04
fluorene	33.2	1.805E-04
phenanthrene	36	1.439E-04
anthracene	38.6	1.528E-04
fluoranthene	41.7	1.283E-04
pyrene	43.8	1.334E-04
benz[ <i>a</i> ]anthracene	50.7	1.113E-04
chrysene	52.1	1.206E-04
benzo[ <i>b</i> ]fluoranthene	57.8	1.022E-04
benzo[ <i>k</i> ]fluoranthene	60.1	1.025E-04
benzo[ <i>a</i> ]pyrene	62.5	1.438E-04
dibenz[ <i>a,h</i> ]anthracene	65.7	1.038E-04
benzo[ <i>ghi</i> ]perylene	68.6	1.200E-04
indeno[1,2,3- <i>cd</i> ]pyrene	69.7	1.038E-04

Table A5. Surrogate compounds for HPLC calibration.

<b>Compound</b>	<b>LC Response Factor Used</b>
phenalene	fluorene
benz[ <i>e</i> ]indene	fluorene
benz[ <i>f</i> ]indene	fluorene
dibenzofulvene	fluorene
cyclopenta[ <i>def</i> ]phenanthrene	phenanthrene
co-eluting products 2-methylfluoranthene, benzo[ <i>a</i> ]fluorene, and benzo[ <i>b</i> ]fluorene	fluoranthene
benzo[ <i>c</i> ]fluorene	fluoranthene
7 <i>H</i> -benz[ <i>de</i> ]anthracene	pyrene
3,4-dihydrocyclopenta[ <i>cd</i> ]pyrene	pyrene
triphenylene	chrysene
Benzo[ <i>ghi</i> ]fluoranthene	fluoranthene
6 <i>H</i> -benzo[ <i>cd</i> ]pyrene	pyrene
benzo[ <i>e</i> ]pyrene	benzo[ <i>a</i> ]pyrene
benzo[ <i>j</i> ]fluoranthene	benzo[ <i>k</i> ]fluoranthene
benzo[ <i>a</i> ]fluoranthene	benzo[ <i>b</i> ]fluoranthene
perylene	benzo[ <i>ghi</i> ]perylene
naphtho[1,2- <i>a</i> ]fluorene	benzo[ <i>k</i> ]fluoranthene
naphtho[2,3- <i>a</i> ]fluorene	benzo[ <i>k</i> ]fluoranthene
naphtho[2,1- <i>a</i> ]fluorene	benzo[ <i>k</i> ]fluoranthene
dibenzo[ <i>a,h</i> ]fluorene	benzo[ <i>k</i> ]fluoranthene
dibenzo[ <i>a,c</i> ]fluorene	benzo[ <i>k</i> ]fluoranthene
anthanthrene	benzo[ <i>ghi</i> ]perylene
dibenz[ <i>a,c</i> ]anthracene	dibenz[ <i>a,h</i> ]anthracene
dibenz[ <i>a,j</i> ]anthracene	dibenz[ <i>a,h</i> ]anthracene
pentaphene	dibenz[ <i>a,h</i> ]anthracene
benzo[ <i>b</i> ]chrysene	dibenz[ <i>a,h</i> ]anthracene
benzo[ <i>g</i> ]chrysene	dibenz[ <i>a,h</i> ]anthracene
picene	dibenz[ <i>a,h</i> ]anthracene

(Table cont'd)


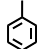
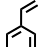
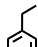
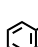
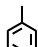
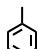
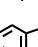
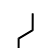

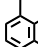
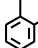
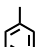


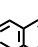
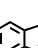
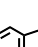
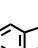
<b>Compound</b>	<b>LC Response Factor Used</b>
benzo[ <i>a</i> ]naphthacene	dibenz[ <i>a,h</i> ]anthracene
coronene	Benzo[ <i>ghi</i> ]perylene
dibenzo[ <i>b,j</i> ]fluoranthene	benzo[ <i>k</i> ]fluoranthene
dibenzo[ <i>j,l</i> ]fluoranthene	benzo[ <i>k</i> ]fluoranthene
naphtho[1,2- <i>b</i> ]fluoranthene	benzo[ <i>k</i> ]fluoranthene
naphtho[2,3- <i>b</i> ]fluoranthene	benzo[ <i>k</i> ]fluoranthene
naphtho[2,3- <i>e</i> ]pyrene	benzo[ <i>a</i> ]pyrene
dibenzo[ <i>a,e</i> ]pyrene	benzo[ <i>a</i> ]pyrene
co-eluting benzo[ <i>b</i> ]perylene and dibenzo[ <i>e,l</i> ]pyrene	benzo[ <i>a</i> ]pyrene
naphtho[2,1- <i>a</i> ]pyrene	benzo[ <i>a</i> ]pyrene
naphtho[2,3- <i>a</i> ]pyrene	benzo[ <i>a</i> ]pyrene
dibenzo[ <i>a,i</i> ]pyrene	benzo[ <i>a</i> ]pyrene
dibenzo[ <i>a,l</i> ]pyrene	benzo[ <i>a</i> ]pyrene
naphtho[1,2- <i>e</i> ]pyrene	benzo[ <i>a</i> ]pyrene
fluoreno[1,9- <i>ab</i> ]pyrene	indeno[1,2,3- <i>cd</i> ]pyrene
benz[ <i>a</i> ]indeno[1,2,3- <i>jk</i> ]pyrene	indeno[1,2,3- <i>cd</i> ]pyrene
benz[ <i>a</i> ]indeno[1,2,3- <i>cd</i> ]pyrene	indeno[1,2,3- <i>cd</i> ]pyrene
dibenzo[ <i>e,ghi</i> ]perylene	benzo[ <i>ghi</i> ]perylene
indeno[1,2,3- <i>cd</i> ]perylene	indeno[1,2,3- <i>cd</i> ]pyrene
dibenzo[ <i>b,ghi</i> ]perylene	benzo[ <i>ghi</i> ]perylene
naphtho[1,2,3,4- <i>ghi</i> ]perylene	benzo[ <i>ghi</i> ]perylene
naphtho[8,1,2- <i>bcd</i> ]perylene	benzo[ <i>ghi</i> ]perylene
dibenzo[ <i>cd,lm</i> ]perylene	benzo[ <i>ghi</i> ]perylene
tribenz[ <i>a,c,h</i> ]anthracene	dibenz[ <i>a,h</i> ]anthracene
benzo[ <i>c</i> ]pentaphene	dibenz[ <i>a,h</i> ]anthracene
benzo[ <i>h</i> ]pentaphene	dibenz[ <i>a,h</i> ]anthracene
benzo[ <i>pqr</i> ]naphtho[8,1,2- <i>bcd</i> ]perylene	benzo[ <i>ghi</i> ]perylene
benzo[ <i>ghi</i> ]naphtho[8,1,2- <i>bcd</i> ]perylene	benzo[ <i>ghi</i> ]perylene

(Table cont'd)



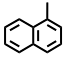
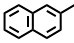
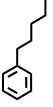
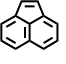
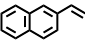
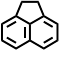
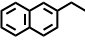
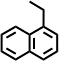
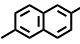
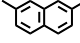
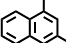
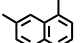
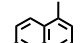
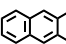
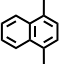
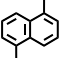
<b>Compound</b>	<b>LC Response Factor Used</b>
co-eluting phenanthro[5,4,3,2- <i>efghi</i> ]perylene and benzo[ <i>cd</i> ]naphtho[3,2,1,8- <i>pqra</i> ]perylene	benzo[ <i>ghi</i> ]perylene
benzo[ <i>a</i> ]coronene	benzo[ <i>ghi</i> ]perylene
tribenzo[ <i>b,j,l</i> ]fluoranthene	benzo[ <i>b</i> ]fluoranthene
benzo[ <i>e</i> ]naphtho[2,3- <i>a</i> ]pyrene	benzo[ <i>a</i> ]pyrene
benzo[ <i>e</i> ]naphtho[2,1- <i>a</i> ]pyrene	benzo[ <i>a</i> ]pyrene
naphtho[8,1,2- <i>abc</i> ]coronene	benzo[ <i>ghi</i> ]perylene
benzo[ <i>cd</i> ]naphtho[1,2,3- <i>lm</i> ]perylene	benzo[ <i>ghi</i> ]perylene

## Appendix B. Supporting Information for Chapter 4 and Chapter 5

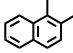
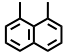
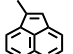
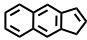
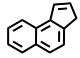
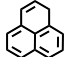
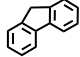
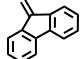
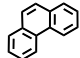
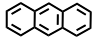
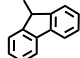
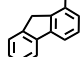
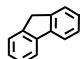
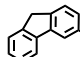
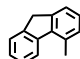
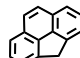
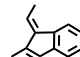
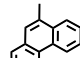
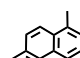
Table B1. Quantified aromatic products of supercritical *n*-decane pyrolysis.

Product Name	Formula	Structure	Code
benzene	C <sub>6</sub> H <sub>6</sub>		78a
toluene	C <sub>7</sub> H <sub>8</sub>		92a
styrene	C <sub>8</sub> H <sub>8</sub>		104a
ethylbenzene	C <sub>8</sub> H <sub>10</sub>		106a
<i>o</i> -xylene	C <sub>8</sub> H <sub>10</sub>		106b
<i>m</i> -xylene	C <sub>8</sub> H <sub>10</sub>		106c
<i>p</i> -xylene	C <sub>8</sub> H <sub>10</sub>		106d
indene	C <sub>9</sub> H <sub>8</sub>		116a
<i>n</i> -propylbenzene	C <sub>9</sub> H <sub>12</sub>		120a
1,2,3-trimethylbenzene	C <sub>9</sub> H <sub>12</sub>		120b
1,2,4-trimethylbenzene	C <sub>9</sub> H <sub>12</sub>		120c
1,3,5-trimethylbenzene	C <sub>9</sub> H <sub>12</sub>		120d
methylethylbenzene	C <sub>9</sub> H <sub>12</sub>		120g
methylethylbenzene	C <sub>9</sub> H <sub>12</sub>		120h
naphthalene	C <sub>10</sub> H <sub>8</sub>		128a
1-methylindene	C <sub>10</sub> H <sub>10</sub>		130a
2-methylindene	C <sub>10</sub> H <sub>10</sub>		130b
3-methylindene	C <sub>10</sub> H <sub>10</sub>		130c
<i>n</i> -butylbenzene	C <sub>10</sub> H <sub>14</sub>		134a

(Table cont'd)

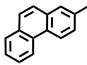
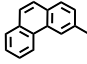
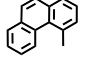
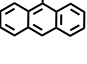
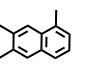
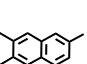
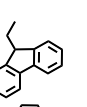
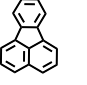
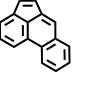
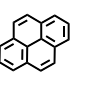
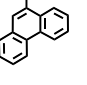
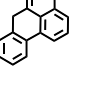
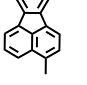
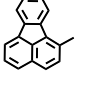
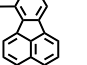
Product Name	Formula	Structure	Code
C <sub>4</sub> -alkylbenzene	C <sub>10</sub> H <sub>14</sub>		134b
C <sub>4</sub> -alkylbenzene	C <sub>10</sub> H <sub>14</sub>		134c
1-methylnaphthalene	C <sub>11</sub> H <sub>10</sub>		142a
2-methylnaphthalene	C <sub>11</sub> H <sub>10</sub>		142b
<i>n</i> -pentylbenzene	C <sub>11</sub> H <sub>16</sub>		148a
acenaphthylene	C <sub>12</sub> H <sub>8</sub>		152a
2-vinylnaphthalene	C <sub>12</sub> H <sub>10</sub>		154a
acenaphthene	C <sub>12</sub> H <sub>10</sub>		154b
2-ethylnaphthalene	C <sub>12</sub> H <sub>12</sub>		156a
1-ethylnaphthalene	C <sub>12</sub> H <sub>12</sub>		156b
2,6-dimethylnaphthalene	C <sub>12</sub> H <sub>12</sub>		156c
2,7-dimethylnaphthalene	C <sub>12</sub> H <sub>12</sub>		156d
1,3-dimethylnaphthalene	C <sub>12</sub> H <sub>12</sub>		156e
1,7-dimethylnaphthalene	C <sub>12</sub> H <sub>12</sub>		156f
1,6-dimethylnaphthalene	C <sub>12</sub> H <sub>12</sub>		156g
2,3-dimethylnaphthalene	C <sub>12</sub> H <sub>12</sub>		156h
1,4-dimethylnaphthalene	C <sub>12</sub> H <sub>12</sub>		156i
1,5-dimethylnaphthalene	C <sub>12</sub> H <sub>12</sub>		156j

(Table cont'd)

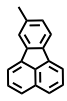
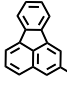
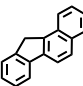
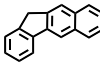
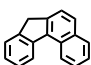
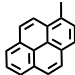
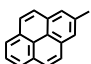
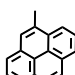
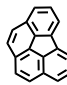
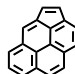
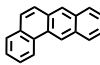
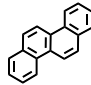
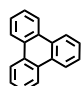
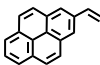
Product Name	Formula	Structure	Code
1,2-dimethylnaphthalene	C <sub>12</sub> H <sub>12</sub>		156k
1,8-dimethylnaphthalene	C <sub>12</sub> H <sub>12</sub>		156l
1-methylacenaphthylene	C <sub>13</sub> H <sub>10</sub>		166a
benz[ <i>f</i> ]indene	C <sub>13</sub> H <sub>10</sub>		166b
benz[ <i>e</i> ]indene	C <sub>13</sub> H <sub>10</sub>		166c
phenalene	C <sub>13</sub> H <sub>10</sub>		166d
fluorene	C <sub>13</sub> H <sub>10</sub>		166e
dibenzofulvene	C <sub>14</sub> H <sub>10</sub>		178a
phenanthrene	C <sub>14</sub> H <sub>10</sub>		178b
anthracene	C <sub>14</sub> H <sub>10</sub>		178c
9-methylfluorene	C <sub>14</sub> H <sub>12</sub>		180a
1-methylfluorene	C <sub>14</sub> H <sub>12</sub>		180b
2-methylfluorene	C <sub>14</sub> H <sub>12</sub>		180c
3-methylfluorene	C <sub>14</sub> H <sub>12</sub>		180d
4-methylfluorene	C <sub>14</sub> H <sub>12</sub>		180e
4 <i>H</i> -cyclopenta[ <i>def</i> ]phenanthrene	C <sub>15</sub> H <sub>10</sub>		190a
9-ethylidene fluorene	C <sub>15</sub> H <sub>12</sub>		192a
9-methylphenanthrene	C <sub>15</sub> H <sub>12</sub>		192b
1-methylphenanthrene	C <sub>15</sub> H <sub>12</sub>		192c

(Table cont'd)

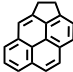
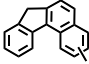
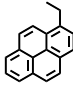
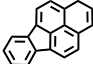
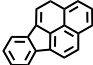
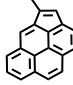
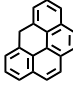
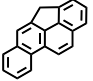
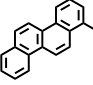
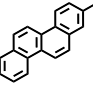
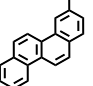
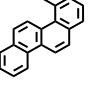
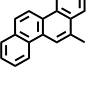
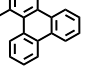


Product Name	Formula	Structure	Code
2-methylphenanthrene	C <sub>15</sub> H <sub>12</sub>		192d
3-methylphenanthrene	C <sub>15</sub> H <sub>12</sub>		192e
4-methylphenanthrene	C <sub>15</sub> H <sub>12</sub>		192f
9-methylanthracene	C <sub>15</sub> H <sub>12</sub>		192g
1-methylanthracene	C <sub>15</sub> H <sub>12</sub>		192h
2-methylanthracene	C <sub>15</sub> H <sub>12</sub>		192i
9-ethylfluorene	C <sub>15</sub> H <sub>14</sub>		194a
fluoranthene	C <sub>16</sub> H <sub>10</sub>		202a
acephenanthrylene	C <sub>16</sub> H <sub>10</sub>		202b
pyrene	C <sub>16</sub> H <sub>10</sub>		202c
9-ethylphenanthrene	C <sub>16</sub> H <sub>14</sub>		206a
7H-benz[de]anthracene	C <sub>17</sub> H <sub>12</sub>		216a
3-methylfluoranthene	C <sub>17</sub> H <sub>12</sub>		216b
1-methylfluoranthene	C <sub>17</sub> H <sub>12</sub>		216c
7-methylfluoranthene	C <sub>17</sub> H <sub>12</sub>		216d

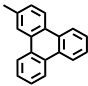
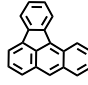
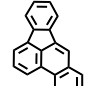
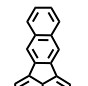
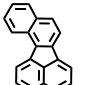
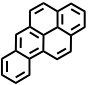
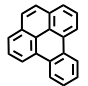
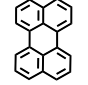
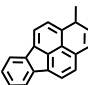
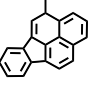
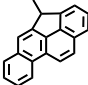
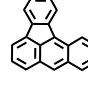
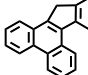
(Table cont'd)

Product Name	Formula	Structure	Code
8-methylfluoranthene	C <sub>17</sub> H <sub>12</sub>		216e
2-methylfluoranthene	C <sub>17</sub> H <sub>12</sub>		216f
benzo[ <i>a</i> ]fluorene	C <sub>17</sub> H <sub>12</sub>		216g
benzo[ <i>b</i> ]fluorene	C <sub>17</sub> H <sub>12</sub>		216h
benzo[ <i>c</i> ]fluorene	C <sub>17</sub> H <sub>12</sub>		216i
1-methylpyrene	C <sub>17</sub> H <sub>12</sub>		216j
2-methylpyrene	C <sub>17</sub> H <sub>12</sub>		216k
4-methylpyrene	C <sub>17</sub> H <sub>12</sub>		216l
benzo[ <i>ghi</i> ]fluoranthene	C <sub>18</sub> H <sub>10</sub>		226a
cyclopenta[ <i>cd</i> ]pyrene	C <sub>18</sub> H <sub>10</sub>		226b
benz[ <i>a</i> ]anthracene	C <sub>18</sub> H <sub>12</sub>		228a
chrysene	C <sub>18</sub> H <sub>12</sub>		228b
triphenylene	C <sub>18</sub> H <sub>12</sub>		228c
2-vinylpyrene	C <sub>18</sub> H <sub>12</sub>		228d

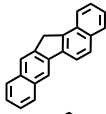
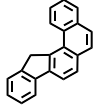
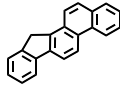
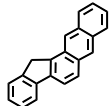
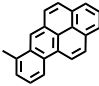
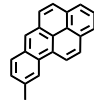
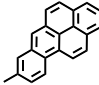
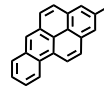
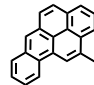
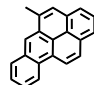
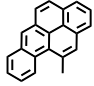
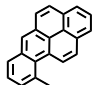
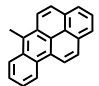
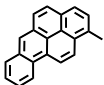
(Table cont'd)

Product Name	Formula	Structure	Code
3,4-dihydrocyclopenta[ <i>cd</i> ]pyrene	C <sub>18</sub> H <sub>12</sub>		228e
methylbenzo[ <i>c</i> ]fluorene	C <sub>18</sub> H <sub>14</sub>		230a
1-ethylpyrene	C <sub>18</sub> H <sub>14</sub>		230b
1 <i>H</i> -benzo[ <i>cd</i> ]fluoranthene <sup>a</sup>	C <sub>19</sub> H <sub>12</sub>		240e
4 <i>H</i> -benzo[ <i>cd</i> ]fluoranthene <sup>a</sup>	C <sub>19</sub> H <sub>12</sub>		240a
4-methylcyclopenta[ <i>cd</i> ]pyrene	C <sub>19</sub> H <sub>12</sub>		240b
6 <i>H</i> -benzo[ <i>cd</i> ]pyrene	C <sub>19</sub> H <sub>12</sub>		240c
4 <i>H</i> -cyclopenta[ <i>def</i> ]chrysene	C <sub>19</sub> H <sub>12</sub>		240d
1-methylchrysene	C <sub>19</sub> H <sub>14</sub>		242a
2-methylchrysene	C <sub>19</sub> H <sub>14</sub>		242g
3-methylchrysene	C <sub>19</sub> H <sub>14</sub>		242d
4-methylchrysene	C <sub>19</sub> H <sub>14</sub>		242h
6-methylchrysene	C <sub>19</sub> H <sub>14</sub>		242f
1-methyltriphenylene	C <sub>19</sub> H <sub>14</sub>		242b

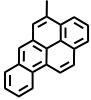
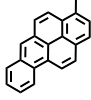
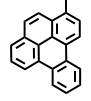
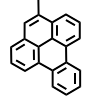
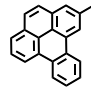
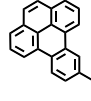
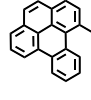
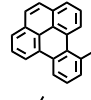
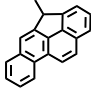
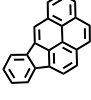
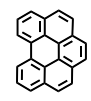
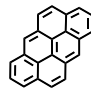
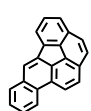
(Table cont'd)

Product Name	Formula	Structure	Code
2-methyltriphenylene	C <sub>19</sub> H <sub>14</sub>		242c
benzo[ <i>a</i> ]fluoranthene	C <sub>20</sub> H <sub>12</sub>		252a
benzo[ <i>b</i> ]fluoranthene	C <sub>20</sub> H <sub>12</sub>		252b
benzo[ <i>k</i> ]fluoranthene	C <sub>20</sub> H <sub>12</sub>		252c
benzo[ <i>j</i> ]fluoranthene	C <sub>20</sub> H <sub>12</sub>		252d
benzo[ <i>a</i> ]pyrene	C <sub>20</sub> H <sub>12</sub>		252e
benzo[ <i>e</i> ]pyrene	C <sub>20</sub> H <sub>12</sub>		252g
perylene	C <sub>20</sub> H <sub>12</sub>		252f
1-methyl-1 <i>H</i> -benzo[ <i>cd</i> ]fluoranthene <sup>a</sup>	C <sub>20</sub> H <sub>14</sub>		254c
4-methyl-4 <i>H</i> -benzo[ <i>cd</i> ]fluoranthene <sup>a</sup>	C <sub>20</sub> H <sub>14</sub>		254a
4-methyl-4 <i>H</i> -cyclopenta[ <i>def</i> ]chrysene	C <sub>20</sub> H <sub>14</sub>		254b
methylbenzo[ <i>a</i> ]fluoranthene	C <sub>21</sub> H <sub>14</sub>		266c
dibenzo[ <i>a,c</i> ]fluorene	C <sub>21</sub> H <sub>14</sub>		266a

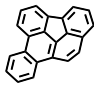
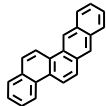
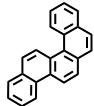
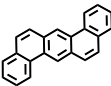
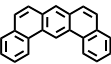
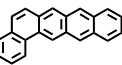
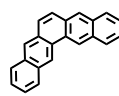
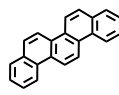
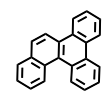
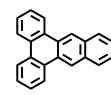
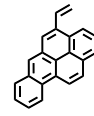
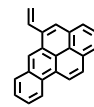
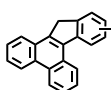
(Table cont'd)

Product Name	Formula	Structure	Code
dibenzo[ <i>a,h</i> ]fluorene	C <sub>21</sub> H <sub>14</sub>		266d
naphtho[1,2- <i>a</i> ]fluorene	C <sub>21</sub> H <sub>14</sub>		266e
naphtho[2,1- <i>a</i> ]fluorene	C <sub>21</sub> H <sub>14</sub>		266f
naphtho[2,3- <i>a</i> ]fluorene	C <sub>21</sub> H <sub>14</sub>		266g
7-methylbenzo[ <i>a</i> ]pyrene	C <sub>21</sub> H <sub>14</sub>		266h
9-methylbenzo[ <i>a</i> ]pyrene	C <sub>21</sub> H <sub>14</sub>		266i
8-methylbenzo[ <i>a</i> ]pyrene	C <sub>21</sub> H <sub>14</sub>		266j
2-methylbenzo[ <i>a</i> ]pyrene	C <sub>21</sub> H <sub>14</sub>		266k
12-methylbenzo[ <i>a</i> ]pyrene	C <sub>21</sub> H <sub>14</sub>		266l
5-methylbenzo[ <i>a</i> ]pyrene	C <sub>21</sub> H <sub>14</sub>		266m
11-methylbenzo[ <i>a</i> ]pyrene	C <sub>21</sub> H <sub>14</sub>		266n
10-methylbenzo[ <i>a</i> ]pyrene	C <sub>21</sub> H <sub>14</sub>		266o
6-methylbenzo[ <i>a</i> ]pyrene	C <sub>21</sub> H <sub>14</sub>		266p
1-methylbenzo[ <i>a</i> ]pyrene	C <sub>21</sub> H <sub>14</sub>		266q

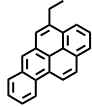
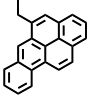
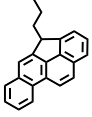
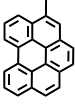
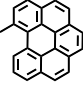
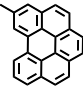

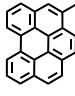
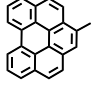
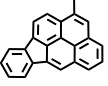
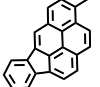
(Table cont'd)

Product Name	Formula	Structure	Code
4-methylbenzo[ <i>a</i> ]pyrene	C <sub>21</sub> H <sub>14</sub>		266r
3-methylbenzo[ <i>a</i> ]pyrene	C <sub>21</sub> H <sub>14</sub>		266s
3-methylbenzo[ <i>e</i> ]pyrene	C <sub>21</sub> H <sub>14</sub>		266b
4-methylbenzo[ <i>e</i> ]pyrene	C <sub>21</sub> H <sub>14</sub>		266t
2-methylbenzo[ <i>e</i> ]pyrene	C <sub>21</sub> H <sub>14</sub>		266u
10-methylbenzo[ <i>e</i> ]pyrene	C <sub>21</sub> H <sub>14</sub>		266v
1-methylbenzo[ <i>e</i> ]pyrene	C <sub>21</sub> H <sub>14</sub>		266w
9-methylbenzo[ <i>e</i> ]pyrene	C <sub>21</sub> H <sub>14</sub>		266x
4-ethyl-4 <i>H</i> -cyclopenta[ <i>def</i> ]chrysene	C <sub>21</sub> H <sub>16</sub>		268a
indeno[1,2,3- <i>cd</i> ]pyrene	C <sub>22</sub> H <sub>12</sub>		276a
benzo[ <i>ghi</i> ]perylene	C <sub>22</sub> H <sub>12</sub>		276b
anthanthrene	C <sub>22</sub> H <sub>12</sub>		276c
dibenzo[ <i>b,ghi</i> ]fluoranthene	C <sub>22</sub> H <sub>12</sub>		276d

(Table cont'd)

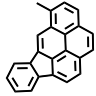
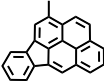
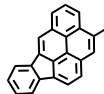
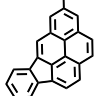
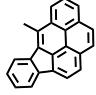
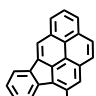
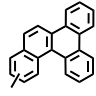
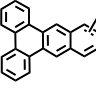

Product Name	Formula	Structure	Code
dibenzo[ <i>e,ghi</i> ]fluoranthene	C <sub>22</sub> H <sub>12</sub>		276e
benzo[ <i>b</i> ]chrysene	C <sub>22</sub> H <sub>14</sub>		278a
benzo[ <i>c</i> ]chrysene	C <sub>22</sub> H <sub>14</sub>		278i
dibenz[ <i>a,h</i> ]anthracene	C <sub>22</sub> H <sub>14</sub>		278b
dibenz[ <i>a,j</i> ]anthracene	C <sub>22</sub> H <sub>14</sub>		278c
benzo[ <i>a</i> ]naphthacene	C <sub>22</sub> H <sub>14</sub>		278d
pentaphene	C <sub>22</sub> H <sub>14</sub>		278e
picene	C <sub>22</sub> H <sub>14</sub>		278f
benzo[ <i>g</i> ]chrysene	C <sub>22</sub> H <sub>14</sub>		278g
dibenz[ <i>a,c</i> ]anthracene	C <sub>22</sub> H <sub>14</sub>		278h
4-vinylbenzo[ <i>a</i> ]pyrene <sup>b</sup>	C <sub>22</sub> H <sub>14</sub>		278j
5-vinylbenzo[ <i>a</i> ]pyrene <sup>b</sup>	C <sub>22</sub> H <sub>14</sub>		278k
methyldibenzo[ <i>a,c</i> ]fluorene	C <sub>22</sub> H <sub>16</sub>		280a

(Table cont'd)

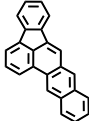
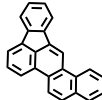
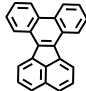
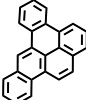
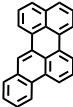
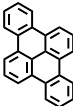
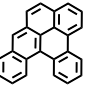
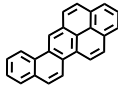
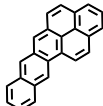
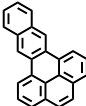
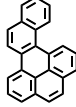
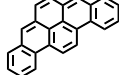
Product Name	Formula	Structure	Code
4-ethylbenzo[ <i>a</i> ]pyrene	C <sub>22</sub> H <sub>16</sub>		280b
5-ethylbenzo[ <i>a</i> ]pyrene	C <sub>22</sub> H <sub>16</sub>		280c
4-propyl-4 <i>H</i> -cyclopenta[ <i>def</i> ]chrysene	C <sub>22</sub> H <sub>18</sub>		282a
4-methylbenzo[ <i>ghi</i> ]perylene	C <sub>23</sub> H <sub>14</sub>		290a
7-methylbenzo[ <i>ghi</i> ]perylene	C <sub>23</sub> H <sub>14</sub>		290b
6-methylbenzo[ <i>ghi</i> ]perylene	C <sub>23</sub> H <sub>14</sub>		290c
5-methylbenzo[ <i>ghi</i> ]perylene	C <sub>23</sub> H <sub>14</sub>		290d
3-methylbenzo[ <i>ghi</i> ]perylene	C <sub>23</sub> H <sub>14</sub>		290e
1-methylbenzo[ <i>ghi</i> ]perylene	C <sub>23</sub> H <sub>14</sub>		290f
1-methylindeno[1,2,3- <i>cd</i> ]pyrene <sup>c</sup>	C <sub>22</sub> H <sub>14</sub>		290g
3-methylindeno[1,2,3- <i>cd</i> ]pyrene <sup>c</sup>	C <sub>22</sub> H <sub>14</sub>		290h

(Table cont'd)

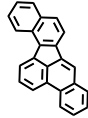
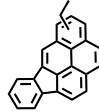

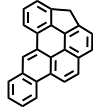
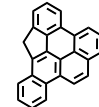
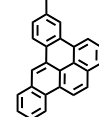
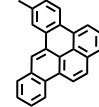
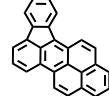
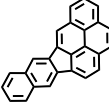
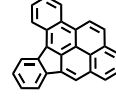
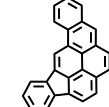


Product Name	Formula	Structure	Code
5-methylindeno[1,2,3- <i>cd</i> ]pyrene <sup>c</sup>	C <sub>22</sub> H <sub>14</sub>		290i
12-methylindeno[1,2,3- <i>cd</i> ]pyrene <sup>c</sup>	C <sub>22</sub> H <sub>14</sub>		290j
2-methylindeno[1,2,3- <i>cd</i> ]pyrene <sup>c</sup>	C <sub>22</sub> H <sub>14</sub>	 }  }  }  }	290k-n
4-methylindeno[1,2,3- <i>cd</i> ]pyrene <sup>c</sup>	C <sub>22</sub> H <sub>14</sub>		
6-methylindeno[1,2,3- <i>cd</i> ]pyrene <sup>c</sup>	C <sub>22</sub> H <sub>14</sub>		
11-methylindeno[1,2,3- <i>cd</i> ]pyrene <sup>c</sup>	C <sub>22</sub> H <sub>14</sub>		
7-methylindeno[1,2,3- <i>cd</i> ]pyrene <sup>c</sup>	C <sub>22</sub> H <sub>14</sub>		
8-methylindeno[1,2,3- <i>cd</i> ]pyrene <sup>c</sup>	C <sub>22</sub> H <sub>14</sub>		
9-methylindeno[1,2,3- <i>cd</i> ]pyrene <sup>c</sup>	C <sub>22</sub> H <sub>14</sub>		
10-methylindeno[1,2,3- <i>cd</i> ]pyrene <sup>c</sup>	C <sub>22</sub> H <sub>14</sub>		
methylbenzo[ <i>g</i> ]chrysene	C <sub>23</sub> H <sub>16</sub>		292a
methyldibenz[ <i>a,c</i> ]anthracene	C <sub>23</sub> H <sub>16</sub>		292b-d
coronene	C <sub>24</sub> H <sub>12</sub>		300a

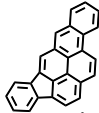
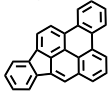
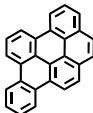
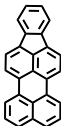
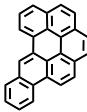
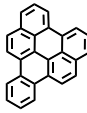
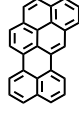
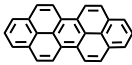
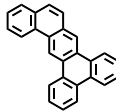
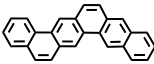
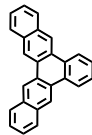
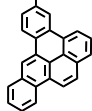
(Table cont'd)

Product Name	Formula	Structure	Code
naphtho[2,3- <i>b</i> ]fluoranthene	C <sub>24</sub> H <sub>14</sub>		302a
naphtho[1,2- <i>b</i> ]fluoranthene	C <sub>24</sub> H <sub>14</sub>		302b
dibenzo[ <i>j,l</i> ]fluoranthene	C <sub>24</sub> H <sub>14</sub>		302c
dibenzo[ <i>a,e</i> ]pyrene	C <sub>24</sub> H <sub>14</sub>		302d
benzo[ <i>b</i> ]perylene	C <sub>24</sub> H <sub>14</sub>		302e
dibenzo[ <i>e,l</i> ]pyrene	C <sub>24</sub> H <sub>14</sub>		302f
dibenzo[ <i>a,l</i> ]pyrene	C <sub>24</sub> H <sub>14</sub>		302g
naphtho[2,1- <i>a</i> ]pyrene	C <sub>24</sub> H <sub>14</sub>		302h
naphtho[2,3- <i>a</i> ]pyrene	C <sub>24</sub> H <sub>14</sub>		302i
naphtho[2,3- <i>e</i> ]pyrene	C <sub>24</sub> H <sub>14</sub>		302j
naphtho[1,2- <i>e</i> ]pyrene	C <sub>24</sub> H <sub>14</sub>		302k
dibenzo[ <i>a,i</i> ]pyrene	C <sub>24</sub> H <sub>14</sub>		302l

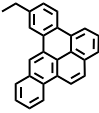
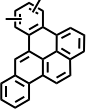
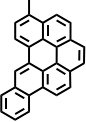
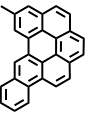
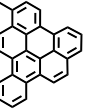
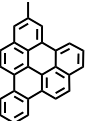
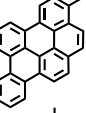
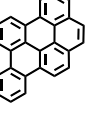
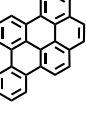
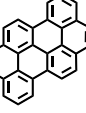
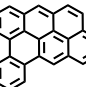
(Table cont'd)

Product Name	Formula	Structure	Code
dibenzo[ <i>b,j</i> ]fluoranthene	C <sub>24</sub> H <sub>14</sub>		302m
ethylindeno[1,2,3- <i>cd</i> ]pyrene	C <sub>24</sub> H <sub>16</sub>		304a
1-methylcoronene	C <sub>25</sub> H <sub>14</sub>		314a
3 <i>H</i> -indeno[4,3,2- <i>efg</i> ]benzo[ <i>a</i> ]pyrene <sup>d</sup>	C <sub>25</sub> H <sub>14</sub>		314 <i>b</i>
7 <i>H</i> -indeno[2,3,4- <i>cde</i> ]benzo[ <i>a</i> ]pyrene <sup>d</sup>	C <sub>25</sub> H <sub>14</sub>		314 <i>c</i>
5-methyldibenzo[ <i>a,e</i> ]pyrene <sup>d</sup>	C <sub>25</sub> H <sub>16</sub>		316 <i>a</i>
6-methyldibenzo[ <i>a,e</i> ]pyrene <sup>d</sup>	C <sub>25</sub> H <sub>16</sub>		316 <i>b</i>
fluoreno[1,9- <i>ab</i> ]pyrene	C <sub>26</sub> H <sub>14</sub>		326 <i>a</i>
benz[5,6]indeno[1,2,3- <i>cd</i> ]pyrene	C <sub>26</sub> H <sub>14</sub>		326m
benz[ <i>a</i> ]indeno[1,2,3- <i>cd</i> ]pyrene	C <sub>26</sub> H <sub>14</sub>		326 <i>c</i>
benz[ <i>h</i> ]indeno[1,2,3- <i>cd</i> ]pyrene	C <sub>26</sub> H <sub>14</sub>		326 <i>b</i>

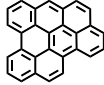
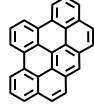
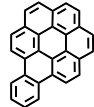
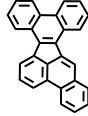
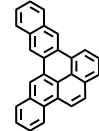
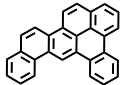
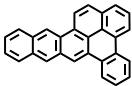
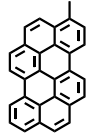

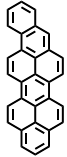
(Table cont'd)

Product Name	Formula	Structure	Code
benz[ <i>i</i> ]indeno[1,2,3- <i>cd</i> ]pyrene	C <sub>26</sub> H <sub>14</sub>		326j
benz[ <i>l</i> ]indeno[1,2,3- <i>cd</i> ]pyrene	C <sub>26</sub> H <sub>14</sub>		326k
dibenzo[ <i>e,ghi</i> ]perylene	C <sub>26</sub> H <sub>14</sub>		326d
indeno[1,2,3- <i>cd</i> ]perylene	C <sub>26</sub> H <sub>14</sub>		326e
dibenzo[ <i>b,ghi</i> ]perylene	C <sub>26</sub> H <sub>14</sub>		326f
naphtho[1,2,3,4- <i>ghi</i> ]perylene	C <sub>26</sub> H <sub>14</sub>		326g
naphtho[8,1,2- <i>bcd</i> ]perylene	C <sub>26</sub> H <sub>14</sub>		326h
dibenzo[ <i>cd,lm</i> ]perylene	C <sub>26</sub> H <sub>14</sub>		326i
tribenz[ <i>a,c,h</i> ]anthracene	C <sub>26</sub> H <sub>16</sub>		328a
benzo[ <i>c</i> ]pentaphene	C <sub>26</sub> H <sub>16</sub>		328b
benzo[ <i>h</i> ]pentaphene	C <sub>26</sub> H <sub>16</sub>		328c
5-ethyldibenzo[ <i>a,e</i> ]pyrene <sup>d</sup>	C <sub>26</sub> H <sub>16</sub>		330a

(Table cont'd)

Product Name	Formula	Structure	Code
6-ethylidibenzo[ <i>a,e</i> ]pyrene <sup>d</sup>	C <sub>26</sub> H <sub>16</sub>		330b
dimethyldibenzo[ <i>a,e</i> ]pyrene	C <sub>26</sub> H <sub>16</sub>		330c
5-methyldibenzo[ <i>b,ghi</i> ]perylene <sup>e</sup>	C <sub>27</sub> H <sub>16</sub>		340a
6-methyldibenzo[ <i>b,ghi</i> ]perylene <sup>e</sup>	C <sub>27</sub> H <sub>16</sub>		340b
1-methylnaphtho[1,2,3,4- <i>ghi</i> ]perylene <sup>e</sup>	C <sub>27</sub> H <sub>16</sub>		340c
2-methylnaphtho[1,2,3,4- <i>ghi</i> ]perylene <sup>e</sup>	C <sub>27</sub> H <sub>16</sub>		340d
3-methyldibenzo[ <i>e,ghi</i> ]perylene <sup>e</sup>	C <sub>27</sub> H <sub>16</sub>		340e
4-methyldibenzo[ <i>e,ghi</i> ]perylene <sup>e</sup>	C <sub>27</sub> H <sub>16</sub>		340f
7-methyldibenzo[ <i>e,ghi</i> ]perylene <sup>e</sup>	C <sub>27</sub> H <sub>16</sub>		340g
benzo[ <i>pqr</i> ]naphtho[8,1,2- <i>bcd</i> ]perylene	C <sub>28</sub> H <sub>14</sub>		350a
benzo[ <i>ghi</i> ]naphtho[8,1,2- <i>bcd</i> ]perylene	C <sub>28</sub> H <sub>14</sub>		350b

(Table cont'd)

Product Name	Formula	Structure	Code
benzo[ <i>cd</i> ]naphtho[8,1,2,3- <i>fg</i> hi]perylene	C <sub>28</sub> H <sub>14</sub>		350c
phenanthro[5,4,3,2- <i>ef</i> ghi]perylene	C <sub>28</sub> H <sub>14</sub>		350d
benzo[ <i>a</i> ]coronene	C <sub>28</sub> H <sub>14</sub>		350e
tribenzo[ <i>b,j,l</i> ]fluoranthene	C <sub>28</sub> H <sub>16</sub>		352a
benzo[ <i>a</i> ]naphtho[2,3- <i>e</i> ]pyrene	C <sub>28</sub> H <sub>16</sub>		352d
benzo[ <i>e</i> ]naphtho[2,1- <i>a</i> ]pyrene	C <sub>28</sub> H <sub>16</sub>		352b
benzo[ <i>e</i> ]naphtho[2,3- <i>a</i> ]pyrene	C <sub>28</sub> H <sub>16</sub>		352c
3-methylbenzo[ <i>pqr</i> ]naphtho[8,1,2- <i>bcd</i> ]perylene	C <sub>29</sub> H <sub>16</sub>		364g
naphtho[8,1,2- <i>abc</i> ]coronene	C <sub>30</sub> H <sub>14</sub>		374a
benzo[ <i>cd</i> ]naphtho[1,2,3- <i>lm</i> ]perylene	C <sub>30</sub> H <sub>16</sub>		376a

<sup>a</sup> The identifications of 4*H*-benzo[*cd*]fluoranthene (240a), 4-methyl-4*H*-benzo[*cd*]fluoranthene (254a), 1*H*-benzo[*cd*]fluoranthene (240e), and 1-methyl-1*H*-benzo[*cd*]fluoranthene (254c) are based on their UV and mass spectra but cannot be unequivocally confirmed, due to a lack of reference standards and published UV spectra for these PAH.

<sup>b</sup> For the identifications of the two vinylbenzo[*a*]pyrenes (278*j* and 278*k*), the UV and mass spectra establish that they are vinylbenzo[*a*]pyrenes. We do not have reference standards of all of the vinylbenzo[*a*]pyrenes, so we cannot be certain about the positions of the vinyl substituents on these two products' benzo[*a*]pyrene structures. However, since the only methyl- and ethylbenzo[*a*]pyrene products whose yields increase with 4-methylchrysene doping<sup>51</sup> are the 4- and 5-methyl- and ethylbenzo[*a*]pyrenes, we believe that the two vinylbenzo[*a*]pyrene products identified (whose yields increase with doping<sup>51</sup>) are 4-vinylbenzo[*a*]pyrene and 5-vinylbenzo[*a*]pyrene. They would result from the dehydrogenation of 4-ethylbenzo[*a*]pyrene and 5-ethylbenzo[*a*]pyrene, respectively.

<sup>c</sup> There are twelve possible isomers of methylindeno[1,2,3-*cd*]pyrenes. We know that the *n*-decane products contain at least nine methylindeno[1,2,3-*cd*]pyrenes because our product chromatograms show eight chromatographic peaks whose UV and mass spectra indicate are methylindeno[1,2,3-*cd*]pyrenes and another peak whose UV and mass spectra indicate are a methylindeno[1,2,3-*cd*]pyrene and an ethylindeno[1,2,3-*cd*]pyrene co-eluting. Three of the methylindeno[1,2,3-*cd*]pyrene peaks show no increase in yield with 4-methylchrysene doping,<sup>51</sup> and five do. The peak of co-elutants increases some with doping, but we cannot tell if the increase is due to the methylindeno[1,2,3-*cd*]pyrene or the ethylindeno[1,2,3-*cd*]pyrene. As explained in the chapter 5, we believe that the methylindeno[1,2,3-*cd*]pyrenes 290*g*, 290*h*, 290*i*, and 290*j* are four of the isomers that exhibit increases with doping, since they would be the ones formed in the reactions of Figure 5.13. We believe that any other isomers whose yields increase with doping would be among the group 290*k*, 290*l*, 290*m*, and 290*n*, for the reasons outlined in the chapter 5.

<sup>d</sup> The present experiments show that 4-methylchrysene doping<sup>51</sup> brings about increased production of dibenzo[*a,e*]pyrene (302*d*) as well as six PAH products whose UV and mass spectra indicate are: two methylene-bridged dibenzo[*a,e*]pyrenes, two methyl-substituted dibenzo[*a,e*]pyrenes, and two ethyl-substituted dibenzo[*a,e*]pyrenes. Noting that 1-butene's reactions with 5-benzo[*a*]pyrenylmethyl and 4-benzo[*a*]pyrenylmethyl would each give a bay-region methyl-substituted dibenzo[*a,e*]pyrene and that each of these, like 4-methylchrysene itself, would form a methylene-bridged derivative and a non-bay-region methyl-substituted "neighbor" isomer, we have deduced the two methylene-bridged dibenzo[*a,e*]pyrene products to be 3*H*-indeno[4,3,2-*efg*]benzo[*a*]pyrene (314*b*) and 7*H*-indeno[2,3,4-*cde*]benzo[*a*]pyrene (314*c*) and the two methyl-dibenzo[*a,e*]pyrene products to be 5-methyl-dibenzo[*a,e*]pyrene (316*a*) and 6-methyl-dibenzo[*a,e*]pyrene (316*b*). Since the methyl groups of 5-methyl-dibenzo[*a,e*]pyrene and 6-methyl-dibenzo[*a,e*]pyrene are not in bay regions, their arylmethyl radicals can easily combine with methyl, producing 5-ethyl-dibenzo[*a,e*]pyrene (330*a*) and 6-ethyl-dibenzo[*a,e*]pyrene (330*b*), so we deduce these to be the identities of the two ethyl-dibenzo[*a,e*]pyrenes whose yields increase with 4-methylchrysene doping.<sup>51</sup>

<sup>e</sup> The present experiments show that there are seven methyl-substituted C<sub>26</sub>H<sub>14</sub> products whose yields increase with 4-methylchrysene doping.<sup>51</sup> The UV and mass spectra of these seven products reveal that three of them are methyl-dibenzo[*e,ghi*]perylene, two of them are methyl-dibenzo[*b,ghi*]perylene, and two of them are methyl-naphtho[1,2,3,4-*ghi*]perylene. Our supercritical *n*-decane pyrolysis experiments with the dopants 1-methylnaphthalene,<sup>49</sup> 2-

methylnaphthalene,<sup>49</sup> 1-methylphenanthrene,<sup>50</sup> and 4-methylchrysene<sup>51</sup> have shown that when the reaction of 1-butene with either an arylmethyl radical or a phenalenyl-type radical produces a non-bay-region methyl-substituted PAH, that product does not convert to another isomer. However, when that reaction produces a bay-region methyl-substituted PAH, a large portion of that product converts to its non-bay-region methyl-substituted “neighbor” isomer. We have incorporated that finding, along with our findings<sup>49,50</sup> on the reactions of 1-butene with phenalenyl-type radicals, to construct the reaction pathways of Figure 5.11. Those pathways show that 1-butene’s reactions with the phenalenyl-type radicals of Figure 5.9 should produce exactly three methyl-dibenzo[*e,ghi*]perylene, two methyl-dibenzo[*b,ghi*]perylene, and two methyl-naphtho[1,2,3,4-*ghi*]perylene—and that those products would be: 3-methyl-dibenzo[*e,ghi*]perylene (340e), 4-methyl-dibenzo[*e,ghi*]perylene (340f), 7-methyl-dibenzo[*e,ghi*]perylene (340g), 5-methyl-dibenzo[*b,ghi*]perylene (340a), 6-methyl-dibenzo[*b,ghi*]perylene (340b), 1-methyl-naphtho[1,2,3,4-*ghi*]perylene (340c), and 2-methyl-naphtho[1,2,3,4-*ghi*]perylene (340d). We have therefore deduced these PAH to be the seven methyl-substituted C<sub>26</sub>H<sub>14</sub> products whose yields increase with 4-methylchrysene doping.<sup>51</sup>



Table B2. PAH growth reactions of 1-naphthylmethyl and phenalenyl, as determined from supercritical *n*-decane pyrolysis experiments<sup>49</sup> with the dopant 1-methylnaphthalene.

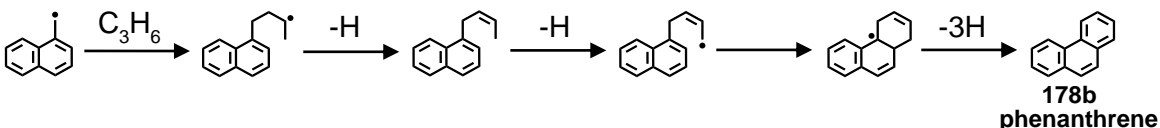
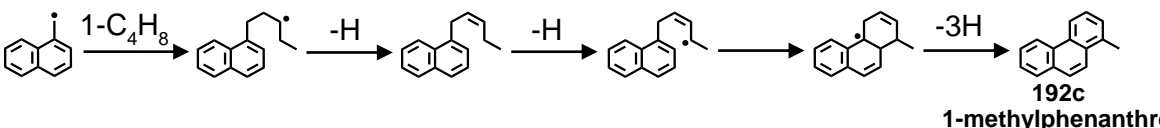
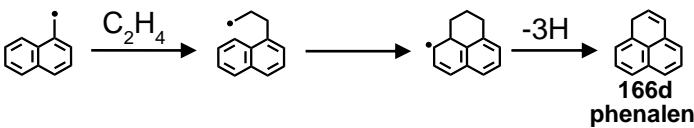
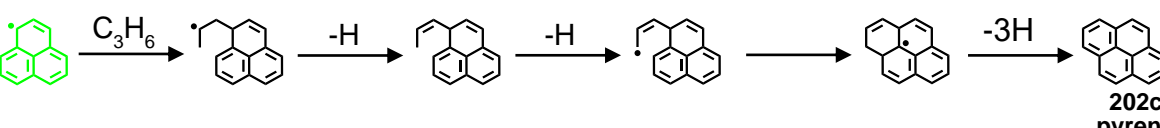
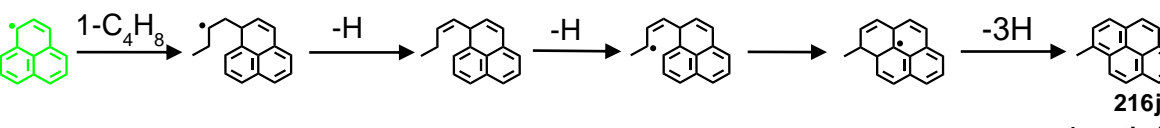
Reaction	Equation
	(B1) 178b phenanthrene
	(B2) 192c 1-methylphenanthrene
	(B3) 166d phenalene
	(B4) 202c pyrene
	(B5) 216j 1-methylpyrene

Table B3. PAH growth reactions of 1-pyrenylmethyl and benzo[*cd*]pyrenyl, as determined from supercritical *n*-decane pyrolysis experiments<sup>49</sup> with the dopant 1-methylnaphthalene (which greatly increased the production of 1-methylpyrene).

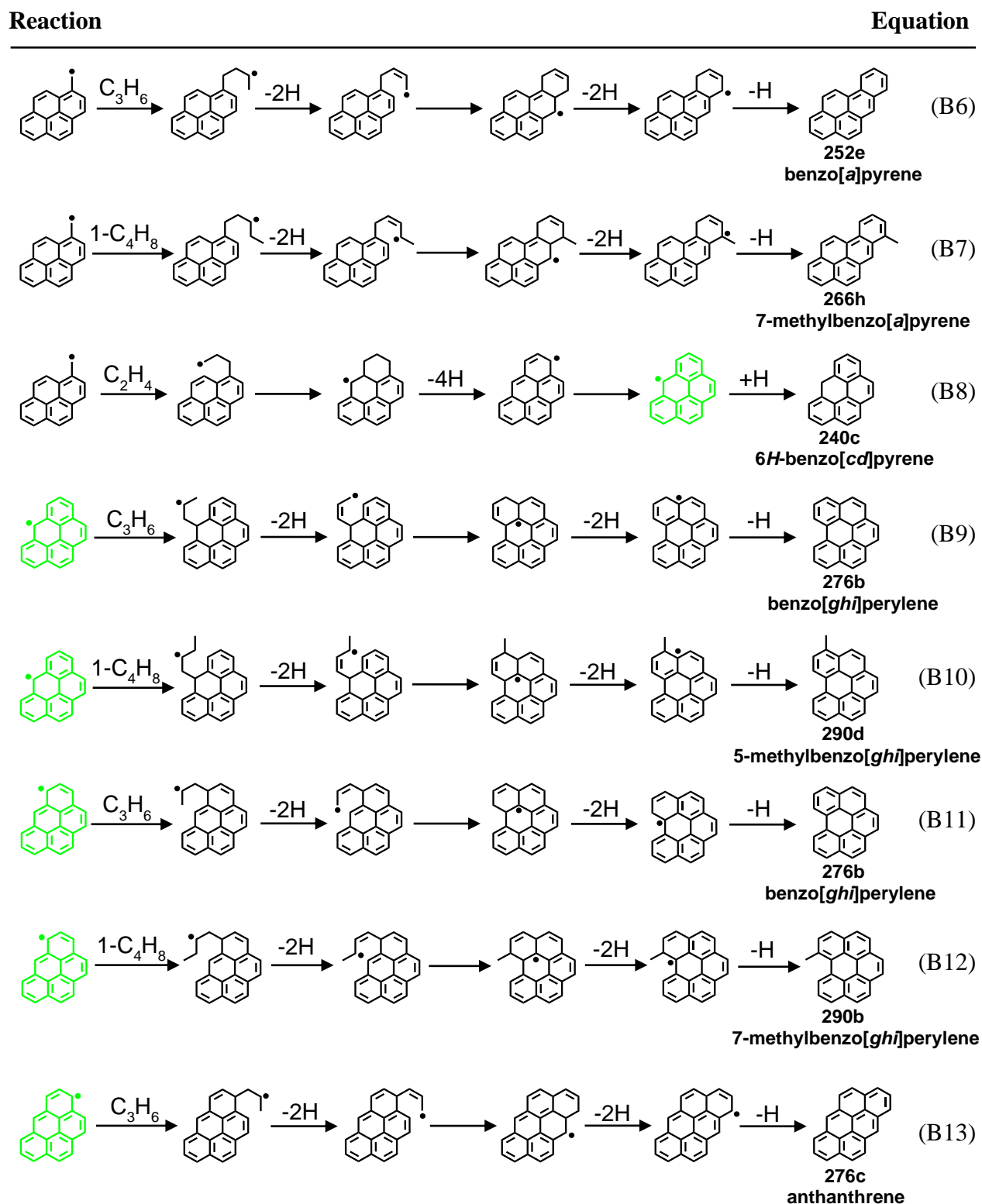


Table B4. PAH growth reactions of 1-phenanthrylmethyl and benz[de]anthracenyl, as determined from supercritical *n*-decane pyrolysis experiments<sup>50</sup> with the dopant 1-methylphenanthrene.

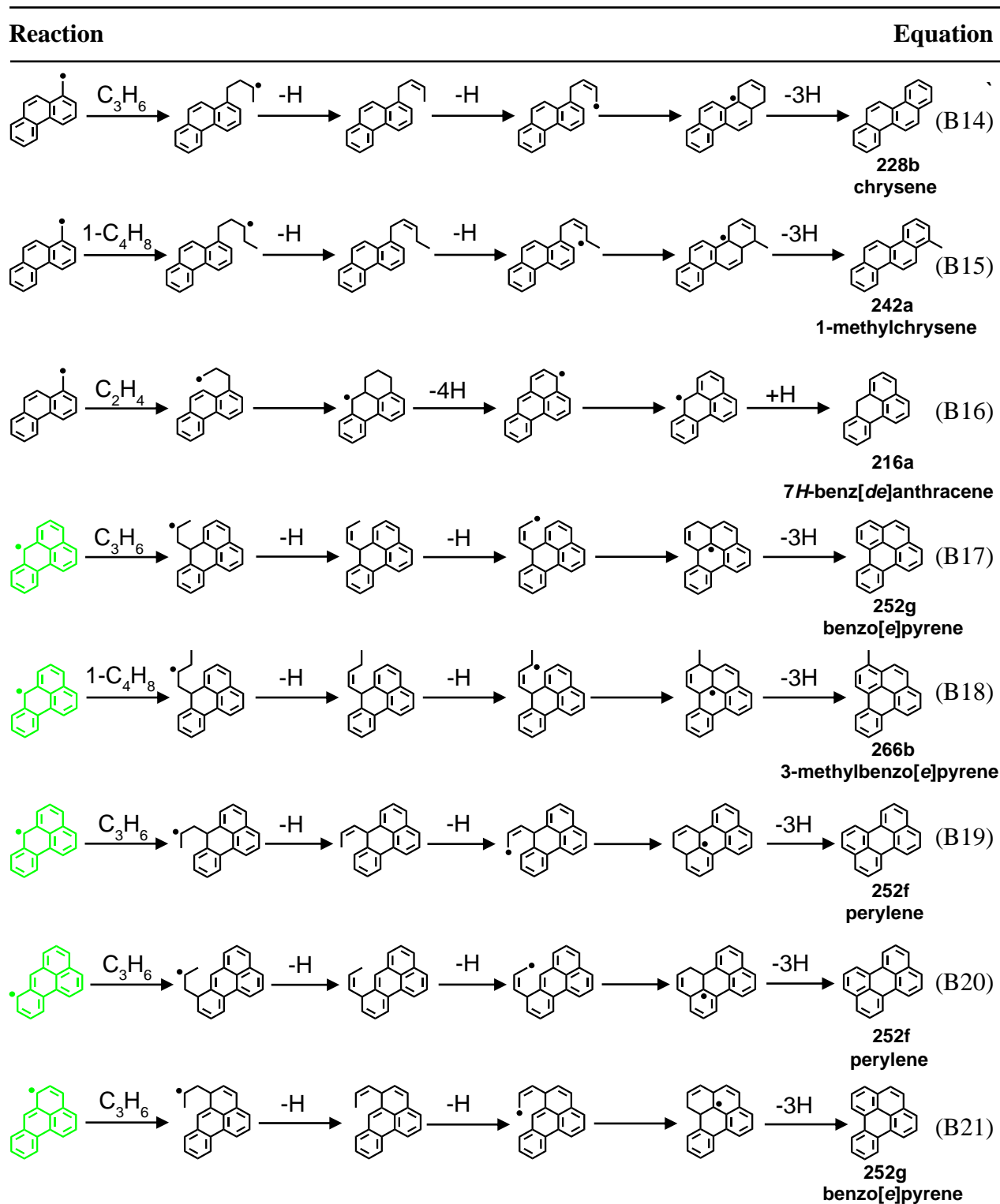
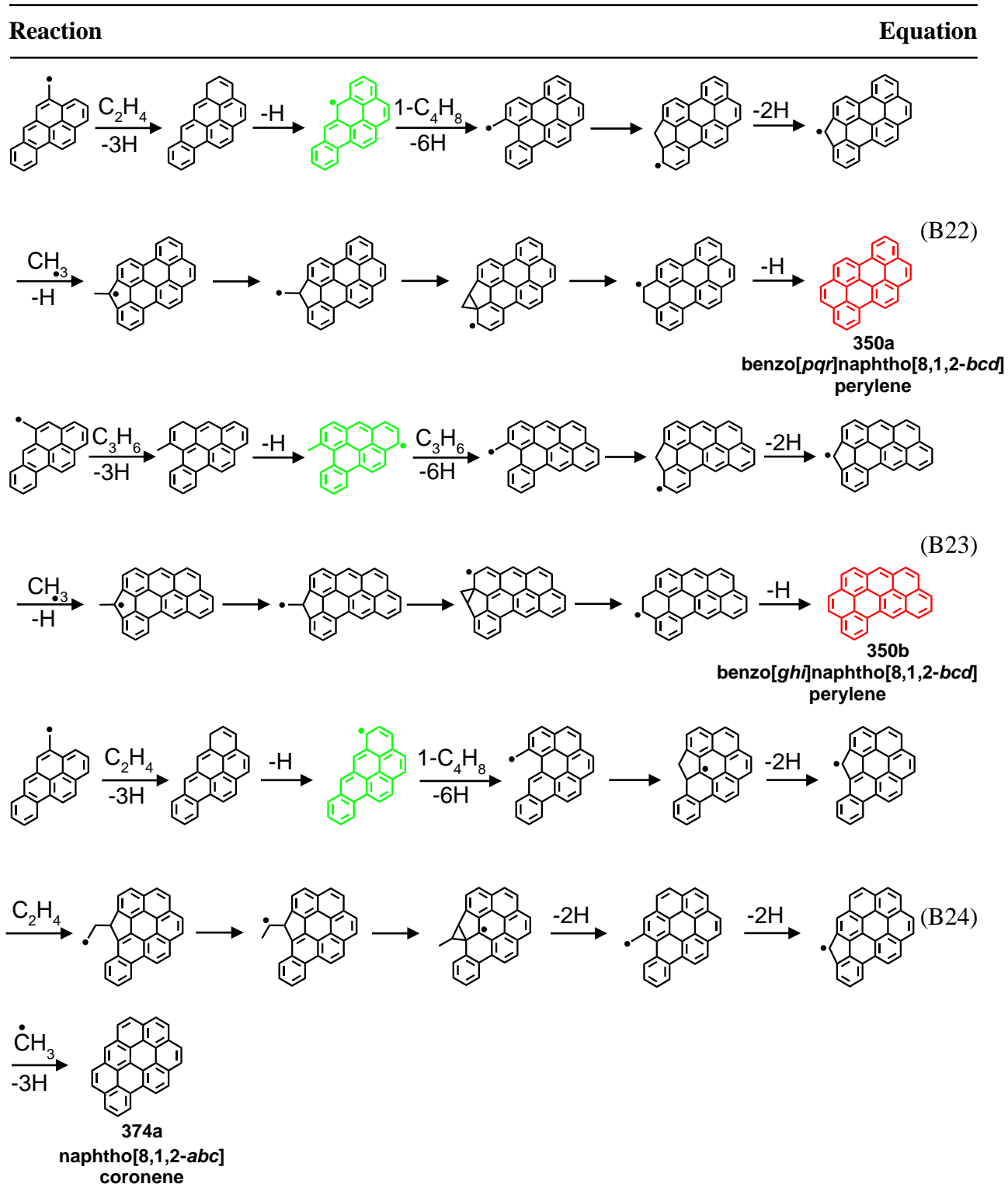


Table B5. Proposed pathways for the formation of benzo[*pqr*]naphtho[8,1,2-*bcd*]perylene, benzo[*ghi*]naphtho[8,1,2-*bcd*]perylene, and naphtho[8,1,2-*abc*]coronene from reactions of 4-benzo[*a*]pyrenylmethyl and 5-benzo[*a*]pyrenylmethyl with the principal aliphatic growth species—methyl, ethylene, propene, and 1-butene—in the supercritical *n*-decane pyrolysis environment.



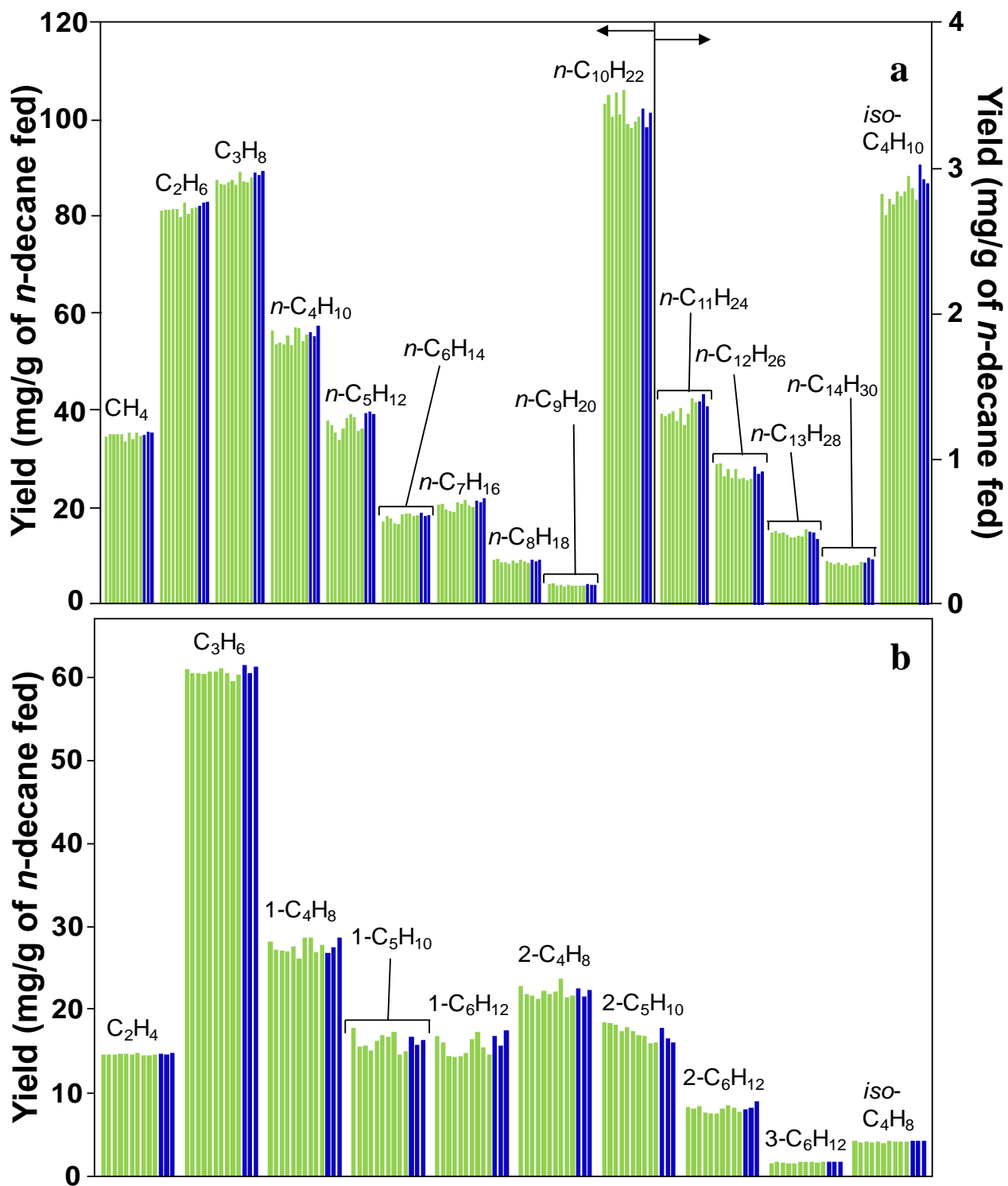


Figure B1. Yields of (a) alkanes (including unreacted fuel *n*-decane) and (b) C<sub>2</sub>-C<sub>6</sub> alkenes from the supercritical pyrolysis of *n*-decane at 568 °C, 94.6 atm, and 133 sec. Experiments: (■) without dopant and (■) with 4-methylchrysene dopant (684 μg 4-methylchrysene / g *n*-decane fed). For the 2- and 3-alkenes in (b), the reported yields are those summed for the *cis* and *trans* isomers.

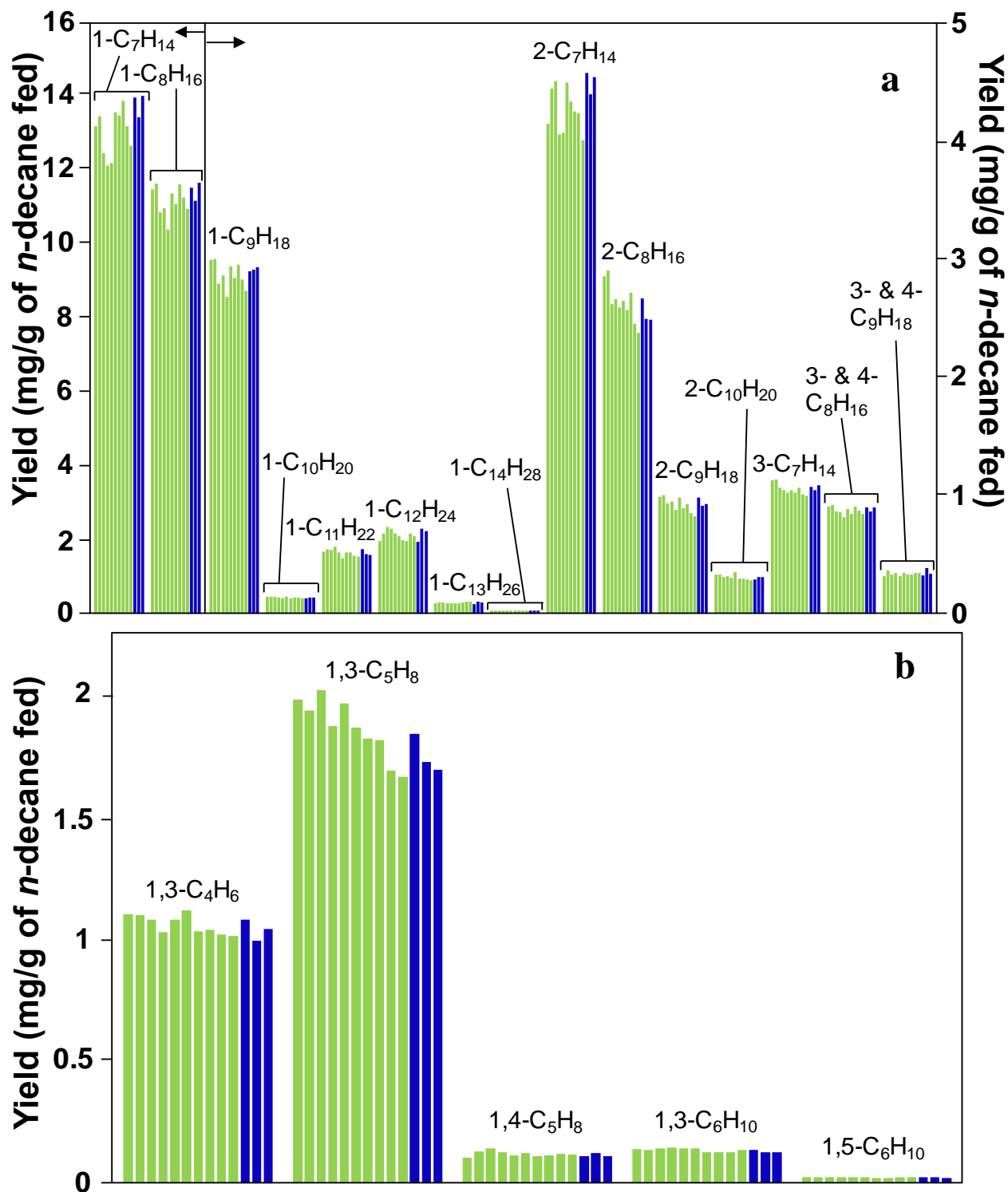


Figure B2. Yields of (a) C<sub>7</sub>-C<sub>14</sub> alkenes and (b) dienes from the supercritical pyrolysis of *n*-decane at 568 °C, 94.6 atm, and 133 sec. Experiments: (■) without dopant and (■) with 4-methylchrysene dopant (684 μg 4-methylchrysene / g *n*-decane fed). For the 2-, 3-, and 4-alkenes in (a), and 1,3-pentadiene in (b), the reported yields are those summed for the *cis* and *trans* isomers.

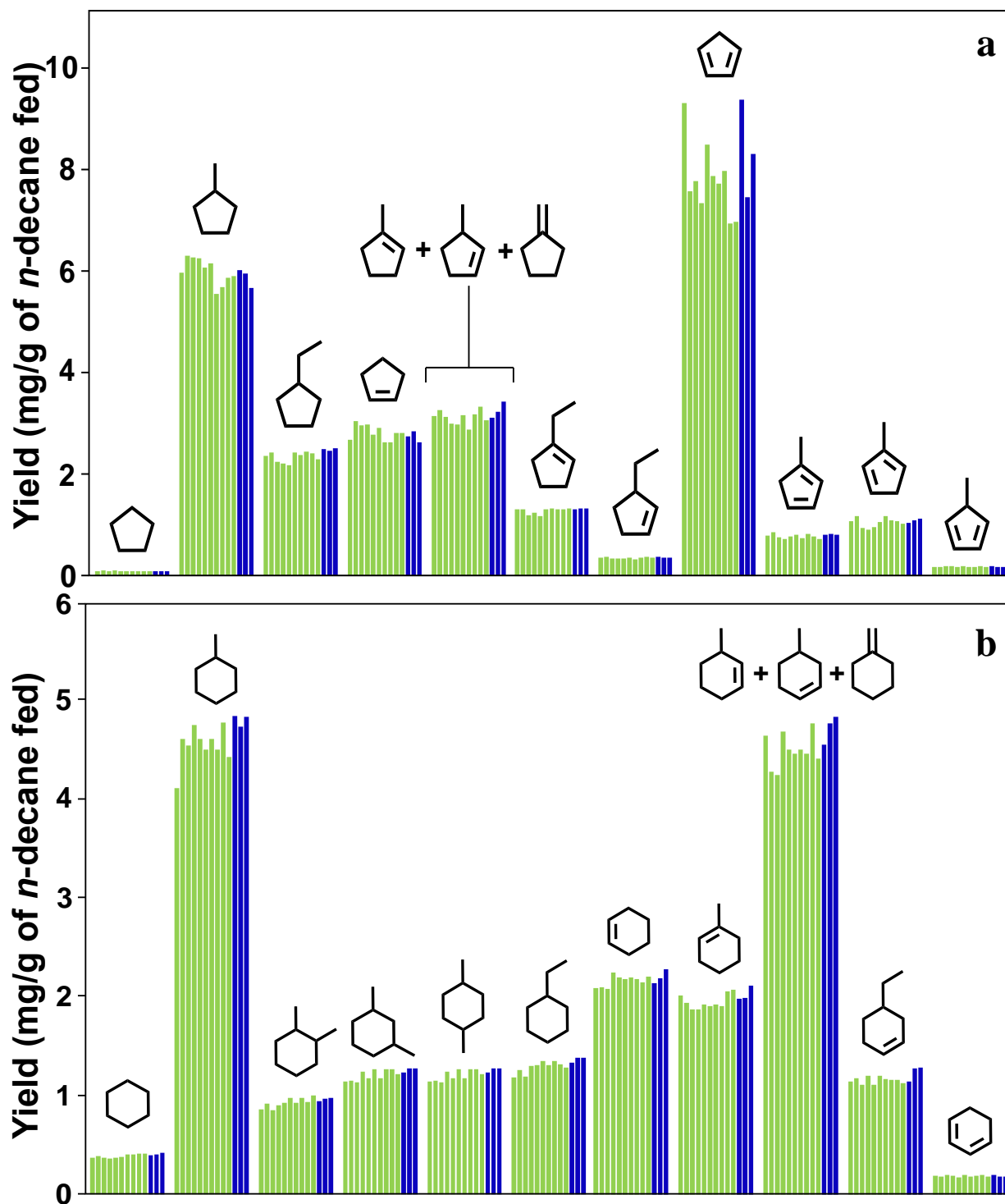


Figure B3. Yields of (a) C<sub>5</sub>-ring and (b) C<sub>6</sub>-ring cyclic aliphatic products from the supercritical pyrolysis of *n*-decane at 568 °C, 94.6 atm, and 133 sec. Experiments: (■) without dopant and (■) with 4-methylchrysene dopant (684 μg 4-methylchrysene / g *n*-decane fed). For the three dimethylcyclohexanes in (b), the reported yields are those summed for the *cis* and *trans* isomers. The variations in the experimental yields of cyclopentadiene in (a) and methylcyclohexane in (b) stem from their volatility in the liquid-phase products.

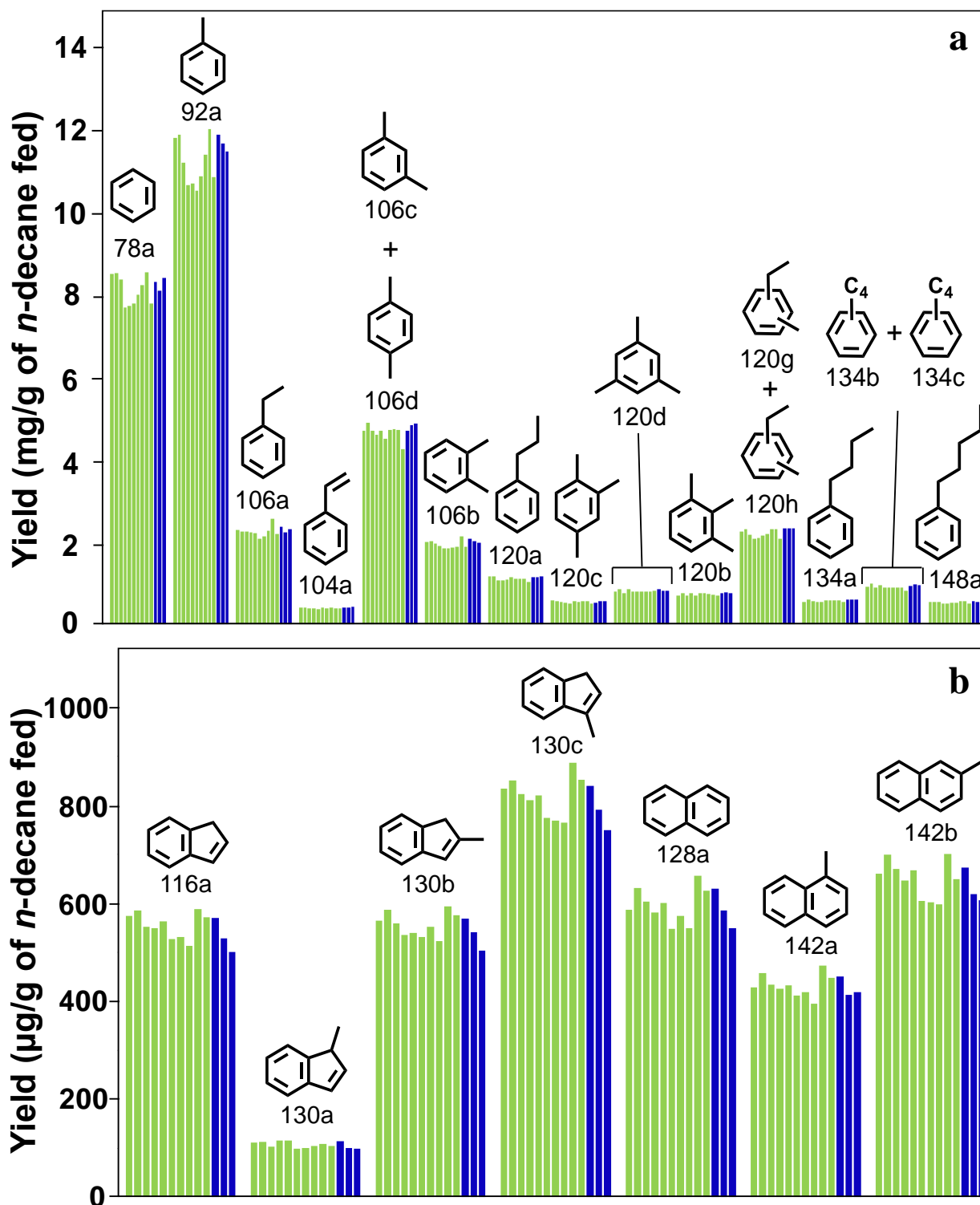


Figure B4. Yields of one- and two-ring aromatics from supercritical *n*-decane pyrolysis at 568 °C, 94.6 atm, and 133 sec: (a) benzene and substituted benzenes; (b) indene (116a), 1-methylindene (130a), 2-methylindene (130b), 3-methylindene (130c), naphthalene (128a), 1-methylnaphthalene (142a), and 2-methylnaphthalene (142b). Experiments: (■) without dopant and (■) with 4-methylchrysene dopant (684 µg 4-methylchrysene / g *n*-decane fed).



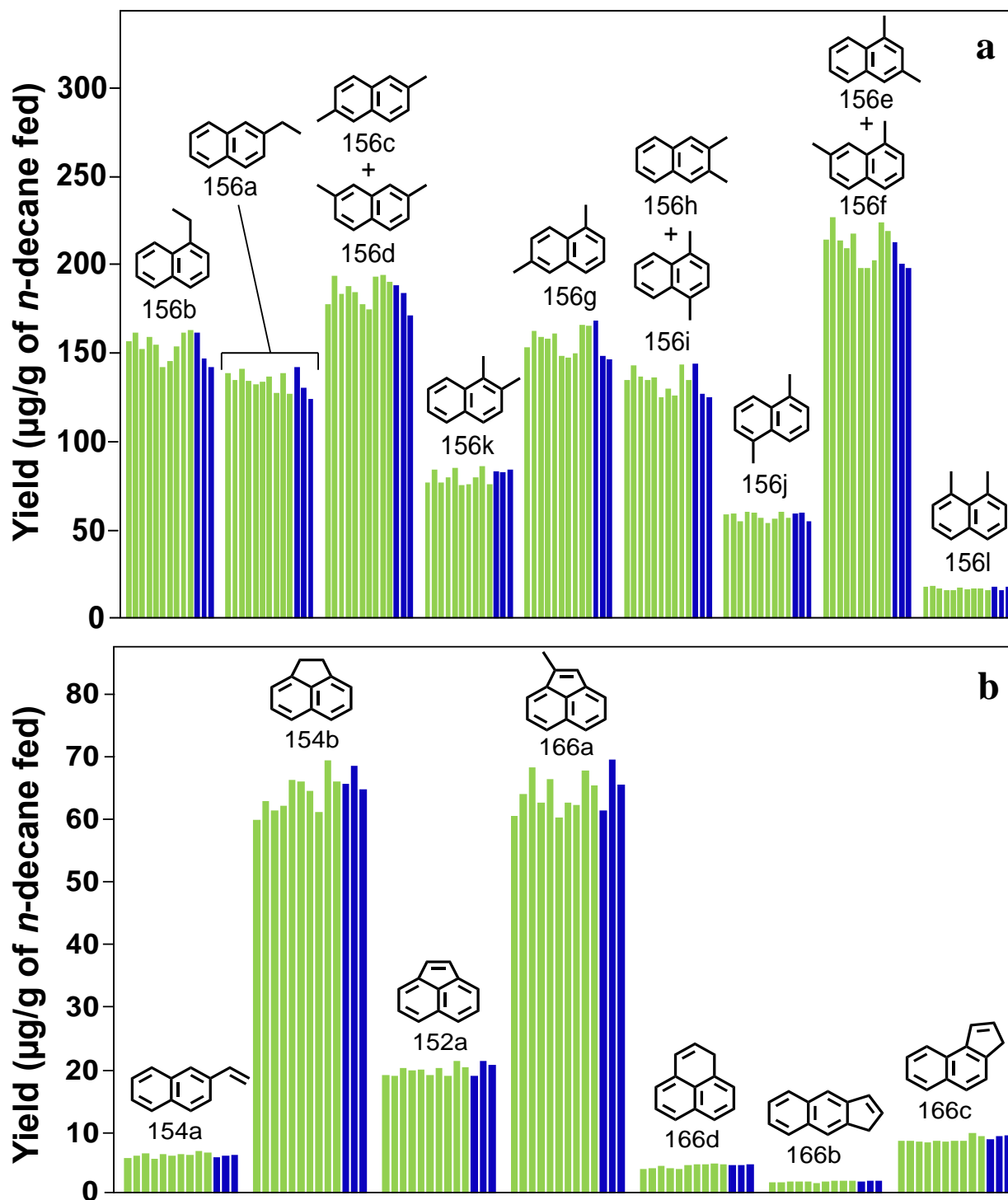


Figure B5. Yields of two- and three-ring aromatics from supercritical *n*-decane pyrolysis at 568 °C, 94.6 atm, and 133 sec: (a) 1-ethylnaphthalene (156b), 2-ethylnaphthalene (156a), and the ten dimethylnaphthalenes (156c-l); (b) 2-vinylnaphthalene (154a), acenaphthene (154b), acenaphthylene (152a), 1-methylacenaphthylene (166a), phenalene (166d), benz[*f*]indene (166b), and benz[*e*]indene (166c). Experiments: (■) without dopant and (■) with 4-methylchrysene dopant (684  $\mu\text{g}$  4-methylchrysene / g *n*-decane fed).

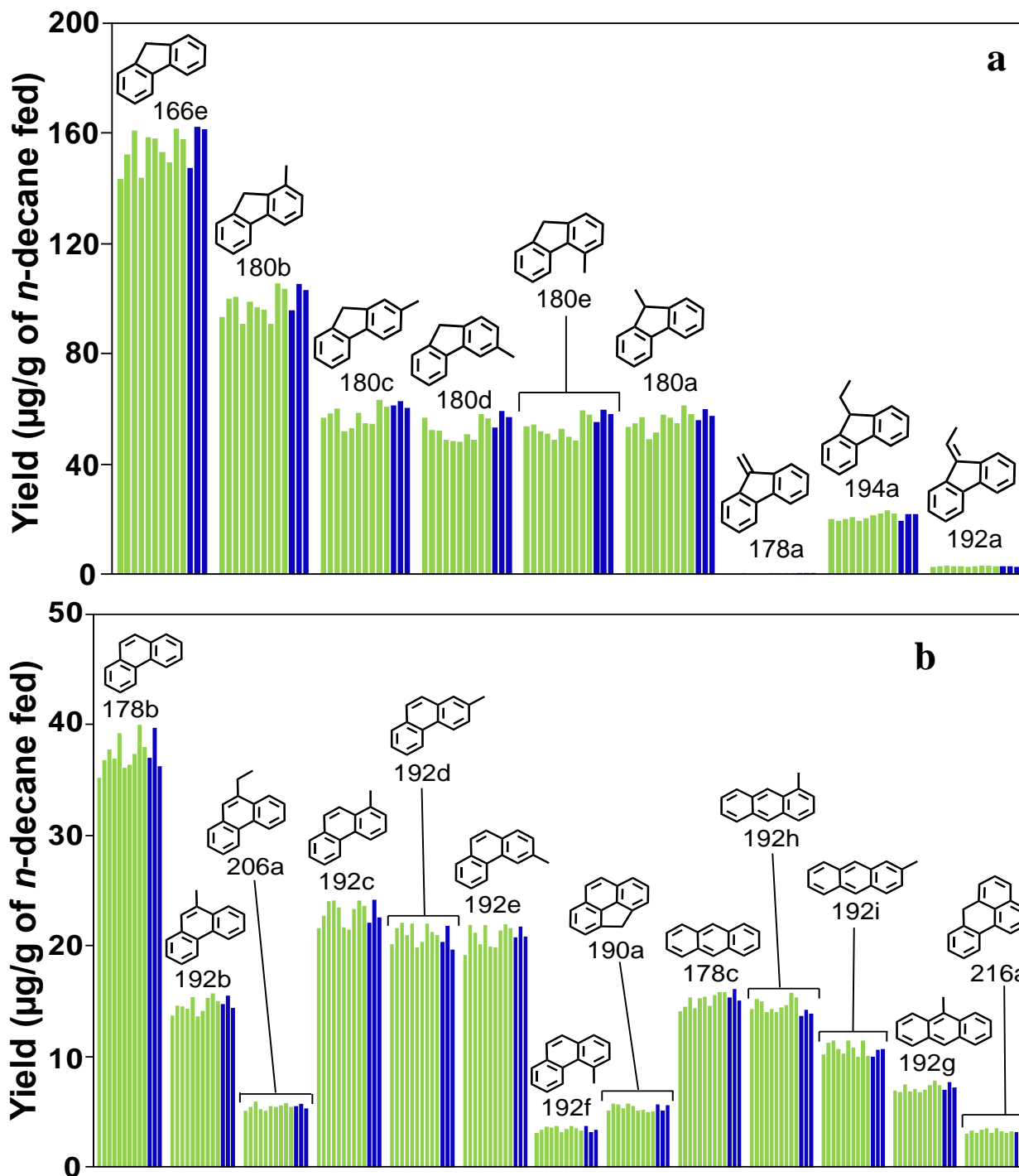


Figure B6. Yields of three- and four-ring PAH from supercritical *n*-decane pyrolysis at 568 °C, 94.6 atm, and 133 sec: (a) fluorene (166e), the five methylfluorenes (180a–e), dibenzofulvene (178a), 9-ethylfluorene (194a), and 9-ethylidene fluorene (192a); (b) phenanthrene (178b), the five methylphenanthrenes (192b–f), 4*H*-cyclopenta[*def*]phenanthrene (190a), anthracene (178c), the three methylanthracenes (192g–i), and 7*H*-benz[*de*]anthracene (216a). Experiments: (■) without dopant and (■) with 4-methylchrysene dopant (684  $\mu\text{g}$  4-methylchrysene / g *n*-decane fed).

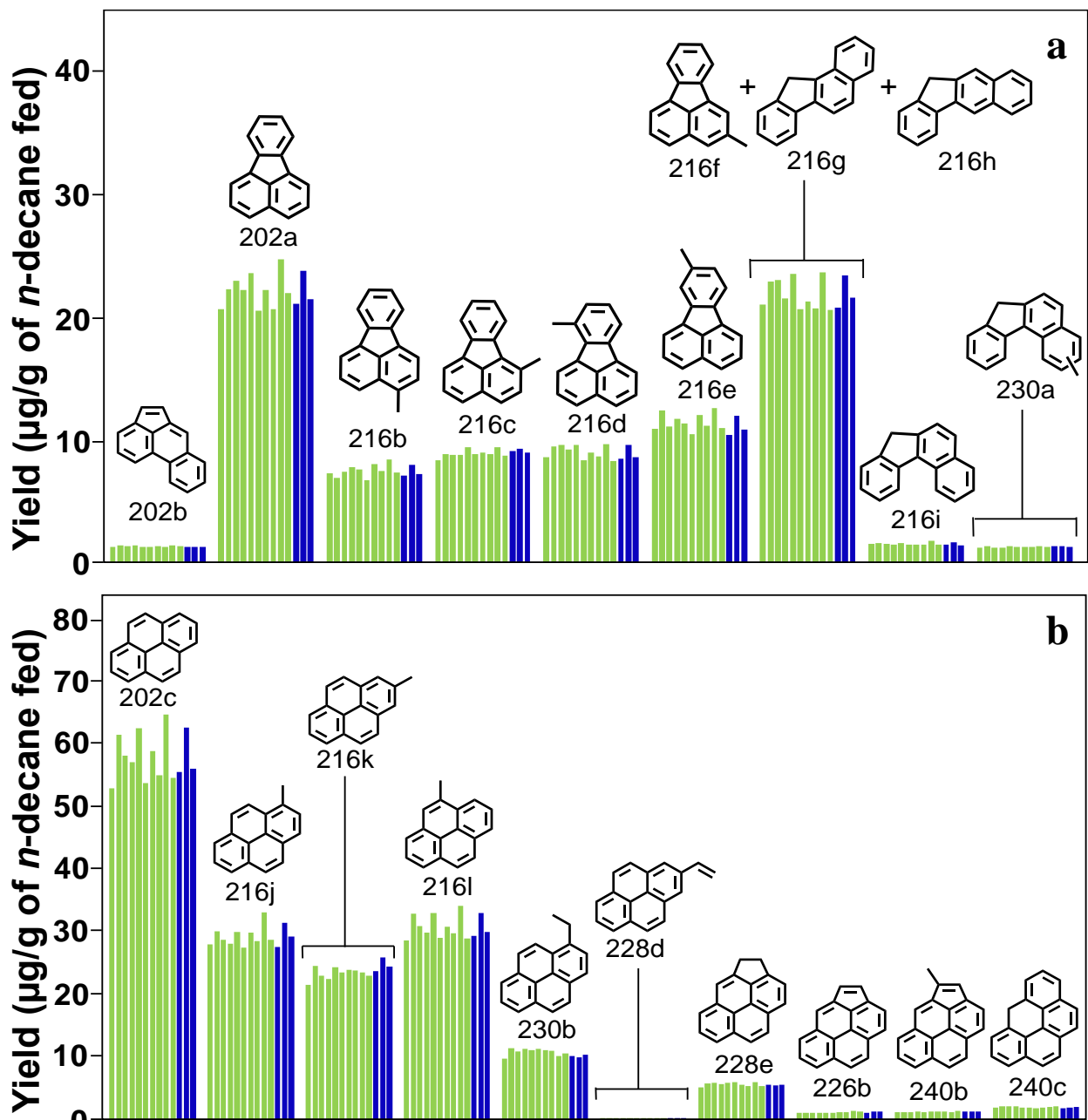


Figure B7. Yields of four-ring PAH, and their derivatives, from supercritical *n*-decane pyrolysis at 568 °C, 94.6 atm, and 133 sec: (a) acephenanthrylene (202b), fluoranthene (202a), the five methylfluoranthenes (216b-f) (one of which co-elutes with benzo[*a*]fluorene (216g) and benzo[*b*]fluorene (216h)), benzo[*c*]fluorene (216i), and a methylbenzo[*c*]fluorene (230a); (b) pyrene (202c), 1-methylpyrene (216j), 2-methylpyrene (216k), 4-methylpyrene (216l), 1-ethylpyrene (230b), 2-vinylpyrene (228d), 3,4-dihydrocyclopenta[*cd*]pyrene (228e), cyclopenta[*cd*]pyrene (226b), 4-methylcyclopenta[*cd*]pyrene (240b), and 6*H*-benzo[*cd*]pyrene (240c). Experiments: (■) without dopant and (■) with 4-methylchrysene dopant (684 µg 4-methylchrysene / g *n*-decane fed). The yield reported in (b) for 1-ethylpyrene might include contributions from co-eluting ethylpyrenes or dimethylpyrenes; hence it is a maximum possible 1-ethylpyrene yield.

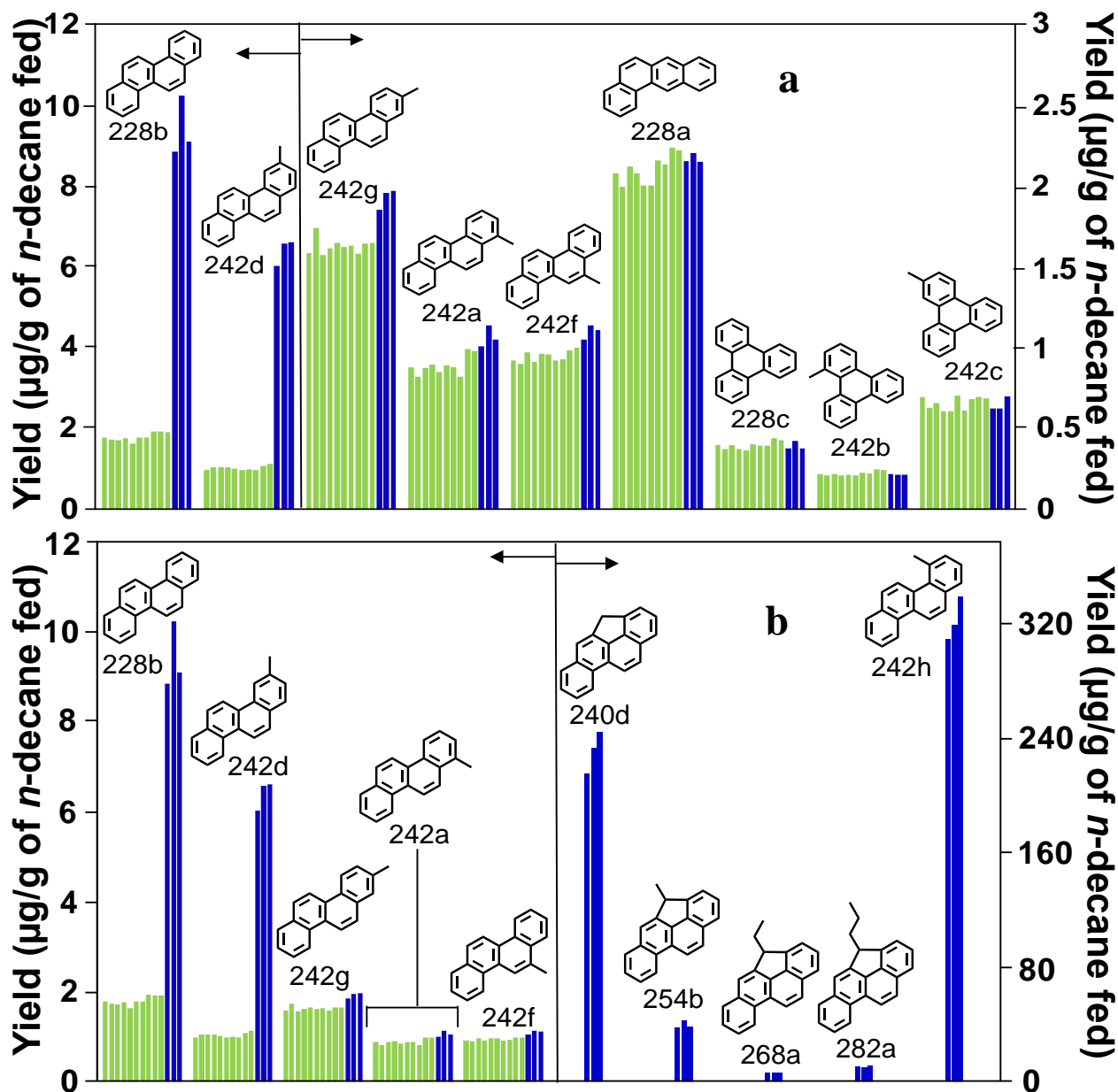


Figure B8. Yields of four-ring  $C_{18}H_{12}$  and five-ring  $C_{19}H_{12}$  PAH, and their alkyl derivatives, from supercritical *n*-decane pyrolysis at 568 °C, 94.6 atm, and 133 sec: (a) chrysene (228b), 3-methylchrysene (242d), 2-methylchrysene (242g), 1-methylchrysene (242a), 6-methylchrysene (242f), benz[*a*]anthracene (228a), triphenylene (228c), 1-methyltriphenylene (242b), and 2-methyltriphenylene (242c); (b) chrysene (228b), 3-methylchrysene (242d), 2-methylchrysene (242g), 1-methylchrysene (242a), 6-methylchrysene (242f), 4*H*-cyclopenta[*def*]chrysene (240d), 4-methyl-4*H*-cyclopenta[*def*]chrysene (254b), 4-ethyl-4*H*-cyclopenta[*def*]chrysene (268a), 4-propyl-4*H*-cyclopenta[*def*]chrysene (282a), and 4-methylchrysene (242h). Experiments: (■) without dopant and (■) with 4-methylchrysene dopant (684 µg 4-methylchrysene / g *n*-decane fed). For the experiments with the 4-methylchrysene dopant, the yields of chrysene (178c), 3-methylchrysene (242d), and benz[*a*]anthracene (228a) have been corrected to account for their levels as impurities—0.952, 0.145, and 0.025 µg/ g *n*-decane fed, respectively—introduced with the dopant.

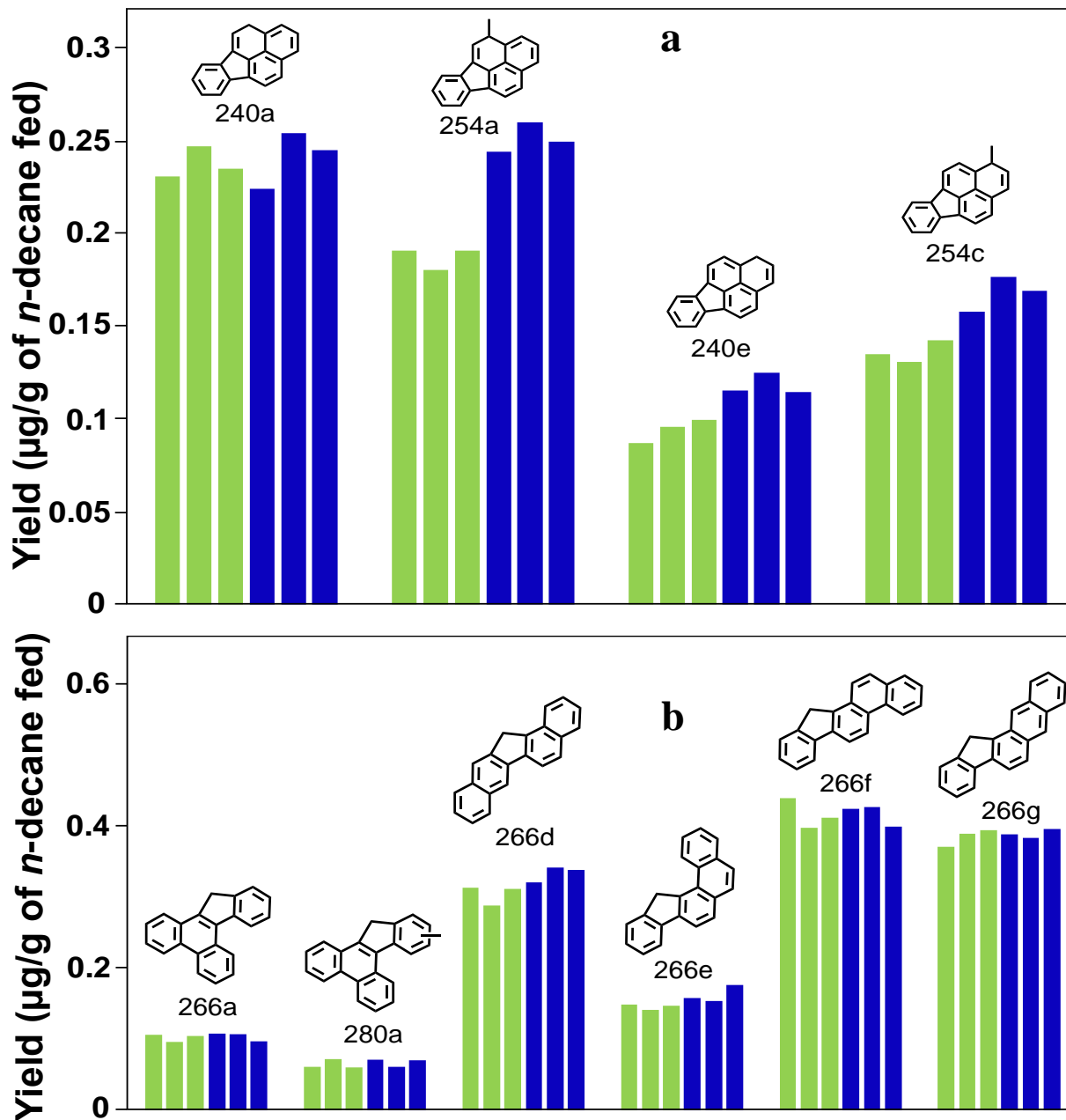


Figure B9. Yields of five-ring  $C_{19}H_{12}$  and  $C_{21}H_{14}$  PAH, and their methyl derivatives, from supercritical *n*-decane pyrolysis at 568 °C, 94.6 atm, and 133 sec: (a) 4*H*-benzo[*cd*]fluoranthene (240a), 4-methyl-4*H*-benzo[*cd*]fluoranthene (254a), 1*H*-benzo[*cd*]fluoranthene (240e), and 1-methyl-1*H*-benzo[*cd*]fluoranthene (254c); (b) dibenzo[*a,c*]fluorene (266a), methyl-dibenzo[*a,c*]fluorene (280a), dibenzo[*a,h*]fluorene (266d), naphtho[1,2-*a*]fluorene (266e), naphtho[2,1-*a*]fluorene (266f), and naphtho[2,3-*a*]fluorene (266g). Experiments: (■) without dopant and (■) with 4-methylchrysene dopant (684 µg 4-methylchrysene / g *n*-decane fed). The identifications of 4*H*-benzo[*cd*]fluoranthene (240a), 4-methyl-4*H*-benzo[*cd*]fluoranthene (254a), 1*H*-benzo[*cd*]fluoranthene (240e), and 1-methyl-1*H*-benzo[*cd*]fluoranthene (254c) are based on their UV and mass spectra but cannot be unequivocally confirmed, due to a lack of reference standards and published UV spectra for these PAH.

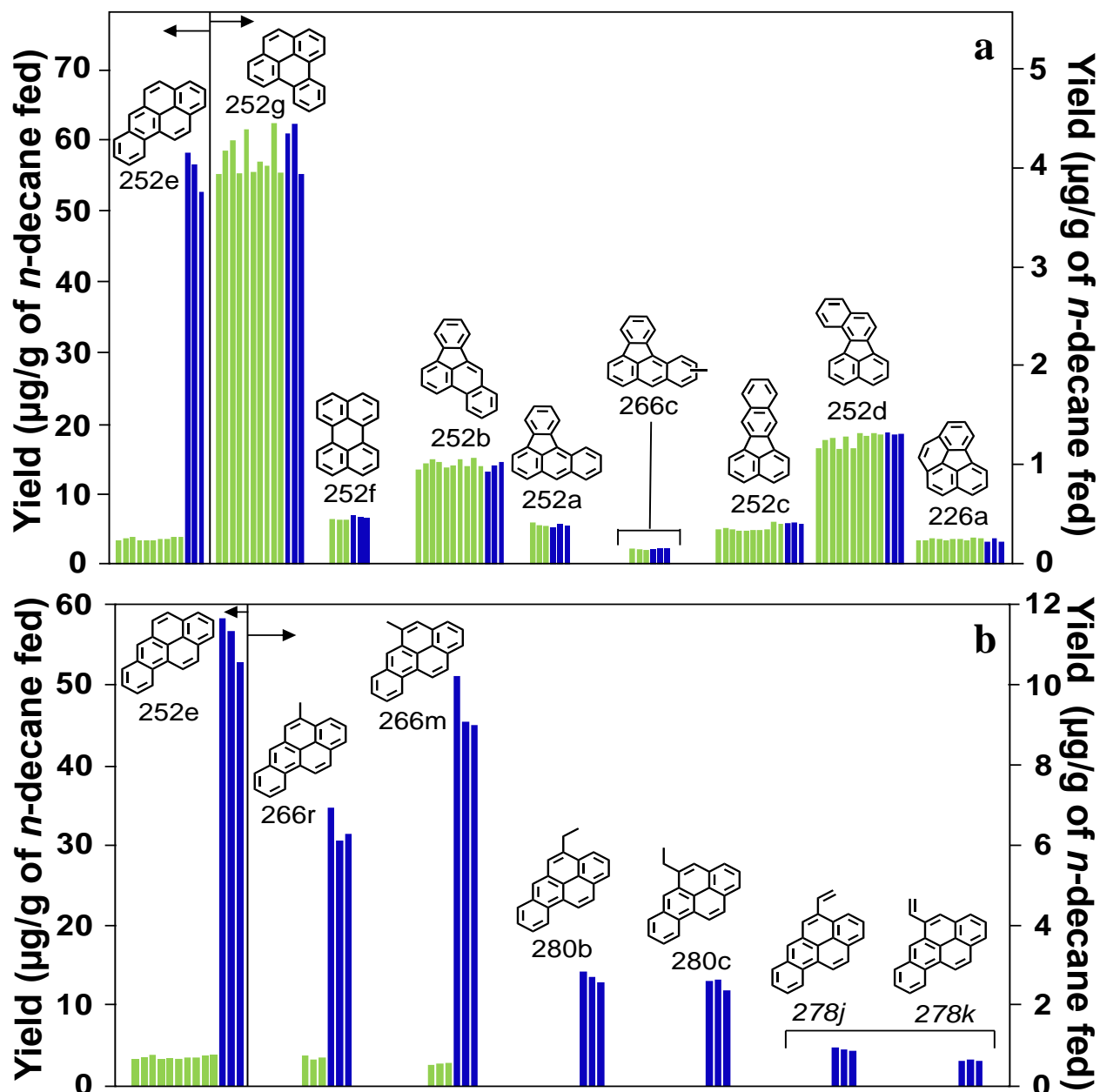


Figure B10. Yields of five-ring C<sub>20</sub>H<sub>12</sub> PAH, their derivatives, and an associated C<sub>18</sub>H<sub>10</sub> PAH product from supercritical *n*-decane pyrolysis at 568 °C, 94.6 atm, and 133 sec: (a) benzo[*a*]pyrene (252e), benzo[*e*]pyrene (252g), perylene (252f), benzo[*b*]fluoranthene (252b), benzo[*a*]fluoranthene (252a), a methylbenzo[*a*]fluoranthene (266c), benzo[*k*]fluoranthene (252c), benzo[*j*]fluoranthene (252d), and benzo[*ghi*]fluoranthene (226a); (b) benzo[*a*]pyrene (252e), 4-methylbenzo[*a*]pyrene (266r), 5-methylbenzo[*a*]pyrene (266m), 4-ethylbenzo[*a*]pyrene (280b), 5-ethylbenzo[*a*]pyrene (280c), 4-vinylbenzo[*a*]pyrene (278j), and 5-vinylbenzo[*a*]pyrene (278k). Experiments: (■) without dopant and (■) with 4-methylchrysene dopant (684 µg 4-methylchrysene / g *n*-decane fed). For the identifications of the two vinylbenzo[*a*]pyrenes (278j and 278k), the UV and mass spectra establish that they are vinylbenzo[*a*]pyrenes, but the positions of the vinyl substituents on the benzo[*a*]pyrene structure have been deduced, as noted in Table B1.

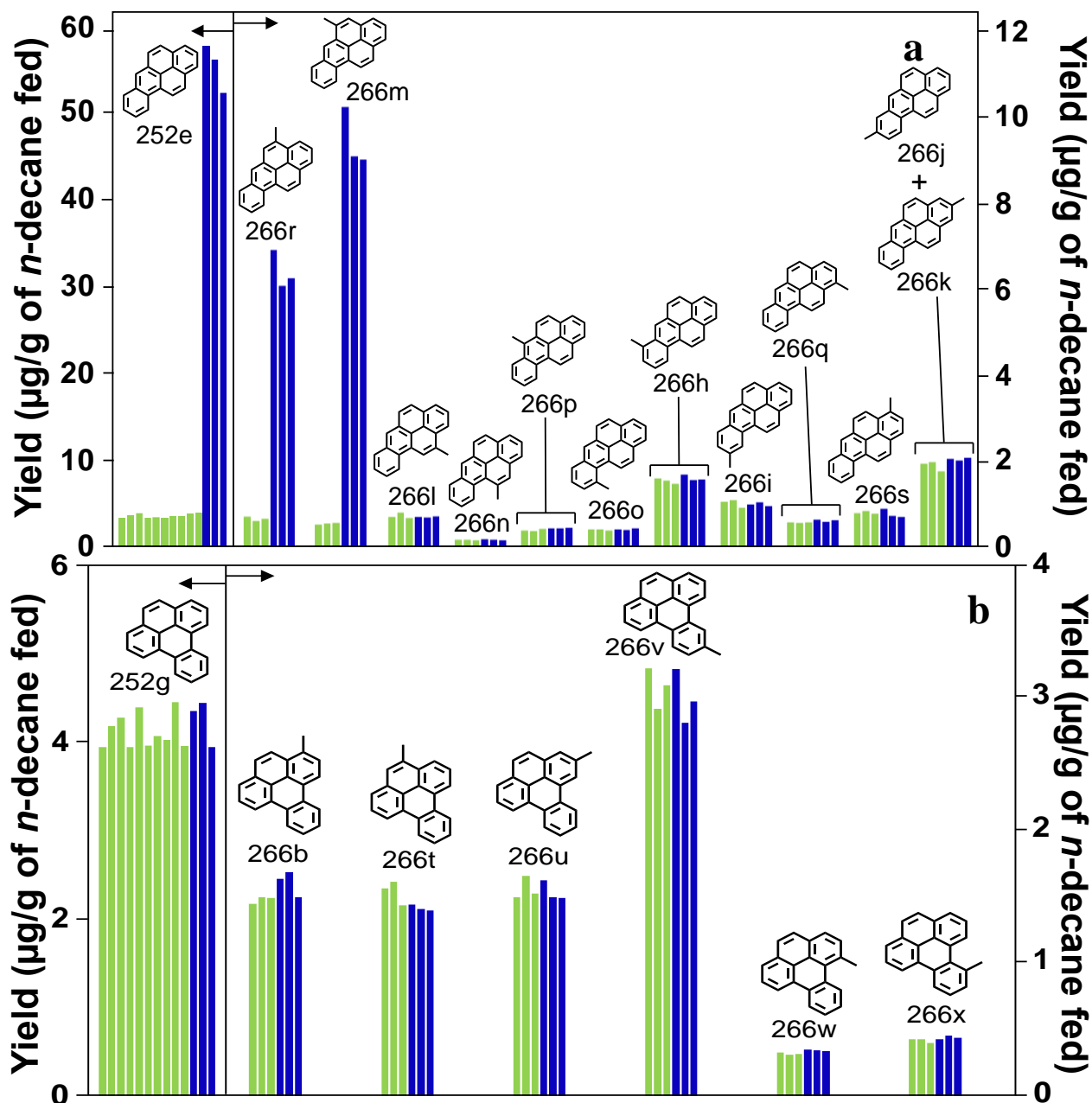


Figure B11. Yields of five-ring C<sub>20</sub>H<sub>12</sub> PAH, and their methyl derivatives, from supercritical *n*-decane pyrolysis at 568 °C, 94.6 atm, and 133 sec: (a) benzo[*a*]pyrene (252e), 4-methylbenzo[*a*]pyrene (266r), 5-methylbenzo[*a*]pyrene (266m), 12-methylbenzo[*a*]pyrene (266l), 11-methylbenzo[*a*]pyrene (266n), 6-methylbenzo[*a*]pyrene (266p), 10-methylbenzo[*a*]pyrene (266o), 7-methylbenzo[*a*]pyrene (266h), 9-methylbenzo[*a*]pyrene (266i), 1-methylbenzo[*a*]pyrene (266q), 3-methylbenzo[*a*]pyrene (266s), and 2-methylbenzo[*a*]pyrene (266k) co-eluting with 8-methylbenzo[*a*]pyrene (266j); (b) benzo[*e*]pyrene (252g), 3-methylbenzo[*e*]pyrene (266b), 4-methylbenzo[*e*]pyrene (266t), 2-methylbenzo[*e*]pyrene (266u), 10-methylbenzo[*e*]pyrene (266v), 1-methylbenzo[*e*]pyrene (266w), and 9-methylbenzo[*e*]pyrene (266x). Experiments: (■) without dopant and (■) with 4-methylchrysene dopant (684 µg 4-methylchrysene / g *n*-decane fed).

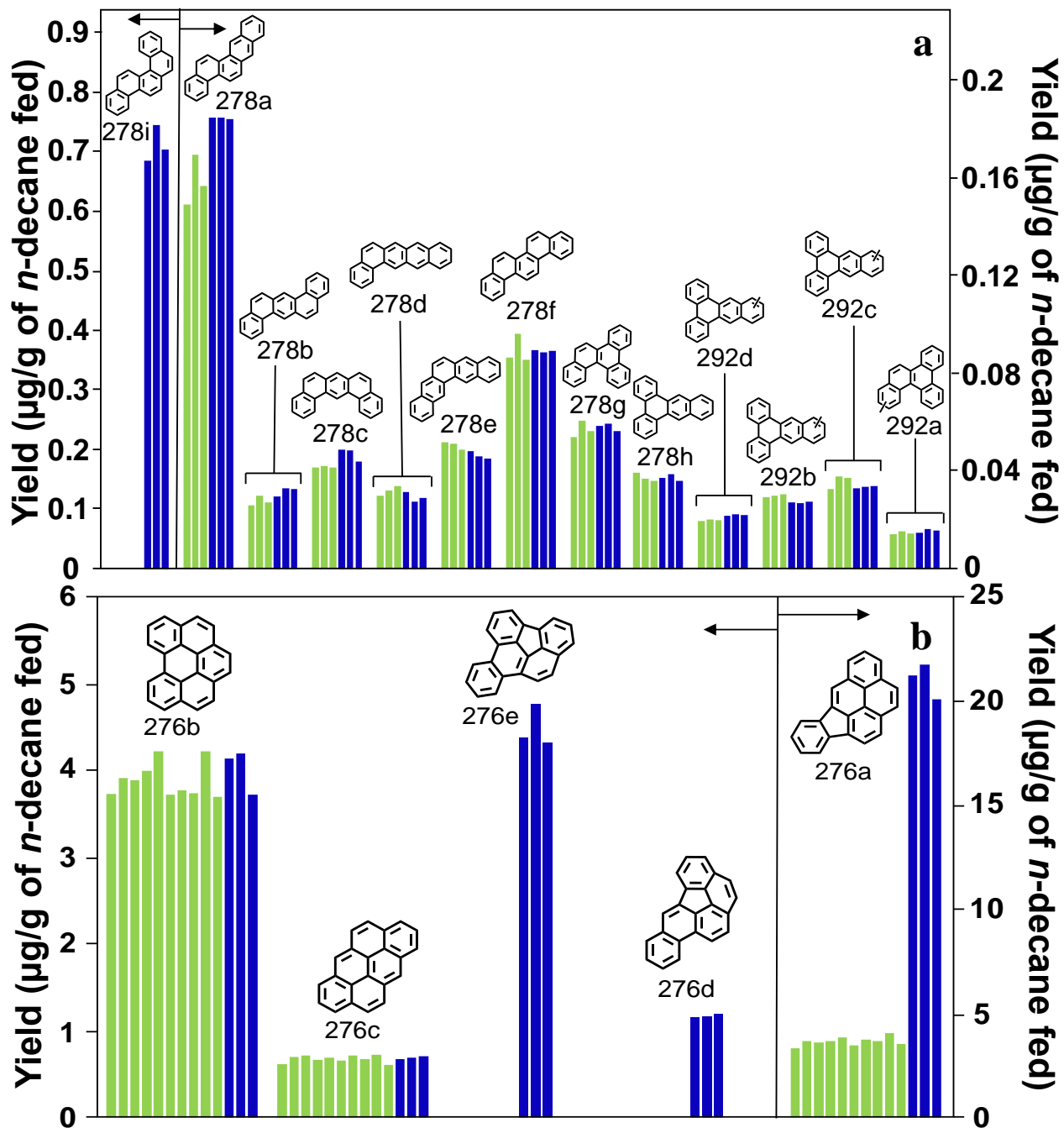


Figure B12. Yields of five-ring C<sub>22</sub>H<sub>14</sub> PAH, and their methyl derivatives, and six-ring C<sub>22</sub>H<sub>12</sub> PAH from supercritical *n*-decane pyrolysis at 568 °C, 94.6 atm, and 133 sec: (a) benzo[*c*]chrysene (278i), benzo[*b*]chrysene (278a), dibenz[*a,h*]anthracene (278b), dibenz[*a,j*]anthracene (278c), benzo[*a*]naphthacene (278d), pentaphene (278e), picene (278f), benzo[*g*]chrysene (278g), dibenz[*a,c*]anthracene (278h), three methyl dibenz[*a,c*]anthracenes (292b-d), and a methyl benzo[*g*]chrysene (292a); (b) benzo[*ghi*]perylene (276b), anthanthrene (276c), dibenzo[*e,ghi*]fluoranthene (276e), dibenzo[*b,ghi*]fluoranthene (276d), and indeno[1,2,3-*cd*]pyrene (276a). Experiments: (■) without dopant and (■) with 4-methylchrysene dopant (684 µg 4-methylchrysene / g *n*-decane fed).



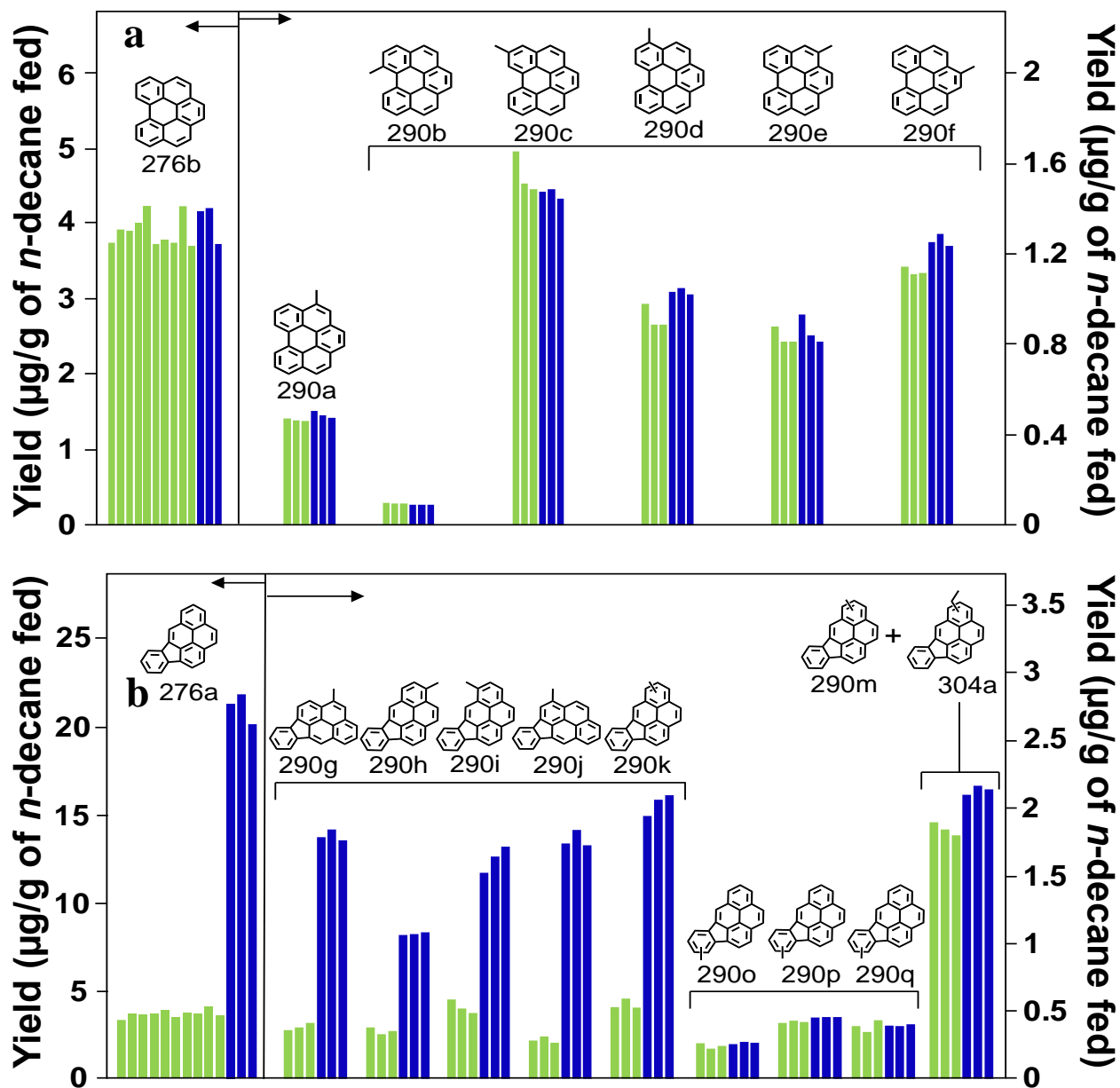


Figure B13. Yields of  $\text{C}_{22}\text{H}_{12}$  PAH, and their alkyl derivatives, from supercritical *n*-decane pyrolysis at 568 °C, 94.6 atm, and 133 sec: (a) benzo[*ghi*]perylene (276b) and the six methylbenzo[*ghi*]perylenes (290a-f); (b) indeno[1,2,3-*cd*]pyrene (276a), five methylindeno[1,2,3-*cd*]pyrenes (290g-k) whose yields increase with doping, three methylindeno[1,2,3-*cd*]pyrenes (290o-q) whose yields do not increase with doping, and another methylindeno[1,2,3-*cd*]pyrene (290m) co-eluting with an ethylindeno[1,2,3-*cd*]pyrene (304a). Experiments: (■) without dopant and (■) with 4-methylchrysene dopant (684  $\mu\text{g}$  4-methylchrysene / g *n*-decane fed). Among the sets of bars associated with the six methylbenzo[*ghi*]perylene products in (a), the set for 4-methylbenzo[*ghi*]perylene (290a) is assigned to that isomer since we have a reference standard for that isomer; a lack of reference standards for the other five methylbenzo[*ghi*]perylene isomers prevents assigning the other sets of bars to particular isomers.

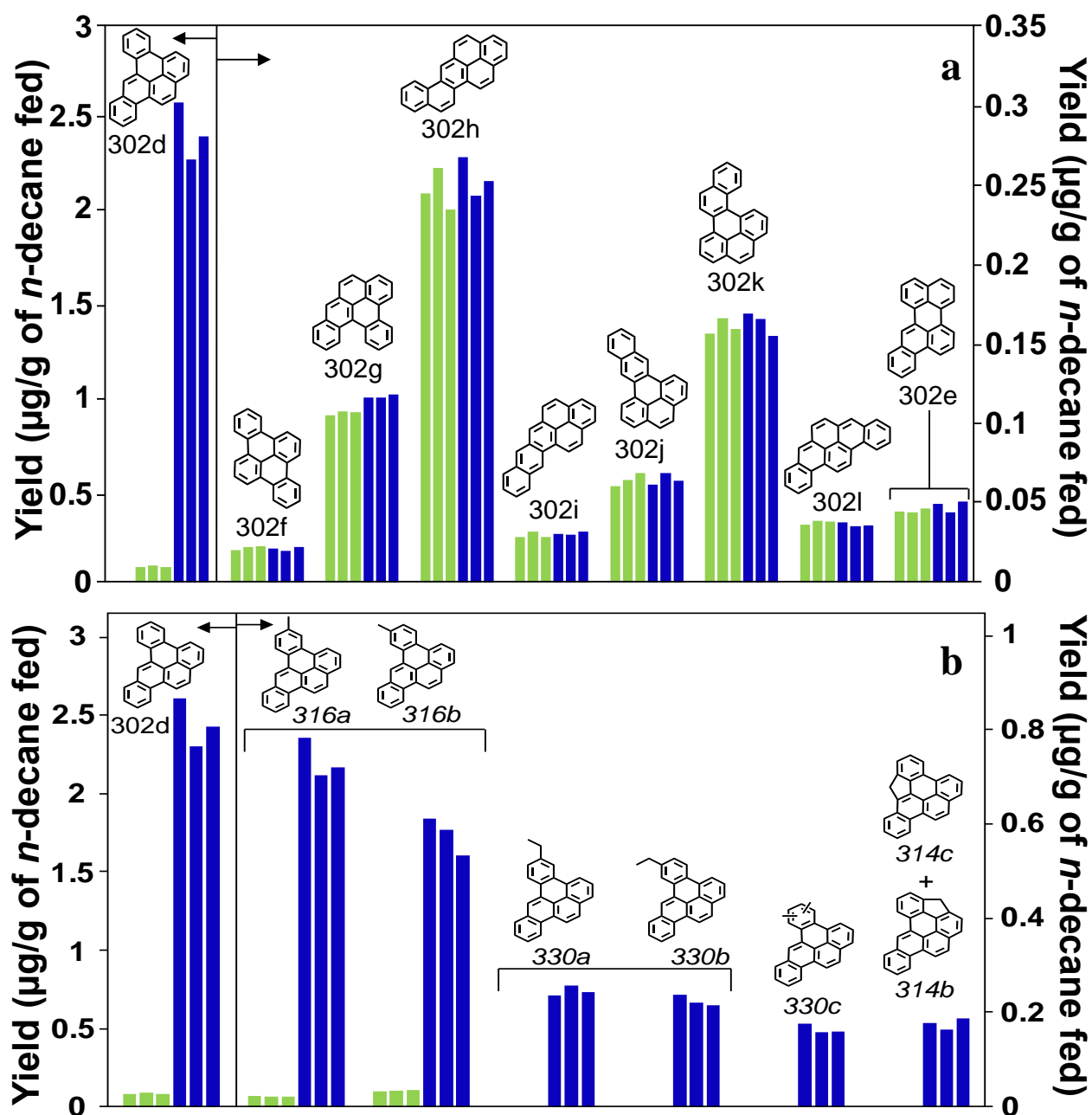


Figure B14. Yields of six-ring C<sub>24</sub>H<sub>14</sub> PAH, and the derivatives of one of these C<sub>24</sub>H<sub>14</sub> PAH, from supercritical *n*-decane pyrolysis at 568 °C, 94.6 atm, and 133 sec: (a) dibenzo[*a,e*]pyrene (302d), dibenzo[*e,l*]pyrene (302f), dibenzo[*a,l*]pyrene (302g), naphtho[2,1-*a*]pyrene (302h), naphtho[2,3-*a*]pyrene (302i), naphtho[2,3-*e*]pyrene (302j), naphtho[1,2-*e*]pyrene (302k), dibenzo[*a,i*]pyrene (302l), and benzo[*b*]perylene (302e); (b) dibenzo[*a,e*]pyrene (302d), two methyl-dibenzo[*a,e*]pyrenes (316a and 316b), two ethyl-dibenzo[*a,e*]pyrenes (330a and 330b), a dimethyl-dibenzo[*a,e*]pyrene (330c), and two methylene-bridged dibenzo[*a,e*]pyrenes (314b and 314c). Experiments: (■) without dopant and (■) with 4-methylchrysene dopant (684 µg 4-methylchrysene / g *n*-decane fed). In (b), the positions of the methyl and ethyl substituents and the methylene bridges on the dibenzo[*a,e*]pyrene structure have been deduced, as noted in Table B1.

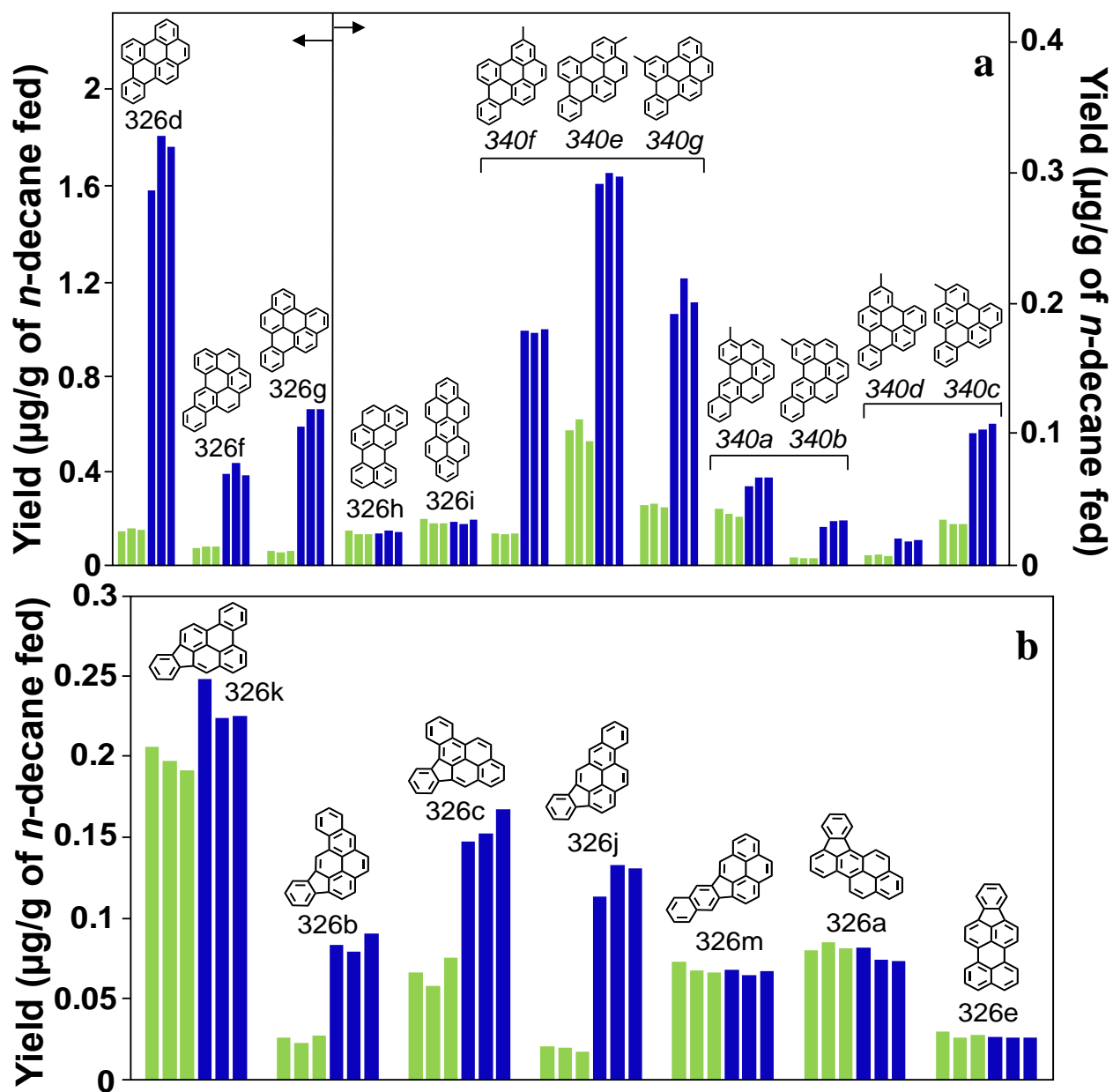


Figure B15. Yields of seven-ring C<sub>26</sub>H<sub>14</sub> PAH, and their methyl derivatives, from supercritical *n*-decane pyrolysis at 568 °C, 94.6 atm, and 133 sec: (a) dibenzo[*e,ghi*]perylene (326d), dibenzo[*b,ghi*]perylene (326f), naphtho[1,2,3,4-*ghi*]perylene (326g), naphtho[8,1,2-*bcd*]perylene (326h), dibenzo[*cd,lm*]perylene (326i), three methyl-dibenzo[*e,ghi*]perylenes (340e-g), two methyl-dibenzo[*b,ghi*]perylenes (340a-b), and two methyl-naphtho[1,2,3,4-*ghi*]perylenes (340c-d); (b) benz[*l*]indeno[1,2,3-*cd*]pyrene (326k), benz[*h*]indeno[1,2,3-*cd*]pyrene (326b), benz[*a*]indeno[1,2,3-*cd*]pyrene (326c), benz[*i*]indeno[1,2,3-*cd*]pyrene (326j), benz[5,6]indeno[1,2,3-*cd*]pyrene (326m), fluoreno[1,9-*ab*]pyrene (326a), and indeno[1,2,3-*cd*]perylene (326e). Experiments: (■) without dopant and (■) with 4-methylchrysene dopant (684 µg 4-methylchrysene / g *n*-decane fed). In (a), the positions of the methyl substituents on the dibenzo[*e,ghi*]perylene, dibenzo[*b,ghi*]perylene, and naphtho[1,2,3,4-*ghi*]perylene structures have been deduced, as noted in Table B1 and Figure 5.11.

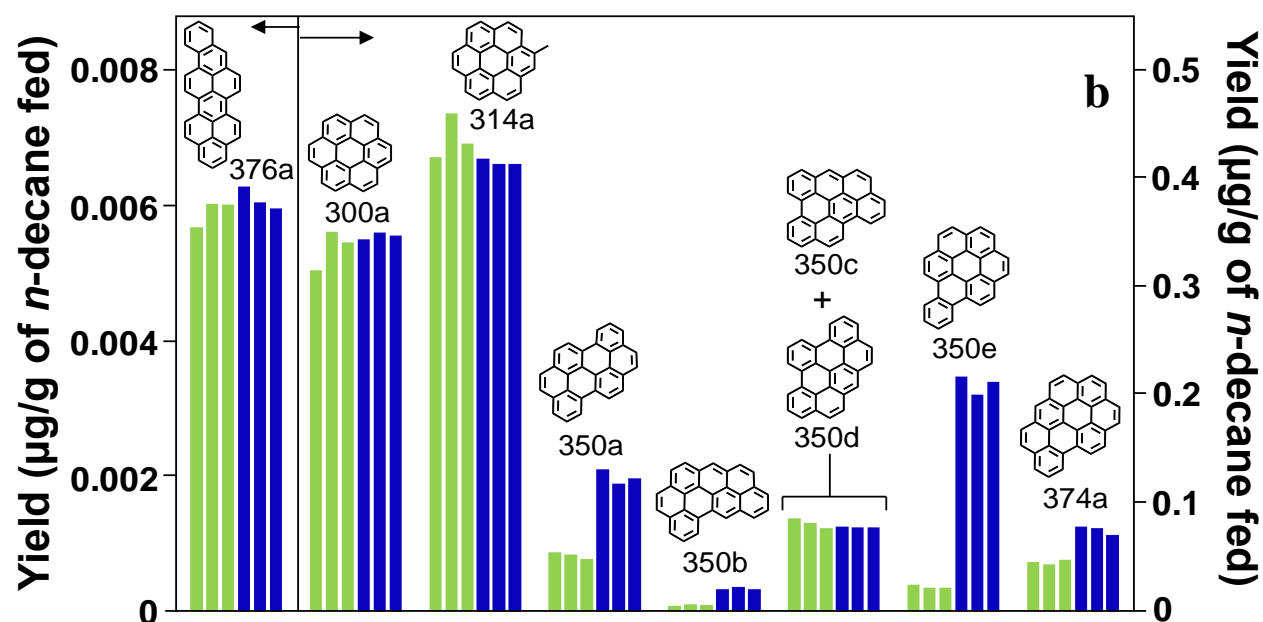
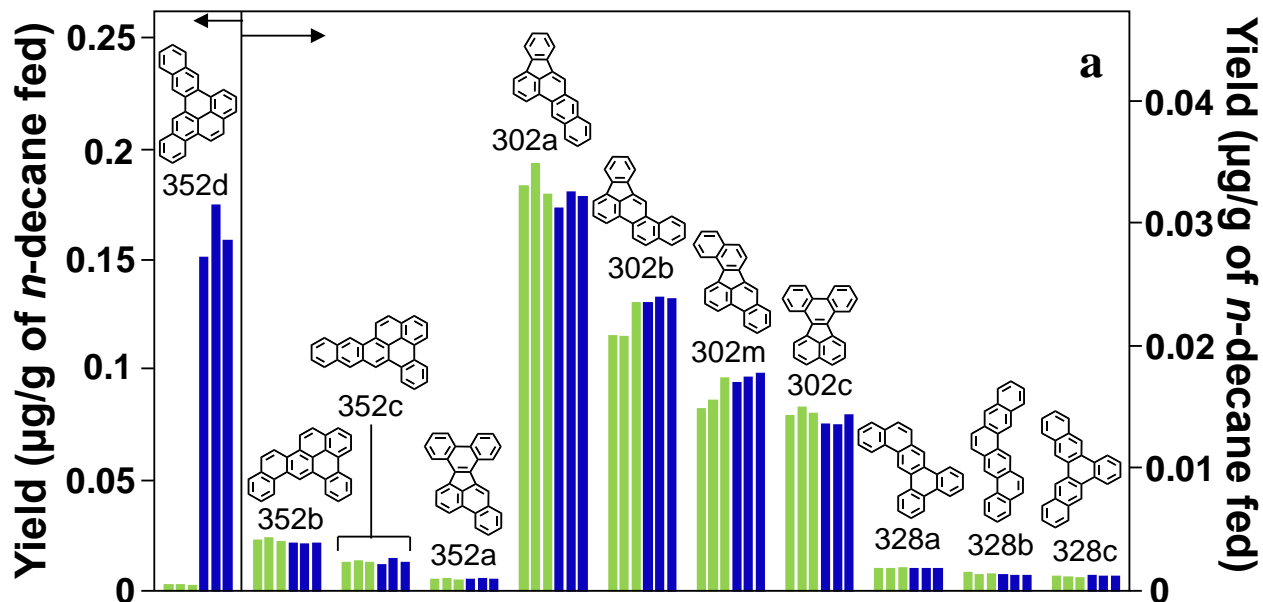

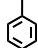
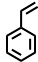
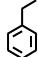
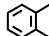
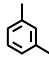
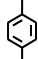
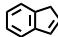
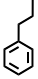
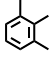
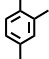
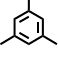


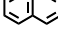
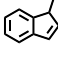
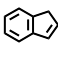
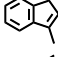
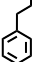


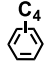
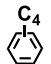
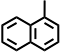
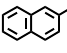
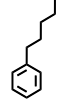
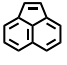
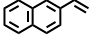
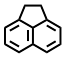
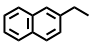
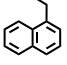
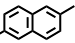
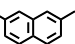
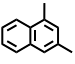
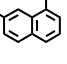
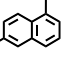
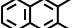
Figure B16. Yields of six- to nine-ring PAH products from supercritical *n*-decane pyrolysis at 568 °C, 94.6 atm, and 133 sec: (a) benzo[*a*]naphtho[2,3-*e*]pyrene (352d), benzo[*e*]naphtho[2,1-*a*]pyrene (352b), benzo[*e*]naphtho[2,3-*a*]pyrene (352c), tribenzo[*b,j,l*]fluoranthene (352a), naphtho[2,3-*b*]fluoranthene (302a), naphtho[1,2-*b*]fluoranthene (302b), dibenzo[*b,j*]fluoranthene (302m), dibenzo[*j,l*]fluoranthene (302c), tribenz[*a,c,h*]anthracene (328a), benzo[*c*]pentaphene (328b), and benzo[*h*]pentaphene (328c); (b) benzo[*cd*]naphtho[1,2,3-*lm*]perylene (376a), coronene (300a), 1-methylcoronene (314a), benzo[*pqr*]naphtho[8,1,2-*bcd*]perylene (350a), benzo[*ghi*]naphtho[8,1,2-*bcd*]perylene (350b), benzo[*cd*]naphtho[8,1,2,3-*fghi*]perylene (350c) co-eluting with phenanthro[5,4,3,2-*efghi*]perylene (350d), benzo[*a*]coronene (350e), and naphtho[8,1,2-*abc*]coronene (374a). Experiments: (■) without dopant and (■) with 4-methylchrysene dopant (684 µg 4-methylchrysene / g *n*-decane fed).

## Appendix C. Supporting Information for Chapter 6

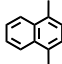
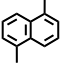
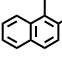
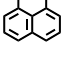
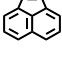
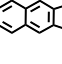
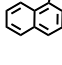
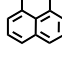
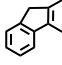
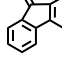
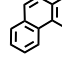
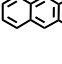
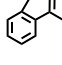
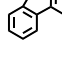
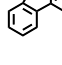
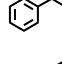

**Table C1.** Quantified aromatic products of supercritical *n*-decane pyrolysis.

Product Name	Formula	Structure	Code
benzene	C <sub>6</sub> H <sub>6</sub>		78a
toluene	C <sub>7</sub> H <sub>8</sub>		92a
styrene	C <sub>8</sub> H <sub>8</sub>		104a
ethylbenzene	C <sub>8</sub> H <sub>10</sub>		106a
<i>o</i> -xylene	C <sub>8</sub> H <sub>10</sub>		106b
<i>m</i> -xylene	C <sub>8</sub> H <sub>10</sub>		106c
<i>p</i> -xylene	C <sub>8</sub> H <sub>10</sub>		106d
indene	C <sub>9</sub> H <sub>8</sub>		116a
<i>n</i> -propylbenzene	C <sub>9</sub> H <sub>12</sub>		120a
1,2,3-trimethylbenzene	C <sub>9</sub> H <sub>12</sub>		120b
1,2,4-trimethylbenzene	C <sub>9</sub> H <sub>12</sub>		120c
1,3,5-trimethylbenzene	C <sub>9</sub> H <sub>12</sub>		120d
methylethylbenzene	C <sub>9</sub> H <sub>12</sub>		120g
methylethylbenzene	C <sub>9</sub> H <sub>12</sub>		120h
naphthalene	C <sub>10</sub> H <sub>8</sub>		128a
1-methylindene	C <sub>10</sub> H <sub>10</sub>		130a
2-methylindene	C <sub>10</sub> H <sub>10</sub>		130b
3-methylindene	C <sub>10</sub> H <sub>10</sub>		130c
<i>n</i> -butylbenzene	C <sub>10</sub> H <sub>14</sub>		134a

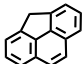
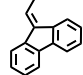
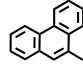
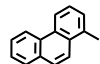
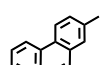
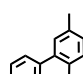
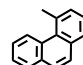
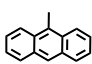
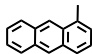
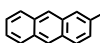
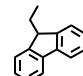
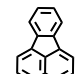
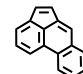
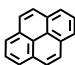
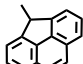
(Table cont'd)

Product Name	Formula	Structure	Code
C <sub>4</sub> -alkylbenzene	C <sub>10</sub> H <sub>14</sub>		134b
C <sub>4</sub> -alkylbenzene	C <sub>10</sub> H <sub>14</sub>		134c
1-methylnaphthalene	C <sub>11</sub> H <sub>10</sub>		142a
2-methylnaphthalene	C <sub>11</sub> H <sub>10</sub>		142b
<i>n</i> -pentylbenzene	C <sub>11</sub> H <sub>16</sub>		148a
acenaphthylene	C <sub>12</sub> H <sub>8</sub>		152a
2-vinylnaphthalene	C <sub>12</sub> H <sub>10</sub>		154a
acenaphthene	C <sub>12</sub> H <sub>10</sub>		154b
2-ethylnaphthalene	C <sub>12</sub> H <sub>12</sub>		156a
1-ethylnaphthalene	C <sub>12</sub> H <sub>12</sub>		156b
2,6-dimethylnaphthalene	C <sub>12</sub> H <sub>12</sub>		156c
2,7-dimethylnaphthalene	C <sub>12</sub> H <sub>12</sub>		156d
1,3-dimethylnaphthalene	C <sub>12</sub> H <sub>12</sub>		156e
1,7-dimethylnaphthalene	C <sub>12</sub> H <sub>12</sub>		156f
1,6-dimethylnaphthalene	C <sub>12</sub> H <sub>12</sub>		156g
2,3-dimethylnaphthalene	C <sub>12</sub> H <sub>12</sub>		156h

(Table cont'd)

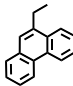
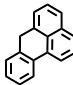
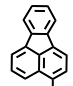
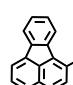
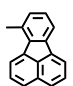
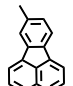
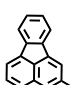
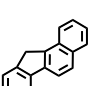
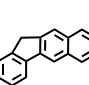
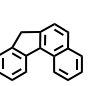
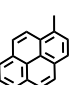
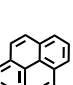
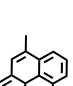
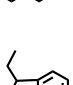
Product Name	Formula	Structure	Code
1,4-dimethylnaphthalene	C <sub>12</sub> H <sub>12</sub>		156i
1,5-dimethylnaphthalene	C <sub>12</sub> H <sub>12</sub>		156j
1,2-dimethylnaphthalene	C <sub>12</sub> H <sub>12</sub>		156k
1,8-dimethylnaphthalene	C <sub>12</sub> H <sub>12</sub>		156l
1-methylacenaphthylene	C <sub>13</sub> H <sub>10</sub>		166a
benz[ <i>f</i> ]indene	C <sub>13</sub> H <sub>10</sub>		166b
benz[ <i>e</i> ]indene	C <sub>13</sub> H <sub>10</sub>		166c
phenalene	C <sub>13</sub> H <sub>10</sub>		166d
fluorene	C <sub>13</sub> H <sub>10</sub>		166e
dibenzofulvene	C <sub>14</sub> H <sub>10</sub>		178a
phenanthrene	C <sub>14</sub> H <sub>10</sub>		178b
anthracene	C <sub>14</sub> H <sub>10</sub>		178c
9-methylfluorene	C <sub>14</sub> H <sub>12</sub>		180a
1-methylfluorene	C <sub>14</sub> H <sub>12</sub>		180b
2-methylfluorene	C <sub>14</sub> H <sub>12</sub>		180c
3-methylfluorene	C <sub>14</sub> H <sub>12</sub>		180d
4-methylfluorene	C <sub>14</sub> H <sub>12</sub>		180e

(Table cont'd)

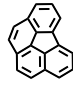
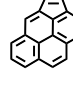
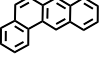
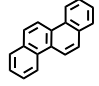
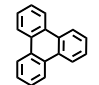
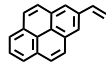
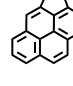
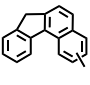
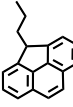
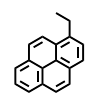
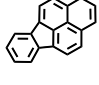
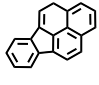
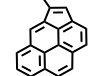
Product Name	Formula	Structure	Code
4 <i>H</i> -cyclopenta[ <i>def</i> ]phenanthrene	C <sub>15</sub> H <sub>10</sub>		190a
9-ethylidene fluorene	C <sub>15</sub> H <sub>12</sub>		192a
9-methylphenanthrene	C <sub>15</sub> H <sub>12</sub>		192b
1-methylphenanthrene	C <sub>15</sub> H <sub>12</sub>		192c
2-methylphenanthrene	C <sub>15</sub> H <sub>12</sub>		192d
3-methylphenanthrene	C <sub>15</sub> H <sub>12</sub>		192e
4-methylphenanthrene	C <sub>15</sub> H <sub>12</sub>		192f
9-methylanthracene	C <sub>15</sub> H <sub>12</sub>		192g
1-methylanthracene	C <sub>15</sub> H <sub>12</sub>		192h
2-methylanthracene	C <sub>15</sub> H <sub>12</sub>		192i
9-ethylfluorene	C <sub>15</sub> H <sub>14</sub>		194a
fluoranthene	C <sub>16</sub> H <sub>10</sub>		202a
acephenanthrylene	C <sub>16</sub> H <sub>10</sub>		202b
pyrene	C <sub>16</sub> H <sub>10</sub>		202c
4-methyl-4 <i>H</i> -cyclopenta[ <i>def</i> ]phenanthrene	C <sub>16</sub> H <sub>12</sub>		204a

(Table cont'd)

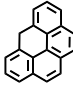
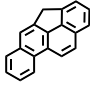
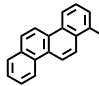
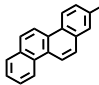
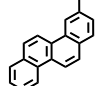
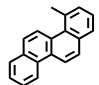
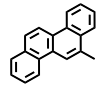
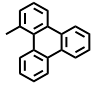
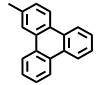
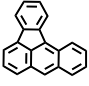
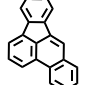
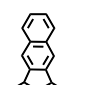
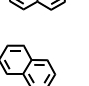
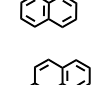


Product Name	Formula	Structure	Code
9-ethylphenanthrene	C <sub>16</sub> H <sub>14</sub>		206a
7H-benz[de]anthracene	C <sub>17</sub> H <sub>12</sub>		216a
3-methylfluoranthene	C <sub>17</sub> H <sub>12</sub>		216b
1-methylfluoranthene	C <sub>17</sub> H <sub>12</sub>		216c
7-methylfluoranthene	C <sub>17</sub> H <sub>12</sub>		216d
8-methylfluoranthene	C <sub>17</sub> H <sub>12</sub>		216e
2-methylfluoranthene	C <sub>17</sub> H <sub>12</sub>		216f
benzo[a]fluorene	C <sub>17</sub> H <sub>12</sub>		216g
benzo[b]fluorene	C <sub>17</sub> H <sub>12</sub>		216h
benzo[c]fluorene	C <sub>17</sub> H <sub>12</sub>		216i
1-methylpyrene	C <sub>17</sub> H <sub>12</sub>		216j
2-methylpyrene	C <sub>17</sub> H <sub>12</sub>		216k
4-methylpyrene	C <sub>17</sub> H <sub>12</sub>		216l
4-ethyl-4H-cyclopenta[def]phenanthrene	C <sub>17</sub> H <sub>14</sub>		218a

(Table cont'd)

Product Name	Formula	Structure	Code
benzo[ <i>ghi</i> ]fluoranthene	C <sub>18</sub> H <sub>10</sub>		226a
cyclopenta[ <i>cd</i> ]pyrene	C <sub>18</sub> H <sub>10</sub>		226b
benz[ <i>a</i> ]anthracene	C <sub>18</sub> H <sub>12</sub>		228a
chrysene	C <sub>18</sub> H <sub>12</sub>		228b
triphenylene	C <sub>18</sub> H <sub>12</sub>		228c
2-vinylpyrene	C <sub>18</sub> H <sub>12</sub>		228d
3,4-dihydrocyclopenta[ <i>cd</i> ]pyrene	C <sub>18</sub> H <sub>12</sub>		228e
methylbenzo[ <i>c</i> ]fluorene	C <sub>18</sub> H <sub>14</sub>		230a
4-propyl-4 <i>H</i> -cyclopenta[ <i>def</i> ]phenanthrene	C <sub>18</sub> H <sub>16</sub>		232a
1-ethylpyrene	C <sub>18</sub> H <sub>14</sub>		230b
1 <i>H</i> -benzo[ <i>cd</i> ]fluoranthene <sup>a</sup>	C <sub>19</sub> H <sub>12</sub>		240e
4 <i>H</i> -benzo[ <i>cd</i> ]fluoranthene <sup>a</sup>	C <sub>19</sub> H <sub>12</sub>		240a
4-methylcyclopenta[ <i>cd</i> ]pyrene	C <sub>19</sub> H <sub>12</sub>		240b

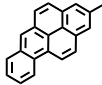
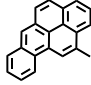
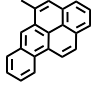
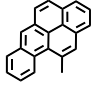
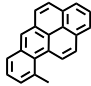
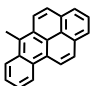
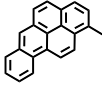
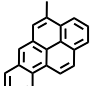
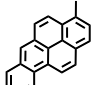
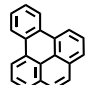
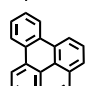
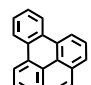
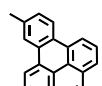
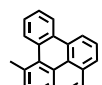
(Table cont'd)

Product Name	Formula	Structure	Code
6 <i>H</i> -benzo[ <i>cd</i> ]pyrene	C <sub>19</sub> H <sub>12</sub>		240c
4 <i>H</i> -cyclopenta[ <i>def</i> ]chrysene	C <sub>19</sub> H <sub>12</sub>		240d
1-methylchrysene	C <sub>19</sub> H <sub>14</sub>		242a
2-methylchrysene	C <sub>19</sub> H <sub>14</sub>		242g
3-methylchrysene	C <sub>19</sub> H <sub>14</sub>		242d
4-methylchrysene	C <sub>19</sub> H <sub>14</sub>		242h
6-methylchrysene	C <sub>19</sub> H <sub>14</sub>		242f
1-methyltriphenylene	C <sub>19</sub> H <sub>14</sub>		242b
2-methyltriphenylene	C <sub>19</sub> H <sub>14</sub>		242c
benzo[ <i>a</i> ]fluoranthene	C <sub>20</sub> H <sub>12</sub>		252a
benzo[ <i>b</i> ]fluoranthene	C <sub>20</sub> H <sub>12</sub>		252b
benzo[ <i>k</i> ]fluoranthene	C <sub>20</sub> H <sub>12</sub>		252c
benzo[ <i>j</i> ]fluoranthene	C <sub>20</sub> H <sub>12</sub>		252d
benzo[ <i>a</i> ]pyrene	C <sub>20</sub> H <sub>12</sub>		252e

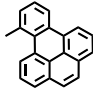
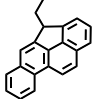
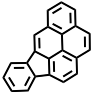

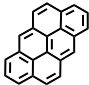
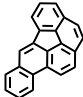
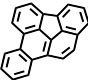
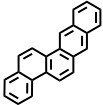
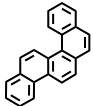
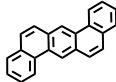
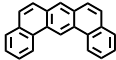
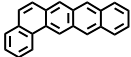
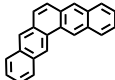
(Table cont'd)

Product Name	Formula	Structure	Code
benzo[ <i>e</i> ]pyrene	C <sub>20</sub> H <sub>12</sub>		252g
perylene	C <sub>20</sub> H <sub>12</sub>		252f
1-methyl-1 <i>H</i> -benzo[ <i>cd</i> ]fluoranthene <sup>a</sup>	C <sub>20</sub> H <sub>14</sub>		254c
4-methyl-4 <i>H</i> -benzo[ <i>cd</i> ]fluoranthene <sup>a</sup>	C <sub>20</sub> H <sub>14</sub>		254a
4-methyl-4 <i>H</i> -cyclopenta[ <i>def</i> ]chrysene	C <sub>20</sub> H <sub>14</sub>		254b
methylbenzo[ <i>a</i> ]fluoranthene	C <sub>21</sub> H <sub>14</sub>		266c
dibenzo[ <i>a,c</i> ]fluorene	C <sub>21</sub> H <sub>14</sub>		266a
dibenzo[ <i>a,h</i> ]fluorene	C <sub>21</sub> H <sub>14</sub>		266d
naphtho[1,2- <i>a</i> ]fluorene	C <sub>21</sub> H <sub>14</sub>		266e
naphtho[2,1- <i>a</i> ]fluorene	C <sub>21</sub> H <sub>14</sub>		266f
naphtho[2,3- <i>a</i> ]fluorene	C <sub>21</sub> H <sub>14</sub>		266g
7-methylbenzo[ <i>a</i> ]pyrene	C <sub>21</sub> H <sub>14</sub>		266h
9-methylbenzo[ <i>a</i> ]pyrene	C <sub>21</sub> H <sub>14</sub>		266i
8-methylbenzo[ <i>a</i> ]pyrene	C <sub>21</sub> H <sub>14</sub>		266j

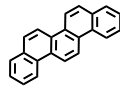
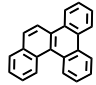
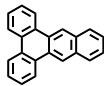
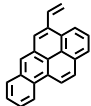
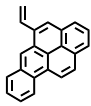
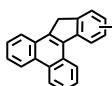
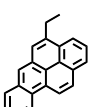
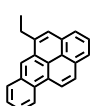
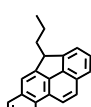
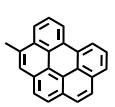
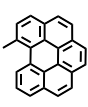
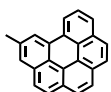
(Table cont'd)

Product Name	Formula	Structure	Code
2-methylbenzo[ <i>a</i> ]pyrene	C <sub>21</sub> H <sub>14</sub>		266k
12-methylbenzo[ <i>a</i> ]pyrene	C <sub>21</sub> H <sub>14</sub>		266l
5-methylbenzo[ <i>a</i> ]pyrene	C <sub>21</sub> H <sub>14</sub>		266m
11-methylbenzo[ <i>a</i> ]pyrene	C <sub>21</sub> H <sub>14</sub>		266n
10-methylbenzo[ <i>a</i> ]pyrene	C <sub>21</sub> H <sub>14</sub>		266o
6-methylbenzo[ <i>a</i> ]pyrene	C <sub>21</sub> H <sub>14</sub>		266p
1-methylbenzo[ <i>a</i> ]pyrene	C <sub>21</sub> H <sub>14</sub>		266q
4-methylbenzo[ <i>a</i> ]pyrene	C <sub>21</sub> H <sub>14</sub>		266r
3-methylbenzo[ <i>a</i> ]pyrene	C <sub>21</sub> H <sub>14</sub>		266s
3-methylbenzo[ <i>e</i> ]pyrene	C <sub>21</sub> H <sub>14</sub>		266b
4-methylbenzo[ <i>e</i> ]pyrene	C <sub>21</sub> H <sub>14</sub>		266t
2-methylbenzo[ <i>e</i> ]pyrene	C <sub>21</sub> H <sub>14</sub>		266u
10-methylbenzo[ <i>e</i> ]pyrene	C <sub>21</sub> H <sub>14</sub>		266v
1-methylbenzo[ <i>e</i> ]pyrene	C <sub>21</sub> H <sub>14</sub>		266w

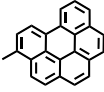
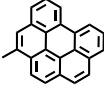
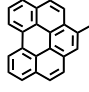
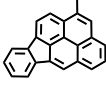
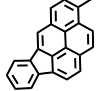
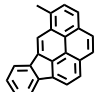
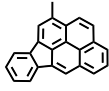
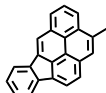
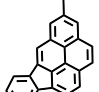
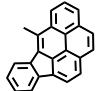
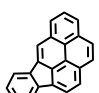
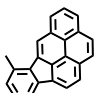
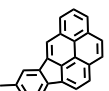
(Table cont'd)

Product Name	Formula	Structure	Code
9-methylbenzo[ <i>e</i> ]pyrene	C <sub>21</sub> H <sub>14</sub>		266x
4-ethyl-4 <i>H</i> -cyclopenta[ <i>def</i> ]chrysene	C <sub>21</sub> H <sub>16</sub>		268a
indeno[1,2,3- <i>cd</i> ]pyrene	C <sub>22</sub> H <sub>12</sub>		276a
benzo[ <i>ghi</i> ]perylene	C <sub>22</sub> H <sub>12</sub>		276b
anthanthrene	C <sub>22</sub> H <sub>12</sub>		276c
dibenzo[ <i>b,ghi</i> ]fluoranthene	C <sub>22</sub> H <sub>12</sub>		276d
dibenzo[ <i>e,ghi</i> ]fluoranthene	C <sub>22</sub> H <sub>12</sub>		276e
benzo[ <i>b</i> ]chrysene	C <sub>22</sub> H <sub>14</sub>		278a
benzo[ <i>c</i> ]chrysene	C <sub>22</sub> H <sub>14</sub>		278i
dibenz[ <i>a,h</i> ]anthracene	C <sub>22</sub> H <sub>14</sub>		278b
dibenz[ <i>a,j</i> ]anthracene	C <sub>22</sub> H <sub>14</sub>		278c
benzo[ <i>a</i> ]naphthacene	C <sub>22</sub> H <sub>14</sub>		278d
pentaphene	C <sub>22</sub> H <sub>14</sub>		278e

(Table cont'd)

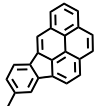
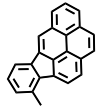
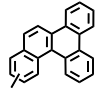
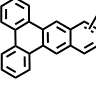
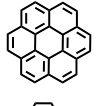
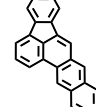
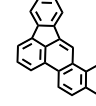
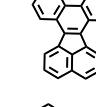
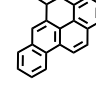
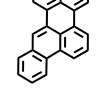
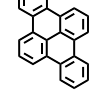
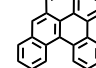
Product Name	Formula	Structure	Code
picene	C <sub>22</sub> H <sub>14</sub>		278f
benzo[ <i>g</i> ]chrysene	C <sub>22</sub> H <sub>14</sub>		278g
dibenz[ <i>a,c</i> ]anthracene	C <sub>22</sub> H <sub>14</sub>		278h
4-vinylbenzo[ <i>a</i> ]pyrene	C <sub>22</sub> H <sub>14</sub>		278j
5-vinylbenzo[ <i>a</i> ]pyrene	C <sub>22</sub> H <sub>14</sub>		278k
methyldibenzo[ <i>a,c</i> ]fluorene	C <sub>22</sub> H <sub>16</sub>		280a
4-ethylbenzo[ <i>a</i> ]pyrene	C <sub>22</sub> H <sub>16</sub>		280b
5-ethylbenzo[ <i>a</i> ]pyrene	C <sub>22</sub> H <sub>16</sub>		280c
4-propyl-4 <i>H</i> -cyclopenta[ <i>def</i> ]chrysene	C <sub>22</sub> H <sub>18</sub>		282a
4-methylbenzo[ <i>ghi</i> ]perylene	C <sub>23</sub> H <sub>14</sub>		290a
7-methylbenzo[ <i>ghi</i> ]perylene	C <sub>23</sub> H <sub>14</sub>		290b
6-methylbenzo[ <i>ghi</i> ]perylene	C <sub>23</sub> H <sub>14</sub>		290c

(Table cont'd)

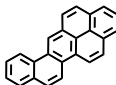
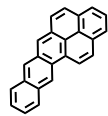
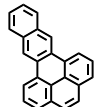
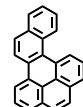
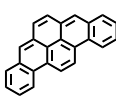
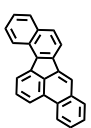
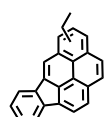
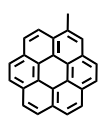
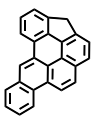
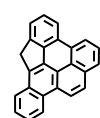
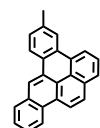
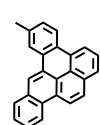
Product Name	Formula	Structure	Code
5-methylbenzo[ghi]perylene	C <sub>23</sub> H <sub>14</sub>		290d
3-methylbenzo[ghi]perylene	C <sub>23</sub> H <sub>14</sub>		290e
1-methylbenzo[ghi]perylene	C <sub>23</sub> H <sub>14</sub>		290f
1-methylindeno[1,2,3-cd]pyrene <sup>b</sup>	C <sub>22</sub> H <sub>14</sub>		290g
3-methylindeno[1,2,3-cd]pyrene <sup>b</sup>	C <sub>22</sub> H <sub>14</sub>		290h
5-methylindeno[1,2,3-cd]pyrene <sup>b</sup>	C <sub>22</sub> H <sub>14</sub>		290i
12-methylindeno[1,2,3-cd]pyrene <sup>b</sup>	C <sub>22</sub> H <sub>14</sub>		290j
2-methylindeno[1,2,3-cd]pyrene <sup>b</sup>	C <sub>22</sub> H <sub>14</sub>		290k-n
4-methylindeno[1,2,3-cd]pyrene <sup>b</sup>	C <sub>22</sub> H <sub>14</sub>		
6-methylindeno[1,2,3-cd]pyrene <sup>b</sup>	C <sub>22</sub> H <sub>14</sub>		
11-methylindeno[1,2,3-cd]pyrene <sup>b</sup>	C <sub>22</sub> H <sub>14</sub>		
7-methylindeno[1,2,3-cd]pyrene <sup>b</sup>	C <sub>22</sub> H <sub>14</sub>		290o-r
8-methylindeno[1,2,3-cd]pyrene <sup>b</sup>	C <sub>22</sub> H <sub>14</sub>		

(Table cont'd)

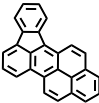
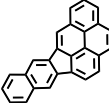
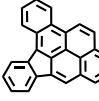
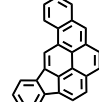
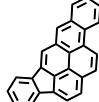
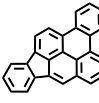
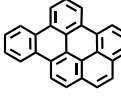
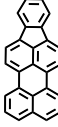
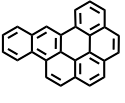
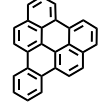
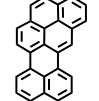


Product Name	Formula	Structure	Code
9-methylindeno[1,2,3- <i>cd</i> ]pyrene <sup>b</sup>	C <sub>22</sub> H <sub>14</sub>		} 290o-r
10-methylindeno[1,2,3- <i>cd</i> ]pyrene <sup>b</sup>	C <sub>22</sub> H <sub>14</sub>		
methylbenzo[ <i>g</i> ]chrysene	C <sub>23</sub> H <sub>16</sub>		292a
methyldibenz[ <i>a,c</i> ]anthracene	C <sub>23</sub> H <sub>16</sub>		292b-d
coronene	C <sub>24</sub> H <sub>12</sub>		300a
naphtho[2,3- <i>b</i> ]fluoranthene	C <sub>24</sub> H <sub>14</sub>		302a
naphtho[1,2- <i>b</i> ]fluoranthene	C <sub>24</sub> H <sub>14</sub>		302b
dibenzo[ <i>j,l</i> ]fluoranthene	C <sub>24</sub> H <sub>14</sub>		302c
dibenzo[ <i>a,e</i> ]pyrene	C <sub>24</sub> H <sub>14</sub>		302d
benzo[ <i>b</i> ]perylene	C <sub>24</sub> H <sub>14</sub>		302e
dibenzo[ <i>e,l</i> ]pyrene	C <sub>24</sub> H <sub>14</sub>		302f
dibenzo[ <i>a,l</i> ]pyrene	C <sub>24</sub> H <sub>14</sub>		302g

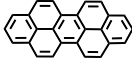
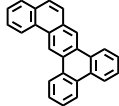
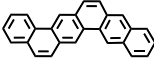
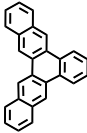
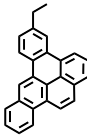
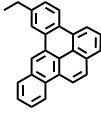
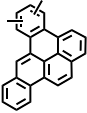
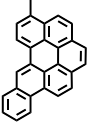
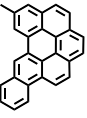
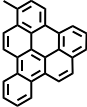
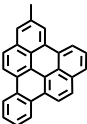
(Table cont'd)

Product Name	Formula	Structure	Code
naphtho[2,1- <i>a</i> ]pyrene	C <sub>24</sub> H <sub>14</sub>		302h
naphtho[2,3- <i>a</i> ]pyrene	C <sub>24</sub> H <sub>14</sub>		302i
naphtho[2,3- <i>e</i> ]pyrene	C <sub>24</sub> H <sub>14</sub>		302j
naphtho[1,2- <i>e</i> ]pyrene	C <sub>24</sub> H <sub>14</sub>		302k
dibenzo[ <i>a,i</i> ]pyrene	C <sub>24</sub> H <sub>14</sub>		302l
dibenzo[ <i>b,j</i> ]fluoranthene	C <sub>24</sub> H <sub>14</sub>		302m
ethylindeno[1,2,3- <i>cd</i> ]pyrene	C <sub>24</sub> H <sub>16</sub>		304a
1-methylcoronene	C <sub>25</sub> H <sub>14</sub>		314a
3 <i>H</i> -indeno[4,3,2- <i>efg</i> ]benzo[ <i>a</i> ]pyrene	C <sub>25</sub> H <sub>14</sub>		314b
7 <i>H</i> -indeno[2,3,4- <i>cde</i> ]benzo[ <i>a</i> ]pyrene	C <sub>25</sub> H <sub>14</sub>		314c
5-methyldibenzo[ <i>a,e</i> ]pyrene	C <sub>25</sub> H <sub>16</sub>		316a
6-methyldibenzo[ <i>a,e</i> ]pyrene	C <sub>25</sub> H <sub>16</sub>		316b

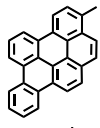
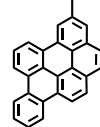
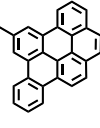
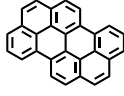
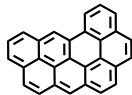
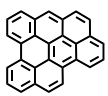
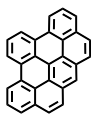
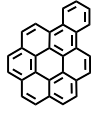
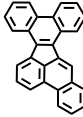
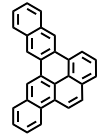
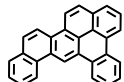
(Table cont'd)

Product Name	Formula	Structure	Code
fluoreno[1,9- <i>ab</i> ]pyrene	C <sub>26</sub> H <sub>14</sub>		326a
benz[5,6]indeno[1,2,3- <i>cd</i> ]pyrene	C <sub>26</sub> H <sub>14</sub>		326m
benz[ <i>a</i> ]indeno[1,2,3- <i>cd</i> ]pyrene	C <sub>26</sub> H <sub>14</sub>		326c
benz[ <i>h</i> ]indeno[1,2,3- <i>cd</i> ]pyrene	C <sub>26</sub> H <sub>14</sub>		326b
benz[ <i>i</i> ]indeno[1,2,3- <i>cd</i> ]pyrene	C <sub>26</sub> H <sub>14</sub>		326j
benz[ <i>l</i> ]indeno[1,2,3- <i>cd</i> ]pyrene	C <sub>26</sub> H <sub>14</sub>		326k
dibenzo[ <i>e,ghi</i> ]perylene	C <sub>26</sub> H <sub>14</sub>		326d
indeno[1,2,3- <i>cd</i> ]perylene	C <sub>26</sub> H <sub>14</sub>		326e
dibenzo[ <i>b,ghi</i> ]perylene	C <sub>26</sub> H <sub>14</sub>		326f
naphtho[1,2,3,4- <i>ghi</i> ]perylene	C <sub>26</sub> H <sub>14</sub>		326g
naphtho[8,1,2- <i>bcd</i> ]perylene	C <sub>26</sub> H <sub>14</sub>		326h

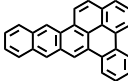
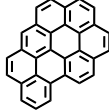
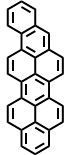
(Table cont'd)

Product Name	Formula	Structure	Code
dibenzo[ <i>cd,lm</i> ]perylene	C <sub>26</sub> H <sub>14</sub>		326i
tribenz[ <i>a,c,h</i> ]anthracene	C <sub>26</sub> H <sub>16</sub>		328a
benzo[ <i>c</i> ]pentaphene	C <sub>26</sub> H <sub>16</sub>		328b
benzo[ <i>h</i> ]pentaphene	C <sub>26</sub> H <sub>16</sub>		328c
5-ethyldibenzo[ <i>a,e</i> ]pyrene	C <sub>26</sub> H <sub>16</sub>		330a
6-ethyldibenzo[ <i>a,e</i> ]pyrene	C <sub>26</sub> H <sub>16</sub>		330b
dimethyldibenzo[ <i>a,e</i> ]pyrene	C <sub>26</sub> H <sub>16</sub>		330c
5-methyldibenzo[ <i>b,ghi</i> ]perylene	C <sub>27</sub> H <sub>16</sub>		340a
6-methyldibenzo[ <i>b,ghi</i> ]perylene	C <sub>27</sub> H <sub>16</sub>		340b
1-methylnaphtho[1,2,3,4- <i>ghi</i> ]perylene	C <sub>27</sub> H <sub>16</sub>		340c
2-methylnaphtho[1,2,3,4- <i>ghi</i> ]perylene	C <sub>27</sub> H <sub>16</sub>		340d

(Table cont'd)

Product Name	Formula	Structure	Code
3-methyldibenzo[ <i>e,ghi</i> ]perylene	C <sub>27</sub> H <sub>16</sub>		340e
4-methyldibenzo[ <i>e,ghi</i> ]perylene	C <sub>27</sub> H <sub>16</sub>		340f
7-methyldibenzo[ <i>e,ghi</i> ]perylene	C <sub>27</sub> H <sub>16</sub>		340g
benzo[ <i>pqr</i> ]naphtho[8,1,2- <i>bcd</i> ]perylene	C <sub>28</sub> H <sub>14</sub>		350a
benzo[ <i>ghi</i> ]naphtho[8,1,2- <i>bcd</i> ]perylene	C <sub>28</sub> H <sub>14</sub>		350b
benzo[ <i>cd</i> ]naphtho[8,1,2,3- <i>fghi</i> ]perylene	C <sub>28</sub> H <sub>14</sub>		350c
phenanthro[5,4,3,2- <i>efghi</i> ]perylene	C <sub>28</sub> H <sub>14</sub>		350d
benzo[ <i>a</i> ]coronene	C <sub>28</sub> H <sub>14</sub>		350e
tribenzo[ <i>b,j,l</i> ]fluoranthene	C <sub>28</sub> H <sub>16</sub>		352a
benzo[ <i>a</i> ]naphtho[2,3- <i>e</i> ]pyrene	C <sub>28</sub> H <sub>16</sub>		352d
benzo[ <i>e</i> ]naphtho[2,1- <i>a</i> ]pyrene	C <sub>28</sub> H <sub>16</sub>		352b

(Table cont'd)

Product Name	Formula	Structure	Code
benzo[ <i>e</i> ]naphtho[2,3- <i>a</i> ]pyrene	C <sub>28</sub> H <sub>16</sub>		352c
naphtho[8,1,2- <i>abc</i> ]coronene	C <sub>30</sub> H <sub>14</sub>		374a
benzo[ <i>cd</i> ]naphtho[1,2,3- <i>lm</i> ]perylene	C <sub>30</sub> H <sub>16</sub>		376a

<sup>a</sup> The identifications of 4*H*-benzo[*cd*]fluoranthene (240a), 4-methyl-4*H*-benzo[*cd*]fluoranthene (254a), 1*H*-benzo[*cd*]fluoranthene (240e), and 1-methyl-1*H*-benzo[*cd*]fluoranthene (254c) are based on their UV and mass spectra but cannot be unequivocally confirmed, due to a lack of reference standards and published UV spectra for these PAH.

<sup>b</sup> There are twelve possible isomers of methylindeno[1,2,3-*cd*]pyrenes. We know that the *n*-decane products contain at least nine methylindeno[1,2,3-*cd*]pyrenes because our product chromatograms show eight chromatographic peaks whose UV and mass spectra indicate are methylindeno[1,2,3-*cd*]pyrenes and another peak whose UV and mass spectra indicate are a methylindeno[1,2,3-*cd*]pyrene and an ethylindeno[1,2,3-*cd*]pyrene co-eluting. Three of the methylindeno[1,2,3-*cd*]pyrene peaks show no increase in yield with 4-methylphenanthrene doping, and five do. As explained in the chapter 6, we believe that the methylindeno[1,2,3-*cd*]pyrenes 290g, 290h, 290i, and 290j are four of the isomers that exhibit increases with doping, since they would be the ones formed in the reactions of Figure 6.10. We also believe that the other isomer whose yields increase with doping would be 290q, for the reasons outlined in the chapter 6.

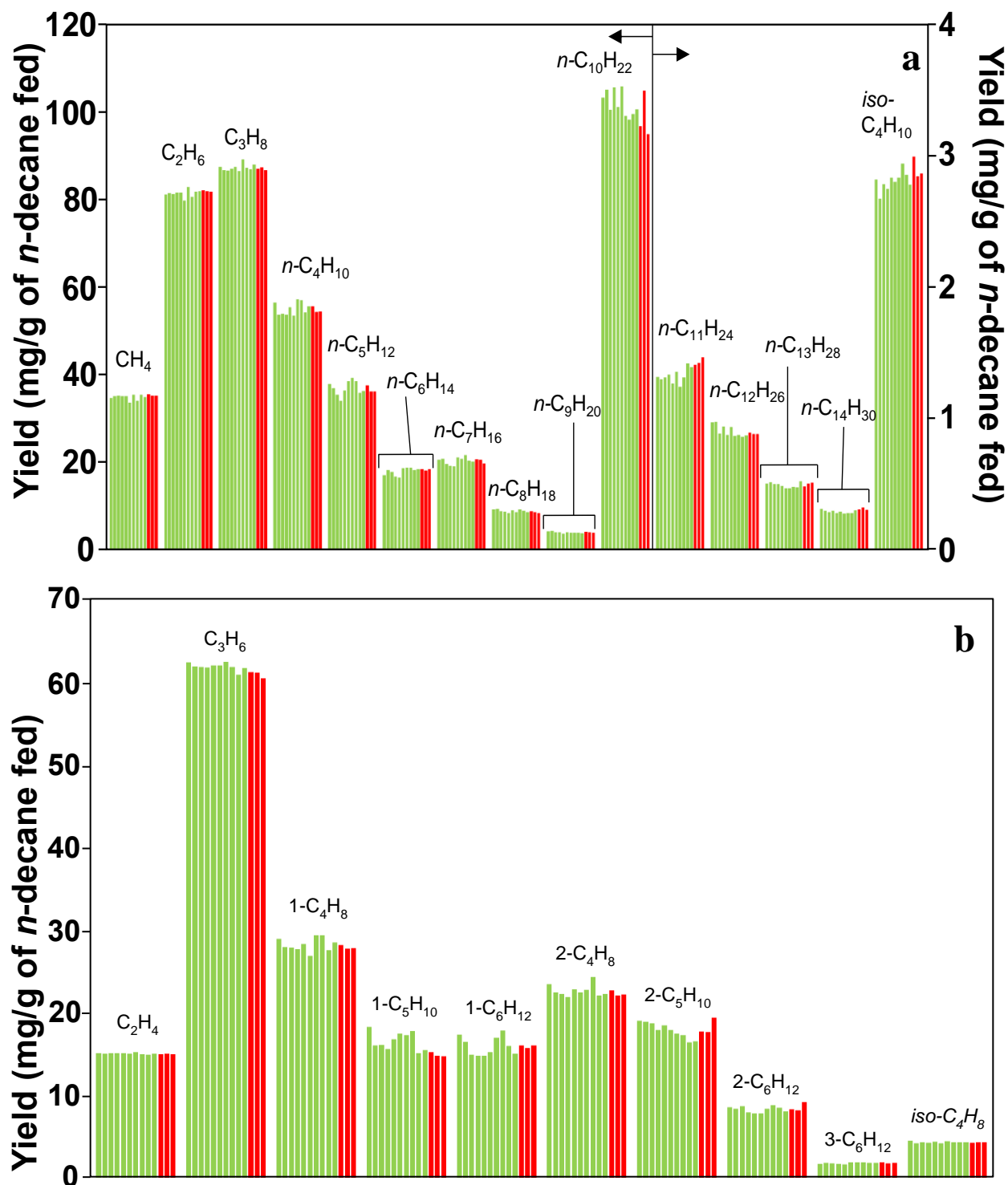


Figure C1. Yields of (a) alkanes (including unreacted fuel *n*-decane) and (b) C<sub>2</sub>-C<sub>6</sub> alkenes from the supercritical pyrolysis of *n*-decane at 568 °C, 94.6 atm, and 133 sec. Experiments: (■) without dopant and (■) with 4-methylphenanthrene dopant (685 μg 4-methylphenanthrene / g *n*-decane fed). For the 2- and 3-alkenes in (b), the reported yields are those summed for the *cis* and *trans* isomers.

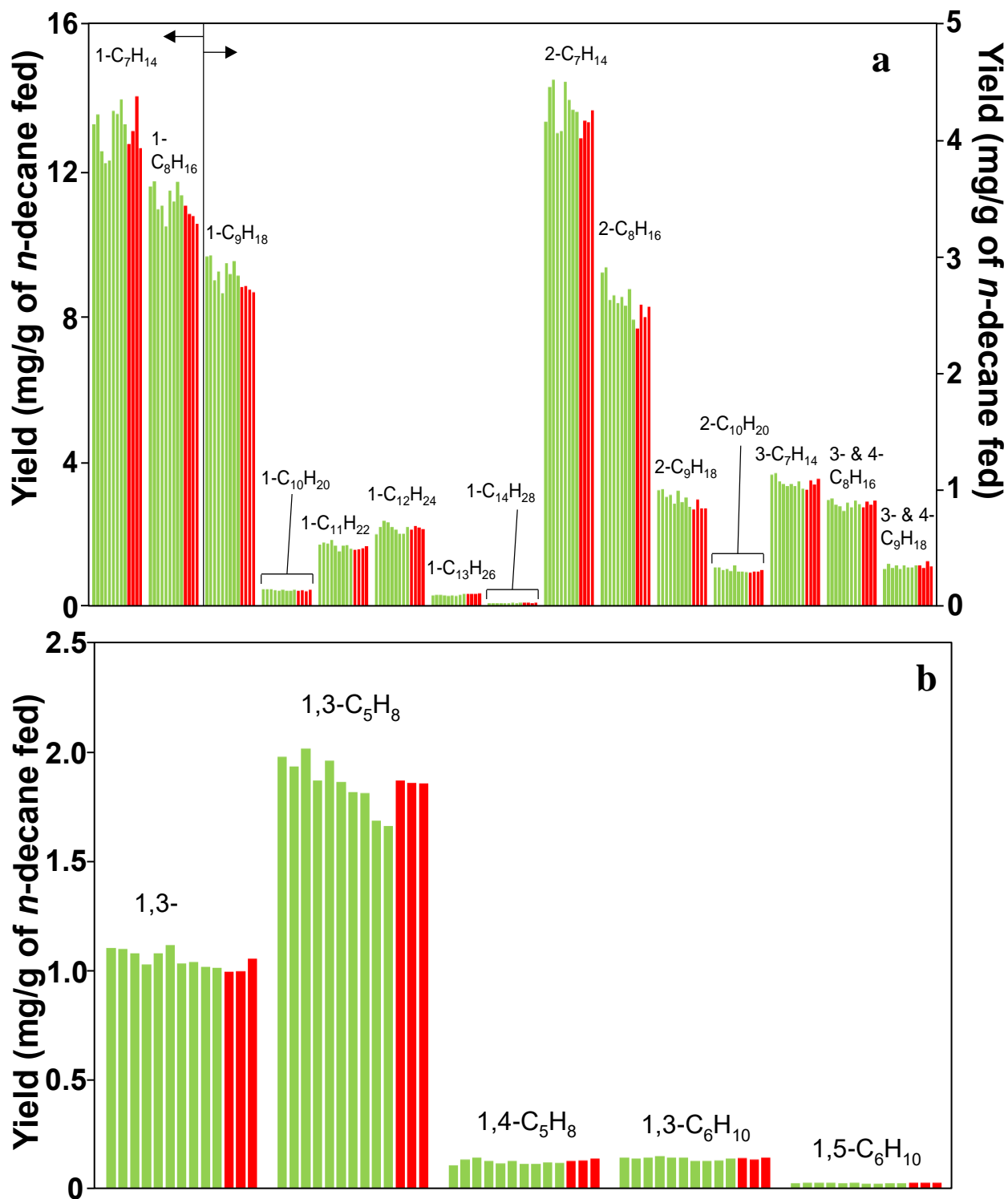


Figure C2. Yields of (a) C<sub>7</sub>-C<sub>14</sub> alkenes and (b) dienes from the supercritical pyrolysis of *n*-decane at 568 °C, 94.6 atm, and 133 sec. Experiments: (■) without dopant and (■) with 4-methylphenanthrene dopant (685 μg 4-methylphenanthrene / g *n*-decane fed). For the 2-, 3-, and 4-alkenes in (a), and 1,3-pentadiene in (b), the reported yields are those summed for the *cis* and *trans* isomers.



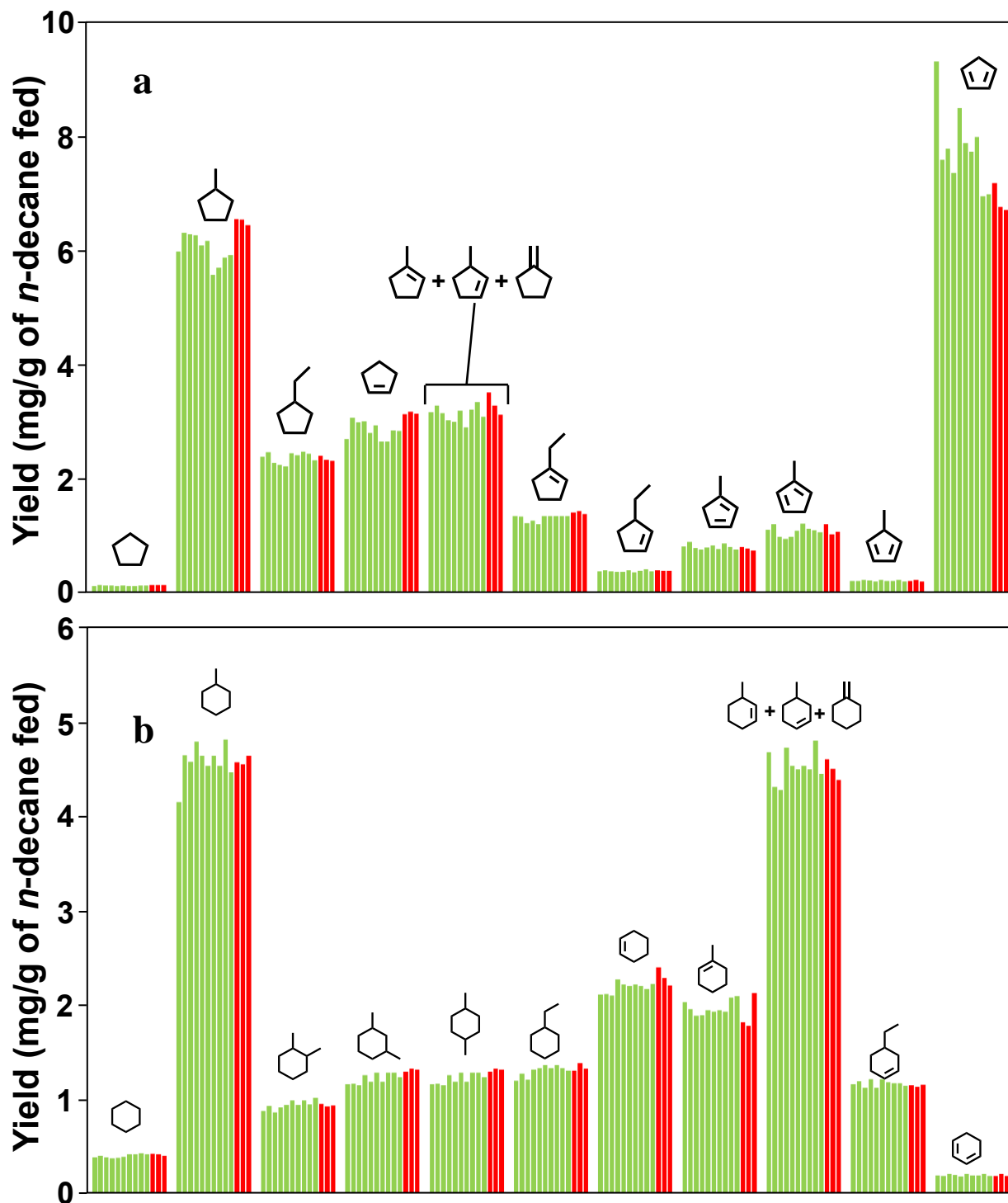


Figure C3. Yields of (a) C<sub>5</sub>-ring and (b) C<sub>6</sub>-ring cyclic aliphatic products from the supercritical pyrolysis of *n*-decane at 568 °C, 94.6 atm, and 133 sec. Experiments: (■) without dopant and (■) with 4-methylphenanthrene dopant (685 μg 4-methylphenanthrene / g *n*-decane fed). For the three dimethylcyclohexanes in (b), the reported yields are those summed for the *cis* and *trans* isomers. The variations in the experimental yields of cyclopentadiene in (a) and methylcyclohexane in (b) stem from their volatility in the liquid-phase products.

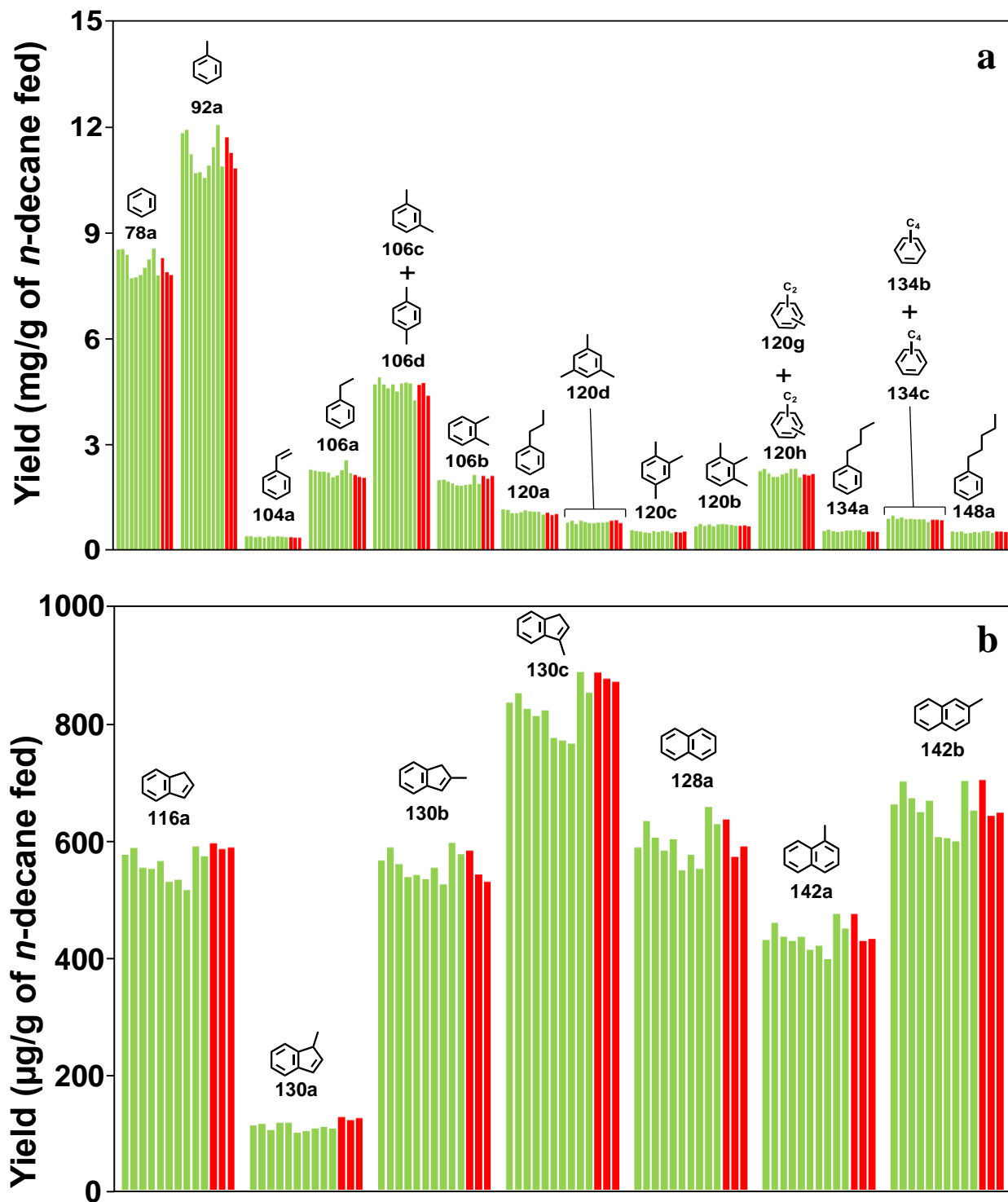


Figure C4. Yields of one- and two-ring aromatics from supercritical *n*-decane pyrolysis at 568 °C, 94.6 atm, and 133 sec: (a) benzene and substituted benzenes; (b) indene (116a), 1-methylindene (130a), 2-methylindene (130b), 3-methylindene (130c), naphthalene (128a), 1-methylnaphthalene (142a), and 2-methylnaphthalene (142b). Experiments: (■) without dopant and (■) with 4-methylphenanthrene dopant (685 µg 4-methylphenanthrene / g *n*-decane fed).

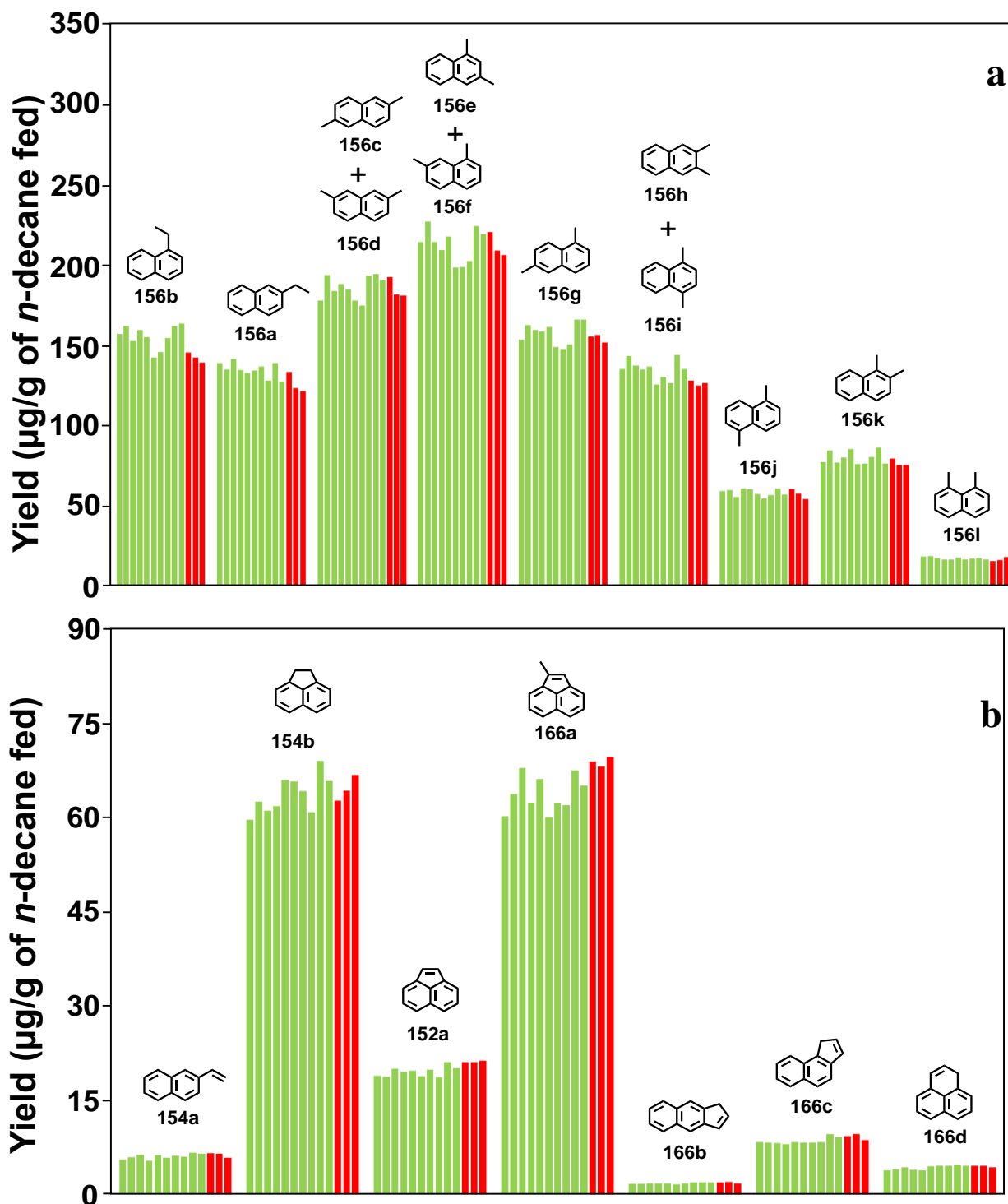


Figure C5. Yields of two- and three-ring aromatics from supercritical *n*-decane pyrolysis at 568 °C, 94.6 atm, and 133 sec: (a) 1-ethylnaphthalene (156b), 2-ethylnaphthalene (156a), and the ten dimethylnaphthalenes (156c-l); (b) 2-vinylnaphthalene (154a), acenaphthene (154b), acenaphthylene (152a), 1-methylacenaphthylene (166a), phenalene (166d), benz[*f*]indene (166b), and benz[*e*]indene (166c). Experiments: (■) without dopant and (■) with 4-methylphenanthrene dopant (685 µg 4-methylphenanthrene / g *n*-decane fed).

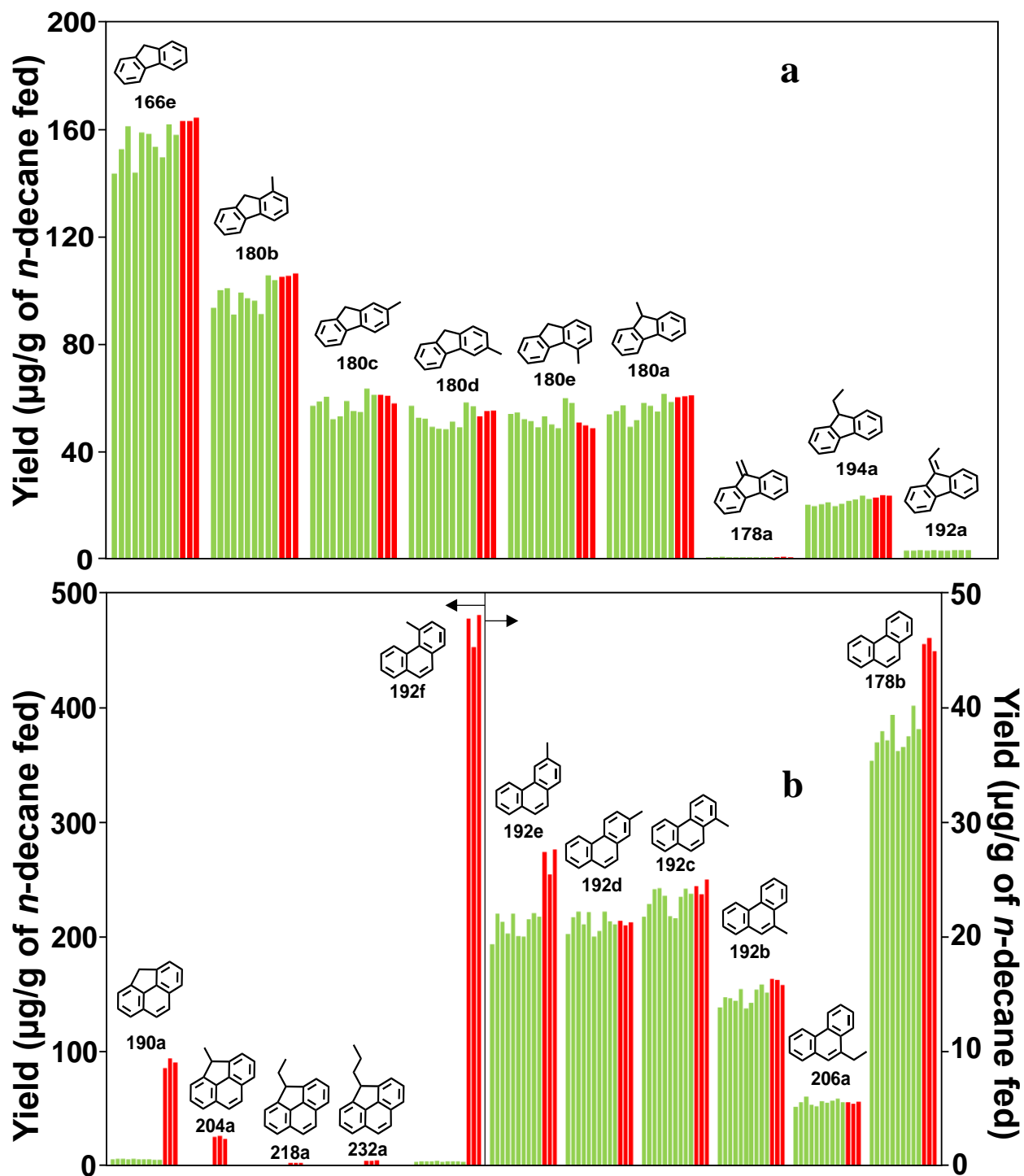


Figure C6. Yields of three- and four-ring PAH from supercritical *n*-decane pyrolysis at 568 °C, 94.6 atm, and 133 sec: (a) fluorene (166e), the five methylfluorenes (180a–e), dibenzofulvene (178a), 9-ethylfluorene (194a), and 9-ethylidene fluorene (192a); (b) 4H-cyclopenta[def]phenanthrene (190a) and its alkylated derivatives (204a, 218a, and 232a), 4-methylphenanthrene (192f), phenanthrene (178b), the four methylphenanthrenes (192b–e), and 9-ethylphenanthrene (206a). Experiments: (■) without dopant and (■) with 4-methylphenanthrene dopant (685  $\mu\text{g}$  4-methylphenanthrene / g *n*-decane fed).

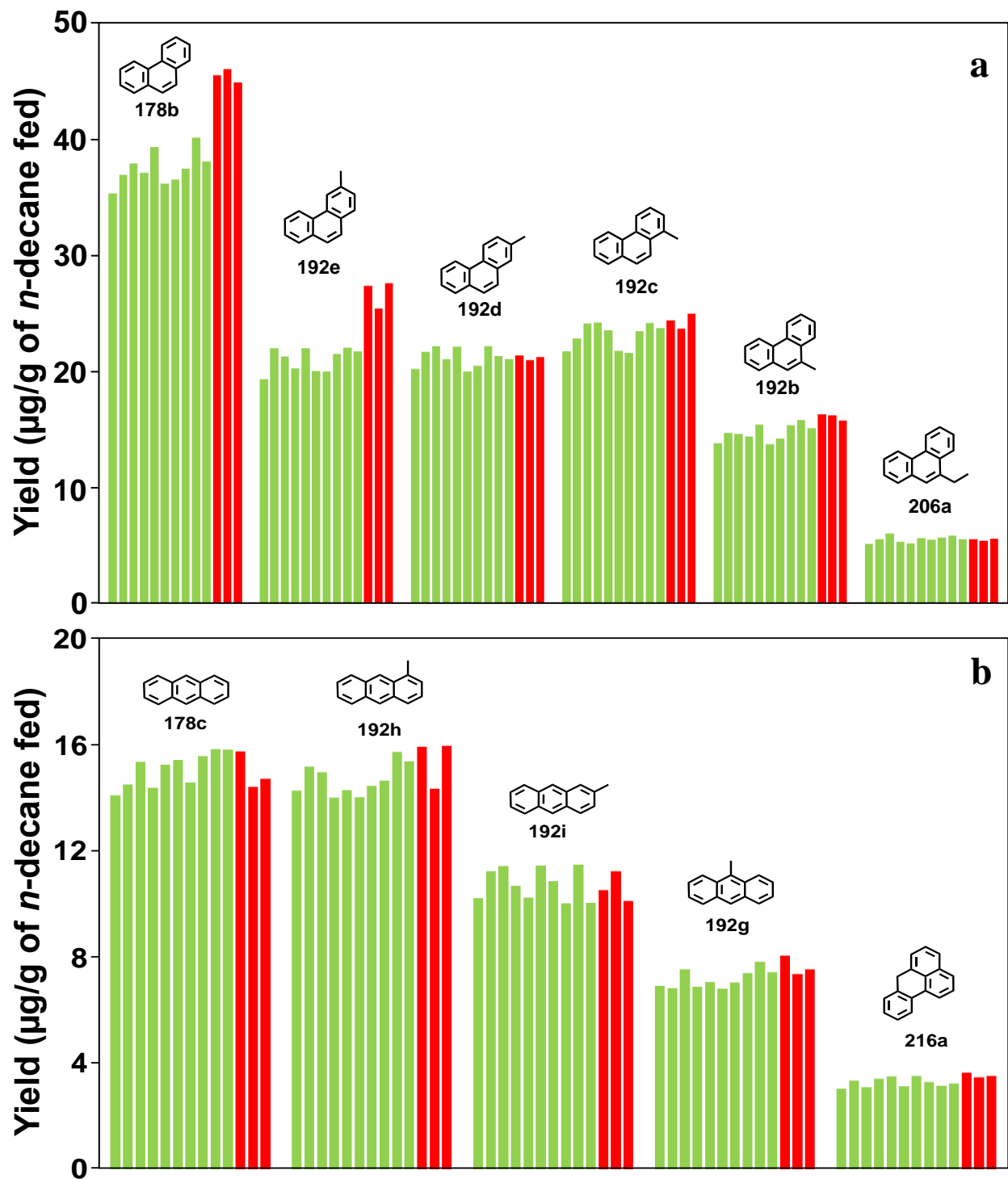


Figure C7. Yields of three- and four-ring PAH from supercritical *n*-decane pyrolysis at 568 °C, 94.6 atm, and 133 sec: (a) phenanthrene (178b), the four methylphenanthrenes (192b-e), and 9-ethylphenanthrene (206a); (b) anthracene (178c), the three methylanthracenes (192g-i), and 7*H*-benz[*de*]anthracene (216a). Experiments: (■) without dopant and (■) with 4-methylphenanthrene dopant (685  $\mu\text{g}$  4-methylphenanthrene / g *n*-decane fed). anthracene (178c), the three methylanthracenes (192g-i), and 7*H*-benz[*de*]anthracene (216a).

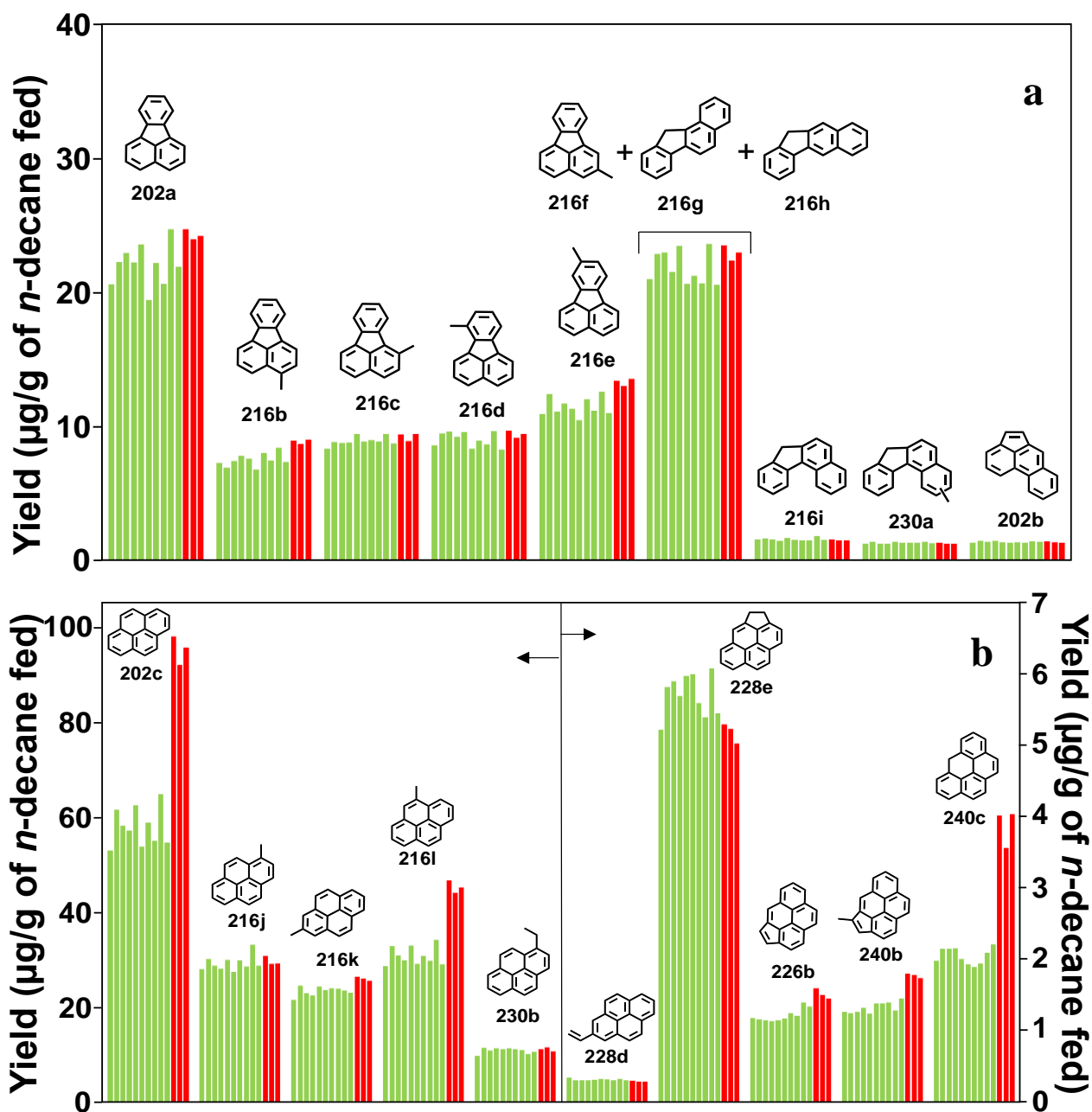
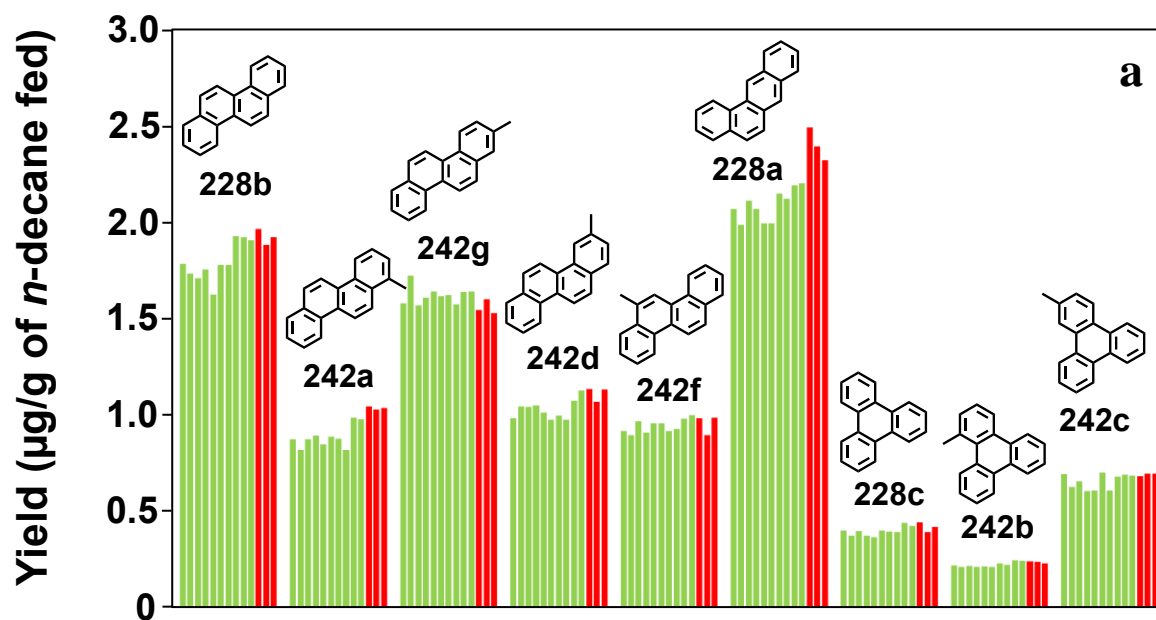


Figure C8. Yields of four-ring PAH, and their derivatives, from supercritical *n*-decane pyrolysis at 568 °C, 94.6 atm, and 133 sec: (a) acephenanthrylene (202b), fluoranthene (202a), the five methylfluoranthenes (216b-f) (one of which co-elutes with benzo[*a*]fluorene (216g) and benzo[*b*]fluorene (216h)), benzo[*c*]fluorene (216i), and a methylbenzo[*c*]fluorene (230a); (b) pyrene (202c), 1-methylpyrene (216j), 2-methylpyrene (216k), 4-methylpyrene (216l), 1-ethylpyrene (230b), 2-vinylpyrene (228d), 3,4-dihydrocyclopenta[*cd*]pyrene (228e), cyclopenta[*cd*]pyrene (226b), 4-methylcyclopenta[*cd*]pyrene (240b), and 6*H*-benzo[*cd*]pyrene (240c). Experiments: (■) without dopant and (■) with 4-methylphenanthrene dopant (685  $\mu\text{g}$  4-methylphenanthrene / g *n*-decane fed). The yield reported in (b) for 1-ethylpyrene might include contributions from co-eluting ethylpyrenes or dimethylpyrenes; hence it is a maximum possible 1-ethylpyrene yield.



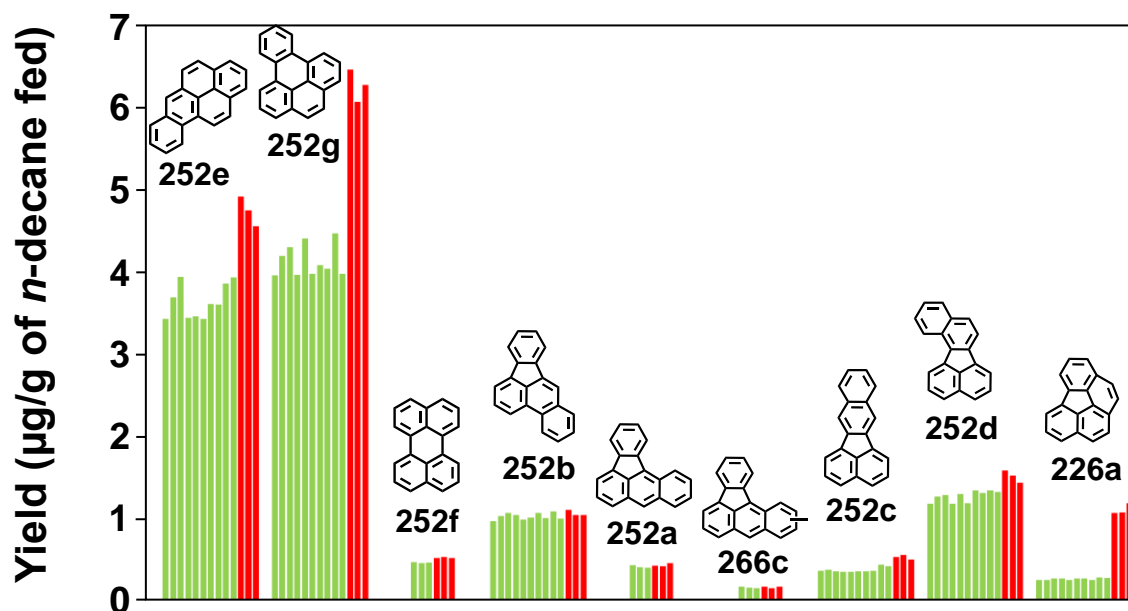


Figure C10. Yields of five-ring  $C_{20}H_{12}$  PAH, their derivatives, and an associated  $C_{18}H_{10}$  PAH product from supercritical *n*-decane pyrolysis at 568 °C, 94.6 atm, and 133 sec: (a) benzo[*a*]pyrene (252e), benzo[*e*]pyrene (252g), perylene (252f), benzo[*b*]fluoranthene (252b), benzo[*a*]fluoranthene (252a), a methylbenzo[*a*]fluoranthene (266c), benzo[*k*]fluoranthene (252c), benzo[*j*]fluoranthene (252d), and benzo[*ghi*]fluoranthene (226a). Experiments: (■) without dopant and (■) with 4-methylphenanthrene dopant (685 µg 4-methylphenanthrene / g *n*-decane fed).



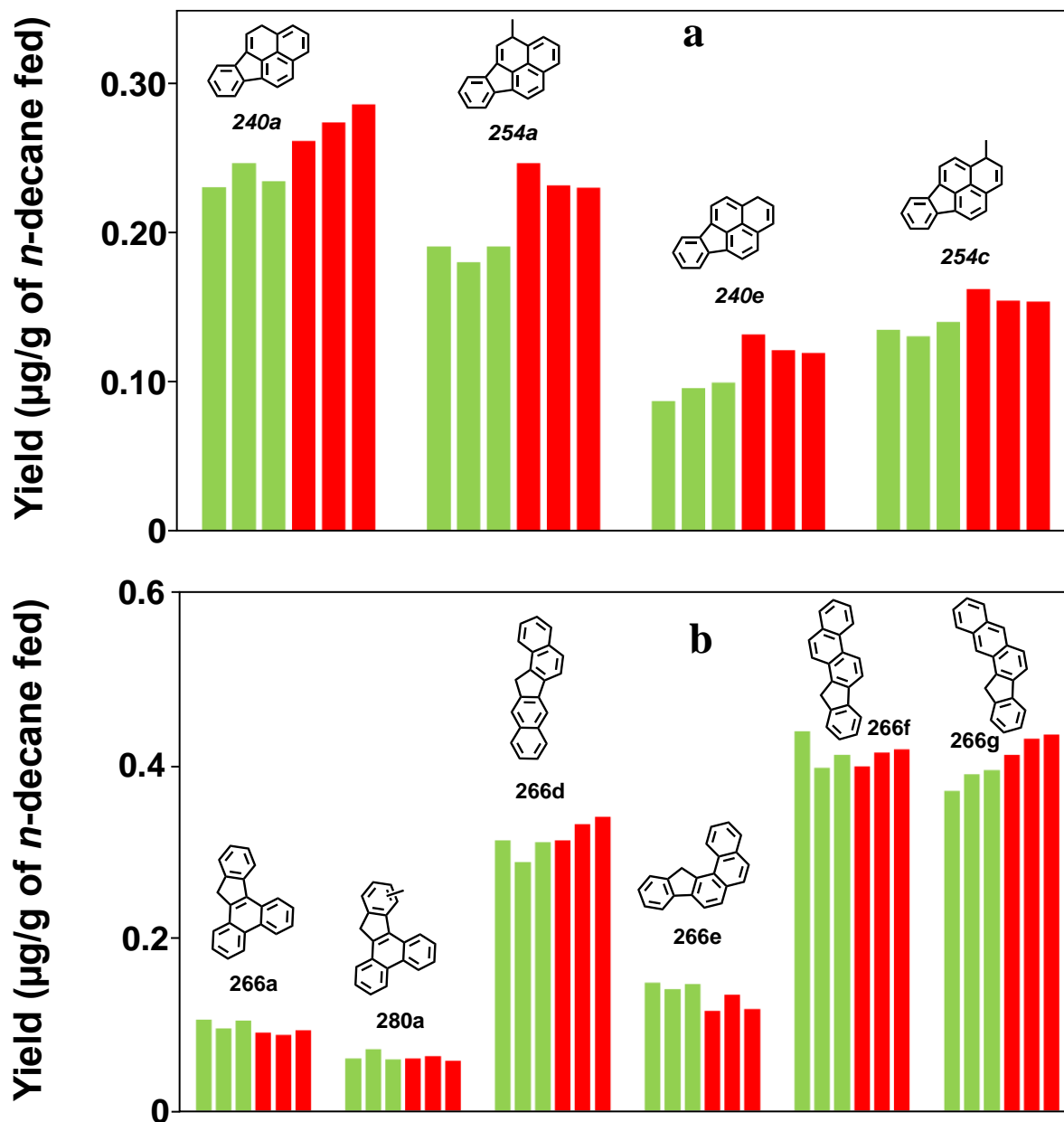


Figure C11. Yields of five-ring  $C_{19}H_{12}$  and  $C_{21}H_{14}$  PAH, and their methyl derivatives, from supercritical *n*-decane pyrolysis at 568 °C, 94.6 atm, and 133 sec: (a) 4*H*-benzo[*cd*]fluoranthene (240a), 4-methyl-4*H*-benzo[*cd*]fluoranthene (254a), 1*H*-benzo[*cd*]fluoranthene (240e), and 1-methyl-1*H*-benzo[*cd*]fluoranthene (254c); (b) dibenzo[*a,c*]fluorene (266a), methyl-dibenzo[*a,c*]fluorene (280a), dibenzo[*a,h*]fluorene (266d), naphtho[1,2-*a*]fluorene (266e), naphtho[2,1-*a*]fluorene (266f), and naphtho[2,3-*a*]fluorene (266g). Experiments: (■) without dopant and (■) with 4-methylphenanthrene dopant (685 µg 4-methylphenanthrene / g *n*-decane fed). The identifications of 4*H*-benzo[*cd*]fluoranthene (240a), 4-methyl-4*H*-benzo[*cd*]fluoranthene (254a), 1*H*-benzo[*cd*]fluoranthene (240e), and 1-methyl-1*H*-benzo[*cd*]fluoranthene (254c) are based on their UV and mass spectra but cannot be unequivocally confirmed, due to a lack of reference standards for these PAH.

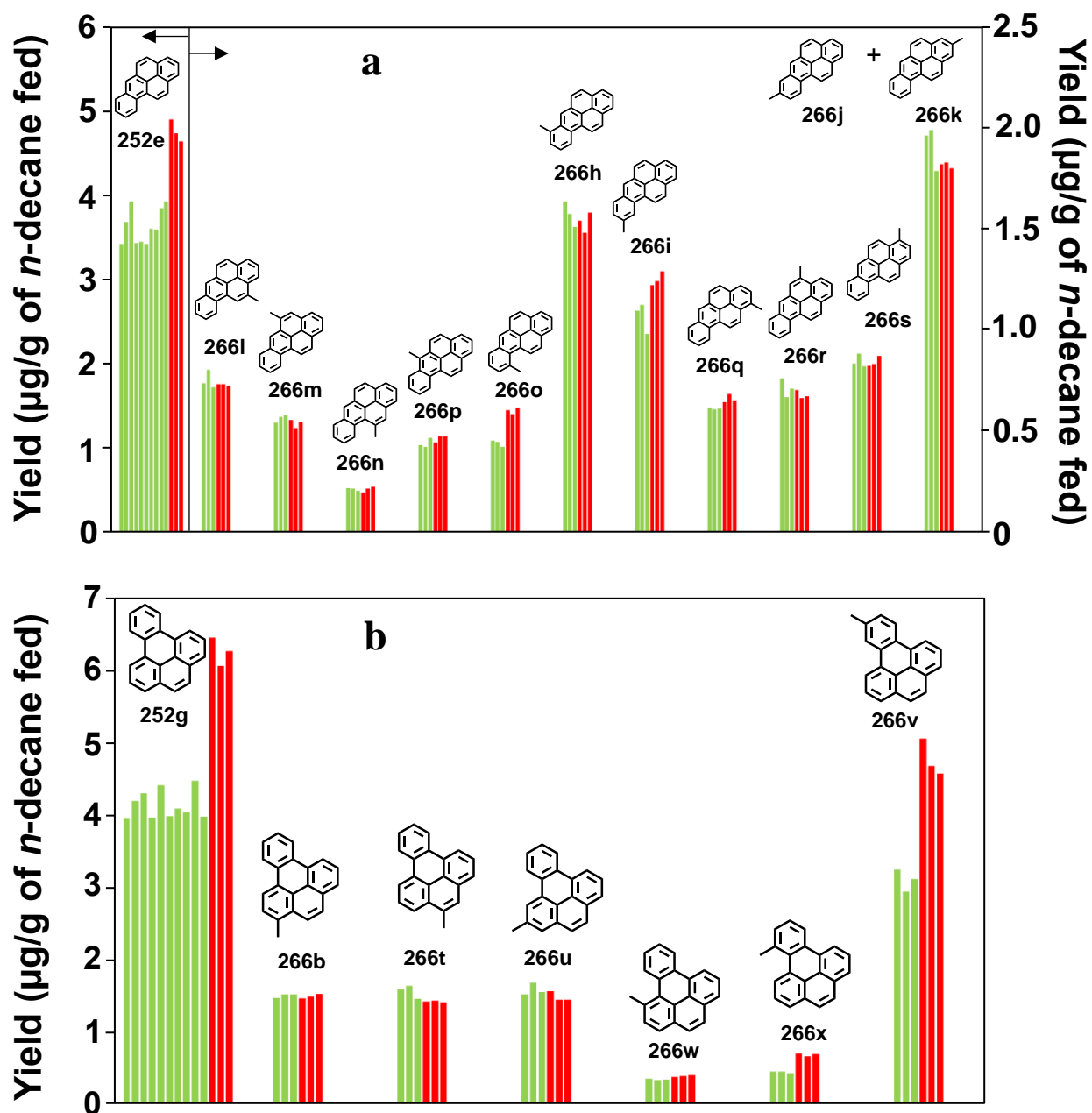


Figure C12. Yields of five-ring  $C_{20}H_{12}$  PAH, and their methyl derivatives, from supercritical *n*-decane pyrolysis at 568 °C, 94.6 atm, and 133 sec: (a) benzo[*a*]pyrene (252e), 12-methylbenzo[*a*]pyrene (266l), 5-methylbenzo[*a*]pyrene (266m), 11-methylbenzo[*a*]pyrene (266n), 6-methylbenzo[*a*]pyrene (266p), 10-methylbenzo[*a*]pyrene (266o), 7-methylbenzo[*a*]pyrene (266h), 9-methylbenzo[*a*]pyrene (266i), 1-methylbenzo[*a*]pyrene (266q), 4-methylbenzo[*a*]pyrene (266r), 3-methylbenzo[*a*]pyrene (266s), and 2-methylbenzo[*a*]pyrene (266k) co-eluting with 8-methylbenzo[*a*]pyrene (266j); (b) benzo[*e*]pyrene (252g), 3-methylbenzo[*e*]pyrene (266b), 4-methylbenzo[*e*]pyrene (266t), 2-methylbenzo[*e*]pyrene (266u), 1-methylbenzo[*e*]pyrene (266w), 9-methylbenzo[*e*]pyrene (266x), and 10-methylbenzo[*e*]pyrene (266v). Experiments: (■) without dopant and (■) with 4-methylphenanthrene dopant (685 µg 4-methylphenanthrene / g *n*-decane fed).

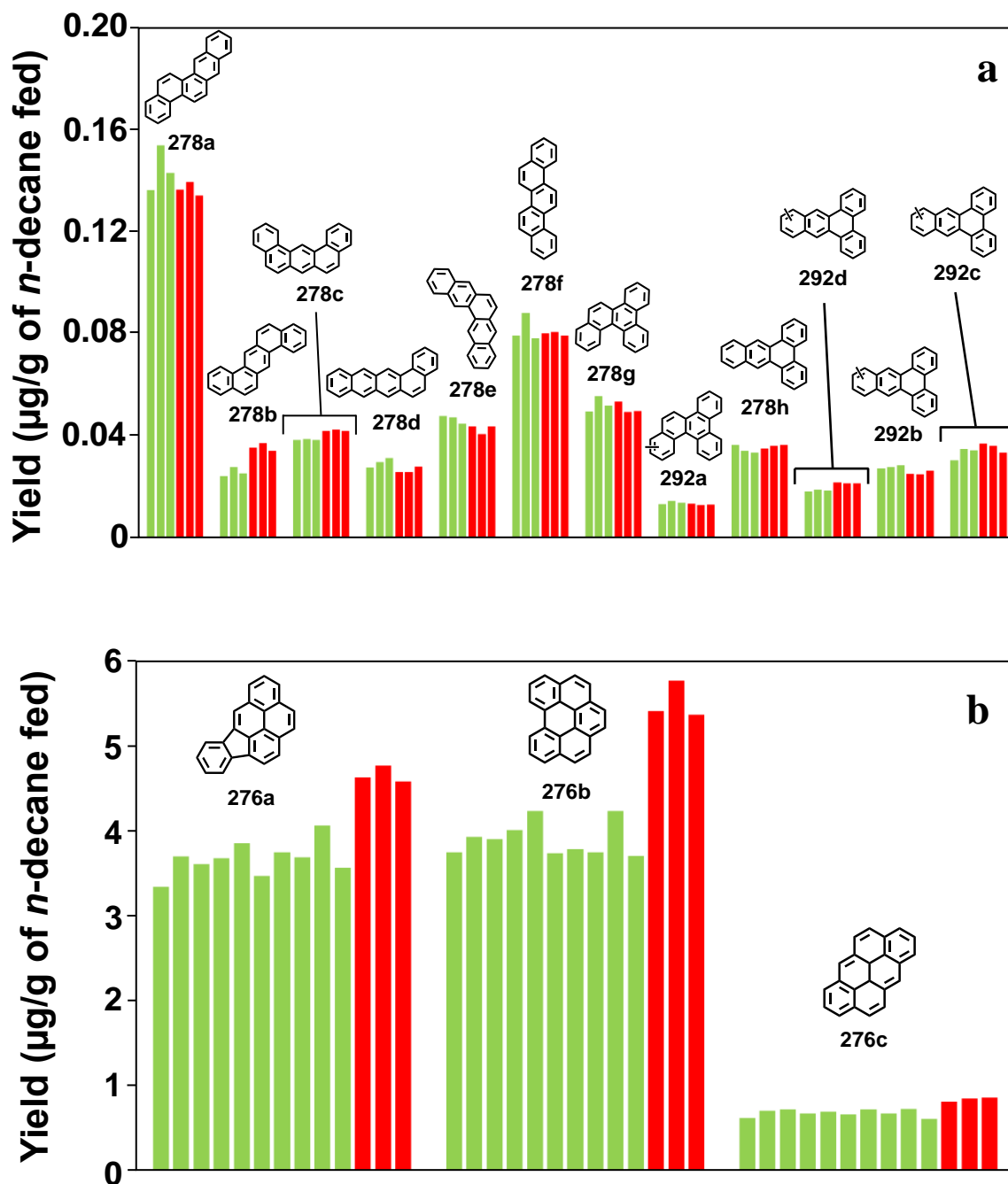


Figure C13. Yields of five-ring  $\text{C}_{22}\text{H}_{14}$  PAH, and their methyl derivatives, and six-ring  $\text{C}_{22}\text{H}_{12}$  PAH from supercritical *n*-decane pyrolysis at 568 °C, 94.6 atm, and 133 sec: (a) benzo[*b*]chrysene (278a), dibenz[*a,h*]anthracene (278b), dibenz[*a,j*]anthracene (278c), benzo[*a*]naphthacene (278d), pentaphene (278e), picene (278f), benzo[*g*]chrysene (278g), dibenz[*a,c*]anthracene (278h), three methyl dibenz[*a,c*]anthracenes (292b-d), and a methylbenzo[*g*]chrysene (292a); (b) indeno[1,2,3-*cd*]pyrene (276a), benzo[*ghi*]perylene (276b), and anthanthrene (276c). Experiments: (■) without dopant and (■) with 4-methylphenanthrene dopant (685  $\mu\text{g}$  4-methylphenanthrene / g *n*-decane fed).

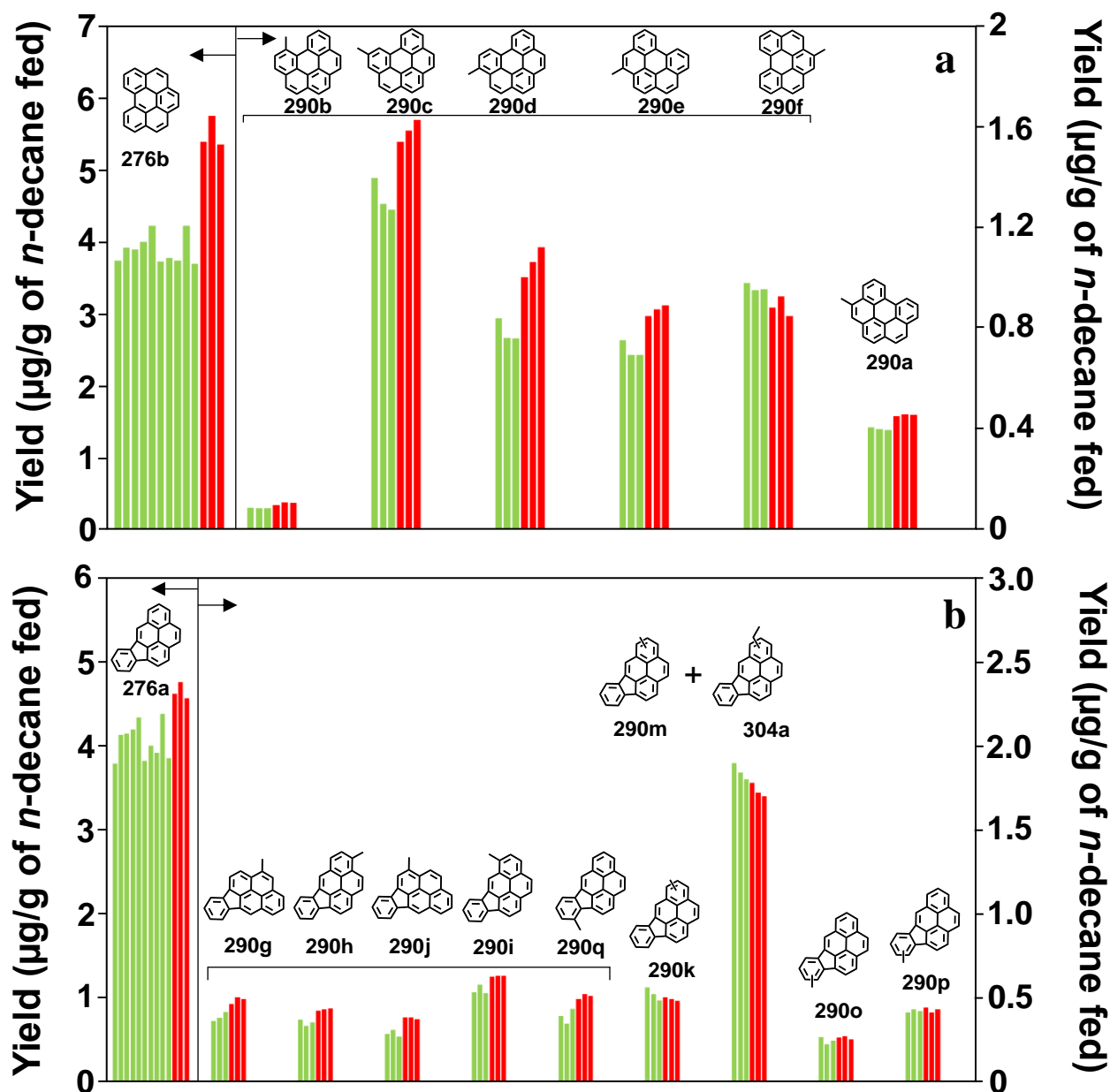


Figure C14. Yields of  $\text{C}_{22}\text{H}_{12}$  PAH, and their alkyl derivatives, from supercritical *n*-decane pyrolysis at 568 °C, 94.6 atm, and 133 sec: (a) benzo[ghi]perylene (276b) and the six methylbenzo[ghi]perylenes (290a-f); (b) indeno[1,2,3-*cd*]pyrene (276a), five methylindeno[1,2,3-*cd*]pyrenes (290g-j, 290q) whose yields increase with doping, three methylindeno[1,2,3-*cd*]pyrenes (290o-p, 290k) whose yields do not increase with doping, and a methylindeno[1,2,3-*cd*]pyrene (290m) co-eluting with an ethylindeno[1,2,3-*cd*]pyrene (304a). Experiments: (■) without dopant and (■) with 4-methylphenanthrene dopant (685  $\mu\text{g}$  4-methylphenanthrene / g *n*-decane fed). Among the sets of bars associated with the six methylbenzo[ghi]perylene products in (a), the set for 4-methylbenzo[ghi]perylene (290a) is assigned to that isomer since we have a reference standard for that isomer; a lack of reference standards for the other five methylbenzo[ghi]perylene isomers prevents assigning the other sets of bars to particular isomers.

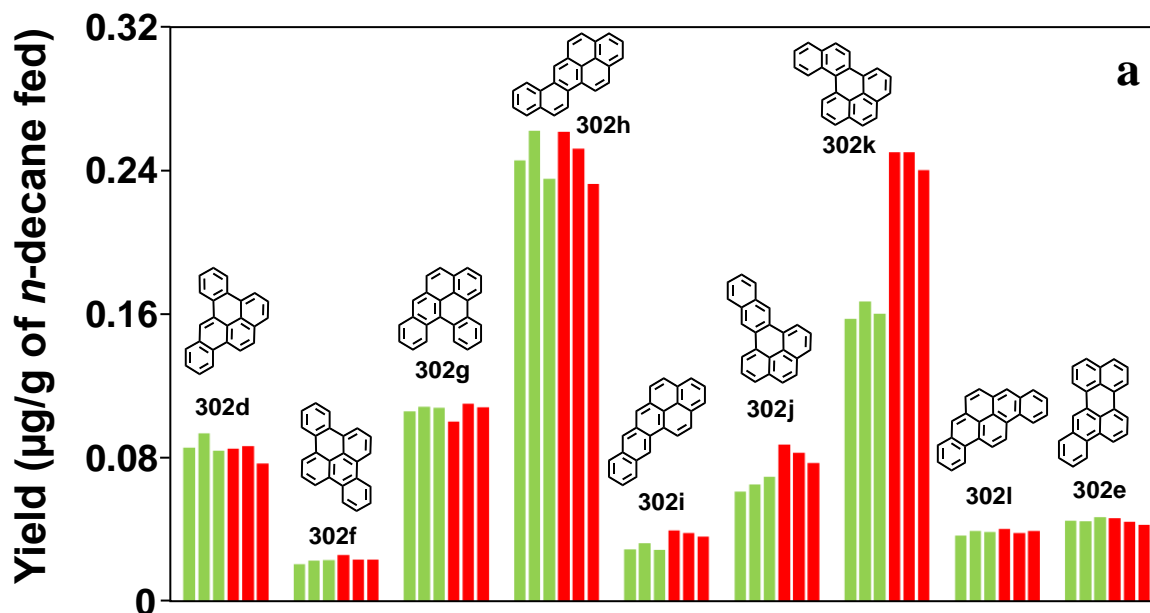


Figure C15. Yields of six-ring  $C_{24}H_{14}$  PAH from supercritical *n*-decane pyrolysis at 568 °C, 94.6 atm, and 133 sec: (a) dibenzo[*a,e*]pyrene (302d), dibenzo[*e,l*]pyrene (302f), dibenzo[*a,l*]pyrene (302g), naphtho[2,1-*a*]pyrene (302h), naphtho[2,3-*a*]pyrene (302i), naphtho[2,3-*e*]pyrene (302j), naphtho[1,2-*e*]pyrene (302k), dibenzo[*a,i*]pyrene (302l), and benzo[*b*]perylene (302e); Experiments: (■) without dopant and (■) with 4-methylphenanthrene dopant (685 µg 4-methylphenanthrene / g *n*-decane fed).

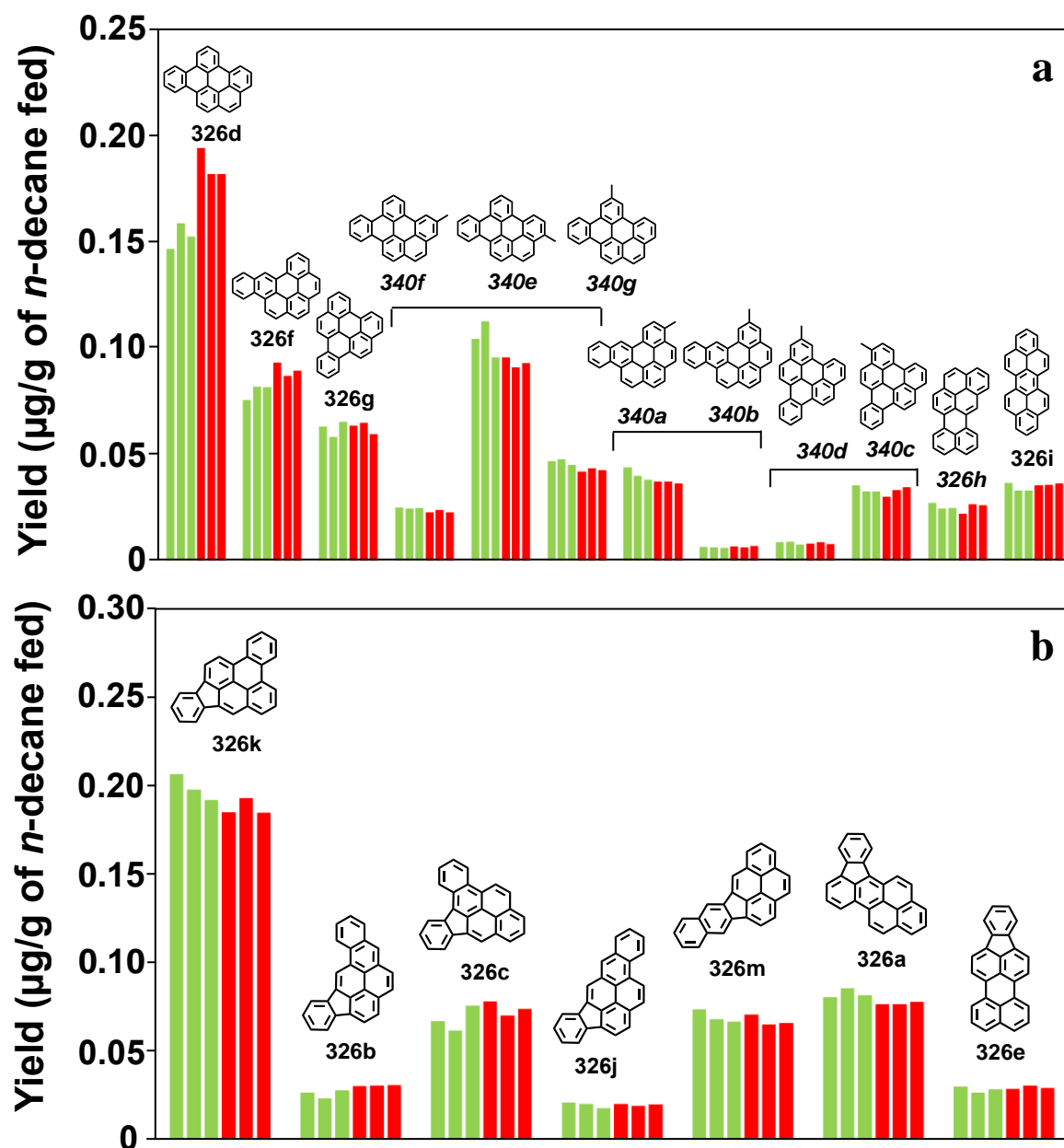


Figure C16. Yields of seven-ring  $C_{26}H_{14}$  PAH, and their methyl derivatives, from supercritical *n*-decane pyrolysis at 568 °C, 94.6 atm, and 133 sec: (a) dibenzo[*e,ghi*]perylene (326d), dibenzo[*b,ghi*]perylene (326f), naphtho[1,2,3,4-*ghi*]perylene (326g), naphtho[8,1,2-*bcd*]perylene (326h), dibenzo[*cd,lm*]perylene (326i), three methyl derivatives (340e-g), two methyl derivatives (340a-b), and two methyl derivatives (340c-d); (b) benz[*l*]indeno[1,2,3-*cd*]pyrene (326k), benz[*h*]indeno[1,2,3-*cd*]pyrene (326b), benz[*a*]indeno[1,2,3-*cd*]pyrene (326c), benz[*i*]indeno[1,2,3-*cd*]pyrene (326j), benz[5,6]indeno[1,2,3-*cd*]pyrene (326m), fluoreno[1,9-*ab*]pyrene (326a), and indeno[1,2,3-*cd*]perylene (326e). Experiments: (■) without dopant and (■) with 4-methylphenanthrene dopant (685 µg 4-methylphenanthrene / g *n*-decane fed). In (a), the positions of the methyl substituents on the dibenzo[*e,ghi*]perylene, dibenzo[*b,ghi*]perylene, and naphtho[1,2,3,4-*ghi*]perylene structures have been deduced, as noted in Table B1 in Appendix B.

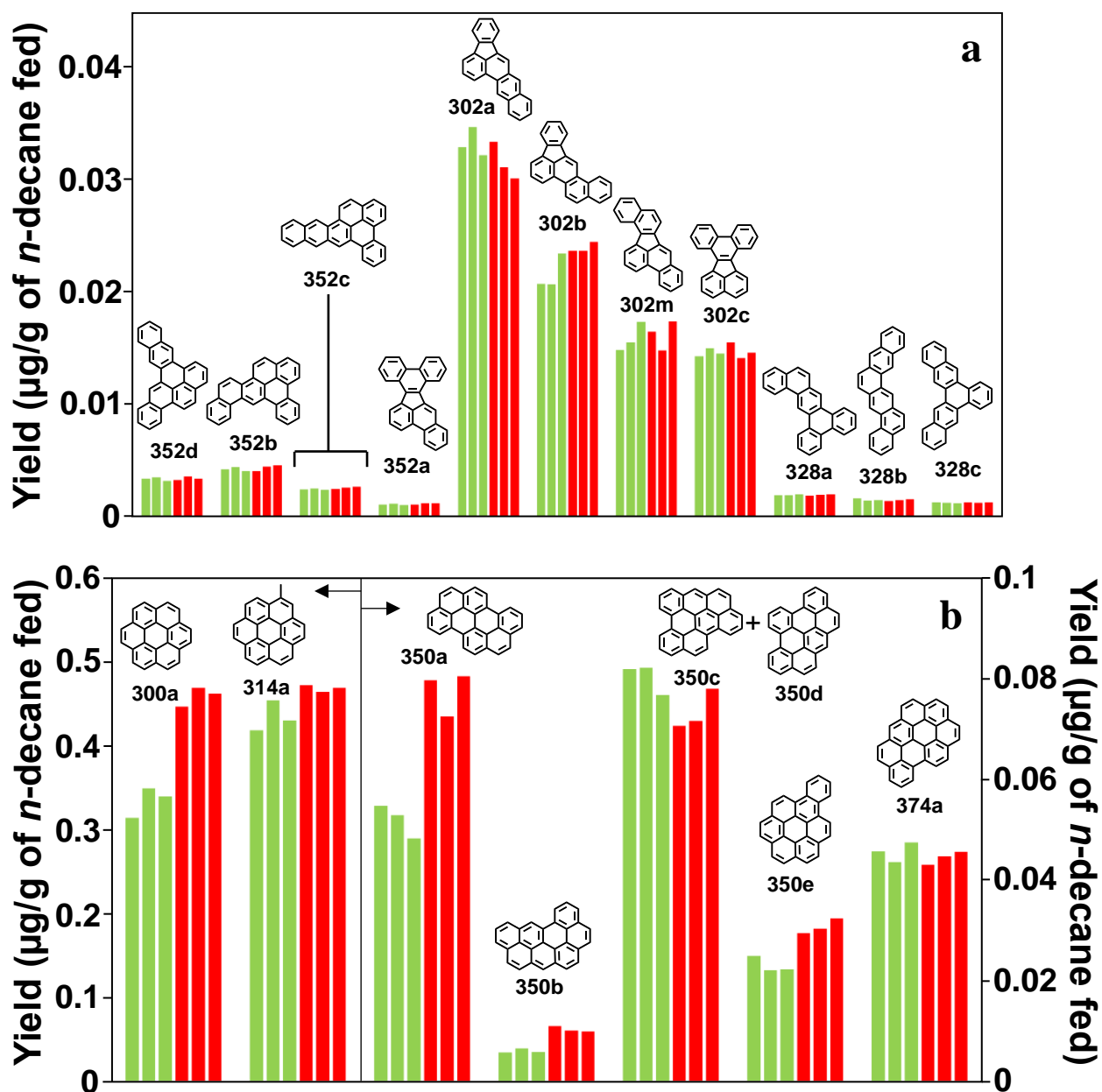



Figure C17. Yields of six- to nine-ring PAH products from supercritical *n*-decane pyrolysis at 568 °C, 94.6 atm, and 133 sec: (a) benzo[*a*]naphtho[2,3-*e*]pyrene (352d), benzo[*e*]naphtho[2,1-*a*]pyrene (352b), benzo[*e*]naphtho[2,3-*a*]pyrene (352c), tribenzo[*b,j,l*]fluoranthene (352a), naphtho[2,3-*b*]fluoranthene (302a), naphtho[1,2-*b*]fluoranthene (302b), dibenzo[*b,j*]fluoranthene (302m), dibenzo[*j,l*]fluoranthene (302c), tribenz[*a,c,h*]anthracene (328a), benzo[*c*]pentaphene (328b), and benzo[*h*]pentaphene (328c); (b) coronene (300a), 1-methylcoronene (314a), benzo[*pqr*]naphtho[8,1,2-*bcd*]perylene (350a), benzo[*ghi*]naphtho[8,1,2-*bcd*]perylene (350b), benzo[*cd*]naphtho[8,1,2,3-*fghi*]perylene (350c) co-eluting with phenanthro[5,4,3,2-*efghi*]perylene (350d), benzo[*a*]coronene (350e), and naphtho[8,1,2-*abc*]coronene (374a). Experiments: (■) without dopant and (■) with 4-methylphenanthrene dopant (685 µg 4-methylphenanthrene / g *n*-decane fed).

## Appendix D. Letter of Permission

10/25/21, 12:03 PM

Rightslink® by Copyright Clearance Center

Home Help ▾ Live Chat Sign in Create Account



Reaction pathways of molecular growth for bay-region methyl-substituted polycyclic aromatic hydrocarbons during supercritical pyrolysis of n-decane, as determined from experiments with 4-methylchrysene dopant

Author: Karthik Vutukuru, Avinash R. Mali, Mary J. Wornat

Publication: Proceedings of the Combustion Institute

Publisher: Elsevier

Date: 2021

© 2020 The Combustion Institute. Published by Elsevier Inc. All rights reserved.

### Journal Author Rights

Please note that, as the author of this Elsevier article, you retain the right to include it in a thesis or dissertation, provided it is not published commercially. Permission is not required, but please ensure that you reference the journal as the original source. For more information on this and on your other retained rights, please visit: <https://www.elsevier.com/about/our-business/policies/copyright#Author-rights>

BACK

CLOSE WINDOW

© 2021 Copyright - All Rights Reserved | [Copyright Clearance Center, Inc.](#) | [Privacy statement](#) | [Terms and Conditions](#)  
Comments? We would like to hear from you. E-mail us at [customercare@copyright.com](mailto:customercare@copyright.com)



## References

1. Edwards, T. *Combust. Sci. Technol.* **2006**, 178, 307-334.
2. Huang, H.; Spadaccini, L. J.; Sobel, D. R. *Trans. ASME* **2004**, 126, 284-293.
3. Maurice, L. Q.; Lander, H.; Edwards, T.; Harrison III, W. E. *Fuel* **2001**, 80, 747-756.
4. Edwards, T.; Zabarnick, S. *Ind. Eng. Chem. Res.* **1993**, 32, 3117-3122.
5. Huang, H.; Sobel, D. R.; Spadacini, L. J. *AIAA 2002-3871*, **2002**.
6. Yu, J.; Eser, S. *Ind. Eng. Chem. Res.* **1995**, 34, 404-409.
7. Dewitt, M. J.; Edwards, T.; Shafer, L.; Brooks, D.; Striebich, R.; Bagley, S. P.; Wornat, M. J. *Ind. Eng. Chem. Res.* **2011**, 50, 10434-10451.
8. Hazlett, R. N. Ed. American Society for Testing and Materials, Philadelphia, PA, **1991**.
9. Huang, H.; Spadaccini, L. J. *Ind. Eng. Chem. Res.* **2005**, 44, 267-278.
10. Bates, R.; Edward T.; Myer, M. *41<sup>st</sup> Aerospace Sciences Meeting and Exhibit*: Reno, NV. **2003**.
11. Edwards, T. *AIAA 2002-3874*, **2002**.
12. Edwards, T. *J. Propul. Power.* **2003**, 19, 1089-1107.
13. Song, C.; Lai, W. C.; Schobert, H. H. *Ind. Eng. Chem. Res.* **1994**, 33, 534-547.
14. Fabuss, B. M.; Smith, J. O.; Lait, R. I.; Borsanyi, A. S.; Satterfield, C. N. *Ind. Eng. Chem. Process Des. Dev.* **1962**, 1, 293-299.
15. Stewart, J.; Brezinsky, K.; Glassman, I. *Combust. Sci. Technol.* **1998**, 136, 373-390.
16. Fabuss, B. M.; Kafesjian, R.; Smith, J. O.; Satterfield, C. N. *Ind. Eng. Chem. Process Des. Dev.* **1964**, 3, 248-254.
17. Somers M. L.; McClaine, J. W.; Wornat, M. J. *Proc. Combust. Inst.* **2007**, 31, 501-509.
18. Bagley, S. P. *Supercritical Pyrolysis of n-Decane*, Ph.D. Thesis, Department of Chemical Engineering, Louisiana State University, **2010**.
19. Kalpathy, S. V. *Growth of Polycyclic Aromatic Hydrocarbons During the Supercritical Pyrolysis of n-Decane* . Ph.D. Thesis, Department of Chemical Engineering, Louisiana State University, **2016**.

20. Rice, F. O.; Herzfeld, K. F. *J. Am. Chem. Soc.* **1934**, 56, 284-289.
21. Kossiakoff, A.; Rice, F. O. *J. Am. Chem. Soc.* **1943**, 65, 590-595.
22. Ward, T. A.; Ervin, J. S.; Zabarnick, S.; Shafer, L. *J. Propul. Power* **2005**, 21, 344-355.
23. Ward, T. A.; Ervin, J. S.; Striebich, R. C.; Zabarnick, S. *J. Propul. Power* **2004**, 20, 394-402.
24. Jia, Z.; Huang, H.; Zhou, W.; Qi, F.; Zeng, M. *Energy Fuels* **2014**, 28, 6019-6028.
25. Zhou, W.; Jia Z.; Qin, J.; Bao, W.; Yu, B. *Chem. Eng. J.* **2014**, 243, 127-136.
26. Zhu, Y.; Liu, B.; Jiang, P. *Energy Fuels* **2014**, 28, 466-474.
27. Yu, J.; Eser, S. *Ind. Eng. Chem. Res.* **1997**, 36, 574-584.
28. Jiang, R.; Liu, G.; He, X.; Yang, C.; Wang, L.; Zhang, X.; Mi, Z. *J. Anal. Appl. Pyrolysis* **2011**, 92, 292-306.
29. Zhou, P.; Crynes, B. L. *Ind. Eng. Chem. Process Des. Dev.* **1986**, 25, 508-514.
30. Khorasheh, F.; Gray, M. R. *Ind. Eng. Chem. Res.* **1993**, 32, 1853-1863.
31. Shabtai, J.; Ramakrishnan, R.; Oblad, A. G. Hydropyrolysis of Model Compounds. *In Thermal Hydrocarbon Chemistry*; Oblad, A. G.; Davis, H. G.; Eddinger R. G., Eds.; Advances in Chemistry Series 183; American Chemical Society: Washington, DC, **1979**; pp 297-328.
32. Blouri, B.; Hamdan, F.; Herault, D. *Ind. Eng. Chem. Process Des. Dev.* **1985**, 24, 30-37.
33. Doue, F.; Guiochon, G. *J. Chim. Phys.* **1968**, 64, 395-409.
34. Voge, H. H.; Good, G. M. *J. Am. Chem. Soc.* **1949**, 71, 593-597.
35. Watanabe, M.; Tsukagoshi, M.; Hirakoso, H.; Adschiri, T.; Arai, K. *AIChE J.* **2000**, 46, 843-856.
36. Dominé, F. *Energy Fuels* **1989**, 3, 89-96.
37. Lai, W.-C.; Song, C. *Fuel* **1995**, 74, 1436-1451.
38. Luo, Y.-R. *Handbook of Bond Dissociation Energies in Organic Chemistry*; CRC Press: Boca Raton, FL, **2003**.
39. Zhou, P.; Hollis, O. L.; Crynes, B. L. *Ind. Eng. Chem. Res.* **1987**, 26, 846-852.
40. Safarik, I.; Strausz, O. P. *Res. Chem. Intermed.* **1996**, 22, 275-314.

41. Fabuss, B. M.; Smith, J. O.; Satterfield, C. N. *Adv. Pet. Chem. Refin.* **1964**, 9, 157-201.
42. Andrésen, J. M.; Strohm, J. J.; Sun, L.; Song, C. *Energy Fuels* **2001**, 15, 714-723.
43. Ivanovski, L.; Sapgir, G. *AIAA 1996-2683*, **1996**.
44. Somers M. L.; McClaine, J. W.; Wornat, M. J. *Proc. Combust. Inst.* **2007**, 31, 501-509.
45. Walker, M. S.; Wornat, M. J. *J. Chromatogr. A* **2010**, 1217, 4568-4574.
46. Bagley, S. P.; Wornat, M. J. *Energy Fuels*, **2011**, 25, 4517-4527.
47. Bagley, S. P.; Wornat, M. J. *Energy Fuels*, **2013**, 27, 1321-1330.
48. Kalpathy, S. V.; Bagley, S. P.; Wornat, M. J. *Ind. Eng. Chem. Res.* **2015**, 54, 7014-7027.
49. Kalpathy, S. V.; Poddar, N. B.; Bagley, S. P.; Wornat, M. J. *Proc. Combust. Inst.* **2015**, 35, 1833-1841.
50. Kalpathy, S.V.; Poddar, N.B.; Hurst, E.A.; Caspary, E.C.; Wornat, M.J. *Proc. Combust. Inst.* **2017**, 36, 965-973.
51. K. Vutukuru, A.R. Mali, and M.J. Wornat *Proc. Combust. Inst.* **2021**, 38, 1355-1364.
52. Hemelsoet, K.; Van Speybroeck, V.; Waroquier, M.; *J. Phys. Chem. A*, **2008**, 112, 13566-13573.
53. Brooks, M.A.; Scott, L.T.; *J. Am. Chem. Soc.* ,**1999**,121, 5444-5449.
54. Hurst, E.A.; Poddar, N.B.; Vutukuru, K.; Wornat, M.J.; *Proc. Combust. Inst.* **2019**, 37, 1107-1115.
55. Davis, G. T. *An Experimental Study of Supercritical Methylcyclohexane pyrolysis*. M.S.E. Thesis, Department of Mechanical and Aerospace Engineering, Princeton University, **1994**.
56. Stewart, J. F. *Supercritical Pyrolysis of the Endothermic Fuels of Methylcyclohexane, Decalin, and Tetralin*. Ph.D. Thesis, Department of Mechanical and Aerospace Engineering, Princeton University, **1999**.
57. Ledesma, E. B.; Wornat, M. J.; Felton, P. G.; Sivo, J. A. *Proc. Combust. Inst.* **2005**, 30, 1371-1379.
58. Nguyen, K. D. *Supercritical Pyrolysis of Toluene*. M.S. Thesis, Department of Chemical Engineering, Louisiana State University, **2011**.

59. Grubb, C. A. *An Experimental Investigation of the Effects of n-Decane on the Supercritical Pyrolysis of Toluene*. M.S. Thesis, Department of Chemical Engineering, Louisiana State University, **2014**.
60. McClaine, J. W.; Wornat M. J. *J. Phys. Chem. C*, **2007**, 111, 86-95.
61. Hurst, E.A. *The Effects of Temperature on the Yields of Aliphatic and Aromatic Products from the Supercritical Pyrolysis of 1-Octene*. Ph.D. Thesis, Department of Chemical Engineering, Louisiana State University, **2019**.
62. Darrah, S. *Jet Fuel Deoxygenation*, AFWAL-TR-88-20811988.
63. Wise, S. A.; Chesler, S. N.; Hertz, H. S.; Hilpert, L. R.; May, W. E., *Analytical Chemistry*, **1977**, 49, 2306-2310.
64. Ehrenhauser, F. S.; Wornat, M. J.; Valsaraj, K. T.; Rodriguez, P. *Rapid Commun. Mass Spectrom.* **2010**, 24, 1351–1357.
65. Lafleur, A. L.; Monchamp, P. A.; Plummer, E. F.; Wornat, M. J. *Anal. Lett.* **1987**, 20, 1171–1192.
66. Fetzer, J. C.: *Large (C<sub>n</sub>≥24) Polycyclic Aromatic Hydrocarbons: Chemistry and Analysis*, Wiley-Interscience, New York, **2000**.
67. Jones, R. N., *Journal of American Chemical Society*, **1945**, 67, 2127-2150.
68. Yahyaoui, M.; Djebaili-Chaumeix, N.; Dagaut, P., Paillard, C. -E.; Gail, S. *Combust. Flame* **2006**, 147, 67-68.
69. Fridlyand, A.; Goldsborough, S. S.; Brezinsky, K.; Merchant, S. S.; Green, W. H. *Proc. Combust. Inst.* **2015**, 35, 333-340.
70. Wang, K.; Villano, S. M.; Dean, A. M. *Energy Fuels* **2017**, 31, 6515-6524.
71. Lai, W. C.; Song, C. *Fuel Process. Technol.* **1996**, 48, 1-27.

## **Vita**

Venkata Sai Krishna Karthik Vutukuru was born in Guntur, India. He grew up in Hyderabad, India. He attended Osmania University where he earned his bachelor's degree in chemical engineering in May 2015. In the same year, he attended graduate school at Louisiana State University to further his studies in chemical engineering. As a graduate student, he has authored/co-authored two peer-reviewed journal articles and one more article is in preparation for submission. He also had the opportunity to present his research work at conferences in San Francisco, Dublin, and Adelaide. He plans to graduate in the fall of 2021.